POLITECNICO DI TORINO

Master Degree course in Physics of Complex Systems

Master Degree Thesis

Andreev reflection in spin-orbit nanowires proximized by superconductors

Supervisor
Prof. Fabrizio Dolcini

Candidate
Leonardo Musca

Academic Year 2024-2025

Acknowledgements

I would like to express my deepest gratitude to Prof. Fabrizio Dolcini for his kindness and wise guidance throughout this final part of my academic journey, and for constantly encouraging me to pursue scientific rigor and critical thinking.
I am also sincerely grateful to Dr. Alessandro Braggio and Dr. Fabio Taddei from the CNR Institute of Nanoscience in Pisa for the inspiring discussions and valuable suggestions they shared during their visit to the Nanoscience and Quantum Systems group at Politecnico di Torino.
Finally, my heartfelt thanks go to Mamma, Papà and Carmelo. Thank you for your unwavering support, especially during the most challenging moments. Your love and encouragement have been the primary source of my strength and determination. This work is dedicated to you.

Ringraziamenti

Vorrei esprimere la mia più profonda gratitudine al Prof. Fabrizio Dolcini per la sua gentilezza e la sua sapiente guida durante questa fase finale del mio percorso accademico, e per avermi costantemente incoraggiato a perseguire il rigore scientifico e il pensiero critico.
Sono inoltre sinceramente grato al Dr. Alessandro Braggio e al Dr. Fabio Taddei dell'Istituto di Nanoscienze del CNR di Pisa per le stimolanti discussioni e i preziosi suggerimenti condivisi durante la loro visita al gruppo Nanoscience and Quantum Systems del Politecnico di Torino.
Infine, un ringraziamento speciale va a Mamma, Papà e Carmelo. Grazie per il vostro sostegno incrollabile, soprattutto nei momenti più difficili. Il vostro amore e il vostro incoraggiamento sono stati la fonte primaria della mia forza e determinazione. Questo lavoro è dedicato a voi.

Abstract

Superconductivity is one of the most important macroscopic quantum coherent phenomena in physics, where at sufficiently low temperatures electrons form Cooper pairs sharing the same phase. When an interface is realized between a superconductor (S) and a normal (N) material, a phenomenon called Andreev reflection occurs: an electron impinging from the normal side towards the interface cannot penetrate the superconductor as a single quasiparticle and is back-reflected as a hole.

Recently, one of the most interesting and studied setups involving a normal and a superconducting material is the case of semiconductor nanowires with spin-orbit coupling (SOC), where a nanowire portion, covered by a superconducting film, acquires a superconducting pairing by proximity effect. Nanowires characterized by strong SOC, such as InAs and InSb, exhibit ballistic transport and a wide tunability of the SOC, and have been predicted to host Majorana quasiparticles that are robust to decoherence, with potential applications in quantum technology.

While experimental evidence for Majorana quasiparticles is still debated, a key open problem is to understand how Andreev Reflection is affected by SOC inhomogeneities. Indeed, while most theoretical models assume a homogeneous SOC, in actual experiments inhomogeneities are present mainly for two reasons: firstly, when a nanowire portion is covered by a superconducting film, its structural inversion asymmetry underlying the Rashba SOC is modified as compared to the bare nanowire portion. Secondly, the SOC in the normal portion can be controlled in magnitude and direction by wrap metallic gates, with the purpose of tuning the conduction properties of the system. So far, these aspects have been mainly overlooked in the literature.

This MS Thesis is an attempt to bridge this gap, by investigating how Andreev reflection is affected by the inhomogeneities of the SOC. In order to describe a homogeneous single channel semiconductor nanowire proximized by a superconducting pairing, we first consider the generalization of the Bardeen-Cooper-Schrieffer model including the effects of SOC and of an external magnetic field. Then, by adopting the Bogoliubov-de Gennes formalism, we further extend this model to describe inhomogeneous systems, specifically a Normal-Superconducting (N/S) nanowire junction where the SOC profile is non-uniform across the interface.

By combining analytical and numerical methods, we analyze the effects of two specific types of spin-orbit inhomogeneities on Andreev reflection. The first one is an inhomogeneity in the direction of the SOC field, defined by a misalignment angle between the N and S sides. The second type is the inhomogeneity in the magnitude of the Rashba SOC. Our results show that, while Andreev Reflection is independent of the misalignment angle, it can be significantly affected by the difference in the spin-orbit magnitude. We analyze this effect in two distinct regimes, where the spin-orbit energy is much larger

than the superconducting gap, and in the opposite case of a large superconducting gap. Furthermore, we also discuss how these effects are modified by the presence of a magnetic field.

In conclusion, this work provides a rigorous framework for modeling quantum transport in N/S nanowire junctions. Our findings clarify the distinct roles of directional and magnitude-based SOC inhomogeneities in modulating Andreev reflection, providing a solid basis for the design of future quantum devices.

Contents

Chapter 1

Superconductivity and nanowires with spin-orbit coupling

1.1 Superconductivity and Andreev reflection

1.1.1 A quick overview of supercoductivity

Superconductivity stands as one of the most fascinating macroscopic quantum phenomena in condensed matter physics. It was first observed by Heike Kamerlingh Onnes in 1911 while cooling Mercury and other metals down to temperatures of a few Kelvin using liquid Helium. Kamerlingh Onnes observed that below a certain critical temperature T_c, the electrical resistance of these materials dropped abruptly to zero, thereby characterizing them as *perfect conductors*. Later, further experiments have demonstrated that currents in superconducting rings can flow indefinitely without any measurable decay, indicating a truly zero-resistance state. The critical temperature T_c represents the first fundamental parameter characterizing a superconductor and it depends on the material type [1, 2]. In particular, for a given superconducting element, T_c depends on its specific isotopic variant. This phenomenon, known as the Isotope Effect[3], reveals that T_c changes with the mass M of the constituent ions.
A second feature characterizing a superconductor, discovered in 1933 by Walther Meissner and Robert Ochsenfeld, is the *Meissner effect*[4]. It was observed that below T_c, and for magnetic fields below a certain critical value $H_c(T)$, superconductors behave as perfect diamagnets, actively expelling applied magnetic fields from their interior. This expulsion is spontaneous and reversible. The critical magnetic field H_c is temperature-dependent, typically following a universal empirical parabolic law (for materials characterized by low T_c), and vanishing at T_c, namely

$$H_c(T) \approx H_c(0)\left[1 - \left(\frac{T}{T_c}\right)^2\right] \tag{1.1}$$

Above the critical field H_c, superconductivity is destroyed, and the material exhibits its normal resistive state.

The discovery of the Meissner effect was crucial to identify superconductivity as a thermodynamic state of matter, which differs from a mere hypothetical "perfect conductor" (a material with just zero resistance). Indeed let us highlight their difference by considering two possible scenarios. In the first one, both materials are cooled below T_c in zero magnetic field, and then a magnetic field is applied. In this case both of them will expel the field, without showing any response to it. For the perfect conductor, this is due to Faraday's law of induction ($\nabla \times \mathbf{E} = -\partial \mathbf{B}/\partial t$): zero resistance implies zero internal electric field, which means the internal magnetic field cannot change over time ($\partial \mathbf{B}/\partial t = 0$), i.e. remainingvanishing in the material.
In contrast, if a magnetic field is applied above T_c and the materials are subsequently cooled, a perfect conductor would trap the field inside (maintaining $\partial \mathbf{B}/\partial t = 0$ as it becomes perfectly conducting), whereas a superconductor will spontaneously expel the field as it crosses T_c, as observed in the Meissner effect. The reversibility of this effect and the observations that the transition and the final state depend only on the thermodynamic variables (T, H) and not on the cooling history, suggests prove that the superconducting state is a distinct, stable thermodynamic phase of matter.
The evidence that the transition to a superconductivity state represents a phase transition, in which the system enter in a lower energy state, is also supported by the observations of a discontinuity in the specific heat c_v at T_c in zero magnetic field [2]. This represents a second order phase transition, since it involves the second derivative of the Gibbs free energy, and it is characterized by a discontinuos increase of the specific heat at T_c, followed by an exponentially decrease towards zero. This jump indicates an internal reordering of the system (the formation of the superconducting order) that does not require an energy cost, but changes the way in which the system stores heat.
In contrast, in presence of a field H, the superconductivity transition is of the first order, since it involves a discontinuity in entropy and therefore an associated latent heat. Indeed in this case an energetic cost is required to expel the magnetic field in order to enter in the new state([1, 2]).
Over the years further research led to the discovery of a second type of low T_c superconductors (predicted by Abrikosov in 1957), called type II superconductors. The classification of these materials into two types is based on their magnetic response:

- *Type-I* Superconductors that exhibit complete Meissner effect up to a single critical field H_c, above which superconductivity is completely lost.

- *Type-II* Superconductors characterized by two critical fields, H_{c1} and H_{c2}. Below H_{c1}, they are perfect diamagnets. Between H_{c1} and H_{c2}, they enter a mixed state (or vortex state) where magnetic flux penetrates the material in quantized vortices while remaining superconducting. Above H_{c2}, the bulk superconductivity is destroyed.

Furthermore, in 1986 scientists Georg Bednorz and K. Alex Müller discovered the first high-T_c superconductors [5], characterized by a high critical temperature with respect the superconductors discovered up to that time. Tipically, a superconductor is classified as an high-T_c one, when the critical temperature is above the boiling point of liquid nitrogen, i.e. $77\,K$. All known high-Tc superconductors are Type-II ones.

1.1.2 The phenomenological Ginzburg–Landau theory of superconductivity

Before a thorough microscopic theory of superconductivity was formulated, Ginzburg and Landau (1950) proposed a powerful phenomenological approach to explain this phenomenon . Their approach is based on Landau's theory of continuous phase transitions (1937). The central concept is the introduction of an order parameter, a quantity that is non-zero below the critical temperature T_c (in the ordered superconducting phase) and identically zero above it (in the normal phase). Landau suggested that the free energy $\mathcal{F}$ of the system near the critical point can be expanded as a power series of this order parameter and its derivatives, constrained by the fundamental symmetries of the system. In the context of superconductivity, the order parameter is a complex macroscopic wavefunction $\psi(\mathbf{r})$, whose squared modulus represents

$$|\psi(\mathbf{r})|^2 = n_s = \text{density of superconducting charge carriers}$$

whose charge and mass are denoted by e^* and m^*, respectively. Denoting by $\mathcal{F}_n$ the free energy of the normal state, the physical value taken by the superconducting order parameter is determined by minimizing the free energy functional

$$\mathcal{F} = \mathcal{F}_n + \int d\mathbf{r} \left[\frac{|(-i\hbar\boldsymbol{\nabla} - e^*\mathbf{A}(\mathbf{r}))\psi(\mathbf{r})|^2}{2m^*} + \alpha|\psi(\mathbf{r})|^2 + \frac{\beta}{2}|\psi(\mathbf{r})|^4 + \frac{\mathbf{B}^2(\mathbf{r})}{2\mu_0} \right] \tag{1.2}$$

with respect to ψ, ψ^* and $\mathbf{A}$ [1, 2]. In particular, for a spatially uniform order parameter ψ and in the absence of external fields ($\mathbf{A} \equiv 0$), the free energy difference $\mathcal{F} - \mathcal{F}_n$ exhibits two qualitatively different behaviors depicted in Fig.1.1. As one can see, while for $\alpha > 0$

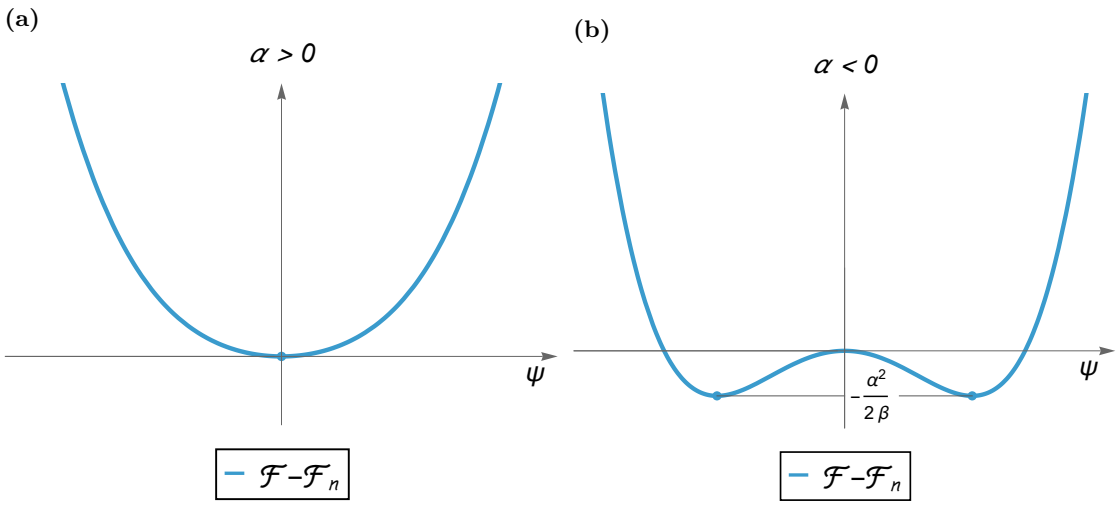

Figure 1.1: The Ginzburg-Landau free energy difference $\mathcal{F} - \mathcal{F}_n$ for $\alpha > 0$(left panel) and $\alpha < 0$(right panel). For $\alpha > 0$ the minimum is reached at energy value $-\frac{\alpha^2}{2\beta}$.

the minimal free energy is obtained for $\psi = 0$ (no superconductivity), for $\alpha < 0$ the free

energy exhibits two local minima, corresponding to the order parameter value

$$|\psi|^2 = -\frac{\alpha}{\beta} \tag{1.3}$$

thereby causing the emergence of a superconducting state. This suggests that $\alpha(T) = a(T - T_c)$ with $a > 0$.
In the most general case (1.2) where also the spatial variations of the order parameter are included, the minimization leads to the Ginzburg Landau equations

$$-\frac{\hbar^2}{2m^*}\left(-\boldsymbol{\nabla} - i\frac{e^*}{\hbar}\mathbf{A}(\mathbf{r})\right)^2 \psi(\mathbf{r}) + \alpha\psi(\mathbf{r}) + \beta|\psi(\mathbf{r})|^2\psi(\mathbf{r}) = 0 \tag{1.4}$$

and

$$\mathbf{J} = -\frac{ie^*\hbar}{2m^*}\left(\psi^*\boldsymbol{\nabla}\psi - \boldsymbol{\nabla}\psi^*\,\psi\right) - \frac{(e^*)^2}{m^*}\mathbf{A}|\psi(\mathbf{r})|^2 \tag{1.5}$$

The former equation (1.4) resembles a non-linear Schrödinger equation for the superconducting order parameter, while the second one returns the value of the current density. In particular, by expressing the order parameter in terms of its modulus and phase

$$\psi(\mathbf{r}) = |\psi(\mathbf{r})|\, e^{i\varphi(\mathbf{r})} \tag{1.6}$$

the current density (1.5) can be re-expressed as

$$\mathbf{J} = \frac{e^*}{m^*}|\Psi|^2\left(\hbar\boldsymbol{\nabla}\varphi - e^*\,\mathbf{A}\right) \tag{1.7}$$

The spatial variations of the *phase* of the order parameter are related to the current due to the superconducting carriers.
The Ginzburg-Landau theory enables one to identify the coherence length ξ, i.e. the typical lengthscale over which the density of superconducting carriers spatially changes, the penetration depth of the magnetic field inside the superconductor. Moreover, it enables one to predict the existence of type-I and type-II superconductors, to compute the critical magnetic fields and current, and to demonstrate the existence of magnetic vortices and fluxoid quantization.

1.1.3 The microscopic theory of superconductivity by Bardeen, Cooper and Schrieffer

The first comprehensive microscopic theory describing superconductivity was proposed in 1957 by Bardeen, Cooper and Schrieffer, known as the *BCS theory*[6]. Unlike previous phenomenological approaches, this theory provides an explanation of the phenomenon starting from fundamental quantum mechanical principles. BCS theory is founded on the second quantization formalism, which is essential for treating many-body systems characteristic of condensed matter. Within this framework, the system is described by considering the fundamental constituents and their couplings:

- The crystal lattice of positively charged ions.

- The "sea" of conduction electrons (Fermi sea).
- The mutual interactions between these entities: specifically, the direct electron-electron Coulomb repulsion and the electron-lattice (electron-phonon) interaction.

A first, simplified attempt to describe condensed matter relies on the Born-Oppenheimer approximation[7, 8]. This approach decouples the motion of electrons from that of the ions, based on the significant difference in their respective velocities due to their vastly different masses. Following this observation, the approximation assumes that the electrons perceive the ionic configuration as a static attractive potential, instantaneously adjusting to any change in ionic positions, whereas Ions move much slower and feel an effective potential generated by the average distribution of the electron cloud.
Going beyond the Born-Oppenheimer approximation, the crucial starting point for effectively modeling the interaction between electrons and ions is the Fröhlich Hamiltonian [9]. This Hamiltonian represents a first attempt in which the dynamics of electrons and ions become coupled. It is composed by three terms and reads

$$\mathcal{H}_{Fr} = \sum_{\mathbf{k}\sigma} \epsilon_{\mathbf{k}} c^{\dagger}_{\mathbf{k}\sigma} c_{\mathbf{k}\sigma} + \sum_{\mathbf{q}} \hbar\omega_{\mathbf{q}} a^{\dagger}_{\mathbf{q}} a_{\mathbf{q}} + \sum_{\mathbf{kq}\sigma} \nu_{\mathbf{q}} c^{\dagger}_{\mathbf{k}+\mathbf{q}\sigma} c_{\mathbf{k}\sigma} (a_{\mathbf{q}} + a^{\dagger}_{-\mathbf{q}}) \tag{1.8}$$

where

- $\mathcal{H}_{el} = \sum_{\mathbf{k}\sigma} \epsilon_{\mathbf{k}} c^{\dagger}_{\mathbf{k}\sigma} c_{\mathbf{k}\sigma}$ describes the kinetic energy of the non-interacting Fermi Sea;
- $\mathcal{H}_{ph} = \sum_{\mathbf{q}} \hbar\omega_{\mathbf{q}} a^{\dagger}_{\mathbf{q}} a_{\mathbf{q}}$ represents the vibrational energy of the lattice in the harmonic approximation. In particular $\hbar\omega_{\mathbf{q}}$ denotes the quanta of energy of the quasi-particle with momentum $\mathbf{q}$, called phonons;
- $\mathcal{H}_{el-ph} = \sum_{\mathbf{kq}\sigma} \nu_{\mathbf{q}} c^{\dagger}_{\mathbf{k}+\mathbf{q}\sigma} c_{\mathbf{k}\sigma} (a_{\mathbf{q}} + a^{\dagger}_{-\mathbf{q}})$ accounts for the electron-phonon interaction, i.e. the fundamental process through which an electron interacts with the lattice by absorbing or emitting a phonon. Specifically $\nu_{\mathbf{q}}$ denotes the coupling constants of such process where an electron is scattered from momentum $\mathbf{k} \to \mathbf{k} + \mathbf{q}$ by absorbing a phonon with momentum $\mathbf{q}$ or by emitting one with momentum $-\mathbf{q}$.

Thus, this Hamiltonian isolates the interaction between electrons and the vibrational modes of the lattice, neglecting the electron-electron interaction. Indeed, in the Frḧlich model, electrons experience the vibrating lattice as a perturbation of the periodic potential in which they are embedded, and this perturbation induces a scattering process between electrons and phonons.
In this framework it is possible to demonstrate that, under certain conditions, the interaction mediated by the exchange of virtual phonons can overcompensate for the natural Coulomb repulsion between two electrons, resulting in a net effective attractive interaction between electrons near the Fermi surface. This counterintuitive effective attraction is the key ingredient required for the formation of bound electron states, a central concept that is formally explored through *Cooper's* theorem [10].

Cooper Theorem

The foundational step towards a microscopic theory of superconductivity was taken by Leon Cooper in 1956 [10]. He demonstrated that the normal ground state of a metal (the filled Fermi sea) becomes unstable in the presence of an arbitrarily small attractive interaction between electrons.
Before deriving the theorem formally, it is crucial to understand the origin of this attractive interaction. In a simple picture, as an electron moves through the crystal lattice, it attracts the surrounding positive ions, creating a local lattice deformation (a region of increased positive charge density). Due to the much larger mass of the ions compared to the electron mass ($M_{ion} \gg m_e$), the lattice response is slow ($v_{ion} \ll v_e$). The ion lattice deformation persists for a short time after the electron has passed. A second electron can then be attracted to this region of enhanced positive charge before the lattice relaxes back to equilibrium. This process effectively results in a net *attractive* interaction between the two electrons, mediated by the exchange of virtual phonons, which may overcome the direct Coulomb repulsion, which is strongly screened in a metal.
The Cooper theorem, which reveals the instability of the Fermi Sea to attractive interaction [1]. Cooper considered a simplified model with a non-interacting Fermi sea at $T = 0K$, filled up to the Fermi energy E_F. Let us now add two extra electrons to the Fermi sea. By Pauli exclusion principle, they must have energies $E > E_F$. We assume that these two electrons interact via a weak attractive potential $V(\mathbf{r}_1, \mathbf{r}_2)$. All other electrons in the Fermi sea are treated as a non-interacting background whose role is to exclude states with $E \leq E_F$.
We look for a two-electron bound state with total energy $E < 2E_F$. If such a state exists, it is energetically favorable for electrons to pair up, destabilizing the normal Fermi sea.

Let us start by writing the Schrödinger equation for the two-electron wavefunction $\psi(\mathbf{r}_1, \mathbf{r}_2)$, namely

$$\left(-\frac{\hbar^2}{2m}(\nabla_1^2 + \nabla_2^2) + V(\mathbf{r}_1, \mathbf{r}_2)\right)\psi(\mathbf{r}_1, \mathbf{r}_2) = E\,\psi(\mathbf{r}_1, \mathbf{r}_2) \tag{1.9}$$

We look for solutions in the form

$$\psi(\mathbf{r}_1, \mathbf{r}_2) = \frac{1}{\sqrt{\Omega}} e^{i\mathbf{K}\cdot\mathbf{R}}\phi(\mathbf{r})\chi(\sigma_1, \sigma_2) \tag{1.10}$$

where R is the center of mass coordinates, $\mathbf{r} = \mathbf{r}_1 - \mathbf{r}_2$ represents the relative distance of the two electrons, $\phi(\mathbf{r})$ represents the wavefunction in the center of mass, and $\chi(\sigma_1, \sigma_2)$ denotes the spin wavefunction. Expanding $\phi(\mathbf{r})$ in plane waves, we enforce the constraint that states $k < k_F$ are occupied:

$$\phi(\mathbf{r}) = \frac{1}{\Omega}\sum_{\mathbf{k},|\mathbf{k}|>k_F} g_{\mathbf{k}} e^{i\mathbf{k}\cdot\mathbf{r}} \tag{1.11}$$

where Ω represent the volume. Assuming the electrons to have opposite spin we obtain the following spin wavefunction (spin singlet)

$$\chi(\uparrow,\downarrow) = \frac{1}{\sqrt{2}}\Big[\,|\uparrow\rangle\,|\downarrow\rangle - |\downarrow\rangle\,|\uparrow\rangle\,\Big]. \tag{1.12}$$

which characterizes the so-called convential (low T_c) superconductivity. We remark that, since the total wavefunction must be antisymmetric, then $\phi(\mathbf{r})$ must be symmetric, implying that $\phi(\mathbf{r}) = \phi(-\mathbf{r})$ and thus $g_{\mathbf{k}} = g_{-\mathbf{k}}$. Finally, to minimize the kinetic energy of the pairs and to maximize the number of available final states of the scattering process between the two electrons, we consider solutions with the center of mass at rest (i.e. total momentum $\mathbf{K} = 0$) obtaining

$$\psi(\mathbf{r}) = \frac{1}{\Omega} \sum_{|\mathbf{k}|>k_F} g_{\mathbf{k}} e^{i\mathbf{k}\cdot\mathbf{r}} \chi(\uparrow,\downarrow) \tag{1.13}$$

Then, inserting Eq.(1.13) in Eq.(1.9) we obtain

$$\sum_{\mathbf{k}} \left[-\frac{\hbar^2}{2m}(\nabla_1^2 + \nabla_2^2) + V(\mathbf{r}_1 - \mathbf{r}_2) \right] g_{\mathbf{k}} e^{i\mathbf{k}\cdot(\mathbf{r}_1-\mathbf{r}_2)} = E \sum_{\mathbf{k}} g_{\mathbf{k}} e^{i\mathbf{k}\cdot(\mathbf{r}_1-\mathbf{r}_2)} \tag{1.14}$$

Assuming translation invariance for the potential $V(\mathbf{r}_1 - \mathbf{r}_2)$, multiplying both side by $e^{-i\mathbf{k}'\mathbf{r}}$ and integrating over $\mathbf{r}$, one obtains

$$\Omega(2\epsilon_{\mathbf{k}} - E) g_{\mathbf{k}} + \sum_{\mathbf{k}'} V_{\mathbf{k}\mathbf{k}'} g_{\mathbf{k}'} = 0 \tag{1.15}$$

where $2\epsilon_{\mathbf{k}} = \frac{\hbar^2 k^2}{m}$ is the kinetic energy of the pair and $V_{\mathbf{k}\mathbf{k}'}$ represents the Fourier transform of the potential.
We now assume that the two electrons interact via a weak attractive potential $-V$ only when their energies are within a small range $\hbar\omega_D$ above E_F (where ω_D is the Debye frequency, characteristic of lattice vibrations), namely

$$V_{\mathbf{k}\mathbf{k}'} = \begin{cases} -V & \text{if } E_F < \epsilon_{\mathbf{k}}, \epsilon_{\mathbf{k}'} < E_F + \hbar\omega_D \\ \\ 0 & \text{otherwise} \end{cases} \tag{1.16}$$

The equation simplifies to:

$$\Omega(2\epsilon_{\mathbf{k}} - E) g_{\mathbf{k}} = V \sum_{\mathbf{k}'}^{*} g_{\mathbf{k}'} \tag{1.17}$$

where the symbol "*" indicates that the summation is performed over the spherical energy shell $E_F < \epsilon_{\mathbf{k}'} < E_F + \hbar\omega_D$. Summing over $\mathbf{k}$ in the spherical energy shell yields the self-consistency condition:

$$\frac{1}{\Omega} \sum_{\mathbf{k}} \frac{V}{2\epsilon_{\mathbf{k}} - E} = 1 \tag{1.18}$$

Converting the sum to an integral over energy using the density of states $N(\xi)$ (where $\xi = \epsilon_{\mathbf{k}} - E_F$)

$$1 = V \int_0^{\hbar\omega_D} N(\xi) \frac{d\xi}{2\xi - (E - 2E_F)} \approx VN(0) \int_0^{\hbar\omega_D} \frac{d\xi}{2\xi + \Delta} \tag{1.19}$$

Here we defined the binding energy $\Delta = 2E_F - E$ (whence $E = 2E_F - \Delta$, and we are looking for $\Delta > 0$) and approximated the density of states as constant $N(0)$ over the range of integration

$$1 = \frac{VN(0)}{2} \ln\left(\frac{2\hbar\omega_D + \Delta}{\Delta}\right) \tag{1.20}$$

Solving for the binding energy Δ in the weak coupling limit $VN(0) \ll 1$,(implying $\Delta \ll \hbar\omega_D$) it follows that

$$\Delta \approx 2\hbar\omega_D e^{-\frac{2}{N(0)V}} \tag{1.21}$$

Since $\Delta > 0$ for any $V > 0$, a bound state always exists for any attractive interaction, no matter how weak. Furthermore, the binding energy depends on V as $\propto e^{-1/V}$. This function cannot be expanded in a Taylor series at $V = 0$, meaning that this result cannot be obtained by standard perturbation theory.
Thus, the existence of a state with energy $E < 2E_F$ implies that adding electrons to form pairs, lowers the system total energy. This suggests that the normal Fermi sea is unstable against the formation of such pairs, leading to a new ground state: the superconducting ground state.

The BCS wavefunction

As demonstrated by Cooper's calculation, the Fermi sea becomes unstable against the formation of electron pairs (Cooper pairs) when the net interaction between them is attractive. This occurs when the mutual Coulomb repulsion is overcome by a stronger attractive interaction mediated by phonons.
Furthermore, the implications of this theorem are strongly supported by experimental observations of the Isotope Effect. For many conventional superconductors, this effect shows that the critical temperature T_c depends on the isotopic mass M of the constituent ions:

$$T_c \propto M^{-\alpha} \tag{1.22}$$

where the exponent $\alpha \approx 0.5$. This mass dependence provided crucial evidence that the attractive pairing mechanism was not purely electronic, but must be mediated by lattice vibrations (phonons). This conclusion is strongly supported by the fact that characteristic phonon frequencies (such as the Debye frequency, ω_D) scale precisely the same manner, $\omega_D \propto M^{-1/2}$.
Cooper's theorem further implies the opening of an energy gap (Δ) in the excitation spectrum relative to the Cooper pair ground state. This theoretical result is supported by experimental observations of an exponential decay in specific heat as temperatures approach absolute zero. Consequently, the only electrons available for thermal transport are those that, thanks to thermal excitations, can cross this gap via tunneling.
Given these experimental observations and the implications of Cooper's theorem, the thermodynamic superconducting phase is expected to arise when these Cooper pairs condense to form a new stable ground state with lower energy compared to the normal ground state.
The N-electron ground state can be constructed starting from the individual Cooper pair

wavefunctions as:

$$\Psi_N = \hat{\mathcal{A}} \prod_{j=1}^{N/2} \psi(\mathbf{r}_{2j-1} - \mathbf{r}_{2j}) \tag{1.23}$$

Here, $\psi(\mathbf{r}_{2j-1} - \mathbf{r}_{2j})$ is the pair wavefunction (analogous to Eq. (1.13)), where we have considered the center of mass at rest, meaning the wavefunction depends only on the relative distance between the electrons in the pair. The antisymmetrization operator $\hat{\mathcal{A}}$ ensures that the total wavefunction satisfy the Pauli exclusion principle.
In real space, handling this antisymmetrization for an N-electron wavefunction typically involves an $N \times N$ Slater determinant. This determinant finds a much more compact expression using the second quantization formalism, utilizing creation ($c^\dagger_{\mathbf{k}\sigma}$) and annihilation ($c_{\mathbf{k}\sigma}$) operators. In this formalism, the wavefunction in Eq. (1.23) becomes

$$\Psi_N = \sum_{\mathbf{k}_1} \sum_{\mathbf{k}_2} ... \sum_{\mathbf{k}_{N/2}} g_{\mathbf{k}_1} g_{\mathbf{k}_2} \, ... g_{\mathbf{k}_{N/2}} c^\dagger_{\mathbf{k}_1\uparrow} c^\dagger_{-\mathbf{k}_1\downarrow} ... c^\dagger_{\mathbf{k}_{N/2}\uparrow} c^\dagger_{-\mathbf{k}_{N/2}\downarrow} \, |0\rangle \tag{1.24}$$

where $|0\rangle$ represents the electron vacuum state.

Bardeen, Cooper, and Schrieffer in their theory [6] proposed an alternative formulation of the superconducting state, which captures the crucial physical ingredients of the phenomenon of superconductivity, allowing much more efficient calculations. The BCS state

$$|BCS\rangle = \prod_{\mathbf{k}} (u_{\mathbf{k}} + v_{\mathbf{k}} c^\dagger_{\mathbf{k}\uparrow} c^\dagger_{-\mathbf{k}\downarrow}) \, |0\rangle \tag{1.25}$$

consists of products of superpositions of empty and paired state ($\mathbf{k}\uparrow, -\mathbf{k}\downarrow$), with $|v_{\mathbf{k}}|^2$ denoting the probability that the pair state is occupied, while $|u_{\mathbf{k}}|^2$ the probability that it is empty. The normalization condition for the $|BCS\rangle$ state requires that the coefficients $u_{\mathbf{k}}$ and $v_{\mathbf{k}}$ are related by $|u_{\mathbf{k}}|^2 + |v_{\mathbf{k}}|^2 = 1$. The relative complex phase between $v_{\mathbf{k}}$ and $u_{\mathbf{k}}$ identifies the phase of the pair. The crucial feature of the $|BCS\rangle$ state is that it describes a macroscopic quantum *coherent* state, since all pairs acquire a well specified phase, rather than a randomly distributed one. In this way the system gains a finite energy with respect to remaining in a normal state. Scattering of one electron is suppressed because it would cause a pair breaking, which requires the supply of a finite energy. This is the gist of the superconductivity phenomenon. Moreover, $|BCS\rangle$ is also referred to as a pair *condensate*, for all pairs ($\mathbf{k}\uparrow, -\mathbf{k}\downarrow$) are in the same state of (vanishing) center-of-mass momentum.
Importantly, the BCS state (1.25) can be shown to be the ground state of the following BCS Hamiltonian [2, 6]:

$$\mathcal{H}_{BCS} = \sum_{\mathbf{k}\sigma} \xi_{\mathbf{k}} c^\dagger_{\mathbf{k}\sigma} c_{\mathbf{k}\sigma} + \sum_{\mathbf{k}} \left(\Delta_{\mathbf{k}} c^\dagger_{\mathbf{k}\uparrow} c^\dagger_{-\mathbf{k}\downarrow} + \Delta^*_{\mathbf{k}} c_{-\mathbf{k}\downarrow} c_{\mathbf{k}\uparrow} \right) + \text{const.} \tag{1.26}$$

which describes ($\mathbf{k}\uparrow, -\mathbf{k}\downarrow$) pairs moving in a mean pairing field

$$\Delta_{\mathbf{k}} = + \sum_{\mathbf{k}'} V_{\mathbf{k}\mathbf{k}'} \langle c_{-\mathbf{k}'\downarrow} c_{\mathbf{k}'\uparrow} \rangle \tag{1.27}$$

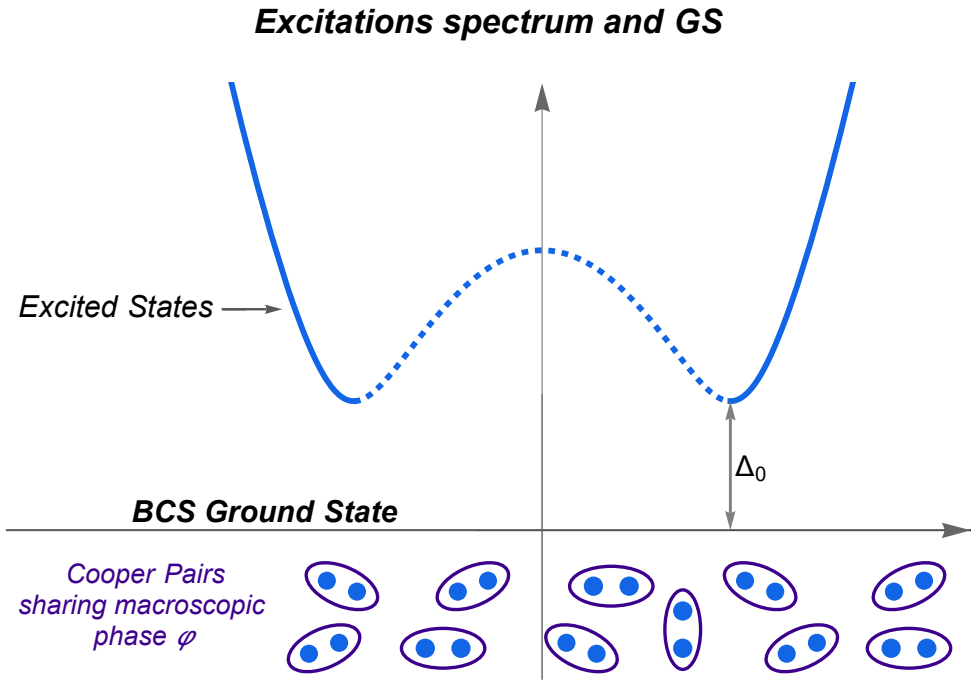

Figure 1.2: The BCS state (1.25) is a macroscopically coherent quantum states formed by pairs that all share the same phase. This state is robust to perturbation and is separated by a gap Δ_0 from the excitations.

generated by all other pairs a caused by the attractive potential $V_{\mathbf{k}\mathbf{k}'}$. The $\mathbf{k}$-dependence of the pairing potential determines the $\mathbf{k}$-dependence of the pair phases. In conventional superconductors, it turns out that the pairing field can be taken as $\mathbf{k}$-independent (s-wave superconductors)

$$\Delta_{\mathbf{k}} = \Delta_0 \, e^{i\varphi} \quad . \tag{1.28}$$

Its phase φ is also the phase shared coherently by all Cooper pairs. It therefore characterizes the superconducting state macroscopically and is essential for phenomena like the Josephson effect. The modulus Δ_0 has the meaning of the *superconducting gap*, i.e. the minimal energy one has to supply in order to excite a quasi-particle above the BCS condensate, see Fig.1.2.
The main difference between the BCS form in Eq.(1.25) and the expression in Eq.(1.24) lies in the total number of particles N. Although, the ground state in Eq.(1.24) has a fixed number of particles, this is no longer true for the BCS ground state. These two different representations of the GS can be related by rewriting Eq.(1.25) as a coherent superposition of states with different particle numbers $N = 0, 2, 4, \ldots, \infty$,namely

$$|BCS\rangle = \sum_N \lambda_N \, |\Psi_N\rangle \tag{1.29}$$

with the normalization condition $|\lambda_N| = 1$.
The reason beyond the BCS proposal for $|BCS\rangle$ is that such theory represents effectively

a *mean-field* theory where the exact particle number N is not conserved ($[\mathcal{H}, \hat{N}] \neq 0$) [2, 6]. In contrast, what is fixed is the average particle number $\bar{N}$, defined as

$$\bar{N} = \langle BCS| \hat{N} |BCS\rangle \tag{1.30}$$

where $\hat{N}$ is the number operator defined as

$$\hat{N} = \sum_{\mathbf{k}\sigma} c^{\dagger}_{\mathbf{k}\sigma} c_{\mathbf{k}\sigma} = \sum_{\mathbf{k}} (c^{\dagger}_{\mathbf{k}\uparrow} c_{\mathbf{k}\uparrow} + c^{\dagger}_{-\mathbf{k}\downarrow} c_{-\mathbf{k}\downarrow}) \tag{1.31}$$

This approach is justified because, in a typical metal, the average number of electrons is enormous ($\bar{N} \approx 10^{23}$). From statistical considerations, the root-mean-square fluctuations δN are

$$\delta N = \sqrt{\langle \hat{N}^2 \rangle - \langle \hat{N} \rangle^2} \approx \sqrt{\bar{N}} \tag{1.32}$$

These fluctuations are around 10^{11} particle, which might seem large absolutely, however the relative fluctuations $\delta N/\bar{N}$ are extremely small ($\approx 10^{-12}$), meaning the distribution is extremely sharply peaked around the average value. This fully justifies using a grand canonical ensemble approach (mean-field) to describe the superconducting state.

1.1.4 The Andreev reflection phenomenon

In 1964 the physicist Alexander F. Andreev discovered that, at the interface between a normal (N), i.e. non superconducting, material, and a superconductor (S), a unique particle-hole conversion effect occurs [11]. This phenomenon, which occurs under general conditions at any N/S interface, is called Andreev Reflection (AR) and underlies the physical behavior of most nanodevices based on superconductors.
In order illustrate this effect, let us consider an electron impinging from the N region onto the interface with the superconductor S, as depicted in Fig.1.3. For the electron the possible outcomes are being either back-reflected into the N region or transmitted into the S region. The probabilities for these events, which depend on the incident electron energy (E) and the system parameters, must satisfy the conservation law $R + T = 1$.
If the incident electron has an energy below the superconducting gap value ($E < \Delta_0$), it cannot penetrate the S region as a single-particle excitation, as no propagating quasi-particle states are available within the gap energy range. Indeed, the probability amplitude for a quasi-particle decays exponentially inside S.
The crucial observation is that, because the superconducting ground state is formed by Cooper pairs, an incoming electron with $E < \Delta_0$ is transmitted by forming a Cooper pair, with an electron in the S region with (almost) opposite momentum and spin. This partner electron is drawn from the Fermi sea on the N side, leaving behind a hole (with opposite charge, momentum, and spin) that is back-reflected into the N region. The same process, with the appropriate differences, holds for a hole incident onto the interface.
Andreev Reflection thus enables the flow of supercurrent across the interface by converting the charge current in the normal region into a pair current in the superconducting region.

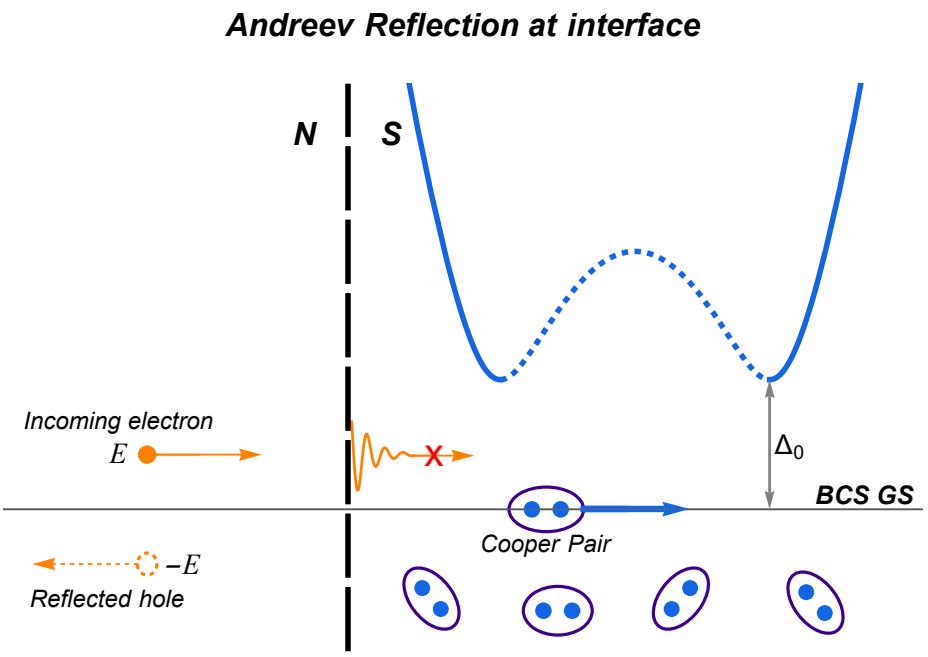

Figure 1.3: The Andreev Reflection effect occurs at the interface between a Normal (non superconducting) material and a Superconductor. An electron impinging from the N side with an energy $E < \Delta_0$ cannot penetrate inside the superconductor, due to the absence of propagating states inside the superconducting gap. Instead, it is back-reflected as a hole, while a Cooper pair travels into the superconductor.

One of the seminal theoretical frameworks for the quantitative study of reflection and transmission at a non-ideal N/S interface is the model developed by Blonder, Tinkham, and Klapwijk [12] (BTK) in 1982. The BTK model uses a scattering approach to calculate the probabilities for Andreev Reflection and Normal Reflection at the interface, including also a potential barrier strength (Z) to account for non-ideal interface transparency, which is characterized by a strength parameter Z. The differential Conductance $G(V) = dI/dV$ of the N/S junction as a function of the bias voltage (V), i.e.

$$G(V) = \frac{dI}{dV} = G_N \int_{-\infty}^{\infty} dE[1 + R_a(E) - R_n(E)] \left(-\frac{\partial f}{\partial E}(E - eV)\right) \tag{1.33}$$

where

- G_N is the conductance in the normal state, experimentally obtained when the bias energy is much larger than the superconducting gap, i.e., $eV \gg \Delta$;
- $R_a(E)$ is the probability for Andreev Reflection, which is a function of the energy E and the barrier strength Z;
- $R_n(E)$ is the probability for Normal Reflection;
- $f(E - eV)$ is the Fermi-Dirac distribution function at finite temperature T.

The BTK formula shows that in the high-transparency limit ($Z \to 0$), when $E < \Delta_0$, the Normal Reflection probability B tends to zero, while the Andreev Reflection probability A tends to unity. This leads to the characteristic doubling of the conductance at zero bias, where $G(V = 0) = 2G_N$, a hallmark signature used extensively in experiments.
The phenomenon of Andreev Reflection serves as the fundamental microscopic mechanism underlying a wide range of transport phenomena in superconducting hybrid structures. Most notably, it governs the Josephson effect in weak links [13, 14] and the superconducting proximity effect[15] at normal-superconductor interfaces. These phenomena are the cornerstones of modern quantum technologies, enabling devices such as Superconductor-Normal-Superconductor (SNS) junctions and proximized semiconductor nanowires. In particular, a crucial application of the proximity effect-specifically its role in the search for Majorana zero modes—will be discussed in detail in the following sections.

1.2 Spin-orbit coupling (SOC)

1.2.1 Origin and derivation of the SOC in atomic structures

Spin-orbit coupling is a purely relativistic effect intrinsically that is present in the atomic structure. It is typically first encountered in the study of hydrogen-like atoms, where this interaction, along with other relativistic corrections, is responsible for the so-called fine structure, i.e. the splitting of the single atomic energy levels in more levels. These deviations are typically characterized by the fine-structure constant, $\alpha \approx 1/137 \approx 10^{-2}$. This term was introduced by Arnold Sommerfeld to explain experimental observations of spectral lines splitting.
Given its relativistic origin, the spin-orbit interaction can be derived directly from the Dirac equation . Indeed, unlike the Schrödinger equation, the former intrinsically accounts for both the electron spin and special relativity laws. Then, considering the non relativistic-limit ($v/c \ll 1$) of the Dirac equation, by performing a low-velocity expansion (e.g., using the Foldy-Wouthuysen transformation), one naturally obtains a Hamiltonian term describing the SOC [16, 17].
However, a physically intuitive derivation can be equally obtained by considering the implications of special relativity for an electron orbiting around a nucleus [18, 19]. Thus, let us consider a classical picture, in which an electron moves with velocity $\mathbf{v}$ around the positively charged nucleus. In the rest frame of the electron, the nucleus orbits around it, generating an effective current loop. This moving charge creates a magnetic field $\mathbf{B}_{eff}$ perceived by the electron. According to the Biot-Savart law, this field is:

$$\mathbf{B}_{eff} = \frac{\mu_0 Ze}{4\pi r^3}(\mathbf{r} \times \mathbf{v}) \tag{1.34}$$

where μ_0 is the vacuum permeability and $\mathbf{r}$ represents the nucleus position in the electron reference frame. Exploiting the definition of orbital angular momentum $\mathbf{L} = \mathbf{r} \times \mathbf{p} = m(\mathbf{r} \times \mathbf{v})$, then $\mathbf{B}eff$ reads

$$\mathbf{B}_{eff} = \frac{\mu_0 Ze}{4\pi m r^3}\mathbf{L} \tag{1.35}$$

Note that the effective magnetic field points in same direction as the orbital angular moment, $\mathbf{B}_{eff} \parallel \mathbf{L}$. To express this in terms of the *central* electrostatic potential energy

$V(r) = -\frac{Ze^2}{4\pi\epsilon_0 r}$, we note that $\frac{1}{r}\frac{dV}{dr} = \frac{Ze^2}{4\pi\epsilon_0 r^3}$, and recalling that $\epsilon_0\mu_0 = 1/c^2$, we can rewrite the magnetic field as

$$\mathbf{B}_{eff} = \frac{1}{mec^2}\frac{1}{r}\frac{dV}{dr}\mathbf{L} \tag{1.36}$$

Considering now that the electron exhibits an intrinsic magnetic dipole moment associated with its spin $\mathbf{S}$, the effective magnetic field $\mathbf{B}_{eff}$ gives rise to a torque applied to the electron, trying to align the spin along its direction. The interaction energy between this magnetic moment and the effective magnetic field is given by the standard Zeeman energy interaction term and reads

$$U_{SO} = -\boldsymbol{\mu}_S \cdot \mathbf{B}_{eff} \tag{1.37}$$

The magnetic moment $\boldsymbol{\mu}_S$ for the electron is defined as

$$\boldsymbol{\mu}_S = -g_s\frac{e}{2m}\mathbf{S} \approx -\frac{e}{m}\mathbf{S} \tag{1.38}$$

where g_s represents the electron spin g-factor and is $g_s \approx 2$. The interaction energy becomes

$$U_{SOC} = \frac{1}{m^2c^2}\frac{1}{r}\frac{dV}{dr}\mathbf{S}\cdot\mathbf{L} \tag{1.39}$$

In fact, the above naive derivation requires a correction factor of $1/2$, known as Thomas precession, because the electron rest frame is not inertial, as it rotates around the nucleus. The correct SOC energy term is thus:

$$U_{SOC} = \frac{1}{2m^2c^2}\frac{1}{r}\frac{dV}{dr}\mathbf{S}\cdot\mathbf{L} \tag{1.40}$$

This formula clearly shows that the interaction depends on the scalar product $\mathbf{S}\cdot\mathbf{L}$, hence the name "spin-orbit coupling." We remark here that this represents a naive derivation in a semiclassical picture, in which the electron performs a loop around its nucleous. As will be clear in the following section, the SOC coupling is actually a quite general phenomenon experienced by an electron whenever an electric field is present.

1.2.2 Derivation of the SOC in crystalline structures

After illustrating the origin and the name of the spin-orbit coupling in atoms, it is natural to ask whether it can be generalized to situations where electrons move freely within a background electromagnetic field without performing any loop, such as in a crystalline solid. The fundamental ingredients remain the same, i.e. the intrinsic electron magnetic moment due to the spin $\mathbf{S}$ and the motion through an electric field $\mathbf{E}$. In a crystalline structure, an electron moves through a static periodic potential generated by the lattice ions. In the rest frame of the crystal, there is a purely electrostatic field $\mathbf{E}$ and no magnetic field ($\mathbf{B} = 0$). The electric field is related to the gradient of the potential energy V through:

$$\mathbf{E} = \frac{1}{e}\nabla V(\mathbf{r}) \tag{1.41}$$

Consider now the rest frame of the electron, which is moving with velocity $\mathbf{v}$ relative to the crystal. According to special relativity, the electromagnetic fields transform between

inertial frames. The magnetic field $\mathbf{B}'$ observed in the electron's rest frame is given by the Lorentz transformation:

$$\mathbf{B}' = \gamma \left(\mathbf{B} - \frac{\mathbf{v} \times \mathbf{E}}{c^2} \right) \tag{1.42}$$

where $\gamma = (1 - v^2/c^2)^{-1/2}$ is the Lorentz factor. In the non-relativistic limit ($v \ll c$), $\gamma \approx 1$. Since $\mathbf{B} = 0$ in the lattice frame, the effective magnetic field experienced by the electron is:

$$\mathbf{B}' \approx -\frac{1}{c^2}(\mathbf{v} \times \mathbf{E}) \tag{1.43}$$

Substituting the expression for the electric field in the crystal

$$\mathbf{B}' = -\frac{1}{c^2 e}\Big(\mathbf{v} \times \boldsymbol{\nabla} V(\mathbf{r})\Big) \tag{1.44}$$

The interaction energy between the electron intrinsic magnetic dipole moment $\boldsymbol{\mu}_S \approx -\frac{e}{m}\mathbf{S}$ and this field is

$$U' = -\boldsymbol{\mu}_S \cdot \mathbf{B}' \approx \left(\frac{e}{m}\mathbf{S}\right) \cdot \left[-\frac{1}{c^2 e}\Big(\mathbf{v} \times \boldsymbol{\nabla} V(\mathbf{r})\Big)\right] = -\frac{1}{mc^2}\mathbf{S} \cdot \Big(\mathbf{v} \times \boldsymbol{\nabla} V(\mathbf{r})\Big) \tag{1.45}$$

Using the canonical momentum $\mathbf{p} = m\mathbf{v}$, and exchanging the terms of the cross product, we obtain

$$U' = +\frac{1}{m^2 c^2}\mathbf{S} \cdot \Big(\boldsymbol{\nabla} V(\mathbf{r}) \times \mathbf{p}\Big) \tag{1.46}$$

Just like in the atomic case, the above result must be corrected by the Thomas precession factor of 1/2 due to the non-inertial nature of the electron frame during acceleration. Thus, the final, correct Hamiltonian term in the first quantization formalism, describing Spin-Orbit Coupling interaction, due to a general potential $V(\mathbf{r})$ reads

$$H_{SOC} = +\frac{1}{2m^2 c^2}\mathbf{S} \cdot \Big(\boldsymbol{\nabla} V(\mathbf{r}) \times \mathbf{p}\Big) \tag{1.47}$$

Note that, for a central potential $V(\mathbf{r}) = V(r)$, one has $\nabla V(\mathbf{r}) = r^{-1}\frac{dV}{dr}\mathbf{r}$, and one recovers the atomic result (1.40). Finally, recalling that the spin operators is expressed as $\mathbf{S} = \frac{\hbar}{2}\boldsymbol{\sigma}$ in terms of the the Pauli matrices, one can also rewrite

$$H_{SOC} = +\frac{\hbar}{4m^2 c^2}\boldsymbol{\sigma} \cdot \Big(\boldsymbol{\nabla} V(\mathbf{r}) \times \mathbf{p}\Big) \tag{1.48}$$

The specific symmetries of this potential determine the nature of the spin splitting, which in a crystal has the periodicity of the lattice. Specifically, there are two main types of spin-orbit coupling in this context, known as the Rashba and Dresselhaus interactions.

1.2.3 Symmetries and SOC: The Rashba and Dresselhaus effect

When studying the band structure of a crystal, spatial and temporal symmetries play a fundamental role. In the absence of an external magnetic field, a crystal structure fulfills Time-Reversal Symmetry (TRS). The time-reversal operation maps an electron

state with momentum $\mathbf{k}$ and spin $\boldsymbol{\sigma}$ onto a state with momentum $-\mathbf{k}$ and flipped spin $(-\boldsymbol{\sigma})$. The most important consequence is a mandatory energy degeneracy, known as Kramers degeneracy

$$E_{\mathbf{k},\uparrow} = E_{-\mathbf{k},\downarrow} \quad \text{and} \quad E_{\mathbf{k},\downarrow} = E_{-\mathbf{k},\uparrow} \tag{1.49}$$

If the system also exhibits Spatial Inversion Symmetry (IS)—meaning a center of inversion exists such that the operation $\mathbf{r} \to -\mathbf{r}$ leaves the system unchanged—states with opposite momenta but the same spin are degenerate:

$$E_{\mathbf{k},\uparrow} = E_{-\mathbf{k},\uparrow} \quad \text{and} \quad E_{\mathbf{k},\downarrow} = E_{-\mathbf{k},\downarrow} \tag{1.50}$$

Consequently, a system respecting both symmetries (TRS + IS) will be characterized by the following degeneracy at every point $\mathbf{k}$ in the Brillouin zone:

$$E_{\mathbf{k},\uparrow} = E_{\mathbf{k},\downarrow} \tag{1.51}$$

In such a system, every band is at least doubly spin-degenerate, and the bands are symmetric around the center of the Brillouin zone ($\mathbf{k} = 0$) [20].

Breaking at least one of these two symmetries can lift this degeneracy, causing a spin splitting of the bands. It is known that TRS is broken by applying an external magnetic field (Zeeman effect), which establishes a preferred orientation for the spins.
Recalling the general form of the SOC Hamiltonian, $H_{SO} \propto (\nabla V \times \mathbf{p}) \cdot \mathbf{S}$, one can straightforwardly realize that it fulfills TRS. Moreover, in a system with inversion symmetry, the local contributions to SOC due to an atom at position $\mathbf{r}$ are perfectly cancelled by an opposite contribution from the symmetric atom at $-\mathbf{r}$. However, when inversion symmetry of $V(\mathbf{r})$ is broken, this cancellation fails and a net spin-splitting emerges.
Then, the electron experiences an asymmetric potential ($V(\mathbf{r}) \neq V(-\mathbf{r})$), which leads to a net, non-zero expectation value for the $\mathbf{p} \times \nabla V$ term. This generates the effective, $\mathbf{k}$-dependent magnetic field that ultimately removes the spin degeneracy, even in zero magnetic field (IS broken, TRS preserved).
The lack of spatial inversion symmetry can be primarily ascribed to two factors, either intrinsic to the material (Bulk Inversion Asymmetry, BIA) or caused by external intervention (Structural Inversion Asymmetry, SIA).

Rashba effect

The structural inversion asymmetry represents the source of the Rashba SOC effect [21]. SIA is not an intrinsic property of the bulk crystal, but is imposed on the system by the application of an external field, or due to the setup geometry. It typically occurs in low-dimensional systems, such as quantum wells, heterostructures, or surfaces, where a confining potential -e.g. along the z direction- $V(z)$ creates a strong electric field $\mathbf{E} = E_z \hat{\mathbf{z}}$, which restricts the electron motion to the perpendicular 2D plane (the xy-plane).
To derive the corresponding Hamiltonian contribution, we start from the general SOC term H_{SO} displayed in Eq.(1.48). Expanding the electric potential energy $V(\mathbf{r})$ up to the first order as

$$V(\mathbf{r}) = V_0 + e\,\mathbf{E}(\mathbf{r}) \cdot \mathbf{r} \tag{1.52}$$

then the electric field $\mathbf{E}(\mathbf{r})$ governs the inversion asymmetry breaking [20].
Assuming that the electron is well described by plane waves, then the velocity and the momentum are related by $\mathbf{p} = \hbar\mathbf{k}$. Thus, the Rashba SOC interaction term H_{SO} an external electric field applied along the z-direction, i.e. $\mathbf{E} = \mathbf{E}(z)$ and $\boldsymbol{\nabla} V = (\partial V/\partial z)\hat{\mathbf{z}}$, is proportional to:

$$H_{RSOC} \propto (\hat{\mathbf{z}} \times \mathbf{k}) \cdot \boldsymbol{\sigma} = (k_x\sigma_y - k_y\sigma_x) \tag{1.53}$$

By grouping all the constants (related to $\boldsymbol{\nabla} V$, m, c, etc.) in Eq.(1.48) into a single parameter α_R, known as the Rashba SOC parameter, we obtain the effective 2D Rashba Hamiltonian:

$$H_{RSOC} = \alpha_R(\mathbf{k} \times \boldsymbol{\sigma}) \cdot \hat{\mathbf{z}} = \alpha_R(k_x\sigma_y - k_y\sigma_x) \tag{1.54}$$

The strength parameter α_R is proportional to the electric field E_z and can therefore be tuned externally, for example, by a gate voltage. This tunability is the operating principle of the proposed Datta-Das spin transistor, which we will describe in the following.
A primary example of a system characterized by the Rashba SOC is the case of 2D electron gas, realized in doped semiconductor heterostuctures such as GaAs/AlGaAs or InGaAs/InAlAs, InAs/GaSb. Other examples are InAs, InSb nanowires, oxide interfaces ($LaAlO_3/SrTiO_3$), heavy-element surfaces and surface alloys (Au(111), Bi/Ag) and polar Rashba crystals (BiTeI, GeTe) [22].

Dresselhaus effect

The Dresselhaus effect is a type of spin-orbit coupling caused by a symmetry breaking that is intrinsic to the material itself, known as Bulk Inversion Asymmetry (BIA) [20, 23]. This effect is prominent in materials with a *zinc-blende crystal* structure, which lacks a center of inversion. Common examples include III-V zinc-blende semiconductors such as GaAs, AlAs, InAs, and InSb,or II-VI zinc-blende such as ZnSe, CdTe.
For the 3D bulk crystal, the Dresselhaus Hamiltonian (or BIA term) acquires the following form

$$H_{DSO}^{(3D)} = \alpha_D \left[k_x(k_y^2 - k_z^2)\sigma_x + k_y(k_z^2 - k_x^2)\sigma_y + k_z(k_x^2 - k_y^2)\sigma_z\right] \tag{1.55}$$

where α_D is the Dresselhaus coefficient. This Hamiltonian is derived within the framework of the Kane model using $\mathbf{k} \cdot \mathbf{p}$ perturbation theory.
Differently from the Rashba SOC, which is typically linear in k, the Dresselhaus SOC (1.55) exhibits a cubic dependence on the wave vector. However, in a two-dimensional system (e.g. a two-dimensional electron gas, 2DEG) confined to the x-y-plane, the 2D Dresselhaus Hamiltonian reduces to the sum of a linear and a cubic term in k, namely

$$H_{DSO}^{(2D)} = \beta(k_y\sigma_y - k_x\sigma_x) + \alpha_D(k_x k_y^2\sigma_x - k_y k_x^2\sigma_y) \tag{1.56}$$

Here, the linear coefficient is $\beta = \alpha_D\langle k_z^2\rangle$, which is often the dominant term, and the cubic coefficient α_D is the original bulk coefficient α_D.

Rashba vs Dresselhaus effect

As previously discussed, the main difference between these two types of spin–orbit interaction lies in how spatial inversion symmetry is broken, namely BIA vs SIA.
As a result, while the Dresselhaus effect essentially represents an intrinsic BIA property of the crystal, the Rashba effect stems from SIA and depends on an interfacial or gate–induced electric field, which in turn can be externally tuned.
It is also possible to have materials where both effects are present. Indeed, this is the case in many III–V semiconductors with zinc–blende structure, which do not exhibit a center of inversion in the unit cell (BIA), and which, in heterostructures or gated devices, acquire additional structural inversion asymmetry via asymmetric quantum wells or externally applied electric fields (SIA).
In many InAs/InSb nanowire devices, the Rashba SOC typically dominates over the Dresselhaus SOC, which is often negligible. However, recent studies have shown that, depending on the growth direction and geometry, it is possible to engineer materials where the Dresselhaus contribution can become relevant and change the effective direction of the spin–orbit field along the wire[24].
The goal of achieving an external tuning of the Rashba SOC in materials is a primary has fostered various theoretical proposals and subsequent experimental realizations. The applications range from proposed spintronic devices (like the Datta–Das spin transistor), gate–programmable spin precession and spin filters, and the generation/detection of pure spin currents (via the spin Hall and inverse spin Hall effects). Quite interestingly, applications also include the design of superconducting hybrid devices and, more broadly, platforms for novel topological phases of matter.
In particular, semiconductor nanowires featuring strong Rashba SOC, such as InAs or InSb, are currently on the spotlight of this research field, for reasons that will be described in the subsequent sections [25, 26].

1.2.4 1D Nanowires: Quantum Confinement, Phenomena and Applications

Nanowires (NWs) are cylindrical semiconductor structures, typically characterized by a diameter of the order of nanometers (10–100 nm) and a length that can reach several micrometers (1–10 μm). Due to their extremely high length-to-diameter aspect ratio, they are considered quasi-one-dimensional (1D) channels. In practice, electrons are quantum-confined in the two transverse dimensions (the diameter), and their motion occurs along the longitudinal direction (the axis of the wire).
The physical feature that distinguishes NWs from bulk solid-state structures is that the electron de Broglie wavelength (λ_B) is comparable to the wire diameter. Consequently, classical transport laws no longer apply, and quantum effects become dominant, leading to quantum transport. For this reason, NWs are a remarkable example of quantum wires.
Several relevant quantum phenomena can be observed in quantum wires. The most fundamental one is the conductance quantization, where the conductance G exhibits discrete steps of conductance $G_0 = 2e^2/h$ quantum as a function of the transversal confinement potential [27]. Another key phenomenon is ballistic transport that occurs

when the electron mean free path l_m, i.e. the average distance traveled between scattering events (e.g., off impurities or phonons), is longer than the length of the nanowire (L) [28]. This means that electrons can cross the wire with minimal or no scattering, resulting in very low resistance (though non-zero, unlike superconductors). Others widely studied effects include Spin Hall effect, Aharonov–Bohm and Aharonov–Casher phase-coherent oscillations and universal conductance fluctuations [29].
One-dimensional (1D) NWs represent an evolving technological frontier with applications across different fields. The main physical reasons why they are so investigated are :

(i) the transverse confinement yields few (sometimes single) well-resolved 1D modes, enabling clean tests of quantum transport and scattering;

(ii) local gates allow precise control of carrier density, potential profiles, and the *magnitude/direction* of spin–orbit coupling (SOC), enabling engineered spin textures [30, 31];

(iii) hybrid normal/superconducting (NS, SNS, NF) devices show Andreev reflection, Josephson effects, and spin filtering useful for metrology and spintronics [32];

(iv) their large surface-to-volume ratio underpins sensitive chemical/biological sensors and efficient light–matter interaction for photonics/photodetectio [33].

1.2.5 Nanowires and SOC : an effective 1D model

In this subsection, we will briefly illustrate the main qualitative aspects regarding the importance of 1D nanowires with SOC. A quantitative discussion (i.e., the calculation of the eigensolutions of the corresponding Hamiltonian) for this type of system will be provided extensively in the following chapters in this thesis. A suitable starting point to derive an effective model for a 1D nanowire is a two-dimensional electron gas (2DEG) system [34]. By applying an additional lateral confinement to the latter in, e.g., the y direction, the motion transverse to the transport axis is quantized. The wavefucntion describing such a system reads

$$\Psi(x, y, z) \approx \phi_n(y, z)\, \psi_n(x) \quad , \tag{1.57}$$

where ϕ_n solves the transverse Schrodinger problem with energy eigenenvalues $E_n^{\perp}$. In the *locally uniform* (adiabatic) limit, i.e. when the confinement varies slowly along x, the longitudinal dynamics in each transverse mode decouples and is governed by an effective 1D dispersion

$$E_n(k_x) = E_n^{\perp} + \frac{\hbar^2 k_x^2}{2m^*} - \mu, \tag{1.58}$$

so that the 2DEG is mapped onto a set of 1D subbands indexed by n, i.e. we are neglecting the contribution from the mixing-subbands term, which naturally arises when a confinement potential is applied. If the chemical potential lies close to the bottom of the first subband and the spacing $\Delta_{\perp} \equiv E_2^{\perp} - E_1^{\perp}$ exceeds thermal and bias energies ($k_B T$, $eV \ll \Delta_{\perp}$), only one the two lowest subbands are occupied (two because of spin degree of freedom), and transport is effectively one dimensional. In this regime, the small

number of well-resolved channels enables clean tests of quantum transport, including conductance quantization and phase–coherent effects.
This reduction also justifies the effective 1D Hamiltonian used later in the thesis.
Starting from either a single-band effective-mass model or a multiband $\mathbf{k}\cdot\mathbf{p}$ description, one *projects* all single-particle operators onto the occupied transverse mode: the kinetic term yields the parabolic $\hbar^2k_x^2/2m^*$ dispersion, while spin–orbit terms become linear in k_x after averaging over $\phi_n(y,z)$. The 1D SOC term of the form $-k_x\,\boldsymbol{\alpha}\cdot\boldsymbol{\sigma}$ shall be characterized by an *effective* magnitude α and the direction $\boldsymbol{\alpha}$ is determined by the actual geometrical confinement and electrostatics.
The second quantization Hamiltonian describing such an ideal system, written in the spinor basis $\Psi_k^\dagger = (c_{k\uparrow}^\dagger, c_{k\downarrow}^\dagger)$ (where $k \equiv k_x$), is

$$\mathcal{H} = \sum_k \left(c_{k\uparrow}^\dagger, c_{k\downarrow}^\dagger\right)\left(\xi_k^0\sigma_0 - k\boldsymbol{\alpha}\cdot\boldsymbol{\sigma}\right)\begin{pmatrix} c_{k\uparrow} \\ c_{k\downarrow}\end{pmatrix} \tag{1.59}$$

To summarize, the resulting model assumes a strong transverse quantization (no inter-subband mixing), an approximate translational invariance along x (or slowly varying potentials), and a parabolic conduction band with effective mass m^*. Furthermore weak disorder are assumed such that the mean free path is not shorter than the device length in the ballistic/coherent measurements considered. Under these conditions, the 1D description captures the essential physics of transport and interfacial matching in a minimal, analytically transparent form.
In a strictly 1D wire with linear-in-k SOC, the single-particle spectrum splits into two spin bands. A suitable parametrization is

$$H_{\mathrm{SO}}^{\mathrm{1D}} = -\,k\,\boldsymbol{\alpha}\cdot\boldsymbol{\sigma} = -\,|\boldsymbol{\alpha}|\,k\,\sigma_{\hat{\mathbf{n}}}, \quad \hat{\mathbf{n}} \equiv \boldsymbol{\alpha}/|\boldsymbol{\alpha}|, \tag{1.60}$$

so that the strength $|\boldsymbol{\alpha}|$ fixes the spin-precession scale, while the unit vector $\hat{\mathbf{n}}$ sets the spin quantization axis defined by SOC.
In typical III–V NWs the dominant linear SOC is Rashba-like and scales with the transverse electric field. As a result:

- *Magnitude control.* The application of back, side, or wrap gates modify the transverse field and thus the SOC strength $|\boldsymbol{\alpha}|$, enabling continuous tuning of the spin-precession length $\ell_{\mathrm{so}} \sim \hbar^2/(m^*|\boldsymbol{\alpha}|)$. Experiments have demonstrated *large, continuous* electrical tuning in single nanowires [35].

- *Directional control.* Asymmetric gating (e.g., multiple side gates), facet-selective dielectrics, or partial metallic/superconducting coverage can rotate the effective field and hence the SOC axis $\hat{\mathbf{n}}$ in spin space, realizing electrically programmable spin textures along the wire [35, 36].

- *Materials/geometry leverage.* Crystal orientation and cross-section (core/shell, hexagonal facets) set a baseline for the SOC direction $\hat{\mathbf{n}}$; the electrostatic environment (dielectric constant, gate spacing and geometry) sets additional, purely electrical control parameters for tailoring both the magnitude and the orientation of SO vector [37].

1.2.6 SOC and Spintronics : the Datta-Das Transistor

Spintronics is a major research field in electronics aiming to exploit the spin electron degrees of freedom, in addition to its charge, to store, transport, and process information [38, 39]. This pursuit is driven by fundamental physical and technological needs. As conventional silicon-based transistors approach the physical limits of miniaturization (the end of Moore's Law), spintronic devices promise significant advantages, such as lower power consumption, higher processing speeds, and non-volatile memory (retaining information when powered off). While applications like Giant Magnetoresistance (GMR) in hard-drive read heads and MRAM have already proven to be commercially successful, the full potential of spintronics lies in active logic and computation.
A central challenge in spintronics is the efficient control of electron spin. Manipulating spin with external magnetic fields is typically slow, power-intensive, and difficult to integrate at the nanoscale. The key to practical spintronics lies in finding a way to control spin using fast, scalable electric fields. In this context, spin-orbit coupling plays a central role because it links spin to the electron momentum. Thus, by engineering the SOC effects, an applied electric field controlling the electron momentum becomes a "steering wheel" to manipulate the electron spin.

This mechanism drives key spintronic phenomena: in metals and heterostructures with strong SOC, it enables the generation of pure spin currents via the Spin Hall Effect or the conversion of spin currents into transverse charge currents through the Inverse Spin Hall Effect, forming the operating principle of gate-tunable logic devices, most notably the Datta-Das spin transistor or spin-FET. The Datta-Das spin transistor is a field-effect device that exploits gate-tunable spin precession to modulate the source-drain current in the transistor, and was first proposed in 1990 [40]. Its canonical implementation consists of a non-magnetic semiconductor channel with Rashba spin-orbit coupling, contacted by a spin-selective injector and detector. An electron spin, injected with a well-defined orientation, precesses while propagating through the channel because Rashba SOC acts as an effective, momentum-dependent magnetic field, whose magnitude is controlled electrostatically by external gates. The drain behaves as a spin analyzer. Specifically, the transmitted current is maximized when the spin at the exit channel is aligned with the detector polarization axis and minimized when it is orthogonal, yielding a gate-controlled conductance.

Let us illustrate the simplest system where a Datta-Das transistor can be implemented. We consider a toy model where the SOC vector $\boldsymbol{\alpha}$ is aligned with the spin quantization axis z, i.e., $\boldsymbol{\alpha} = (0,0,\alpha_z)$. For this choice of the SOC parameter, the Hamiltonian (1.59) describing the system is diagonal in the $\uparrow$ / $\downarrow$ basis, and its eigenvalues reads

$$E_{\uparrow/\downarrow}(k) = \frac{\hbar^2 k^2}{2m^*} \pm \alpha_z k \tag{1.61}$$

Thus, for a fixing energy value E, a generic propagating spin-polarized state can be

written as superposition of spin-↑ and spin-↓ states, namely

$$\phi(x) = \frac{1}{\sqrt{2}}\left[\begin{pmatrix} 1 \\ 0 \end{pmatrix} e^{ik_\uparrow x} + \begin{pmatrix} 0 \\ 1 \end{pmatrix} e^{ik_\downarrow x} \right] \tag{1.62}$$

where $k_\uparrow$, $k_\downarrow$ are obtained by inverting Eq.(1.61) for a fixed energy E. For a channel of lenght L, the injected ($x = 0$) and detected ($x = L$) spin states read, respectively,

$$\phi(0) = \frac{1}{\sqrt{2}}\left[\begin{pmatrix} 1 \\ 0 \end{pmatrix} + \begin{pmatrix} 0 \\ 1 \end{pmatrix} \right] \tag{1.63}$$

$$\phi(L) = \frac{1}{\sqrt{2}}\left[\begin{pmatrix} 1 \\ 0 \end{pmatrix} e^{ik_\uparrow L} + \begin{pmatrix} 0 \\ 1 \end{pmatrix} e^{ik_\downarrow L} \right] \tag{1.64}$$

At a fixed energy E, the wavevectors of the two spin bands differ in wave vector by

$$\Delta k \;=\; \frac{2m^*|\alpha_z|}{\hbar^2}, \tag{1.65}$$

then, a spin injected at $x = 0$ accumulates a precession angle of

$$\Delta\theta(L) = \Delta k\, L \tag{1.66}$$

If a ferromagnetic detector is also aligned along the x-axis, the current is minimized when the spin is anti-aligned, i.e., $\Delta\theta(L) = \pi$. As a result the current is minimized for $\Delta\theta(L) = \pi$, that is when

$$|\alpha_z| = \frac{\pi\hbar^2}{2m^*L} \tag{1.67}$$

Thus, it is possible to modulate the current by controlling the phase difference $\Delta\theta(L)$, which in turn depends on the SOC parameter $|\alpha_z|$ that can be tuned by external gates. The device works in the regime where the channel is ballistic and phase-coherent over L, and where spin relaxation time is longer than the transit time over the channel.
Furthermore, spin injection/detection can be implemented for 2DEGs as well, not only in semiconductor nanowires.
A significant practical challenge in this architecture is the impedance mismatch between the ferromagnetic metal contacts and the semiconductor channel, which can severely inhibits efficient spin injection and detection. For this reason many experimental efforts have shifted to all-electrical methods, such as the Spin Hall Effect, which can generate and detect spin currents without ferromagnetic contacts.
Regardless of its practical implementation, the Datta-Das architecture remains a guiding paradigm for gate-controlled spin manipulation.

1.3 Nanowires and superconductors

1.3.1 Nanowires as a platform for Andreev spin qubits

A quite interesting applications of NWs is the realization of Andreev spin qubits. A qubit is the building block for encoding and transmitting information at quantum level,

offering the advantage, with respect to classical qubits, to be prepared in a quantum superposition of states. Quantum entanglement is a property that can be exploited to speed up algorithms with respect to the classical physics realm.
Various realizations of qubits have been proposed. Among them, an interesting proposal was formulated by Y. Nazarov and co-workers [41, 42] and is based on the Andreeev bound states of a Josephson junction. Indeed, when a normal region is sandwiched between two superconductors, the Andreev processes occurring at the two N/S interfaces in the energy range within the superconducting gap Δ_0 lead to a finite number of electron-hole bound states, which are characterized by a discrete energy separation caused by the Andreev confinement. For a customary material without any spin-texture, these states are spin-degenerate. However, if the normal region between the two superconductors is characterized by strong spin-orbit coupling, an spin splitting occurs. Thus, such discrete spin states can realize an Andreev spin qubit (ASQ).
Differently from a customary quantum dot, the charge of the ASQ is not fixed, because Andreev bound states carry an electron current. This reduces the effects of electron-electron interaction. Moreover, because the spin state of the ASQ determines the superconducting current in the Josephson junction, it also enables one to readout the qubit state by measuring the current.
Following this idea, A. Levy-Yeyati and co-workers have investigated a model for a Josephson junction based on a semiconductor NWs with strong spin-orbit coupling contacted to two superconducting electrodes, paving the way to an application of NWs as a platform for ASQs [43]. More recently this theoretical proposal was experimentally realized by various groups [44, 45, 46, 47, 48]. Evidence of the resulting spin-split Andreev bound states in the weak link was observed, and the possibility to control, readout and manipulate the spin qubit via microwave radiation has been demonstrated. These results confirm the broad and promising range of applications of NWs in qauntum science and technology.

1.3.2 Topological superconductivity and Majorana quasi-particles

In the last two decades, many research studies in condensed matter physics have focussed on applying concepts borrowed by the field topology to the quantum ground states characterizing gapped systems, i.e models that exhibit a gap in their excitation spectrum. Indeed for such systems—most notably insulators and fully gapped superconductors—a topological classification is possible based on their symmetries. In this context, the underlying idea is to consider continuous variations of the system Hamiltonian and to inspect how they impact on the phase, i.e. on the fundamental properties characterizing its ground states. Specifically, two phases are topologically equivalent if and only if they can be connected by varying the Hamiltonian parameters, without abruptly changing its fundamental nature, i.e. without ever closing the bulk gap, and while preserving the relevant symmetries. Conversely, a transition between topologically distinct phases necessarily involves a gap closing at some critical point in parameter space, followed by a reopening on the other side [49].
The classification of these states is achieved through topological invariants. These are integer (or discrete) quantities that assume a specific value for all states within a given

topological class and a different value for states in another class.
Depending on the system dimensionality and its fundamental symmetries-specifically Time-Reversal Symmetry (TRS), Particle-Hole Symmetry (PHS), and Chiral Symmetry (SLS) -it is possible to categorize all gapped quantum systems into the so-called Ten-Fold Way (or Altland-Zirnbauer classification [50]). For each symmetry class, a specific topological invariant is defined (e.g., Chern number, $\mathbb{Z}_2$ invariant, winding number). Typically, this invariant is zero for a "trivial" phase (like the vacuum or ordinary insulators) and non-zero for a "non-trivial" topological phase[51, 52].
The most profound physical consequence of this mathematical structure is the Bulk-Boundary Correspondence. Consider the interface between two materials belonging to different topological classes (e.g., a non-trivial topological superconductor and a trivial vacuum). Since it is impossible to adiabatically deform the non-trivial state into the trivial one without closing the gap, the topology mismatch enforces gapless boundary states at the interface, allowing the topological invariant to change, while the bulk of the material remains gapped [53].
These states are known as topological edge modes or bound states. The bulk-boundary correspondence principle rigorously links the topological invariant of the bulk (a global property) to the existence and number of these robust gapless modes at the surface.[54, 55, 56, 57].
In particular, in recent years topological superconductivity has attracted a great deal of attention. This is mainly because the boundary states topological superconductors are predicted to host Majorana zero modes (or Majorana quasi-particles). These exotic quasiparticles, which will be briefly described in the following paragraph, hold immense potential for fault-tolerant topological quantum computing.

Majorana quasi-particles

A Majorana quasi-particle was proposed by Ettore Majorana in 1937 as a special solution of the Dirac equation [58]. The Dirac framework, which merges special relativity with quantum mechanics, describes relativistic spin-1/2 particles (e.g., electrons) and predicts their antiparticles (e.g., the positron, with the same mass and spin but opposite charge). By contrast, a Majorana quasi-particle is a particle *identical to its own antiparticle*. In high-energy physics this requires electric neutrality and spin 1/2; the neutrino has long been considered a candidate, although a conclusive experimental evidence remains elusive due to its extremely weak interactions. Over the past two decades, a different route to observe Majorana quasi-particles has been proposed in condensed matter physics: in superconductors, Majorana quasi-particles can emerge as zero-energy Bogoliubov excitations at boundaries or defects of *topological* superconductors[59]. These are not fundamental particles, but collective excitations protected by symmetry and topology. Indeed, the intrinsic particle–hole symmetry of the Bogoliubov–de Gennes (BdG) formalism, implies the following relation for the operators describing a spinless Bogoliubov quasiparticle at energy E, then

$$\gamma^{\dagger}(E) = \gamma(-E) \quad . \tag{1.68}$$

Therefore, a zero-energy excitation necessarily satisfies

$$\gamma^\dagger(0) = \gamma(0), \tag{1.69}$$

implying that the corresponding operator is Hermitian and defines a *Majorana zero mode* (MZM), which represents a spinless, neutral charge quasi-particle [60, 61].
We emphasize here that the emergence of these MZMs is a direct consequence of the bulk-boundary correspondence principle. A superconductor in a non-trivial topological phase must host gapless excitations at its boundaries, which, in a system of this kind, manifest as Majorana quasiparticles [55, 56, 62, 63].
Because condition (1.69) holds, the zero-mode operator γ_0 cannot be viewed as a standard creation operator. Indeed it would lead to a contraddiction.
It is often said that a Majorana zero mode represents "half" of a Dirac fermion. Indeed, two spatially separated MZMs, γ_A and γ_B, can be combined into a nonlocal Dirac fermion

$$c = \frac{\gamma_A + i\gamma_B}{2}, \qquad c^\dagger = \frac{\gamma_A - i\gamma_B}{2}, \tag{1.70}$$

with fermion parity $n = c^\dagger c \in \{0,1\}$. The Majorana operators obey the algebra

$$\gamma_i^\dagger = \gamma_i, \qquad \{\gamma_i, \gamma_j\} = 2\delta_{ij}, \qquad \gamma_i^2 = 1. \tag{1.71}$$

When the two MZMs are well separated, their overlap is exponentially small and they weakly couple to each other. As a consequence, the two configurations $n = 0$, $n = 1$ have essentially the same energy and a twofold ground-state degeneracy is obtained. In this limit for a 1D system the fermionic state built from the two Majoranas is encoded non-locally across the two ends of the device, making it insensitive to local perturbations at a single end.
This topological degeneracy is the key ingredient giving rise to exotic non-Abelian statistics, which fundamentally distinguishes MZMs from standard quantum particles. Indeed, let us consider a simply two non-exotic particles system: while for bosons the exchange operations of the two particles in position space leaves the total system wavefunction unchanged, for fermions, the exchange introduces a sign change (a phase of π) to the wavefunction. However, in both these standard cases, the exchange operation simply multiplies the wavefunction by a scalar phase factor ($e^{i\phi}$). Since the multiplication of scalars is commutative (the order in which we perform multiple exchanges does not matter), these particles obey Abelian statistics.
In contrast, exchanging (or braiding) two MZMs does not simply apply a global phase factor. Instead, because of the ground-state degeneracy, the exchange operation performs a unitary rotation within the degenerate subspace. Mathematically, the operation is described by a matrix (operator) rather than a scalar number. Notably, if one performs multiple exchanges in sequence, the final state of the system depends on the chronological order in which the swaps are performed. Since matrix multiplication is generally non-commutative ($U_1U_2 \neq U_2U_1$), the result of braiding A then B is different from braiding B then A. For this reason, Majorana modes are classified as non-Abelian anyons. For further details on the non-Abelian statistics of Majorana fermions, we refer to [64, 65, 66, 67, 68, 69, 70].

Besides the fascination of non-Abelian exchange statistics, Majorana modes are particularly attractive for quantum information and computation applications due to their intrinsic robustness against decoherence [71, 72].
First, their zero-energy nature is topologically protected by the bulk superconducting gap and particle–hole symmetry. As long as the gap remains open and symmetries are preserved, smooth local perturbations cannot remove a Majorana mode or flip the fermion parity encoded by two spatially separated modes. Indeed, modifying this state would require either closing the bulk gap or inducing a strong hybridization between the distant pair.
Moreover, Majorana excitations are, on average, electrically neutral objects, being coherent superpositions of electron and hole states. Consequently, they couple only weakly to environmental electrostatic noise. Crucially, the quantum information is encoded nonlocally in the parity shared by these spatially separated modes, which suppresses the sensitivity to strictly local disturbances. In the ideal limit, braiding operations depend solely on the topology of the exchange path rather than on precise timing or microscopic details, thus providing an intrinsically robust route to fault-tolerant quantum control. For a more in-depth discussion on the quantum computation research field we refer the reader to [73, 74, 75, 76, 77].

1.3.3 Nanowires as a platform for topological superconductivity

Over the last 20 years, several proposals for the realization of a topological superconductor supporting Majorana quasi-particles have been discussed. The works that marked a turning point in this field were those of Read and Green for 2D systems [78] and the 1D discrete model by Kitaev [79]. Both of these seminal works are based on the fact that pairing in a spinless p-wave superconductor offers an ideal platform, as it admits the closing and reopening of the superconducting gap, thereby allowing for the characterization of a non-trivial topological phase[80, 81]. Unfortunately, the realization of such a system is not trivial for two primary reasons. First, intrinsic p-wave superconductors are quite rare in nature. Although some materials, such as Sr_2RuO_4 [82], $K_2Cr_3As_3$ [83] or iron-based superconductors, have been proposed as possible candidates, there is not a full scientific consensus on the nature of the pairing yet[84]. Second, actual spinless superconductors do not exist, as electrons are spin-1/2 particles. Consequently, to create a spinless system, it is necessary to break the Kramers degeneracy caused by Time-Reversal Symmetry (TRS), for example, by applying a magnetic field.
However, starting from 2010, proposals emerged based on engineering an effective spinless p-wave superconductor by combining semiconductor nanowires with conventional s-wave superconductors. In the literature, this realization is referred to as a Majorana Nanowire and was first proposed in Refs.Lutchyn, Sau, and Das Sarma [85] et al. and Oreg, Refael, and Von Oppen [86] et al.
The fundamental ingredients for creating such a spinless p-wave superconducting platform showing a non trivial topological phase are three: the superconducting proximity effect, a strong spin-orbit coupling, and the application of an external magnetic field.

We will now briefly analyze these three ingredients :

- **Superconducting Proximity Effect**
  This effect was first observed by Holm–Meissner in 1932 [15, 87]. It occurs when a superconductor (S) is placed in electrical contact with a normal conductor (N), such as a metal or a doped semiconductor and due to this contact, the superconducting properties are induced into the normal material. The proximity effect is necessary to give rise to Majorana quasi-particles: a semiconductor nanowire (N), typically InAs or InSb, is "proximized" by coupling it closely to a conventional superconductor (S), such as Aluminum (Al). This induces the necessary s-wave pairing within the nanowire, effectively turning it into a superconductor [49, 60, 88, 89].

- **Spin-orbit coupling and magnetic field**
  In a strictly 1D channel *without* spin-orbit coupling, spin-rotation symmetry is conserved. Therefore, the two spin species form degenerate bands, and a proximity-induced s-wave pairing only couples opposite spins. With no spin mixing, the phase remains topologically trivial and there is no route to an effectively spinless superconducting state. In contrast, the Rashba SOC lifts the spin degeneracy, and the spectrum splits horizontally into two non-degenerate bands. For any value of the chemical potential μ, there exists two Kramers pairs of "helical" states, i.e. states with opposite momenta $\pm k_F$ that exhibit opposite group velocities and carry opposite spin directions. Applying a magnetic field that is *orthogonal* to the spin-orbit field causes the breaking of Time-Reversal Symmetry and the opening of a *helical gap* at $k = 0$. This means that, within such an energy range, the chemical potential only crosses *one* pair of propagating helical states, while the other pair is "frozen out". For the helical states the propagation direction is locked to the spin orientation, e.g. right-moving electrons only have spin-↑, while left-moving electrons only have spin-↓. This makes spin to behave as a redundant degree of freedom and the system becomes effectively spinless. In this regime, the addition of a further proximity s-wave pairing, when projected onto the helical basis, develops an *intraband* component with effective p-wave symmetry. Indeed electrons with the same energy and opposite momenta, are polarized in different directions, therefore they can couple via the s-wave superconducting pairing. As the Zeeman field is increased, the bulk gap *closes and reopens*, marking a transition into a 1D *topological* superconducting phase that supports *Majorana zero modes* localized at the wire ends [49, 60, 61].

The minimal Hamiltonian proposed by Lutchyn [85] and Oreg [86] to model the 1D proximized nanowire reads

$$\mathcal{H} = \int dx \Psi^\dagger \Big(-\frac{\hbar^2}{2m^*}\frac{\partial^2}{\partial x} - \mu + i\alpha\,\sigma_z\partial_x + b_x\,\sigma_x \Big)\,\Psi + \int dx \Big(\Delta\,\Psi_\uparrow^\dagger \Psi_\downarrow^\dagger + h.c.\Big) \quad . \tag{1.72}$$

where $\Psi^\dagger = (\Psi_\uparrow^\dagger,\, \Psi_\downarrow^\dagger)$ and $\Psi = (\Psi_\uparrow,\, \Psi_\downarrow)^T$ describe the creation and annihilation field operators, respectively, for an electron with effective mass m^*, μ is the chemical potential, b_x represents the applied magnetic field along the x-direction, α represents the Rashba SOC coupling which along the z-direction and Δ represents the induced superconducting

pairing by proximity.
The excitation spectrum of this Hamiltonian gives an upper band E_1 and a lower band E_2. In particular, the latter exhibits a minimum at $k = 0$ with energy

$$E_{min}(0) = \left| |b_x| - \sqrt{\Delta^2 + \mu^2} \right| \tag{1.73}$$

where Δ denotes the superconducting gap. The energy value $E_{min}(0)$ represent the energy bulk gap for the system. We observe that this gap closes precisely when the Zeeman field reaches the critical value $b_x^* = \sqrt{\Delta^2 + \mu^2}$. As widely discussed, the closing and subsequent reopening of the bulk gap signals a topological phase transition. This unique feature renders proximized nanowires with strong spin-orbit coupling and magnetic fields a prime candidate for the search of Majorana quasiparticle, as the system can be tuned into a non-trivial topological phase. Specifically, the classification of the system via a topological invariant allows for a sharp distinction between the trivial and the topological superconducting phases, according to the following criterion

$$|b_x| > \sqrt{\Delta_0^2 + \mu^2} \qquad \text{Topological Phase} \tag{1.74}$$

$$|b_x| < \sqrt{\Delta_0^2 + \mu^2} \qquad \text{Trivial Phase} \tag{1.75}$$

Crucially, it is within the topological phase that the system supports Majorana Zero Modes (MZMs) localized at the ends of the nanowire. [49, 60].

Chapter 2

Review of the BCS model

2.1 Derivation of the mean-field BCS Hamiltonian

In order to derive the BCS Hamiltonian, we start from the Fröhlich Hamiltonian displayed in Eq.(1.8). In particular the latter can be rewritten as

$$\mathcal{H} = \mathcal{H}_0 + \lambda \mathcal{H}_1 \tag{2.1}$$

where $\mathcal{H}_0$ represents the unperturbed Hamiltonian related to the phonon and electronic decoupled problem, whereas $\mathcal{H}_1$ represents the perturbation containing the electron-phonon coupling

$$\mathcal{H}_0 = \sum_{\mathbf{k}\sigma} \epsilon_{\mathbf{k}} c^\dagger_{\mathbf{k}\sigma} c_{\mathbf{k}\sigma} + \sum_{\mathbf{q}} \hbar\omega_{\mathbf{q}} a^\dagger_{\mathbf{q}} a_{\mathbf{q}} \tag{2.2}$$

$$\mathcal{H}_1 = \sum_{\mathbf{kq}\sigma} \nu_{\mathbf{q}} c^\dagger_{\mathbf{k+q}\sigma} c_{\mathbf{k}\sigma} (a_{\mathbf{q}} + a^\dagger_{-\mathbf{q}}) \tag{2.3}$$

Applying the Schrieffer-Wolff Transformation it is possible to treat the problem perturbatively and after a series of calcultations one obtain an effective Hamiltonian which describes the electron-electron interaction mediated by phonons [7]. Specifically, it describes a process where an electron with momentum $\mathbf{k}$ exchanges a phonon of momentum $\mathbf{q}$ with another electron with momentum $\mathbf{k}'$, scattering them to states $\mathbf{k}-\mathbf{q}$ and $\mathbf{k}'+\mathbf{q}$, respectively,

$$\mathcal{H}_{eff} = \sum_{\mathbf{q},\mathbf{k},\mathbf{k}',\sigma,\sigma'} |\nu_{\mathbf{q}}|^2 c^\dagger_{\mathbf{k}'+\mathbf{q},\sigma'} c^\dagger_{\mathbf{k}-\mathbf{q},\sigma} c_{\mathbf{k},\sigma'} c_{\mathbf{k},\sigma} \frac{\hbar\omega_q}{(\epsilon_{\mathbf{k}} - \epsilon_{\mathbf{k}-\mathbf{q}})^2 - (\hbar\omega_q)^2} \tag{2.4}$$

where $\epsilon_{\mathbf{k}-\mathbf{q}} - \epsilon_{\mathbf{k}}$ denotes the energy difference between the initial and final state for the electron scattered from $\mathbf{k} \to \mathbf{k}-\mathbf{q}$, whereas the term $(\hbar\omega_q)^2$ represents the energy of the exchanged phonon. The effective interaction potential V_{eff} is given by:

$$V_{eff}(\mathbf{q},\omega) = \frac{|\nu_{\mathbf{q}}|^2 \hbar\omega_{\mathbf{q}}}{(\epsilon_{\mathbf{k}} - \epsilon_{\mathbf{k}-\mathbf{q}})^2 - (\hbar\omega_{\mathbf{q}})^2} \tag{2.5}$$

Crucially, this interaction becomes attractive ($V_{eff} < 0$) when the energy transfer $|\epsilon_{\mathbf{k}} - \epsilon_{\mathbf{k}-\mathbf{q}}|$ is less than the phonon energy $\hbar\omega_{\mathbf{q}}$. Therefore, taking into consideration the result of the Cooper theorem, which highlights the instability of the Fermi sea with respect of Cooper pairs, the pairing Hamiltonian, also referred to as the *reduced Hamiltonian*, only retains the interaction terms that scatter a Cooper pair $(\mathbf{k}' \uparrow, -\mathbf{k}' \downarrow)$ into another pair state $(\mathbf{k} \uparrow, -\mathbf{k} \downarrow)$ (i.e. pairs with total momentum $\mathbf{K} = 0$), as these are the most relevant correlations for forming the superconducting condensate. It reads

$$\mathcal{H}_{pair} = \sum_{\mathbf{k}\sigma} \xi_{\mathbf{k}} c^{\dagger}_{\mathbf{k}\sigma} c_{\mathbf{k}\sigma} + \sum_{\mathbf{k},\mathbf{k}'} V_{\mathbf{k}\mathbf{k}'} c^{\dagger}_{\mathbf{k}\uparrow} c^{\dagger}_{-\mathbf{k}\downarrow} c_{-\mathbf{k}'\downarrow} c_{\mathbf{k}'\uparrow} \tag{2.6}$$

where $\xi_{\mathbf{k}} = \epsilon_{\mathbf{k}} - \mu$ is the single-particle energy relative to the chemical potential. We introduce the chemical potential μ, to account for the constraint related to the average number of particles $\bar{N}$. Indeed in the Grand canonical ensemble the chemical potential μ represents the Lagrange multiplier related to such quantity. Despite this simplification, H_{pair} is still a many-body Hamiltonian containing quartic interaction terms, making it difficult to solve exactly.
To further proceed, considering that the superconducting GS represents a condensed coherent macroscopic state containing Cooper pairs $(\mathbf{k} \uparrow, -\mathbf{k} \downarrow)$, we assume that the pair creation and annihilation operators can be written as their quantum mechanical average plus a small fluctuation:

$$c_{-\mathbf{k}\downarrow} c_{\mathbf{k}\uparrow} = \langle c_{-\mathbf{k}\downarrow} c_{\mathbf{k}\uparrow} \rangle + \delta(c_{-\mathbf{k}\downarrow} c_{\mathbf{k}\uparrow}) \tag{2.7}$$

Note that this approximation represents the standard procedure of any mean-field theory. Because of the large number of involved particles we expect such fluctuations to be small. Then, substituting the decomposition in Eq.(2.7) into the interaction term and neglecting the second-order terms in the fluctuations (i.e., $\delta(\dots)\delta(\dots) \approx 0$), we obtain

$$\begin{aligned} c^{\dagger}_{\mathbf{k}\uparrow} c^{\dagger}_{-\mathbf{k}\downarrow} c_{-\mathbf{k}'\downarrow} c_{\mathbf{k}'\uparrow} \approx \langle c^{\dagger}_{\mathbf{k}\uparrow} c^{\dagger}_{-\mathbf{k}\downarrow} \rangle c_{-\mathbf{k}'\downarrow} c_{\mathbf{k}'\uparrow} + c^{\dagger}_{\mathbf{k}\uparrow} c^{\dagger}_{-\mathbf{k}\downarrow} \langle c_{-\mathbf{k}'\downarrow} c_{\mathbf{k}'\uparrow} \rangle \\ - \langle c^{\dagger}_{\mathbf{k}\uparrow} c^{\dagger}_{-\mathbf{k}\downarrow} \rangle \langle c_{-\mathbf{k}'\downarrow} c_{\mathbf{k}'\uparrow} \rangle \end{aligned} \tag{2.8}$$

We now introduce the superconducting order parameter (or energy gap) $\Delta_{\mathbf{k}}$, defined as:

$$\Delta_{\mathbf{k}} = + \sum_{\mathbf{k}'} V_{\mathbf{k}\mathbf{k}'} \langle c_{-\mathbf{k}'\downarrow} c_{\mathbf{k}'\uparrow} \rangle \tag{2.9}$$

Using this definition, the linearized interaction term can be rewritten in a more compact form. Substituting it back into the original Hamiltonian yields the BCS Mean-Field Hamiltonian [2, 6]:

$$\mathcal{H}_{BCS} = \sum_{\mathbf{k}\sigma} \xi_{\mathbf{k}} c^{\dagger}_{\mathbf{k}\sigma} c_{\mathbf{k}\sigma} + \sum_{\mathbf{k}} \left(\Delta_{\mathbf{k}} c^{\dagger}_{\mathbf{k}\uparrow} c^{\dagger}_{-\mathbf{k}\downarrow} + \Delta^{*}_{\mathbf{k}} c_{-\mathbf{k}\downarrow} c_{\mathbf{k}\uparrow} \right) + \text{const.} \tag{2.10}$$

where the constant term is $\sum_{\mathbf{k}} \Delta_{\mathbf{k}} \langle c^{\dagger}_{\mathbf{k}\uparrow} c^{\dagger}_{-\mathbf{k}\downarrow} \rangle$. This Hamiltonian describes quasiparticles moving in a mean field generated by the condensate of all other pairs. It is now quadratic in the fermionic operators $c, c^{\dagger}$ and can be diagonalized exactly using the *Bogoliubov-de*

Gennes (BdG) method [90, 91]. This method will be extensively used in the following sections to describe excitations in a superconducting material. In particular, it represents the most suitable formalism for describing the scattering phenomenon at the interface between a normal and a superconducting material.

Remark
We remark here that the standard BCS theory provides a valid framework to describe the phenomenon of *conventional* (phonon–mediated) superconductivity, most commonly realized in low-T_c materials. This class of superconductors is generally characterized by an antisymmetric spin wavefunction (spin singlet, $S = 0$). Due to the Pauli exclusion principle, this implies an even spatial part of the total fermionic wavefunction.
In fact, these materials typically exhibit an *even-parity* order parameter, i.e. $\Delta_{\mathbf{k}} = \Delta_{-\mathbf{k}}$, which in simple metals is often nearly isotropic in $\mathbf{k}$ and, to a good approximation, independent of $\mathbf{k}$. For this reason, in analogy with atomic orbital this type of pairing is often dubbed s-wave pairing ($L = 0$) [2, 92]. It should be pointed out, however, that such terminology, borrowed by the atomic classification and based on spin and angular momentum, is evocative, in a crystalline structure it is actually not rigorous, since spin and angular momentum are not good quantum numbers. Strictly speaking, the pairing potential and the spatial wavefunction should be classified on the crystal symmetry.

Any superconducting material not adequately described by standard s-wave BCS pairing falls into the *unconventional* superconductivity category, which often includes the high critical temperature (high-T_c) families [92]. Indeed, beyond (nearly) isotropic s-wave pairing, it is possible for a material to exhibit anisotropic pairing with a non-trivial dependence on $\mathbf{k}$. For instance, a p-wave pairing ($L = 1$) is characterized by a pairing potential that is odd with respect to $\mathbf{k}$ (i.e., $\Delta_{\mathbf{k}} = -\Delta_{-\mathbf{k}}$). This implies an antisymmetric spatial part and, consequently, a symmetric spin wavefunction, known as a spin-triplet state ($S = 1$). Some studies suggested that materials like Sr_2RuO_4 [82] , $K_2Cr_3As_3$ [83] or iron-based superconductors [93] might exhibit a p-wave order parameter. While a clear evidence of an intrinsic p-wave superconductor is still under debate, we will show in subsequent sections that it is possible to engineer *effective* p-wave pairing in the laboratory by combining specific ingredients, such as applied magnetic fields and strong spin–orbit coupling [60].

In addition to p-wave, there is also d-wave pairing ($L = 2$, spin singlet), which has been experimentally observed, for instance, in high-T_c cuprate superconductors [94]. It differs from s-wave pairing in that it produces nodes in the quasiparticle excitation spectrum. Indeed d-wave pairing is characterized by an even and anisotropic pairing.
Finally, we emphasize that the study of high-T_c superconductors represents a major research field in condensed matter, since the mechanism underlying this phenomenon is highly non trivial and it also involves strong electronic correlations [95].

2.2 Diagonalization of the BCS Hamiltonian

Let us now analyze the BCS Hamiltonian derived in Eq.(2.10)

$$\mathcal{H}_{BCS} = \sum_{\mathbf{k}} \left(\xi_{\mathbf{k}} c^{\dagger}_{\mathbf{k}\uparrow} c_{\mathbf{k}\uparrow} + \xi_{\mathbf{k}} c^{\dagger}_{\mathbf{k}\downarrow} c_{\mathbf{k}\downarrow} \right) + \sum_{\mathbf{k}} \left(\Delta_{\mathbf{k}} c^{\dagger}_{\mathbf{k}\uparrow} c^{\dagger}_{-\mathbf{k}\downarrow} + \Delta^{*}_{\mathbf{k}} c_{-\mathbf{k}\downarrow} c_{\mathbf{k}\uparrow} \right) \tag{2.11}$$

where the summation over $\mathbf{k}$ spans the first BZ, (i.e $|\mathbf{k}| \leq \frac{\pi}{a}$ with 'a' denoting the lattice spacing), and $\xi_{\mathbf{k}} = \varepsilon_{\mathbf{k}} - \mu$, where $\varepsilon_{\mathbf{k}}$ is the bare band dispersion relation and μ denotes the chemical potential.
Our goal is to diagonalize $\mathcal{H}_{BCS}$. To this purpose, we first realize that all terms of Eq.(2.11) are bilinears $c^{\dagger}c$, $c^{\dagger}c^{\dagger}$ and cc in the creation/annilahilation operators. This means that $\mathcal{H}_{BCS}$ can be rewritten in a quadratic form, i.e.

$$\mathcal{H}_{BCS} = \frac{1}{2} \sum_{\mathbf{k}} \Psi^{\dagger}_{\mathbf{k}} H_{\mathbf{k}} \Psi_{\mathbf{k}} \ + C \tag{2.12}$$

where C is a constant, $H_{\mathbf{k}}$ is a matrix, and $\Psi_{\mathbf{k}}$ is a spinor of operators and must necessarily contain both the annihilation and the creation operators. This type of operator spinor is called *Nambu* spinor. There are various possible choices of Nambu spinor. Each choice of $\Psi_{\mathbf{k}}$ determines a specific form of the matrix $H_{\mathbf{k}}$, since $\mathcal{H}_{BCS}$ is given.

Here are two customary choices adopted in the literature

$$\Psi_{\mathbf{k}} = \Psi^{(1)}_{\mathbf{k}} = \begin{pmatrix} c_{\mathbf{k}\uparrow} \\ c_{\mathbf{k}\downarrow} \\ c^{\dagger}_{-\mathbf{k}\downarrow} \\ -c^{\dagger}_{-\mathbf{k}\uparrow} \end{pmatrix} \qquad \Rightarrow \qquad H_{\mathbf{k}} = \begin{pmatrix} \xi_{\mathbf{k}} & 0 & \Delta_{\mathbf{k}} & 0 \\ 0 & \xi_{\mathbf{k}} & 0 & \Delta_{-\mathbf{k}} \\ \Delta^{*}_{\mathbf{k}} & 0 & -\xi_{-\mathbf{k}} & 0 \\ 0 & \Delta^{*}_{-\mathbf{k}} & 0 & -\xi_{-\mathbf{k}} \end{pmatrix} \tag{2.13}$$

or

$$\Psi_{\mathbf{k}} = \Psi^{(2)}_{\mathbf{k}} = \begin{pmatrix} c_{\mathbf{k}\uparrow} \\ c_{-\mathbf{k}\downarrow} \\ c^{\dagger}_{-\mathbf{k}\downarrow} \\ -c^{\dagger}_{\mathbf{k}\uparrow} \end{pmatrix} \qquad \Rightarrow \qquad H_{\mathbf{k}} = \begin{pmatrix} \xi_{\mathbf{k}} & 0 & \Delta_{\mathbf{k}} & 0 \\ 0 & \xi_{-\mathbf{k}} & 0 & \Delta_{\mathbf{k}} \\ \Delta^{*}_{\mathbf{k}} & 0 & -\xi_{-\mathbf{k}} & 0 \\ 0 & \Delta^{*}_{\mathbf{k}} & 0 & -\xi_{\mathbf{k}} \end{pmatrix} \tag{2.14}$$

It can be noticed that, in any case, the component of $\Psi_{\mathbf{k}}$ are redundant, in the sense that there are two pairs of hermitian conjugate operators; this induces some symmetries in the structure of $H_{\mathbf{k}}$.

Proof of Eq.(2.14)
In order to rewrite Eq.(2.11) in the form (2.12) with the Nambu spinor and the matrix defined in Eqs.(2.14), we first relabel the summation index $\mathbf{k} \to -\mathbf{k}$ in the spin-$\downarrow$ band term, and rewrite each term as twice its half, obtaining

$$\begin{aligned} \mathcal{H}_{BCS} = & \frac{1}{2} \sum_{\mathbf{k}} \xi_{\mathbf{k}} (c^{\dagger}_{\mathbf{k}\uparrow} c_{\mathbf{k}\uparrow} + c^{\dagger}_{\mathbf{k}\uparrow} c_{\mathbf{k}\uparrow}) + \frac{1}{2} \sum_{\mathbf{k}} \xi_{-\mathbf{k}} (c^{\dagger}_{-\mathbf{k}\downarrow} c_{-\mathbf{k}\downarrow} + c^{\dagger}_{-\mathbf{k}\downarrow} c_{-\mathbf{k}\downarrow}) + \\ & + \frac{1}{2} \sum_{\mathbf{k}} (\Delta_{\mathbf{k}} c^{\dagger}_{\mathbf{k}\uparrow} c^{\dagger}_{-\mathbf{k}\downarrow} + \Delta^{*}_{\mathbf{k}} c_{-\mathbf{k}\downarrow} c_{\mathbf{k}\uparrow}) + \frac{1}{2} \sum_{\mathbf{k}} (\Delta_{\mathbf{k}} c^{\dagger}_{\mathbf{k}\uparrow} c^{\dagger}_{-\mathbf{k}\downarrow} + \Delta^{*}_{\mathbf{k}} c_{-\mathbf{k}\downarrow} c_{\mathbf{k}\uparrow}) \end{aligned} \tag{2.15}$$

Then, using anticommutation rules of the fermionic operators one has

$$c^\dagger_{k\sigma}c_{k\sigma'} = \delta_{\sigma,\sigma'} - c_{k\sigma'}c^\dagger_{k\sigma} \tag{2.16}$$

and

$$\Delta_{\mathbf{k}}c^\dagger_{\mathbf{k}\uparrow}c^\dagger_{-\mathbf{k}\downarrow} = -\Delta_{\mathbf{k}}c^\dagger_{-\mathbf{k}\downarrow}c^\dagger_{\mathbf{k}\uparrow} \tag{2.17}$$

which enables us to rewrite

$$\begin{aligned}\mathcal{H}_{BCS} =& \frac{1}{2}\sum_{\mathbf{k}}\xi_{\mathbf{k}}(c^\dagger_{\mathbf{k}\uparrow}c_{\mathbf{k}\uparrow} - c_{\mathbf{k}\uparrow}c^\dagger_{\mathbf{k}\uparrow}) + \frac{1}{2}\sum_{\mathbf{k}}\xi_{-\mathbf{k}}(c^\dagger_{-\mathbf{k}\downarrow}c_{-\mathbf{k}\downarrow} - c_{-\mathbf{k}\downarrow}c^\dagger_{-\mathbf{k}\downarrow}) \ + \\ &+ \frac{1}{2}\sum_{\mathbf{k}}(\Delta_{\mathbf{k}}c^\dagger_{\mathbf{k}\uparrow}c^\dagger_{-\mathbf{k}\downarrow} \ + \Delta^*_{\mathbf{k}}c_{-\mathbf{k}\downarrow}c_{\mathbf{k}\uparrow}) - \frac{1}{2}\sum_{\mathbf{k}}(\Delta_{\mathbf{k}}c^\dagger_{-\mathbf{k}\downarrow}c^\dagger_{\mathbf{k}\uparrow} \ + \Delta^*_{\mathbf{k}}c_{\mathbf{k}\uparrow}c_{-\mathbf{k}\downarrow}) \ + \sum_{\mathbf{k}}\xi_{\mathbf{k}}\end{aligned} \tag{2.18}$$

Then by comparing (2.18) with (2.12) and using the expression of the *Nambu* spinor (2.14), it is easy to identify the constant C as

$$C = \sum_{\mathbf{k}}\xi_{\mathbf{k}} \tag{2.19}$$

and the matrix $H_{\mathbf{k}}$ is the one given in Eq.(2.14), i.e.

$$H_{\mathbf{k}} = \begin{pmatrix} \xi_{\mathbf{k}} & 0 & \Delta_{\mathbf{k}} & 0 \\ 0 & \xi_{-\mathbf{k}} & 0 & \Delta_{\mathbf{k}} \\ \Delta^*_{\mathbf{k}} & 0 & -\xi_{-\mathbf{k}} & 0 \\ 0 & \Delta^*_{\mathbf{k}} & 0 & -\xi_{\mathbf{k}} \end{pmatrix} \tag{2.20}$$

End of proof.

The proof for Eq.(2.13) follows similar lines.

The reformulation in a quadratic form is now completed and we can proceed to diagonalize $H_{\mathbf{k}}$. Let us e.g. consider the Nambu spinor and the matrix $H_{\mathbf{k}}$ given in Eq.(2.14). The latter is the matrix representation of the Hamiltonian in first quantization formalism, therefore it is Hermitian and can be always diagonalized by an orthonormal matrix, whose columns are the orthonormal eigenvectors of $H_{\mathbf{k}}$, forming a basis of our space.

We observe that the matrix (2.20) consists of two decoupled 2×2 blocks, related to (1,3) and (2,4) entries, respectively. Moreover, under the reasonable hypothesis that $\varepsilon_{\mathbf{k}}$ is even in $\mathbf{k}$, then

$$\boxed{\xi_{-\mathbf{k}} = \xi_{\mathbf{k}}} \tag{2.21}$$

i.e. $\xi_{\mathbf{k}}$ is even too, and the matrix (2.20) reduces to

$$H_{\mathbf{k}} = \begin{pmatrix} \xi_{\mathbf{k}} & 0 & \Delta_{\mathbf{k}} & 0 \\ 0 & \xi_{\mathbf{k}} & 0 & \Delta_{\mathbf{k}} \\ \Delta^*_{\mathbf{k}} & 0 & -\xi_{\mathbf{k}} & 0 \\ 0 & \Delta^*_{\mathbf{k}} & 0 & -\xi_{\mathbf{k}} \end{pmatrix} \tag{2.22}$$

implying that the two 2×2 blocks are exactly equal to

$$h_{\mathbf{k}} = \begin{pmatrix} \xi_{\mathbf{k}} & \Delta_{\mathbf{k}} \\ \Delta_{\mathbf{k}}^* & -\xi_{\mathbf{k}} \end{pmatrix} \tag{2.23}$$

This means that we can proceed to diagonalize one single block to diagonalize the entire 4×4 matrix. Denoting

$$\Delta_{\mathbf{k}} = |\Delta_{\mathbf{k}}| \, e^{i\varphi_{\mathbf{k}}} \tag{2.24}$$

from the diagonalization of Eq.(2.23) two eigenvalues are obtained

$$E_{\mathbf{k},\pm} = \pm E_{\mathbf{k}} \qquad \text{where} \qquad E_{\mathbf{k}} = \sqrt{\xi_{\mathbf{k}}^2 + |\Delta_{\mathbf{k}}|^2} \tag{2.25}$$

and the corresponding eigenvectors are

$$\begin{aligned} w_{\mathbf{k},+} &= \begin{pmatrix} u_{\mathbf{k}} \\ v_{\mathbf{k}} \end{pmatrix} \qquad \text{eigenvalue } E_{\mathbf{k},+} \\ w_{\mathbf{k},-} &= \begin{pmatrix} -v_{\mathbf{k}}^* \\ u_{\mathbf{k}}^* \end{pmatrix} \qquad \text{eigenvalue } E_{\mathbf{k},-} \end{aligned} \tag{2.26}$$

where

$$u_{\mathbf{k}} = \sqrt{\frac{1}{2}\left(1 + \frac{\xi_{\mathbf{k}}}{E_{\mathbf{k}}}\right)} \tag{2.27}$$

$$v_{\mathbf{k}} = e^{-i\varphi_{\mathbf{k}}} \sqrt{\frac{1}{2}\left(1 - \frac{\xi_{\mathbf{k}}}{E_{\mathbf{k}}}\right)} \tag{2.28}$$

and $\varphi_{\mathbf{k}}$ is the phase of $\Delta_{\mathbf{k}}$ [see Eq.(2.24)].
We remark here that the quantity $|v_{\mathbf{k}}|^2$ represents the probability that the pair state $(\mathbf{k}\uparrow, -\mathbf{k}\downarrow)$ is occupied, while $|u_{\mathbf{k}}|^2$ represents the probability that it is empty. In particular, for $|\Delta_{\mathbf{k}}| = 0$ we obtain the occupation probability for the Normal ground state at $T = 0\,K$, i.e. $|v_{\mathbf{k}}|^2 = 1$ for $\mathbf{k} < \mathbf{k}_F$ and $|v_{\mathbf{k}}|^2 = 0$ for $\mathbf{k} > \mathbf{k}_F$, as shown in Fig.2.1. The particular structure of $w_{\mathbf{k},+}$ and $w_{\mathbf{k},-}$ stems from the structure of $h_{\mathbf{k}}$, and it can be proven by the following theorem.

Theorem 2.1. *For any eigenvector* $w_{\mathbf{k}} = \begin{pmatrix} u_{\mathbf{k}} \\ v_{\mathbf{k}} \end{pmatrix}$ *with eigenvalue* $E_{\mathbf{k}}$ *of the* 2×2 *Hermitian matrix* $h_{\mathbf{k}}$ *defined in Eq.(2.23), the vector* $(-i\sigma_y)\cdot w_{\mathbf{k}}^* = \begin{pmatrix} -v_{\mathbf{k}}^* \\ u_{\mathbf{k}}^* \end{pmatrix}$ *is also an eigenvector of* $h_{\mathbf{k}}$*, with eigenvalue* $-E_{\mathbf{k}}$ *.*

Proof. Let us start by noting that, if $w_{\mathbf{k}}$ is an eigenvector for $h_{\mathbf{k}}$, with eigenvalue $E_{\mathbf{k}}$, i.e. $h_{\mathbf{k}} w_{\mathbf{k}} = E_{\mathbf{k}} w_{\mathbf{k}}$, then, taking the complex conjugate of the previous expression, we obtain $h_{\mathbf{k}}^* w_{\mathbf{k}}^* = E_{\mathbf{k}} w_{\mathbf{k}}^*$. One can now observe that the very structure of the matrix (2.23) straightforwardly implies the following identity :

$$-h_{\mathbf{k}} = (-i\sigma_y)(h_{\mathbf{k}}^*)(i\sigma_y)$$

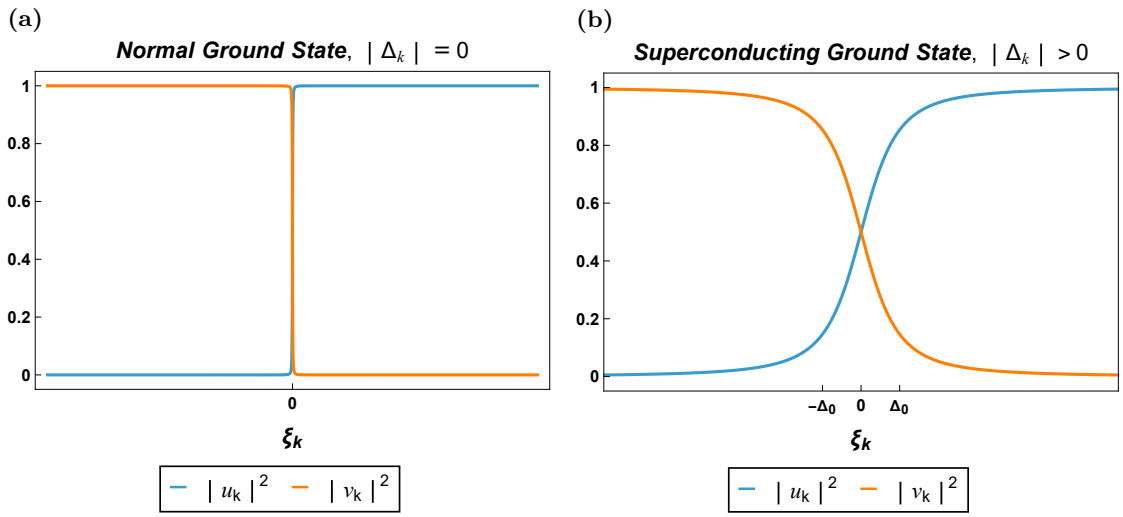

Figure 2.1: Graphic representations of $|u_{\mathbf{k}}|^2$ and $|v_{\mathbf{k}}|^2$ as a function of $\xi_{\mathbf{k}}$. The left panel shows the Normal Ground State $|\Delta_{\mathbf{k}}| = 0$, while the right panel refers to the Superconducting Ground State $|\Delta_{\mathbf{k}}| \neq 0$. The plot has been realized by considering a gap parameter with constant modulus $|\Delta_{\mathbf{k}}| = \Delta_0$ [see Eq.(1.28]. In the Normal GS $|v_{\mathbf{k}}|^2$ reproduces the Fermi distribution at $T = 0\,K$.

By applying the above matrix identity on the vector $(-i\sigma_y)\, w^*_{\mathbf{k}}$, we obtain

$$h_{\mathbf{k}}\,(i\sigma_y)\,w^*_{\mathbf{k}} = (-i\sigma_y)\,h^*_{\mathbf{k}}\,w^*_{\mathbf{k}}$$

Then, substituting $h^*_{\mathbf{k}} w^*_{\mathbf{k}}$ with $E_{\mathbf{k}} w^*_{\mathbf{k}}$ (and multiplying both side by -1), it follows that

$$h_{\mathbf{k}}(-i\sigma_y\, w^*_{\mathbf{k}}) = -E_{\mathbf{k},+}(-i\sigma_y w^*_{\mathbf{k}})$$

which shows that $(-i\sigma_y)\cdot w^*_{\mathbf{k}} = \begin{pmatrix} -v^*_{\mathbf{k}} \\ u^*_{\mathbf{k}} \end{pmatrix}$ is an eigenvector of $h_{\mathbf{k}}$ with eigenvalue $-E_{\mathbf{k}}$.

□

On account of the above theorem, in Eqs.(2.25) and (2.26), we have denoted by $w^*_{\mathbf{k},+}$ the eigenvector with positive eigenvalue $E_{\mathbf{k},+}$ and by $w_{\mathbf{k},-} = (-i\sigma_y)\cdot w^*_{\mathbf{k},+} = \begin{pmatrix} -v^*_{\mathbf{k}} \\ u^*_{\mathbf{k}} \end{pmatrix}$ the eigenvector with negative eigenvalue $E_{\mathbf{k},-} = -E_{\mathbf{k},+}$.

The diagonal matrix of the full problem is

$$H_{diag} = \begin{pmatrix} E_{\mathbf{k},+} & 0 & 0 & 0 \\ 0 & E_{\mathbf{k},+} & 0 & 0 \\ 0 & 0 & E_{\mathbf{k},-} & 0 \\ 0 & 0 & 0 & E_{\mathbf{k},-} \end{pmatrix} \tag{2.29}$$

while the four orthonormal eigenvectors are

$$w^{(1)}_{\mathbf{k},+} = \begin{pmatrix} u_{\mathbf{k}} \\ 0 \\ v_{\mathbf{k}} \\ 0 \end{pmatrix} \qquad w^{(2)}_{\mathbf{k},+} = \begin{pmatrix} 0 \\ u_{\mathbf{k}} \\ 0 \\ v_{\mathbf{k}} \end{pmatrix} \qquad w^{(1)}_{\mathbf{k},-} = \begin{pmatrix} -v^*_{\mathbf{k}} \\ 0 \\ u^*_{\mathbf{k}} \\ 0 \end{pmatrix} \qquad w^{(2)}_{\mathbf{k},-} = \begin{pmatrix} 0 \\ -v^*_{\mathbf{k}} \\ 0 \\ u^*_{\mathbf{k}} \end{pmatrix} \tag{2.30}$$

Then the matrix U, such that $U^\dagger H_{\mathbf{k}} U = H_{diag}$, acquires the form

$$U = \begin{pmatrix} u_{\mathbf{k}} & 0 & -v^*_{\mathbf{k}} & 0 \\ 0 & u_{\mathbf{k}} & 0 & -v^*_{\mathbf{k}} \\ v_{\mathbf{k}} & 0 & u^*_{\mathbf{k}} & 0 \\ 0 & v_{\mathbf{k}} & 0 & u^*_{\mathbf{k}} \end{pmatrix} \tag{2.31}$$

Inverting the previous relation as $H_{\mathbf{k}} = U H_{diag} U^\dagger$ and inserting it in (2.12) , we obtain

$$\mathcal{H}_{BCS} = \frac{1}{2}\sum_{\mathbf{k}} \Psi^\dagger_{\mathbf{k}} H_{\mathbf{k}} \Psi_{\mathbf{k}} + C = \frac{1}{2}\sum_{k} \Psi^\dagger_{\mathbf{k}} U H_{diag} U^\dagger \Psi_{\mathbf{k}} + C = \frac{1}{2}\sum_{k} \Gamma^\dagger_{\mathbf{k}} H_{diag} \Gamma_{\mathbf{k}} + C \tag{2.32}$$

where two new spinors $\Gamma_{\mathbf{k}}$ and $\Gamma^\dagger_{\mathbf{k}}$ are introduced. They are defined as

$$\Gamma_{\mathbf{k}} = U^\dagger \Psi_{\mathbf{k}} \quad \text{and} \quad \Gamma^\dagger_{\mathbf{k}} = \Psi^\dagger_{\mathbf{k}} U \tag{2.33}$$

Assigning to $\Gamma_{\mathbf{k}}$ the same structure of $\Psi_{\mathbf{k}}$, it follows that

$$\Gamma_{\mathbf{k}} = \begin{pmatrix} \gamma_{\mathbf{k}\uparrow} \\ \gamma_{-\mathbf{k}\downarrow} \\ \gamma^\dagger_{-\mathbf{k}\downarrow} \\ -\gamma^\dagger_{\mathbf{k}\uparrow} \end{pmatrix} = \begin{pmatrix} u^*_{\mathbf{k}} c_{\mathbf{k}\uparrow} + v^*_{\mathbf{k}} c^\dagger_{-\mathbf{k}\downarrow} \\ u^*_{\mathbf{k}} c_{-\mathbf{k}\downarrow} - v^*_{\mathbf{k}} c^\dagger_{\mathbf{k}\uparrow} \\ u_{\mathbf{k}} c^\dagger_{-\mathbf{k}\downarrow} - v_{\mathbf{k}} c_{\mathbf{k}\uparrow} \\ -u_{\mathbf{k}} c^\dagger_{\mathbf{k}\uparrow} - v_{\mathbf{k}} c_{-\mathbf{k}\downarrow} \end{pmatrix} \tag{2.34}$$

Because the latter is linear in $\Psi_{\mathbf{k}}$, it contains the same redundancy encountered in (2.14). Moreover, operators γ and $\gamma^\dagger$ are obviously fermionic operators, therefore they satisfy the usual anticommutator relations

$$\{\gamma^\dagger_{\mathbf{k}\sigma}, \gamma_{\mathbf{k}'\sigma'}\} = \delta_{\mathbf{k},\mathbf{k}'}\delta_{\sigma,\sigma'}, \quad \{\gamma^\dagger_{\mathbf{k}\sigma}, \gamma^\dagger_{\mathbf{k}'\sigma'}\} = 0\,, \quad \{\gamma_{\mathbf{k}\sigma}, \gamma_{\mathbf{k}'\sigma'}\} = 0 \tag{2.35}$$

It is also useful to express $\Psi_{\mathbf{k}}$ in terms of $\Gamma_{\mathbf{k}}$ by inverting formula (2.33. It follows that

$$\Psi_{\mathbf{k}} = U\,\Gamma_{\mathbf{k}} = \begin{pmatrix} c_{\mathbf{k}\uparrow} \\ c_{-\mathbf{k}\downarrow} \\ c^\dagger_{-\mathbf{k}\downarrow} \\ -c^\dagger_{\mathbf{k}\uparrow} \end{pmatrix} = \begin{pmatrix} u_{\mathbf{k}}\gamma_{\mathbf{k}\uparrow} - v^*_{\mathbf{k}}\gamma^\dagger_{-\mathbf{k}\downarrow} \\ u_{\mathbf{k}}\gamma_{-\mathbf{k}\downarrow} + v^*_{\mathbf{k}}\gamma^\dagger_{\mathbf{k}\uparrow} \\ u^*_{\mathbf{k}}\gamma^\dagger_{-\mathbf{k}\downarrow} + v_{\mathbf{k}}\gamma_{\mathbf{k}\uparrow} \\ -u^*_{\mathbf{k}}\gamma^\dagger_{\mathbf{k}\uparrow} + v_{\mathbf{k}}\gamma_{-\mathbf{k}\downarrow} \end{pmatrix} \tag{2.36}$$

The expression of $\mathcal{H}_{BCS}$ in terms of γ and $\gamma^\dagger$ is now

$$\mathcal{H}_{BCS} = \frac{1}{2}\sum_{\mathbf{k}} E_{\mathbf{k}}(\gamma^\dagger_{\mathbf{k}\uparrow}\gamma_{\mathbf{k}\uparrow} + \gamma^\dagger_{-\mathbf{k}\downarrow}\gamma_{-\mathbf{k}\downarrow} - \gamma_{-\mathbf{k}\downarrow}\gamma^\dagger_{-\mathbf{k}\downarrow} - \gamma_{\mathbf{k}\uparrow}\gamma^\dagger_{\mathbf{k}\uparrow}) + C. \tag{2.37}$$

where C is given by Eq.(2.19). Using now anticommutator relations (2.35) and relabelling the summation index $-\mathbf{k} \rightarrow \mathbf{k}$ in the spin-$\downarrow$ terms, $\mathcal{H}_{BCS}$ acquires the desired diagonal form

$$\mathcal{H}_{BCS} = -\sum_{\mathbf{k}}(E_{\mathbf{k}} - \xi_{\mathbf{k}}) + \sum_{\mathbf{k}} E_{\mathbf{k}}(\gamma^{\dagger}_{\mathbf{k}\uparrow}\gamma_{\mathbf{k}\uparrow} + \gamma^{\dagger}_{\mathbf{k}\downarrow}\gamma_{\mathbf{k}\downarrow}), \tag{2.38}$$

Here, the first term represents the energy of the Ground State, whereas the second term represents the energy of the excitations.

2.3 The BCS Ground State

By definition, the Ground State (GS) of a system is the eigenstate with the lowest energy. Here below, we shall show that the ground state of the BCS Hamiltonian (2.38), denoted as $|BCS\rangle$, is

$$\boxed{|BCS\rangle = \prod_{\mathbf{k}} \left(u^{*}_{\mathbf{k}} + v^{*}_{\mathbf{k}} c^{\dagger}_{-\mathbf{k}\downarrow} c^{\dagger}_{\mathbf{k}\uparrow}\right)|0\rangle} \tag{2.39}$$

and its ground state energy is:

$$E_0 = -\sum_{\mathbf{k}}(E_{\mathbf{k}} - \xi_{\mathbf{k}}) \tag{2.40}$$

In order to prove that, let us first observe that the diagonal form (2.38) of $\mathcal{H}_{BCS}$ exhibits two contributions: the first one is a constant, and is always negative, whereas, in the second one $E_{\mathbf{k}} > 0$ so that its expectation values are non-negative $\langle BCS|\gamma^{\dagger}\gamma|BCS\rangle \geq 0$. Therefore, in the GS energy level the eigenvalue of operators $\gamma^{\dagger}_{\mathbf{k},\sigma}\gamma_{\mathbf{k},\sigma}$ must be zero $\forall\, \mathbf{k}, \sigma$. This means that $\gamma^{\dagger}_{\mathbf{k},\sigma}$ and $\gamma_{\mathbf{k},\sigma}$ represent, respectively, creation and annihilation operators of excitations with respect the GS. In particular these excitations are quasiparticle, sometimes called Bogolubov quasiparticles. As a consequence, the absence of excitations characterizing the GS implies that

$$\gamma_{\mathbf{k}\sigma}\,|BCS\rangle = 0 \quad \forall\, \mathbf{k}\,, \sigma \tag{2.41}$$

has to be satisfied. Therefore $|BCS\rangle$ may be expressed as

$$|BCS\rangle = \mathcal{N}\prod_{\mathbf{k},\sigma}\gamma_{\mathbf{k}\sigma}\,|R\rangle \ , \tag{2.42}$$

where $\mathcal{N}$ is some normalization factor, and $|R\rangle$ is some reference state to be determined. Indeed, by applying $\gamma_{\mathbf{k}\sigma}$ to $|BCS\rangle$ we obtain that

$$\gamma_{\mathbf{k}\sigma}\ |BCS\rangle = \mathcal{N}\,\gamma_{\mathbf{k}\sigma}\prod_{\mathbf{k}',\sigma'}\gamma_{\mathbf{k}'\sigma'}\,|R\rangle \propto \mathcal{N}\left(\prod_{\mathbf{k}'\neq\mathbf{k},\,\sigma\neq\sigma'}\gamma_{\mathbf{k}'\sigma'}\right)(\gamma_{\mathbf{k}\sigma})^2\,|R\rangle = 0 \tag{2.43}$$

$\forall\, \mathbf{k}, \sigma$, because $(\gamma_{\mathbf{k}\sigma})^2 = 0$, i.e. the condition required by Eq.(2.41).
Reorganizing the terms in the product (2.42) in pairs of operators and, up to a minus

sign due to the switching $\gamma_{\mathbf{k}\sigma}\gamma_{\mathbf{k}'\sigma'} = -\gamma_{\mathbf{k}'\sigma'}\gamma_{\mathbf{k}\sigma}$ of the annihilation operators order, we can rewrite

$$|BCS\rangle = \mathcal{N} \prod_{\mathbf{k}} \gamma_{\mathbf{k}\uparrow}\, \gamma_{-\mathbf{k}\downarrow}\, |R\rangle \ . \tag{2.44}$$

STATEMENT
The only eligible states for $|R\rangle$ are the empty state $|0\rangle$ and the completely filled state $|\uparrow\downarrow\rangle$. Moreover, both these choices yield the same expression for the ground state $|BCS\rangle$.

Proof of statement
Using 2.34 , then

$$\begin{aligned} |BCS\rangle &= \mathcal{N} \prod_{\mathbf{k}} \gamma_{\mathbf{k}\uparrow}\, \gamma_{-\mathbf{k}\downarrow}\, |R\rangle = \prod_{\mathbf{k}} \left(u^*_{\mathbf{k}} c_{\mathbf{k}\uparrow} + v^*_{\mathbf{k}} c^\dagger_{-\mathbf{k}\downarrow}\right) \left(u^*_{\mathbf{k}} c_{-\mathbf{k}\downarrow} - v^*_{\mathbf{k}} c^\dagger_{\mathbf{k}\uparrow}\right) |R\rangle = \\ &= \mathcal{N} \prod_{\mathbf{k}} \left[(u^*_{\mathbf{k}})^2 c_{\mathbf{k}\uparrow} c_{-\mathbf{k}\downarrow} - u^*_{\mathbf{k}} v^*_{\mathbf{k}} c_{\mathbf{k}\uparrow} c^\dagger_{\mathbf{k}\uparrow} + u^*_{\mathbf{k}} v^*_{\mathbf{k}} c^\dagger_{-\mathbf{k}\downarrow} c_{-\mathbf{k}\downarrow} - (v^*_{\mathbf{k}})^2 c^\dagger_{-\mathbf{k}\downarrow} c^\dagger_{\mathbf{k}\uparrow}\right] |R\rangle \end{aligned} \tag{2.45}$$

therefore the following condition must be satisfied :

$$\prod_{\mathbf{k}} \left[(u^*_{\mathbf{k}})^2 c_{\mathbf{k}\uparrow} c_{-\mathbf{k}\downarrow} - u^*_{\mathbf{k}} v^*_{\mathbf{k}} c_{\mathbf{k}\uparrow} c^\dagger_{\mathbf{k}\uparrow} + u^*_{\mathbf{k}} v^*_{\mathbf{k}} c^\dagger_{-\mathbf{k}\downarrow} c_{-\mathbf{k}\downarrow} - (v^*_{\mathbf{k}})^2 c^\dagger_{-\mathbf{k}\downarrow} c^\dagger_{\mathbf{k}\uparrow}\right] |R\rangle \neq 0 \tag{2.46}$$

i.e

$$\left[(u^*_{\mathbf{k}})^2 c_{\mathbf{k}\uparrow} c_{-\mathbf{k}\downarrow} - u^*_{\mathbf{k}} v^*_{\mathbf{k}} c_{\mathbf{k}\uparrow} c^\dagger_{\mathbf{k}\uparrow} + u^*_{\mathbf{k}} v^*_{\mathbf{k}} c^\dagger_{-\mathbf{k}\downarrow} c_{-\mathbf{k}\downarrow} - (v^*_{\mathbf{k}})^2 c^\dagger_{-\mathbf{k}\downarrow} c^\dagger_{\mathbf{k}\uparrow}\right] |R\rangle \neq 0 \quad \forall\, \mathbf{k} \ . \tag{2.47}$$

As a consequence, at least one term of (2.47) must be different from zero.
A priori, within the space $(\mathbf{k}\uparrow, -\mathbf{k}\downarrow)$ there are only four possible choices for the reference state $|R\rangle_{\mathbf{k}}$, and we shall analyze Eq.(2.45) for each of these four choices:

1. $|R\rangle = |0\rangle$

$$\begin{aligned} |BCS\rangle &= \mathcal{N} \prod_{\mathbf{k}} \left[(u^*_{\mathbf{k}})^2 c_{\mathbf{k}\uparrow} c_{-\mathbf{k}\downarrow} - u^*_{\mathbf{k}} v^*_{\mathbf{k}} c_{\mathbf{k}\uparrow} c^\dagger_{\mathbf{k}\uparrow} + u^*_{\mathbf{k}} v^*_{\mathbf{k}} c^\dagger_{-\mathbf{k}\downarrow} c_{-\mathbf{k}\downarrow} - (v^*_{\mathbf{k}})^2 c^\dagger_{-\mathbf{k}\downarrow} c^\dagger_{\mathbf{k}\uparrow}\right] |0\rangle = \\ &= \mathcal{N} \prod_{\mathbf{k}} \left[0 - u^*_{\mathbf{k}} v^*_{\mathbf{k}} + 0 - (v^*_{\mathbf{k}})^2 c^\dagger_{-\mathbf{k}\downarrow} c^\dagger_{\mathbf{k}\uparrow}\right] |0\rangle = \\ &= \mathcal{N} \prod_{\mathbf{k}} (-v^*_{\mathbf{k}}) \left(u^*_{\mathbf{k}} + v^*_{\mathbf{k}} c^\dagger_{-\mathbf{k}\downarrow} c^\dagger_{\mathbf{k}\uparrow}\right) |0\rangle = \\ &= \mathcal{N} \left(\prod_{\mathbf{k}} (-v^*_{\mathbf{k}})\right) \prod_{\mathbf{k}} \left(u^*_{\mathbf{k}} + v^*_{\mathbf{k}} c^\dagger_{-\mathbf{k}\downarrow} c^\dagger_{\mathbf{k}\uparrow}\right) |0\rangle \end{aligned} \tag{2.48}$$

where $\prod_{\mathbf{k}} (-v^*_{\mathbf{k}})$ represents a constant contribution, which may be absorbed by $\mathcal{N}$.

2. $|R\rangle = c^\dagger_{\mathbf{k}\uparrow} |0\rangle$

$$\begin{aligned} |BCS\rangle &= \mathcal{N} \prod_{\mathbf{k}} \left((u^*_{\mathbf{k}})^2 c_{\mathbf{k}\uparrow} c_{-\mathbf{k}\downarrow} - u^*_{\mathbf{k}} v^*_{\mathbf{k}} c_{\mathbf{k}\uparrow} c^\dagger_{\mathbf{k}\uparrow} + u^*_{\mathbf{k}} v^*_{\mathbf{k}} c^\dagger_{-\mathbf{k}\downarrow} c_{-\mathbf{k}\downarrow} - (v^*_{\mathbf{k}})^2 c^\dagger_{-\mathbf{k}\downarrow} c^\dagger_{\mathbf{k}\uparrow}\right) c^\dagger_{\mathbf{k}\uparrow} |0\rangle = \\ &= \mathcal{N} \prod_{\mathbf{k}} \left[0 - 0 + 0 - 0\right] |0\rangle = 0 \end{aligned} \tag{2.49}$$

3. $|R\rangle = c^\dagger_{-\mathbf{k}\downarrow}|0\rangle$

$$\begin{aligned}|BCS\rangle &= \mathcal{N}\prod_{\mathbf{k}}\left((u^*_{\mathbf{k}})^2 c_{\mathbf{k}\uparrow}c_{-\mathbf{k}\downarrow} - u^*_{\mathbf{k}}v^*_{\mathbf{k}}c_{\mathbf{k}\uparrow}c^\dagger_{\mathbf{k}\uparrow} + u^*_{\mathbf{k}}v^*_{\mathbf{k}}c^\dagger_{-\mathbf{k}\downarrow}c_{-\mathbf{k}\downarrow} - (v^*_{\mathbf{k}})^2 c^\dagger_{-\mathbf{k}\downarrow}c^\dagger_{\mathbf{k}\uparrow}\right)c^\dagger_{-\mathbf{k}\downarrow}|0\rangle = \\ &= \mathcal{N}\prod_{\mathbf{k}}\left[0 - u^*_{\mathbf{k}}v^*_{\mathbf{k}}(c_{\mathbf{k}\uparrow}c^\dagger_{\mathbf{k}\uparrow}) + u^*_{\mathbf{k}}v^*_{\mathbf{k}}c^\dagger_{-\mathbf{k}\downarrow}c_{-\mathbf{k}\downarrow} + 0\right]c^\dagger_{-\mathbf{k}\downarrow}|0\rangle = \\ &= \mathcal{N}\prod_{\mathbf{k}}\left(-u^*_{\mathbf{k}}v^*_{\mathbf{k}} + u^*_{\mathbf{k}}v^*_{\mathbf{k}}\right)c^\dagger_{-\mathbf{k}\downarrow}|0\rangle = 0 \end{aligned} \tag{2.50}$$

4. $|R\rangle = c^\dagger_{\mathbf{k}\uparrow}c^\dagger_{-\mathbf{k}\downarrow}|0\rangle$

$$\begin{aligned}|BCS\rangle &= \mathcal{N}\prod_{\mathbf{k}}\left((u^*_{\mathbf{k}})^2 c_{\mathbf{k}\uparrow}c_{-\mathbf{k}\downarrow} - u^*_{\mathbf{k}}v^*_{\mathbf{k}}c_{\mathbf{k}\uparrow}c^\dagger_{\mathbf{k}\uparrow} + u^*_{\mathbf{k}}v^*_{\mathbf{k}}c^\dagger_{-\mathbf{k}\downarrow}c_{-\mathbf{k}\downarrow} - (v^*_{\mathbf{k}})^2 c^\dagger_{-\mathbf{k}\downarrow}c^\dagger_{\mathbf{k}\uparrow}\right)c^\dagger_{\mathbf{k}\uparrow}c^\dagger_{-\mathbf{k}\downarrow}|0\rangle = \\ &= \mathcal{N}\prod_{\mathbf{k}}\left[(u^*_{\mathbf{k}})^2 c_{\mathbf{k}\uparrow}c_{-\mathbf{k}\downarrow} + 0 + u^*_{\mathbf{k}}v^*_{\mathbf{k}}c^\dagger_{-\mathbf{k}\downarrow}c_{-\mathbf{k}\downarrow} + 0\right]c^\dagger_{\mathbf{k}\uparrow}c^\dagger_{-\mathbf{k}\downarrow}|0\rangle = \\ &= \mathcal{N}\left(\prod_{\mathbf{k}}u^*_{\mathbf{k}}\right)\prod_{\mathbf{k}}\left(u^*_{\mathbf{k}} + v^*_{\mathbf{k}}c^\dagger_{-\mathbf{k}\downarrow}c^\dagger_{\mathbf{k}\uparrow}\right)|0\rangle \end{aligned} \tag{2.51}$$

where $\prod_{\mathbf{k}} u^*_{\mathbf{k}}$ represents a constant, hence it may be absorbed in $\mathcal{N}$.

We thus have proven that, within the space $(\mathbf{k}\uparrow, -\mathbf{k}\downarrow)$, the reference state must be either $|R\rangle = |0\rangle$ or $|R\rangle = c^\dagger_{\mathbf{k}\uparrow}c^\dagger_{-\mathbf{k}\downarrow}|0\rangle$. Moreover, by comparing Eqs.(2.48) and (2.51), we realize that, up to a normalization factor, both choices yield the same ground state, which acquires the form (2.39), and is normalized because $|u_{\mathbf{k}}|^2 + |v_{\mathbf{k}}|^2 = 1$.

End of proof

2.4 The Excitations

In Eq.(2.38), the positive energies $E_{\mathbf{k}}$ [see Eq.(2.25)]

$$E_{\mathbf{k}} = \sqrt{\xi^2_{\mathbf{k}} + |\Delta_{\mathbf{k}}|^2} \tag{2.52}$$

represent the energies of *excitations* above the ground state. This excitation spectrum is displayed in Fig.2.2.
Because $\gamma^\dagger$ and γ in Eq.(2.38) are fermionic operators describing excitations, we may now investigate what happens by creating one over the GS.
Hence, to create an excitation, for example within the space $(\mathbf{k}\uparrow)$, we shall apply $\gamma^\dagger_{\mathbf{k}\uparrow}$ on

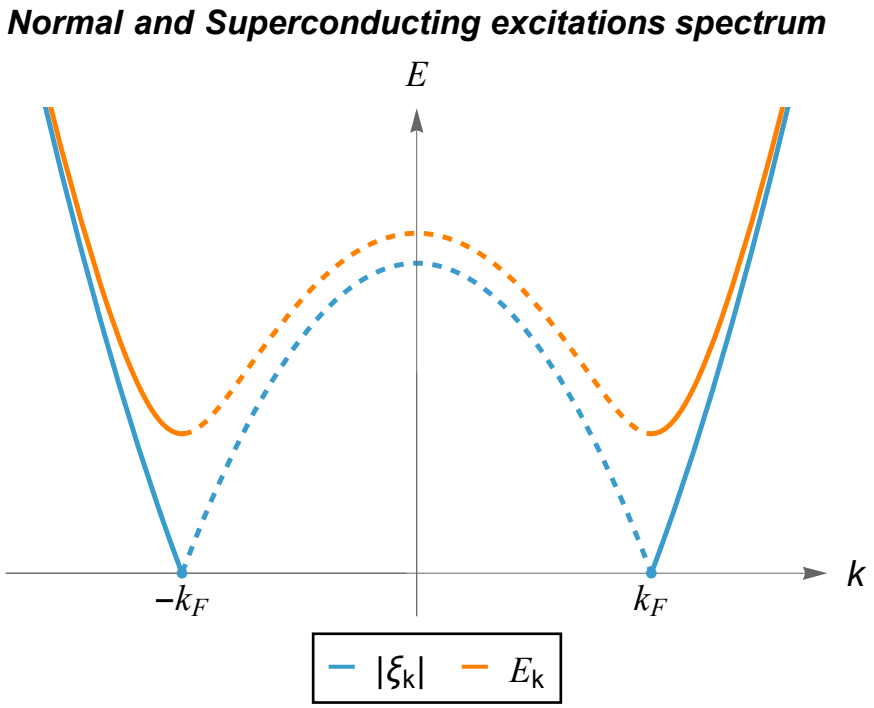

Figure 2.2: The superconducting $E_{\mathbf{k}}$ (orange line) and the Normal $|\xi_{\mathbf{k}}|$ (blue line) excitations spectra are plotted as a function of k, which has been taken as scalar quantities. In particular, the figure has been obtained for a isotropic gap parameter, i.e. $|\Delta_k| = \Delta_0$. The superconducting energy spectrum exhibits a gap in the excitation energies, which prevents the occupation of states with energy $0 < E < \Delta_0$. Furthermore, the dashed lines depict "hole-like" excitations, whereas the solid lines represent "electron-like" excitations for both Normal and Superconducting spectra.

$|BCS\rangle$. Calling the excited state $|ES\rangle_{\mathbf{k}\uparrow} = \gamma^\dagger_{\mathbf{k}\uparrow}|BCS\rangle$ and using (2.34), then

$$
\begin{aligned}
|ES\rangle_{\mathbf{k}\uparrow} &= \mathcal{N}\,\gamma^\dagger_{\mathbf{k}\uparrow}\prod_{\mathbf{k}'}\gamma_{\mathbf{k}'\uparrow}\gamma_{-\mathbf{k}'\downarrow}|0\rangle = \mathcal{N}\left(\prod_{\mathbf{k}'\neq\mathbf{k}}\gamma_{\mathbf{k}'\uparrow}\gamma_{-\mathbf{k}'\downarrow}\right)\gamma^\dagger_{\mathbf{k}\uparrow}\gamma_{\mathbf{k}\uparrow}\gamma_{-\mathbf{k}\downarrow}|0\rangle = \\
&= \mathcal{N}\left(\prod_{\mathbf{k}'\neq\mathbf{k}}\gamma_{\mathbf{k}'\uparrow}\gamma_{-\mathbf{k}'\downarrow}\right)\left(u_{\mathbf{k}}c^\dagger_{\mathbf{k}\uparrow}+v_{\mathbf{k}}c_{-\mathbf{k}\downarrow}\right)\left(u^*_{\mathbf{k}}+v^*_{\mathbf{k}}c^\dagger_{-\mathbf{k}\downarrow}c^\dagger_{\mathbf{k}\uparrow}\right)|0\rangle = \\
&= \mathcal{N}\left(\prod_{\mathbf{k}'\neq\mathbf{k}}\gamma_{\mathbf{k}'\uparrow}\gamma_{-\mathbf{k}'\downarrow}\right)\left(|u_{\mathbf{k}}|^2c^\dagger_{\mathbf{k}\uparrow}+v_{\mathbf{k}}u^*_{\mathbf{k}}c^\dagger_{-\mathbf{k}\downarrow}-u_{\mathbf{k}}v^*_{\mathbf{k}}(c^\dagger_{\mathbf{k}\uparrow})^2c^\dagger_{-\mathbf{k}\downarrow}c+\right. \\
&\qquad \left.+\,|v_{\mathbf{k}}|^2c_{-\mathbf{k}\downarrow}c^\dagger_{-\mathbf{k}\downarrow}c^\dagger_{\mathbf{k}\uparrow}\right)|0\rangle = \qquad (2.53)\\
&= \mathcal{N}\left(\prod_{\mathbf{k}'\neq\mathbf{k}}\gamma_{\mathbf{k}'\uparrow}\gamma_{-\mathbf{k}'\downarrow}\right)\left(|u_{\mathbf{k}}|^2+|v_{\mathbf{k}}|^2\right)c^\dagger_{\mathbf{k}\uparrow}|0\rangle = \\
&= \mathcal{N}\left(\prod_{\mathbf{k}'\neq\mathbf{k}}u^*_{\mathbf{k}'}+v^*_{\mathbf{k}'}c^\dagger_{-\mathbf{k}'\downarrow}c^\dagger_{\mathbf{k}'\uparrow}\right)c^\dagger_{\mathbf{k}\uparrow}|0\rangle
\end{aligned}
$$

up to a minus sign that may appear due to the switching of operators. In the previous equation we made use of $(|u_{\mathbf{k}}|^2 + |v_{\mathbf{k}}|^2) = 1$. From (2.53) it follows that, applying $\gamma^\dagger_{\mathbf{k}\uparrow}$ on $|BCS\rangle$ creates, with certainty, an electron with momentum $\mathbf{k}$ and spin $\uparrow$, hence replacing the quantum superposition $(u^*_{\mathbf{k}} + v^*_{\mathbf{k}} c^\dagger_{-\mathbf{k}\downarrow} c^\dagger_{\mathbf{k}\uparrow})\,|0\rangle$ between an empty and a pair state (Cooper pair) with a singly occupied state $|-\mathbf{k}\downarrow\rangle$.
Repeating the same calculation of (2.53) for the operator $\gamma^\dagger_{-\mathbf{k}\downarrow}$ we obtain

$$|ES\rangle_{-\mathbf{k}\downarrow} = \gamma^\dagger_{-\mathbf{k}\downarrow}\,|BCS\rangle = \mathcal{N}\left(\prod_{\mathbf{k}'\neq\mathbf{k}} u^*_{\mathbf{k}'} + v^*_{\mathbf{k}'} c^\dagger_{-\mathbf{k}'\downarrow} c^\dagger_{\mathbf{k}'\uparrow}\right) c^\dagger_{-\mathbf{k}\downarrow}\,|0\rangle \tag{2.54}$$

Thus, we have created, with certainty, an electron with momentum $-\mathbf{k}$ and spin $\downarrow$, replacing a quantum superposition with a singly occupied state..
The expectation values of $\mathcal{H}_{BCS}$ over the excitated states $|ES\rangle_{\mathbf{k}\uparrow}$ and $|ES\rangle_{-\mathbf{k}\downarrow}$ are defined as

$$\begin{aligned} E_{ES,\mathbf{k}\uparrow} &= \langle ES|\,\mathcal{H}_{BCS}\,|ES\rangle_{\mathbf{k}\uparrow} \\ E_{ES,-\mathbf{k}\downarrow} &= \langle ES|\,\mathcal{H}_{BCS}\,|ES\rangle_{-\mathbf{k}\downarrow} \end{aligned} \tag{2.55}$$

In analogy with operators $c^\dagger_{\mathbf{k},\sigma}$ and $c_{\mathbf{k},\sigma}$, for which it is possible to define a number operator $n_{\mathbf{k},\sigma} = c^\dagger_{\mathbf{k},\sigma} c_{\mathbf{k},\sigma}$, we may define a number operator related to exicitations, i.e. $n_{\gamma,\mathbf{k}\sigma} = \gamma^\dagger_{\mathbf{k},\sigma}\gamma_{\mathbf{k},\sigma}$, which counts the number of excitations within the space $(\mathbf{k},\sigma)$. Therefore, it follows that

$$\begin{aligned} E_{ES,\mathbf{k}\uparrow} &= \langle ES|\,\mathcal{H}_{BCS}\,|ES\rangle_{\mathbf{k}\uparrow} = \\ &= \langle ES|\left(-\sum_{\mathbf{k}'}(E_{\mathbf{k}'} - \xi_{\mathbf{k}'}) + \sum_{\mathbf{k}'} E_{\mathbf{k}'}(\gamma^\dagger_{\mathbf{k}'\uparrow}\gamma_{\mathbf{k}'\uparrow} + \gamma^\dagger_{-\mathbf{k}'\downarrow}\gamma_{-\mathbf{k}'\downarrow})\right)|ES\rangle_{\mathbf{k}\uparrow} = \\ &= \langle ES|\left(-\sum_{\mathbf{k}'}(E_{\mathbf{k}'} - \xi_{\mathbf{k}'})\right)|ES\rangle_{\mathbf{k}\uparrow} + \langle ES|\left(\sum_{\mathbf{k}'} E_{\mathbf{k}'} n_{\gamma,\mathbf{k}'\uparrow}\right)|ES\rangle_{\mathbf{k}\uparrow} + \\ &\quad + \langle ES|\left(\sum_{\mathbf{k}'} E_{\mathbf{k}'} n_{\gamma,-\mathbf{k}'\downarrow}\right)|ES\rangle_{\mathbf{k}\uparrow} = \\ &= -\sum_{\mathbf{k}'}(E_{\mathbf{k}'} - \xi_{\mathbf{k}'}) + E_{\mathbf{k}} = \\ &= E_0 + E_{\mathbf{k}} \end{aligned} \tag{2.56}$$

where we have used

$$n_{\gamma,\mathbf{k}'\sigma}\,|ES\rangle_{\mathbf{k}\uparrow} = \begin{cases} 0 & \textit{if } \mathbf{k}' \neq \mathbf{k} \textit{ and } \sigma \neq \uparrow \\ 1 & \textit{otherwise} \end{cases} \tag{2.57}$$

and E_0 is the ground state energy (2.40).

Repeating the same calculation for state $|ES\rangle_{-\mathbf{k}\downarrow}$, we obtain that

$$\begin{aligned} E_{ES,-\mathbf{k}\downarrow} &= \langle ES|\,\mathcal{H}_{BCS}\,|ES\rangle_{-\mathbf{k}\downarrow} = \langle ES|\left(-\sum_{\mathbf{k}'}(E_{\mathbf{k}'}-\xi_{\mathbf{k}'})\right)|ES\rangle_{-\mathbf{k}\downarrow} + \\ &+ \langle ES|\left(\sum_{\mathbf{k}'}E_{\mathbf{k}'}n_{\gamma,\mathbf{k}'\uparrow}\right)|ES\rangle_{-\mathbf{k}\downarrow} + \langle ES|\left(\sum_{\mathbf{k}'}E_{\mathbf{k}'}n_{\gamma,-\mathbf{k}'\downarrow}\right)|ES\rangle_{-\mathbf{k}\downarrow} = \\ &= -\sum_{\mathbf{k}'}(E_{\mathbf{k}'}-\xi_{\mathbf{k}'}) + E_{\mathbf{k}} = \\ &= E_0 + E_{\mathbf{k}} \end{aligned} \tag{2.58}$$

As expected, the two excited states $|ES\rangle_{-\mathbf{k}\downarrow}$ and $|ES\rangle_{\mathbf{k}\uparrow}$ are degenerate states, and their difference in energy, with respect the GS, is of a single excitation $E_{\mathbf{k}}$.

Chapter 3

Model for nanowire proximized by a superconductor

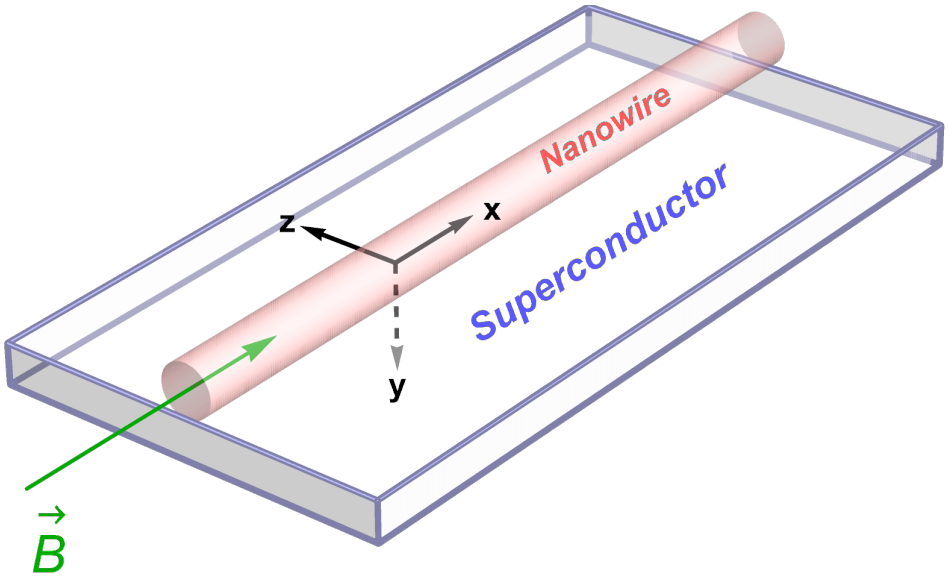

Figure 3.1: Schematic representation of a Nanowire (light red) proximized by a superconductor (light blue) with a magnetic field $\vec{B}$ (green arrow) applied along the x-direction.

As mentioned in Chap.1.3.3, the proximity effect occurs when a superconductor (S) is placed in contact with a normal (N), i.e. non-superconducting conductor, and it consists in the fact that a superconducting pairing is induced in the N material. In this chapter, we shall illustrate and analyze a model to describe a nanowire with spin-orbit coupling that is proximized by a superconducting film covering it.

3.1 Hamiltonian of a proximized nanowire with spin-orbit coupling

We shall now consider a spatially homogeneous single-channel (1D) nanowire with spin-orbit coupling, such as InAs or InSb, proximized by an s-wave superconducting film deposited on it. Furthermore, the possible presence of an applied magnetic field will be considered. We shall model the system with the following Hamiltonian [49, 60, 85, 86, 89]:

$$\mathcal{H} = \sum_k \left(c^\dagger_{k\uparrow}, c^\dagger_{k\downarrow}\right) \left(\xi^0_k\, \sigma_0 - k\boldsymbol{\alpha}\cdot\boldsymbol{\sigma} - \mathbf{b}\cdot\boldsymbol{\sigma}\right) \begin{pmatrix} c_{k\uparrow} \\ c_{k\downarrow} \end{pmatrix} + \sum_k \left(\Delta_k c^\dagger_{k\uparrow} c^\dagger_{-k\downarrow} + \Delta^*_k c_{-k\downarrow} c_{k\uparrow}\right) \quad (3.1)$$

where

$$\xi^0_k = \varepsilon^0_k - \mu \qquad\qquad \varepsilon^0_k = \frac{\hbar^2 k^2}{2m^*} \quad (3.2)$$

is the deviation of the bare electron band energy (in the effective mass m^* approximation) from the chemical potential μ, while $\boldsymbol{\alpha} = (\alpha_x, \alpha_y, \alpha_z)$ is the vector identifying the three components of the spin-orbit coupling, and the term $-\mathbf{b}\cdot\boldsymbol{\sigma}$ denotes the Zeeman coupling with an external magnetic field $\mathbf{b} = (b_x, b_y, b_z)$. Here, σ_0 is the 2×2 identity, while $\boldsymbol{\sigma} = (\sigma_x, \sigma_y, \sigma_z)$ denotes the vector of the three Pauli matrices

$$\sigma_0 = \begin{pmatrix} 1 & 0 \\ 0 & 1 \end{pmatrix} \quad \sigma_x = \begin{pmatrix} 0 & 1 \\ 1 & 0 \end{pmatrix} \quad \sigma_y = \begin{pmatrix} 0 & -i \\ i & 0 \end{pmatrix} \quad \sigma_z = \begin{pmatrix} 1 & 0 \\ 0 & -1 \end{pmatrix}$$

Finally, the s-wave character of the superconducting pairing appearing in Eq.(3.1) is encoded in

$$\Delta_k = \Delta_0\, e^{i\varphi} \quad (3.3)$$

where $\Delta_0 \geq 0$ and φ represent the magnitude and the phase of the pairing, respectively. In analogy with what we have done for the customary BCS model in Eqs.(2.11) and (2.12), it is possible to show that the nanowire Hamiltonian (3.1) can be rewritten in the Bogolubov de Gennes form,

$$\mathcal{H} = \frac{1}{2}\sum_k \Psi^\dagger_k H_{BdG}(k) \Psi_k \; + C \quad (3.4)$$

Here, we choose the Nambu spinor as in Eq.(2.13)

$$\Psi_k = \Psi^{(1)}_k = \begin{pmatrix} c_{k\uparrow} \\ c_{k\downarrow} \\ c^\dagger_{-k\downarrow} \\ -c^\dagger_{-k\uparrow} \end{pmatrix} \qquad\qquad \Psi^\dagger_k = \left(c^\dagger_{k\uparrow}, c^\dagger_{k\downarrow}, c_{-k\downarrow}, -c_{-k\uparrow}\right) \quad (3.5)$$

and the corresponding Bogolubov de Gennes Hamiltonian reads

$$\boxed{H_{BdG}(k) = \begin{pmatrix} \xi^0_k\sigma_0 - k\boldsymbol{\alpha}\cdot\boldsymbol{\sigma} - \mathbf{b}\cdot\boldsymbol{\sigma} & \Delta_0 e^{i\varphi}\sigma_0 \\ \Delta_0 e^{-i\varphi}\sigma_0 & -\xi^0_k\sigma_0 + k\boldsymbol{\alpha}\cdot\boldsymbol{\sigma} - \mathbf{b}\cdot\boldsymbol{\sigma} \end{pmatrix}} \quad (3.6)$$

while, the constant C appearing in Eq.(3.4) is

$$C = \sum_k \xi_k^0 \tag{3.7}$$

Particle and hole blocks
In Eq.(3.6), we denote the two 2×2 blocks

$$\begin{aligned} h_e(k) &= \xi_k^0 \sigma_0 - k\boldsymbol{\alpha} \cdot \boldsymbol{\sigma} - \mathbf{b} \cdot \boldsymbol{\sigma} \\ h_h(k) &= -\xi_k^0 \sigma_0 + k\boldsymbol{\alpha} \cdot \boldsymbol{\sigma} - \mathbf{b} \cdot \boldsymbol{\sigma} \end{aligned} \tag{3.8}$$

related to (1,2) entries as "electron block" $h_e(k)$, and related to (3,4) entries as "hole block" $h_h(k)$, respectively. Using the property

$$\sigma_y \boldsymbol{\sigma}^* \sigma_y = -\boldsymbol{\sigma} \tag{3.9}$$

of the Pauli matrices, it is possible to verify that the following relation holds between the blocks

$$\boxed{h_h(k) = -\sigma_y h_e^*(-k)\sigma_y} \tag{3.10}$$

Proof of Eqs.(3.4)
Let us start from rewriting explicitly the scalar products in Eq.(3.1)

$$\begin{aligned} \mathcal{H} = &\sum_k \left(c_{k\uparrow}^\dagger, c_{k\downarrow}^\dagger\right) \left(\xi_k^0 \sigma_0 - \alpha_x \sigma_x k - \alpha_y \sigma_y k - \alpha_z \sigma_z k \ - b_x \sigma_x - b_y \sigma_y - b_z \sigma_z\right) \begin{pmatrix} c_{k\uparrow} \\ c_{k\downarrow} \end{pmatrix} + \\ &+ \sum_k \left(\Delta_k c_{k\uparrow}^\dagger c_{-k\downarrow}^\dagger + \Delta_k^* c_{-k\downarrow} c_{k\uparrow}\right) \end{aligned} \tag{3.11}$$

It is now convenient to decompose $\mathcal{H}$ as a sum

$$\mathcal{H} = \mathcal{H}_{diag} + \mathcal{H}_{non-diag} \tag{3.12}$$

where $\mathcal{H}_{diag}$ is diagonal in the operators c and $c^\dagger$ and is characterized by σ_0 and σ_z, whereas $\mathcal{H}_{off-diag}$ is off-diagonal in c and $c^\dagger$. Explicitly,

$$\mathcal{H}_{diag} = \sum_k \left(c_{k\uparrow}^\dagger, c_{k\downarrow}^\dagger\right) \left(\xi_k^0 \sigma_0 - k\alpha_z \sigma_z - b_z \sigma_z\right) \begin{pmatrix} c_{k\uparrow} \\ c_{k\downarrow} \end{pmatrix} \tag{3.13}$$

$$\mathcal{H}_{off-diag} = -\sum_k \left(c_{k\uparrow}^\dagger, c_{k\downarrow}^\dagger\right) \left(\alpha_x \sigma_x + \alpha_y \sigma_y + b_x \sigma_x + b_y \sigma_y\right) \begin{pmatrix} c_{k\uparrow} \\ c_{k\downarrow} \end{pmatrix} \tag{3.14}$$

$$+ \sum_k \left(\Delta_k c_{k\uparrow}^\dagger c_{-k\downarrow}^\dagger + \Delta_k^* c_{-k\downarrow} c_{k\uparrow}\right) \tag{3.15}$$

Starting from $\mathcal{H}_{diag}$, we first rewrite such term as twice its half, then relabel one of the two summation index $k \to -k$, obtaining

$$\begin{aligned}\mathcal{H}_{diag} =& \frac{1}{2}\sum_k \begin{pmatrix} c^\dagger_{k\uparrow}, c^\dagger_{k\downarrow}\end{pmatrix} \begin{pmatrix} \xi^0_k - \alpha_z k - b_z & 0 \\ 0 & \xi^0_k + \alpha_z k + b_z \end{pmatrix} \begin{pmatrix} c_{k\uparrow} \\ c_{k\downarrow}\end{pmatrix} + \\ &+ \frac{1}{2}\sum_k \begin{pmatrix} c^\dagger_{-k\uparrow}, c^\dagger_{-k\downarrow}\end{pmatrix} \begin{pmatrix} \xi^0_{-k} + \alpha_z k - b_z & 0 \\ 0 & \xi^0_{-k} - \alpha_z k + b_z \end{pmatrix} \begin{pmatrix} c_{-k\uparrow} \\ c_{-k\downarrow}\end{pmatrix}\end{aligned} \tag{3.16}$$

Using now the anticommutation rules Eq.(2.16) of the fermionic operators, it follows that

$$\begin{aligned}\mathcal{H}_{diag} =& \frac{1}{2}\sum_k \begin{pmatrix} c^\dagger_{k\uparrow}, c^\dagger_{k\downarrow}\end{pmatrix} \begin{pmatrix} \xi^0_k - \alpha_z k - b_z & 0 \\ 0 & \xi^0_k + \alpha_z k + b_z \end{pmatrix} \begin{pmatrix} c_{k\uparrow} \\ c_{k\downarrow}\end{pmatrix} + \\ &- \frac{1}{2}\sum_k (c_{-k\uparrow}, c_{-k\downarrow}) \begin{pmatrix} \xi^0_{-k} + \alpha_z k - b_z & 0 \\ 0 & \xi^0_{-k} - \alpha_z k + b_z \end{pmatrix} \begin{pmatrix} c^\dagger_{-k\uparrow} \\ c^\dagger_{-k\downarrow}\end{pmatrix} + \sum_k \xi^0_{-k} = \\ =& \frac{1}{2}\sum_k \begin{pmatrix} c^\dagger_{k\uparrow}, c^\dagger_{k\downarrow}\end{pmatrix} \begin{pmatrix} \xi^0_k - \alpha_z k - b_z & 0 \\ 0 & \xi^0_k + \alpha_z k + b_z \end{pmatrix} \begin{pmatrix} c_{k\uparrow} \\ c_{k\downarrow}\end{pmatrix} + \\ &+ \frac{1}{2}\sum_k (c_{-k\downarrow}, -c_{-k\uparrow},) \begin{pmatrix} -\left(\xi^0_{-k} - \alpha_z k + b_z\right) & 0 \\ 0 & -\left(\xi^0_{-k} + \alpha_z k - b_z\right) \end{pmatrix} \begin{pmatrix} c^\dagger_{-k\downarrow} \\ -c^\dagger_{-k\uparrow}\end{pmatrix} + \\ &+ \sum_k \xi^0_{-k} = \\ =& \frac{1}{2}\sum_k \begin{pmatrix} c^\dagger_{k\uparrow}, c^\dagger_{k\downarrow}\end{pmatrix} \left(\xi^0_k \sigma_0 - (\alpha_z k + b_z)\sigma_z\right) \begin{pmatrix} c_{k\uparrow} \\ c_{k\downarrow}\end{pmatrix} + \\ &+ \frac{1}{2}\sum_k (c_{-k\downarrow}, -c_{-k\uparrow}) \left(-\xi^0_{-k}\sigma_0 + (\alpha_z k - b_z)\sigma_z\right) \begin{pmatrix} c^\dagger_{-k\downarrow} \\ -c^\dagger_{-k\uparrow}\end{pmatrix} + \sum_k \xi^0_{-k}\end{aligned} \tag{3.17}$$

Recalling now the definition (3.5) of the Nambu spinor, and the fact that $\xi^0_{-k} = \xi^0_k$ is an even function of k [see Eq.(3.2)], we can rewrite $\mathcal{H}_{diag}$ as

$$\mathcal{H}_{diag} = \frac{1}{2}\sum_k \Psi^\dagger_k \begin{pmatrix} \xi^0_k \sigma_0 - k\,\alpha_z\sigma_z - b_z\sigma_z & 0 \\ 0 & -\xi^0_k\sigma_0 + k\,\alpha_z\sigma_z - b_z\sigma_z \end{pmatrix} \Psi_k + \sum_k \xi^0_{-k} \tag{3.18}$$

Let us now consider the off-diagonal term $\mathcal{H}_{off-diag}$. First, by introducing

$$\mathbf{b}_\perp = (b_x, b_y) \qquad \boldsymbol{\alpha}_\perp = (\alpha_x, \alpha_y) \qquad \boldsymbol{\sigma}_\perp = (\sigma_x, \sigma_y) \tag{3.19}$$

one can compactly rewrite Eq.(3.15) as

$$\begin{aligned}\mathcal{H}_{off-diag} =& -\sum_k \begin{pmatrix} c^\dagger_{k\uparrow}, c^\dagger_{k\downarrow}\end{pmatrix} \left((\mathbf{b}_\perp + k\boldsymbol{\alpha}_\perp)\cdot\boldsymbol{\sigma}_\perp\right) \begin{pmatrix} c_{k\uparrow} \\ c_{k\downarrow}\end{pmatrix} + \sum_k \left(\Delta_k c^\dagger_{k\uparrow} c^\dagger_{-k\downarrow} + \Delta^*_k c_{-k\downarrow} c_{k\uparrow}\right) = \\ =& -\sum_k \sum_k \sum_{\sigma,\sigma'=\uparrow,\downarrow} c^\dagger_{k\sigma} \left[(\mathbf{b}_\perp + k\boldsymbol{\alpha}_\perp)\cdot\boldsymbol{\sigma}_\perp\right]_{\sigma,\sigma'} c_{k\sigma'} + \sum_k \left(\Delta_k c^\dagger_{k\uparrow} c^\dagger_{-k\downarrow} + \Delta^*_k c_{-k\downarrow} c_{k\uparrow}\right)\end{aligned} \tag{3.20}$$

Then, by rewriting the above equation as twice 1/2 of itself and by relabelling $k \to -k$ in the second 1/2, one has

$$\begin{aligned}\mathcal{H}_{off-diag} = &-\frac{1}{2}\sum_{k}\sum_{\sigma,\sigma'=\uparrow,\downarrow} c^{\dagger}_{k\sigma}\left((\mathbf{b}_{\perp}+k\boldsymbol{\alpha}_{\perp})\cdot\boldsymbol{\sigma}_{\perp}\right)_{\sigma,\sigma'} c_{k\sigma'} + \\ &-\frac{1}{2}\sum_{k}\sum_{\sigma,\sigma'=\uparrow,\downarrow} c^{\dagger}_{-k\sigma}\left((\mathbf{b}_{\perp}-k\boldsymbol{\alpha}_{\perp})\cdot\boldsymbol{\sigma}_{\perp}\right)_{\sigma,\sigma'} c_{-k\sigma'} + \\ &+\frac{1}{2}\sum_{k}\left(\Delta_k c^{\dagger}_{k\uparrow}c^{\dagger}_{-k\downarrow}+\Delta^{*}_{k}c_{-k\downarrow}c_{k\uparrow}\right)+\frac{1}{2}\sum_{k}\left(\Delta_{-k} c^{\dagger}_{-k\uparrow}c^{\dagger}_{k\downarrow}+\Delta^{*}_{-k}c_{k\downarrow}c_{-k\uparrow}\right) =\end{aligned} \tag{3.21}$$

Now, by noticing that $\boldsymbol{\sigma}_{\perp} = (\sigma_x, \sigma_y)$ are completely off-diagonal matrices, and applying the anticommutation rules (2.16), one can rewrite

$$\begin{aligned}\mathcal{H}_{off-diag} = &-\frac{1}{2}\sum_{k}\sum_{\sigma,\sigma'=\uparrow,\downarrow} c^{\dagger}_{k\sigma}\left((\mathbf{b}_{\perp}+k\boldsymbol{\alpha}_{\perp})\cdot\boldsymbol{\sigma}_{\perp}\right)_{\sigma,\sigma'} c_{k\sigma'} \\ &+\frac{1}{2}\sum_{k}\sum_{\sigma,\sigma'=\uparrow,\downarrow} c_{-k\sigma'}\left((\mathbf{b}_{\perp}-k\boldsymbol{\alpha}_{\perp})\cdot\boldsymbol{\sigma}_{\perp}\right)_{\sigma,\sigma'} c^{\dagger}_{-k\sigma} + \\ &+\frac{1}{2}\sum_{k}\left(\Delta_k c^{\dagger}_{k\uparrow}c^{\dagger}_{-k\downarrow}+\Delta^{*}_{k}c_{-k\downarrow}c_{k\uparrow}\right)-\frac{1}{2}\sum_{k}\left(\Delta_{-k} c^{\dagger}_{k\downarrow}c^{\dagger}_{-k\uparrow}+\Delta^{*}_{-k}c_{-k\uparrow}c_{k\downarrow}\right)\end{aligned} \tag{3.22}$$

The Hermiticity of the Pauli matrices implies that

$$\left((\mathbf{b}_{\perp}-k\boldsymbol{\alpha}_{\perp})\cdot\boldsymbol{\sigma}_{\perp}\right)_{\sigma,\sigma'} = \left((\mathbf{b}_{\perp}-k\boldsymbol{\alpha}_{\perp})\cdot\boldsymbol{\sigma}^{*}_{\perp}\right)_{\sigma',\sigma} \quad .$$

By relabelling $\sigma \leftrightarrow \sigma'$ one can write

$$\begin{aligned}\mathcal{H}_{off-diag} = &-\frac{1}{2}\sum_{k}\left(c^{\dagger}_{k\uparrow}, c^{\dagger}_{k\downarrow}\right)\left((\mathbf{b}_{\perp}+k\boldsymbol{\alpha}_{\perp})\cdot\boldsymbol{\sigma}_{\perp}\right)\begin{pmatrix}c_{k\uparrow}\\ c_{k\downarrow}\end{pmatrix} + \\ &+\frac{1}{2}\sum_{k}\left(c_{-k\uparrow}, c_{-k\downarrow}\right)\left((\mathbf{b}_{\perp}-k\boldsymbol{\alpha}_{\perp})\cdot\boldsymbol{\sigma}^{*}_{\perp}\right)\begin{pmatrix}c^{\dagger}_{-k\uparrow}\\ c^{\dagger}_{-k\downarrow}\end{pmatrix} + \\ &+\frac{1}{2}\sum_{k}\left(\Delta_k c^{\dagger}_{k\uparrow}c^{\dagger}_{-k\downarrow}+\Delta^{*}_{k}c_{-k\downarrow}c_{k\uparrow}\right)-\frac{1}{2}\sum_{k}\left(\Delta_{-k} c^{\dagger}_{k\downarrow}c^{\dagger}_{-k\uparrow}+\Delta^{*}_{-k}c_{-k\uparrow}c_{k\downarrow}\right)\end{aligned} \tag{3.23}$$

Let us now sandwich the $(\mathbf{b}_\perp - k\boldsymbol{\alpha}_\perp)\cdot\boldsymbol{\sigma}_\perp^*$ between two identities $\sigma_0 = (-i\sigma_y)(i\sigma_y)$

$$\begin{aligned}
\mathcal{H}_{off-diag} = &-\frac{1}{2}\sum_k \left(c_{k\uparrow}^\dagger, c_{k\downarrow}^\dagger\right)\left((\mathbf{b}_\perp + k\boldsymbol{\alpha}_\perp)\cdot\boldsymbol{\sigma}_\perp\right)\begin{pmatrix} c_{k\uparrow} \\ c_{k\downarrow}\end{pmatrix} + \\
&+\frac{1}{2}\sum_k \left(c_{-k\uparrow}, c_{-k\downarrow}\right)(-i\sigma_y)\underbrace{i\sigma_y\left((\mathbf{b}_\perp - k\boldsymbol{\alpha}_\perp)\cdot\boldsymbol{\sigma}_\perp^*\right)(-i\sigma_y)}i\sigma_y\begin{pmatrix} c_{-k\uparrow}^\dagger \\ c_{-k\downarrow}^\dagger\end{pmatrix} + \\
&+\frac{1}{2}\sum_k \left(\Delta_k c_{k\uparrow}^\dagger c_{-k\downarrow}^\dagger + \Delta_k^* c_{-k\downarrow}c_{k\uparrow}\right) - \frac{1}{2}\sum_k\left(\Delta_{-k} c_{k\downarrow}^\dagger c_{-k\uparrow}^\dagger + \Delta_{-k}^* c_{-k\uparrow}c_{k\downarrow}\right) = \\
&[\text{use } \sigma_y\boldsymbol{\sigma}_\perp^*\sigma_y = -\boldsymbol{\sigma}_\perp] \\
= &-\frac{1}{2}\sum_k \left(c_{k\uparrow}^\dagger, c_{k\downarrow}^\dagger\right)\left((\mathbf{b}_\perp + k\boldsymbol{\alpha}_\perp)\cdot\boldsymbol{\sigma}_\perp\right)\begin{pmatrix} c_{k\uparrow} \\ c_{k\downarrow}\end{pmatrix} + \\
&-\frac{1}{2}\sum_k \left(c_{-k\downarrow}, -c_{-k\uparrow}\right)\left((\mathbf{b}_\perp - k\boldsymbol{\alpha}_\perp)\cdot\boldsymbol{\sigma}_\perp\right)\begin{pmatrix} c_{-k\downarrow}^\dagger \\ -c_{-k\uparrow}^\dagger\end{pmatrix} + \\
&+\frac{1}{2}\sum_k \left(\Delta_k c_{k\uparrow}^\dagger c_{-k\downarrow}^\dagger + \Delta_k^* c_{-k\downarrow}c_{k\uparrow}\right) - \frac{1}{2}\sum_k\left(\Delta_{-k} c_{k\downarrow}^\dagger c_{-k\uparrow}^\dagger + \Delta_{-k}^* c_{-k\uparrow}c_{k\downarrow}\right)
\end{aligned} \tag{3.24}$$

Recalling now the definition (3.5) of the Nambu spinor, and the s-wave character of the pairing Δ_k, we can rewrite $\mathcal{H}_{off-diag}$ as

$$\mathcal{H}_{off-diag} = \frac{1}{2}\sum_k \Psi_k^\dagger \begin{pmatrix} -(k\boldsymbol{\alpha}_\perp + \mathbf{b}_\perp)\cdot\boldsymbol{\sigma}_\perp & \Delta_0 e^{i\varphi} \\ \Delta_0 e^{-i\varphi} & (k\boldsymbol{\alpha}_\perp - \mathbf{b}_\perp)\cdot\boldsymbol{\sigma}_\perp\end{pmatrix}\Psi_k \tag{3.25}$$

By summing up the two results (3.18) and (3.25), the total Hamiltonian $\mathcal{H} = \mathcal{H}_{diag} + \mathcal{H}_{nondiag}$ acquires the form (3.6).

End of proof.

3.2 The case of magnetic field parallel to the spin-orbit field

Let us consider the case where the spin-orbit coupling $\boldsymbol{\alpha}$ and the magnetic field $\mathbf{b}$ are parallel. Without any loss in generality, we can assume that both these fields point along the z-direction.

$$\boldsymbol{\alpha} = (0,0,\alpha_z) \tag{3.26}$$
$$\mathbf{b} = (0,0,b_z) \tag{3.27}$$

The Bogolubov de Gennes Hamiltonian (3.6) reduces to

$$H_{BdG}(k) = \begin{pmatrix} \xi_k^0\sigma_0 - k\alpha_z\sigma_z - b_z\sigma_z & \Delta_0 e^{i\varphi}\sigma_0 \\ \Delta_0 e^{-i\varphi}\sigma_0 & -\xi_k^0\sigma_0 + k\alpha_z\sigma_z - b_z\sigma_z\end{pmatrix} \tag{3.28}$$

Let us introduce the electron bands for spin-↑ and spin-↓ electrons

$$\begin{cases} \xi_{k\uparrow} &= \varepsilon_k^0 - \mu - \alpha_z k - b_z &= \xi_k^0 - \alpha_z k - b_z \\ \xi_{k\downarrow} &= \varepsilon_k^0 - \mu + \alpha_z k + b_z &= \xi_k^0 + \alpha_z k + b_z \end{cases} , \tag{3.29}$$

with ξ_k^0 given by Eq.(3.2). The band dispersions $\xi_{k\uparrow}$ and $\xi_{k\downarrow}$ are plotted in Fig. 3.2.

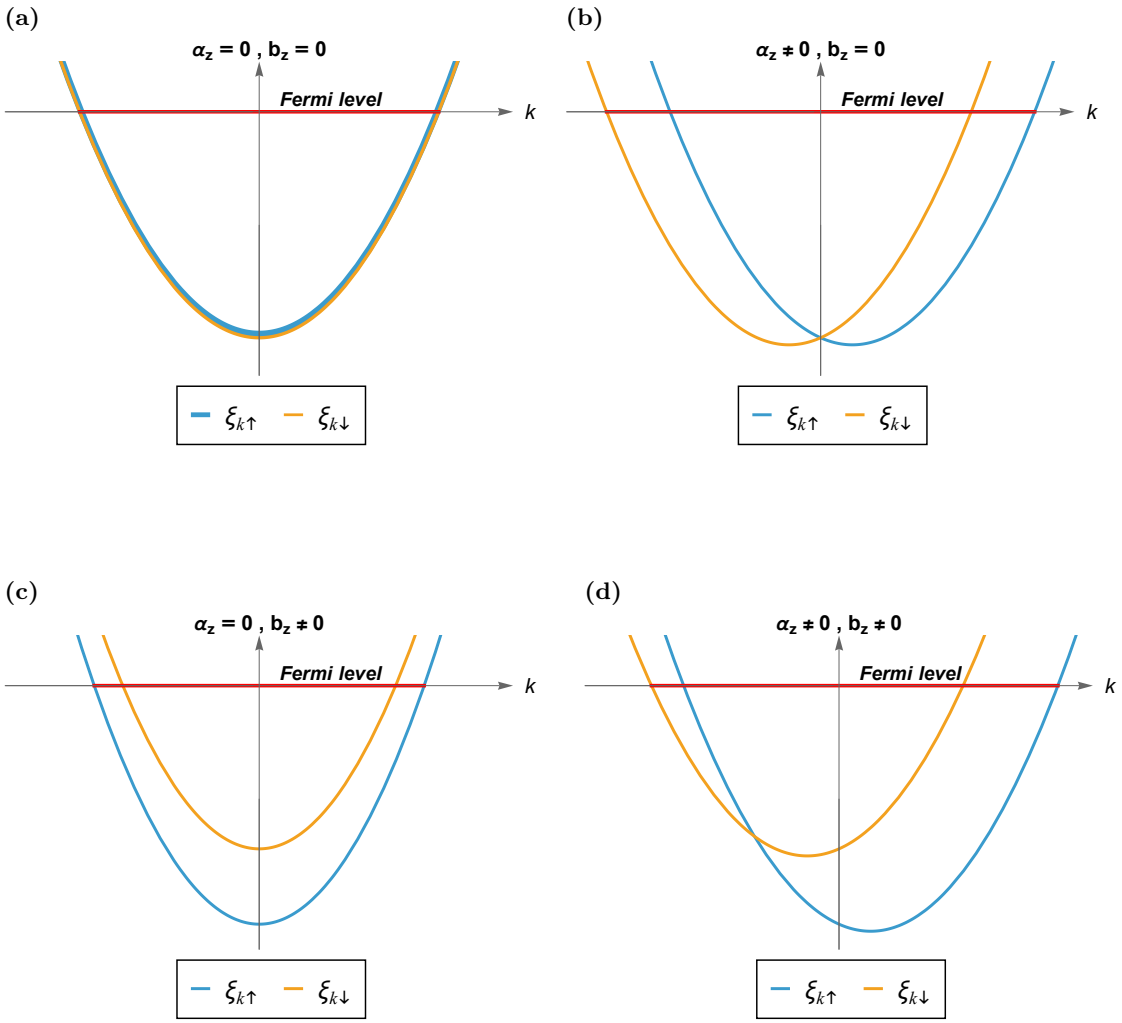

Figure 3.2: Plots of $\xi_{k\uparrow}$ and $\xi_{k\downarrow}$, defined in Eqs.(3.29), for different values of the parameters α_z and b_z. In particular: Panel (a) the doubly degenerate dispersion relation in the absence of SOC and magnetic field; (b) the degeneracy is broken by the SOC and the bands are shifted horizontally; Panel (c) an applied magnetic field open a gap between the two energy branches; (d) the combined effect of the SOC and magnetic field.

The Hamiltonian (3.28) acquires the form

$$H_{BdG}(k) = \begin{pmatrix} \xi_{k\uparrow} & 0 & \Delta_0 e^{i\varphi} & 0 \\ 0 & \xi_{k\downarrow} & 0 & \Delta_0 e^{i\varphi} \\ \Delta_0 e^{-i\varphi} & 0 & -\xi_{-k\downarrow} & 0 \\ 0 & \Delta_0 e^{-i\varphi} & 0 & -\xi_{-k\uparrow} \end{pmatrix} \tag{3.30}$$

where $\xi_{k\sigma}$ are defined in Eqs.(3.29).
We observe that in this case the Bogolubov de Gennes Hamiltonian (3.30) consists of two decoupled 2×2 blocks, related to (1,3) and (2,4) entries, defined as

1. **block (1,3)**

$$h^{(1)}(k) = \begin{pmatrix} \xi_{k\uparrow} & \Delta_0\, e^{i\varphi} \\ \Delta_0\, e^{-i\varphi} & -\xi_{-k\downarrow} \end{pmatrix} = \begin{pmatrix} \xi_k^0 - \alpha_z k - b_z & \Delta_0\, e^{i\varphi} \\ \Delta_0\, e^{-i\varphi} & -(\xi_k^0 - \alpha_z k) - b_z \end{pmatrix} \tag{3.31}$$

2. **block (2,4)**

$$h^{(2)}(k) = \begin{pmatrix} \xi_{k\downarrow} & \Delta_0\, e^{i\varphi} \\ \Delta_0\, e^{-i\varphi} & -\xi_{-k\uparrow} \end{pmatrix} = \begin{pmatrix} \xi_k^0 + \alpha_z k + b_z & \Delta_0\, e^{i\varphi} \\ \Delta_0\, e^{-i\varphi} & -(\xi_k^0 + \alpha_z k) + b_z \end{pmatrix} \tag{3.32}$$

where ξ_k^0 is defined in Eq.(3.2). In particular, it is possible to verify that the relation (3.10) between $h_h(k)$ and $h_e(k)$ is valid also for $h^{(1)}(k)$ and $h^{(2)}(k)$ i.e.

$$\sigma_y \left(h^{(1)}(-k)\right)^* \sigma_y = -h^{(2)}(k) \tag{3.33}$$

As we shall see here below, the blocks (1,3) and (2,4) can be interpreted as

$$\begin{cases} \text{block (1,3)} & \rightarrow & \text{block of spin-}\uparrow\text{ excitations} \\ \\ \text{block (2,4)} & \rightarrow & \text{block of spin-}\downarrow\text{ excitations} \end{cases} \tag{3.34}$$

Let us first proceed by diagonalizing matrices (3.31 and (3.32). In order to do it, we shall make use of the following theorem.

Theorem 3.1. *For any eigenvector $w_k^{(1,2)}$ with eigenvalues $E_k^{(1,2)}$ of the 2×2 Hermitian matrices $h^{(1,2)}(k)$ defined in eq.(3.31) and in eq (3.32), then the vectors $-i\,\sigma_y (w_{-k}^{(1,2)})^*$ are eigenvectors of $h^{(2,1)}(k)$, with eigenvalues $E_k^{(2,1)} = -E_{-k}^{(1,2)}$.*

Proof. For simplicity, let us proceed by proving Theorem (3.1) for an eigenvector $w_k^{(1)}$ of $h^{(1)}(k)$. Proof for an eigenvector $w_k^{(2)}$ of $h^{(2)}(k)$ follows similar lines.
Let us start by noting that, if $w_k^{(1)}$ is an eigenvector for $h^{(1)}(k)$, with eigenvalue $E_k^{(1)}$, i.e. $h^{(1)}(k)\, w_k^{(1)} = E_k^{(1)} w_k^{(1)}$, then, taking the complex conjugate of the previous expression, we obtain

$$\left(h^{(1)}(k)\, w_k^{(1)}\right)^* = E_k^{(1)} (w_k^{(1)})^* \tag{3.35}$$

By applying the matrix identity (3.33) on vector $i\,\sigma_y(w^{(1)}_{-k})^*$ it follows that

$$i\,\sigma_y\left(h^{(1)}(-k)\,w^{(1)}_{-k}\right)^* = -i\,h^{(2)}(k)\,\sigma_y(w^{(1)}_{-k})^*$$

Using now eq (3.35) we obtain that

$$i\sigma_y\,E^{(1)}_{-k}(w^{(1)}_{-k})^* = -i\,h^{(2)}(k)\,\sigma_y(w^{(1)}_{-k})^*,$$

i.e.

$$h^{(2)}(k)\left[-i\sigma_y(w^{(1)}_{-k})^*\right] = -E^{(1)}_{-k}\left[-i\,\sigma_y(w^{(1)}_{-k})^*\right] \tag{3.36}$$

which proves that $-i\,\sigma_y(w^{(1)}_{-k})^*$ is an eigenvector of $h^{(2)}(k)$ with eigenvalue $E^{(2)}_k = -E^{(1)}_{-k}$.

End of proof. □

Theorem 3.2. *Within each block, the eigevectors are independent of the value of* b_z.

Proof. This is simply because, within each block (3.31) and (3.32), b_z multiplies the 2×2 identity matrix.

□

The case of a Normal nanowire ($\Delta_0 = 0$)

The case of a Normal, i.e. non-superconducting, nanowire is obtained by removing the superconducting pairing, i.e. by setting $\Delta_k \equiv 0$. Then, the, matrix (3.30) acquires a diagonal form, i.e.

$$H_{BdG}(k) = \begin{pmatrix} \xi_{k\uparrow} & 0 & 0 & 0 \\ 0 & \xi_{k\downarrow} & 0 & 0 \\ 0 & 0 & -\xi_{-k\downarrow} & 0 \\ 0 & 0 & 0 & -\xi_{-k\uparrow} \end{pmatrix} \tag{3.37}$$

and the Hamiltonian $\mathcal{H}$ reads

$$\mathcal{H} = \frac{1}{2}\sum_k \left(\xi_{k\uparrow}c^\dagger_{k\uparrow}c_{k\uparrow} + \xi_{k\downarrow}c^\dagger_{k\downarrow}c_{k\downarrow} - \xi_{-k\uparrow}c_{-k\uparrow}c^\dagger_{-k\uparrow} - \xi_{-k\downarrow}c_{-k\downarrow}c^\dagger_{-k\downarrow}\right) + C \tag{3.38}$$

where $\xi_{k\sigma}$ is defined in Eqs.(3.29) and the constant C is given by Eq.(3.7).
The Hamiltonian (3.38) can be rewritten in terms of excitation operators $\gamma_{k\sigma}$, as follows. First, we rewrite

$$\xi_{k\sigma} = |\xi_{k\sigma}|\vartheta(\xi_{k\sigma}) - |\xi_{k\sigma}|\vartheta(-\xi_{k\sigma}) \qquad\qquad \sigma = \uparrow,\downarrow \tag{3.39}$$

where $\vartheta(\cdot)$ represents the Heaviside step function.
Then, we re-express the fermion operators $c_{k\sigma}$ in terms of excitation operators $\gamma_{k\sigma\eta}$, as follows

$$c_{k\uparrow} = \begin{cases} \gamma_{k\uparrow e} & \text{if} \quad \xi_{k\uparrow} > 0 \\ \gamma^\dagger_{-k\downarrow h} & \text{if} \quad \xi_{k\uparrow} < 0 \end{cases} \tag{3.40}$$

$$c_{k\downarrow} = \begin{cases} \gamma_{k\downarrow e} & \text{if} \quad \xi_{k\downarrow} > 0 \\ \gamma^\dagger_{-k\uparrow h} & \text{if} \quad \xi_{k\downarrow} < 0 \end{cases} \tag{3.41}$$

where e and h describe electron and hole excitation, respectively. Inserting Eqs.(3.39), (3.40), and (3.41) into Eq.(3.38), the Hamiltonian is rewritten as (proof given below)

$$\begin{aligned}\mathcal{H} &= \sum_k \Big[E^e_{k\uparrow}\left(\gamma^\dagger_{k\uparrow e}\gamma_{k\uparrow e} - \frac{1}{2}\right) + E^h_{k\uparrow}\left(\gamma^\dagger_{k\uparrow h}\gamma_{k\uparrow h} - \frac{1}{2}\right) + \\ &\quad + E^e_{k\downarrow}\left(\gamma^\dagger_{k\downarrow e}\gamma_{k\downarrow e} - \frac{1}{2}\right) + E^h_{k\downarrow}\left(\gamma^\dagger_{k\downarrow h}\gamma_{k\downarrow h} - \frac{1}{2}\right)\Big] + \sum_k \xi^0_k \end{aligned} \tag{3.42}$$

where

$$\begin{aligned} E^e_{k\uparrow} &= |\xi_{k\uparrow}|\vartheta(\xi_{k\uparrow}) > 0 && \text{spin-}\uparrow \text{ excitations (electron type)} \\ E^h_{k\uparrow} &= |\xi_{-k\downarrow}|\vartheta(-\xi_{-k\downarrow}) > 0 && \text{spin-}\uparrow \text{ excitations (hole type)} \\ E^e_{k\downarrow} &= |\xi_{k\downarrow}|\vartheta(\xi_{k\downarrow}) > 0 && \text{spin-}\downarrow \text{ excitations (electron type)} \\ E^h_{k\downarrow} &= |\xi_{-k\uparrow}|\vartheta(-\xi_{-k\uparrow}) > 0 && \text{spin-}\downarrow \text{ excitations (hole type)} \end{aligned} \tag{3.43}$$

Proof of Eq.(3.42):
Inserting Eqs.(3.39), (3.40), and (3.41) into Eq.(3.38) one obtains

$$\begin{aligned}\mathcal{H} =& \sum_k \xi^0_k + \frac{1}{2}\sum_k \Big[\Big(|\xi_{k\uparrow}|\vartheta(\xi_{k\uparrow}) - |\xi_{k\uparrow}|\vartheta(-\xi_{k\uparrow})\Big)c^\dagger_{k\uparrow}c_{k\uparrow} + \\ &+ \Big(|\xi_{k\downarrow}|\vartheta(\xi_{k\downarrow}) - |\xi_{k\downarrow}|\vartheta(-\xi_{k\downarrow})\Big)c^\dagger_{k\downarrow}c_{k\downarrow} + \\ &- \Big(|\xi_{-k\uparrow}|\vartheta(\xi_{-k\uparrow}) - |\xi_{-k\uparrow}|\vartheta(-\xi_{-k\uparrow})\Big)c_{-k\uparrow}c^\dagger_{-k\uparrow} + \\ &+ \Big(|\xi_{-k\downarrow}|\vartheta(\xi_{-k\downarrow}) - |\xi_{-k\downarrow}|\vartheta(-\xi_{-k\downarrow})\Big)c_{-k\downarrow}c^\dagger_{-k\downarrow}\Big] = \\ =& \sum_k \xi^0_k + \frac{1}{2}\sum_k \Big[|\xi_{k\uparrow}|\vartheta(\xi_{k\uparrow})\gamma^\dagger_{k\uparrow e}\gamma_{k\uparrow e} - |\xi_{k\uparrow}|\vartheta(-\xi_{k\uparrow})\gamma_{-k\downarrow h}\gamma^\dagger_{-k\downarrow h} + \\ &+ |\xi_{k\downarrow}|\vartheta(\xi_{k\downarrow})\gamma^\dagger_{k\downarrow e}\gamma_{k\downarrow e} - |\xi_{k\downarrow}|\vartheta(-\xi_{k\downarrow})\gamma^\dagger_{-k\uparrow h}\gamma_{-k\uparrow h} + \\ &- |\xi_{-k\uparrow}|\vartheta(\xi_{-k\uparrow})\gamma_{-k\uparrow e}\gamma^\dagger_{-k\uparrow e} + |\xi_{-k\uparrow}|\vartheta(-\xi_{-k\uparrow})\gamma^\dagger_{k\downarrow h}\gamma_{k\downarrow h} + \\ &- |\xi_{-k\downarrow}|\vartheta(\xi_{-k\downarrow})\gamma_{-k\downarrow e}\gamma^\dagger_{-k\downarrow e} + |\xi_{-k\downarrow}|\vartheta(-\xi_{-k\downarrow})\gamma^\dagger_{k\uparrow h}\gamma_{k\uparrow h}\Big] = \\ =& \sum_k \xi^0_k + \frac{1}{2}\sum_k \Big[|\xi_{k\uparrow}|\vartheta(\xi_{k\uparrow})\left(\gamma^\dagger_{k\uparrow e}\gamma_{k\uparrow e} - \gamma_{k\uparrow e}\gamma^\dagger_{k\uparrow e}\right) + \\ &+ |\xi_{-k\downarrow}|\vartheta(-\xi_{-k\downarrow})\left(\gamma^\dagger_{k\uparrow h}\gamma_{k\uparrow h} - \gamma_{k\uparrow h}\gamma^\dagger_{k\uparrow h}\right) + \\ &+ |\xi_{k\downarrow}|\vartheta(\xi_{k\downarrow})\left(\gamma^\dagger_{k\downarrow e}\gamma_{k\downarrow e} - \gamma_{k\downarrow e}\gamma^\dagger_{k\downarrow e}\right) + \\ &+ |\xi_{-k\uparrow}|\vartheta(-\xi_{-k\uparrow})\left(\gamma^\dagger_{k\downarrow h}\gamma_{k\downarrow h} - \gamma_{k\downarrow h}\gamma^\dagger_{k\downarrow h}\right) \end{aligned}$$

$$
\begin{aligned}
=&\sum_k \xi_k^0 \;+\; \sum_k \Big[|\xi_{k\uparrow}|\vartheta(\xi_{k\uparrow}) \left(\gamma^\dagger_{k\uparrow e}\gamma_{k\uparrow e} - \frac{1}{2}\right) \;+\; |\xi_{-k\downarrow}|\vartheta(-\xi_{-k\downarrow}) \left(\gamma^\dagger_{k\uparrow h}\gamma_{k\uparrow h} - \frac{1}{2}\right) \;+ \\
&\qquad + |\xi_{k\downarrow}|\vartheta(\xi_{k\downarrow}) \left(\gamma^\dagger_{k\downarrow e}\gamma_{k\downarrow e} - \frac{1}{2}\right) + |\xi_{-k\uparrow}|\vartheta(-\xi_{-k\uparrow}) \left(\gamma^\dagger_{k\downarrow h}\gamma_{k\downarrow h} - \frac{1}{2}\right)\Big] \\
=&\sum_k \xi_k^0 \;+\; \sum_k \Big[E^e_{k\uparrow} \left(\gamma^\dagger_{k\uparrow e}\gamma_{k\uparrow e} - \frac{1}{2}\right) \;+\; E^h_{k\uparrow} \left(\gamma^\dagger_{k\uparrow h}\gamma_{k\uparrow h} - \frac{1}{2}\right) \;+ \\
&\qquad + E^e_{k\downarrow} \left(\gamma^\dagger_{k\downarrow e}\gamma_{k\downarrow e} - \frac{1}{2}\right) + E^h_{k\downarrow} \left(\gamma^\dagger_{k\downarrow h}\gamma_{k\downarrow h} - \frac{1}{2}\right)\Big]
\end{aligned}
\tag{3.44}
$$

End of proof.

- **Ground state energy**
  The fact that the energies (3.43) are by definition *positive*, enables us to evaluate the ground state energy E_0, and to interpret also the excitations above the ground state. Indeed, for every k-state, the lower energy is obtained for $\langle \gamma^\dagger_{k\sigma\eta}\gamma_{k\sigma\eta}\rangle = 0$, yielding a ground state energy contribution $-\frac{E^\eta_{k\sigma}}{2} < 0$, while the higher energy is obtained when $\langle \gamma^\dagger_{k\sigma\eta}\gamma_{k\sigma\eta}\rangle = 1$, yielding an excited state with energy $\frac{E^\eta_{k\sigma}}{2} > 0$. As a consequence, the ground state energy is

$$
E_0 = -\frac{1}{2}\sum_k \sum_{\sigma=\uparrow,\downarrow} \sum_{\eta=e,h} E^\eta_{k\sigma} \;+\frac{1}{2}\sum_{k,\sigma} \xi_{k\sigma} \tag{3.45}
$$

  Inserting Eq.(3.43) into Eq.(3.45), and using Eq.(3.39), one can prove that (proof given below)

$$
E_0 = -\sum_{\xi_{k,\sigma}<0} |\xi_{k,\sigma}| \tag{3.46}
$$

  Proof of Eq.(3.46):
  Inserting Eq.(3.43) into Eq.(3.45), and using Eq.(3.39), one obtains

$$
\begin{aligned}
E_0 =& -\frac{1}{2}\sum_{k,\sigma,\eta} E^\eta_{k\sigma} + \frac{1}{2}\sum_{k,\sigma}\xi_{k\sigma} = \\
=& -\frac{1}{2}\sum_k \Big[|\xi_{k\uparrow}|\vartheta(\xi_{k\uparrow}) + |\xi_{-k\downarrow}|\vartheta(-\xi_{-k\downarrow}) + |\xi_{k\downarrow}|\vartheta(\xi_{k\downarrow}) + |\xi_{-k\uparrow}|\vartheta(-\xi_{-k\uparrow})\Big] + \\
&+\frac{1}{2}\sum_k \Big[|\xi_{k\uparrow}|\vartheta(\xi_{k\uparrow}) - |\xi_{k\uparrow}|\vartheta(-\xi_{k\uparrow}) + |\xi_{k\downarrow}|\vartheta(\xi_{k\downarrow}) - |\xi_{k\downarrow}|\vartheta(-\xi_{k\downarrow})\Big] = \\
=& -\frac{1}{2}\sum_k 2\Big[|\xi_{k,\uparrow}|\vartheta(-\xi_{k\uparrow}) + |\xi_{k,\downarrow}|\vartheta(-\xi_{k\downarrow})\Big] = \\
=& -\sum_{\xi_{k,\sigma}<0} |\xi_{k,\sigma}|
\end{aligned}
\tag{3.47}
$$

  End of proof.

- **Fermi wavevectors**
  Taking into account the expressions (3.29), we can re-express Eq.(3.46) by identifying the Fermi wavevectors, i.e. the wavevectors at which $\xi_{k\sigma}$'s vanish. They are given by:

$$k_{F\uparrow}^{(\pm)} = \sigma_\alpha k_{SO} \pm \sqrt{k_{SO}^2 + (k_{F\uparrow}^0)^2} \tag{3.48}$$

$$k_{F\downarrow}^{(\pm)} = -\sigma_\alpha k_{SO} \pm \sqrt{k_{SO}^2 + (k_{F\downarrow}^0)^2} \tag{3.49}$$

  where we have defined

$$k_{SO} = \frac{m^*|\alpha_z|}{\hbar^2} \quad \text{(spin-orbit wavevector)} \tag{3.50}$$

$$\sigma_\alpha = \text{sign}(\alpha_z) \quad \text{(spin-orbit coupling sign)} \tag{3.51}$$

$$k_{F\uparrow}^0 = \frac{\sqrt{2m^*(\mu + b_z)}}{\hbar} \quad \text{(bare spin-}\uparrow\text{ Fermi wavevector)} \tag{3.52}$$

$$k_{F\downarrow}^0 = \frac{\sqrt{2m^*(\mu - b_z)}}{\hbar} \quad \text{(bare spin-}\downarrow\text{ Fermi wavevector)} \tag{3.53}$$

  as it is possible to appreciate in Fig.3.3, where the "$k_F^{(\pm)}$" points are the ones for which the parabolas intersect the Fermi level.

- **Excitations**
  Taking into account the expression (3.42) of the Hamiltonian, and the fact that the ground state is obtained for $\langle \gamma_{k\sigma\eta}^\dagger \gamma_{k\sigma\eta} \rangle = 0$, we also deduce that, for each (k, σ, η), the difference between the higher and the lower energy state is $E_{k\sigma\eta}$, which can therefore be interpreted as the *excitation* energy over the GS. Concerning the nature of such excitations, the structure of Hamiltonian (3.42) and the definition (3.41) of the fermionic operators in terms of excitation operators γ, straightforward implies that by applying the operators $\gamma_{k\sigma\eta}^\dagger$ on the ground state, four different excitation processes are possible.

  1. **spin-↑ excitation of electron type**
     This occur for $\xi_{k\uparrow} > 0$ (i.e. for $k < k_{F\uparrow}^{(-)}$ or $k > k_{F\uparrow}^{(+)}$). In this case $\gamma_{k\uparrow e}^\dagger = c_{k\uparrow}^\dagger$, i.e. one creates a spin-↑ "electron" excitation, depicted by solid blue curves in Fig.3.3;
  2. **spin-↑ excitation of hole type**
     It occurs when $\xi_{-k\downarrow} < 0$ (i.e. for $k \in [k_{F\downarrow}^{(-)}, k_{F\downarrow}^{(+)}]$). In this case $\gamma_{k\uparrow h}^\dagger = c_{-k\downarrow}$, which corresponds to removing from the GS an electron with spin-↓ and momentum $-k$, which means that we are creating a spin-↑ "hole" excitation, depicted by dashed blue curves in Fig.3.3;
  3. **spin-↓ excitation of electron type**
     This is when $\xi_{k\downarrow} > 0$ (i.e. for $k < k_{F\downarrow}^{(-)}$ or $k > k_{F\downarrow}^{(+)}$). In this case, $\gamma_{k\downarrow e}^\dagger = c_{k\downarrow}^\dagger$. This excitation corresponds to creating a spin-↓ "electron" excitation, depicted by solid yellow curves in Fig.3.3;
  4. **spin-↓ excitation of hole type**
     This excitation occurs for $\xi_{-k\uparrow} < 0$ (i.e. for $k \in [k_{F\uparrow}^{(-)}, k_{F\uparrow}^{(+)}]$), then $\gamma_{k\downarrow h}^\dagger = c_{-k\uparrow}$.

In this case one removes from the GS an electron with spin-↑ and momentum $-k$, which means that we are creating a spin-↓ "hole" excitation, depicted by dashed yellow curves in Fig.3.3.

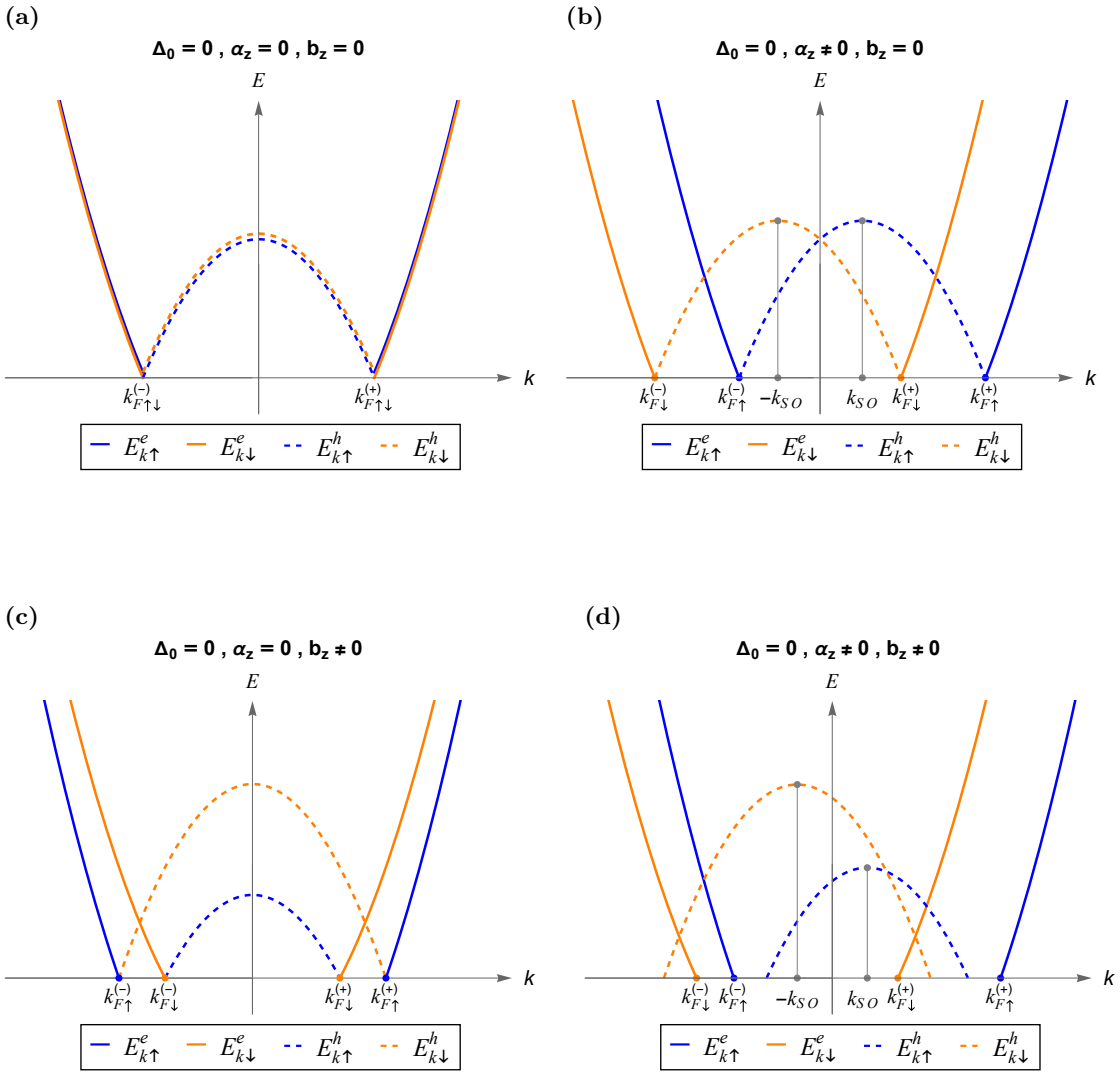

Figure 3.3: The spectrum of the excitation energies of a Normal nanowire ($\Delta_0 = 0$) plotted as a function of k for various values of the parameters α_z and b_z. The spectrum consists of four excitation bands [see Eq.(3.43)], related to two spin degrees of freedom and to the electron/hole character. Compare with the spectrum of Fig.3.2.

The case $\Delta_0 > 0$

When $\Delta_0 > 0$, a superconducting state may appear in the system. Then, let us proceed by diagonalizing the matrix $h^{(1)}(k)$ in Eq.(3.30). In order to do it, we start by computing

the eigenvalues of matrix (3.31). Denoting by $E^{(1)}_{k,+}$ and $E^{(2)}_{k,+}$ the eigenvalues of matrix $h^{(1)}(k)$, we obtain that

$$\begin{aligned} E^{(1)}_{k,+} &= -b_z + \sqrt{\left(\xi^0_k - \alpha_z k\right)^2 + \Delta_0^2} \\ E^{(1)}_{k,-} &= -b_z - \sqrt{\left(\xi^0_k - \alpha_z k\right)^2 + \Delta_0^2} \end{aligned} \tag{3.54}$$

Let us notice that, as a consequence of theorem (3.2), the eigenvectors of matrix (3.31) are the same as the eigenvectors of the following matrix

$$\tilde{h}^{(1)}(k) = \begin{pmatrix} \xi^0_k - \alpha_z k & \Delta_0\, e^{i\varphi} \\ \Delta_0\, e^{-i\varphi} & -(\xi^0_k - \alpha_z k) \end{pmatrix} \tag{3.55}$$

which satisfy the requirements of theorem 2.1. Therefore, we may make use of the latter to compute the eigenvectors of matrix (3.31). It follows that

$$\begin{aligned} w^{(1)}_{k,+} &= \begin{pmatrix} u_k \\ v_k \end{pmatrix} \qquad \text{eigenvalue } E^{(1)}_{k,+} \\ w^{(1)}_{k,-} &= \begin{pmatrix} -v^*_k \\ u^*_k \end{pmatrix} \qquad \text{eigenvalue } E^{(1)}_{k,-} \end{aligned} \tag{3.56}$$

where

$$\begin{aligned} u_k &= \sqrt{\frac{1}{2}\left(1 + \frac{\xi^0_k - \alpha_z k}{\sqrt{(\xi^0_k - \alpha_z k)^2 + \Delta_0^2}}\right)} \\ v_k &= e^{-i\varphi}\sqrt{\frac{1}{2}\left(1 - \frac{\xi^0_k - \alpha_z k}{\sqrt{(\xi^0_k - \alpha_z k)^2 + \Delta_0^2}}\right)} \end{aligned} \tag{3.57}$$

A similar remark holds for the diagonalization of the matrix $h^{(2)}(k)$ in Eq.(3.32). However, in order to diagonalize $h^{(2)}(k)$, we may also make use of theorem 3.1, obtaining eigenvectors and eigenvalues of $h^{(2)}(k)$ from the eigenvectors and eigenvalues of $h^{(1)}(k)$ in Eq.(3.31) as follows

$$-i\sigma_y \left(w^{(1)}_{-k,-}\right)^* = \begin{pmatrix} -u_{-k} \\ -v_{-k} \end{pmatrix} \quad \text{is eigenvector of } h^{(2)}(k) \text{ with eigenvalue } \; E^{(2)}_{k,+} = -E^{(1)}_{-k,-} \tag{3.58}$$

$$-i\sigma_y \left(w^{(1)}_{-k,+}\right)^* = \begin{pmatrix} -v^*_{-k} \\ u^*_{-k} \end{pmatrix} \quad \text{is eigenvector of } h^{(2)}(k) \text{ with eigenvalue } \; E^{(2)}_{k,-} = -E^{(1)}_{-k,+}$$

Since we always have the freedom of redefining such obtained eigenvectors by an overall phase factor, we shall denote

$$\begin{aligned} w^{(2)}_{k,+} &= \begin{pmatrix} u_{-k} \\ v_{-k} \end{pmatrix} \qquad \text{eigenvector of } h^{(2)}(k) \text{ with eigenvalue } E^{(2)}_{k,+} \\ w^{(2)}_{k,-} &= \begin{pmatrix} -v^*_{-k} \\ u^*_{-k} \end{pmatrix} \qquad \text{eigenvector of } h^{(2)}(k) \text{ with eigenvalue } E^{(2)}_{k,-} \end{aligned} \tag{3.59}$$

where

$$\begin{aligned} E^{(2)}_{k,+} &= -E^{(1)}_{-k,-} = b_z + \sqrt{\left(\xi^0_k + \alpha_z k\right)^2 + \Delta_0^2} \\ E^{(2)}_{k,-} &= -E^{(1)}_{-k,+} = b_z - \sqrt{\left(\xi^0_k + \alpha_z k\right)^2 + \Delta_0^2} \end{aligned} \tag{3.60}$$

Therefore, the diagonal form of matrix (3.30) is

$$H_{BdG-d}\,(k) = \begin{pmatrix} E^{(1)}_{k,+} & 0 & 0 & 0 \\ 0 & E^{(2)}_{k,+} & 0 & 0 \\ 0 & 0 & -E^{(2)}_{-k,+} & 0 \\ 0 & 0 & 0 & -E^{(1)}_{-k,+} \end{pmatrix} \tag{3.61}$$

and the four orthonormal eigenvectors $\mathsf{w}^{(1)}_{k,+}$, $\mathsf{w}^{(2)}_{k,+}$, $\mathsf{w}^{(1)}_{k,-}$ and $\mathsf{w}^{(2)}_{k,-}$ for the full 4×4 matrix are

$$\mathsf{w}^{(1)}_{k,+} = \begin{pmatrix} u_k \\ 0 \\ v_k \\ 0 \end{pmatrix} \quad \mathsf{w}^{(2)}_{k,+} = \begin{pmatrix} 0 \\ u_{-k} \\ 0 \\ v_{-k} \end{pmatrix} \quad \mathsf{w}^{(1)}_{k,-} = \begin{pmatrix} -v^*_k \\ 0 \\ u^*_k \\ 0 \end{pmatrix} \quad \mathsf{w}^{(2)}_{k,-} = \begin{pmatrix} 0 \\ -v^*_{-k} \\ 0 \\ u^*_{-k} \end{pmatrix} \tag{3.62}$$

Then, the matrix U_k, such that

$$U^\dagger_k\, H_{BdG}(k)\, U_k = H_{BdG-d}(k) \tag{3.63}$$

acquires the form

$$U_k = \begin{pmatrix} u_k & 0 & -v^*_k & 0 \\ 0 & u_{-k} & 0 & -v^*_{-k} \\ v_k & 0 & u^*_k & 0 \\ 0 & v_{-k} & 0 & u^*_{-k} \end{pmatrix} \tag{3.64}$$

Inverting the above relation (3.63)

$$H_{BdG}(k) = U_k\, H_{BdG-d}(k)\, U^\dagger_k \tag{3.65}$$

and inserting it in Eq.(3.6), we obtain

$$\begin{aligned} \mathcal{H} &= \frac{1}{2}\sum_k \Psi^\dagger_k H_{BdG}\,(k)\,\Psi_k \;+\; C = \frac{1}{2}\sum_k \Psi^\dagger_k U_k H_{BdG-d}\,(k)\,U^\dagger_k \Psi_k \;+\; C \\ &= \frac{1}{2}\sum_k \Gamma^\dagger_k H_{BdG-d}\,(k)\,\Gamma_k \;+\; C \end{aligned} \tag{3.66}$$

where

$$\Gamma_k = U_k^\dagger \Psi_k \quad \text{and} \quad \Gamma_k^\dagger = \Psi_k^\dagger U_k \tag{3.67}$$

and Ψ_k is given by Eq.(3.5).
Assigning to Γ_k the same structure of spinor (3.68), i.e.

$$\Gamma_k = \begin{pmatrix} \tilde{\gamma}_{k\uparrow} \\ \tilde{\gamma}_{k\downarrow} \\ \tilde{\gamma}^\dagger_{-k\downarrow} \\ -\tilde{\gamma}^\dagger_{-k\uparrow} \end{pmatrix} \tag{3.68}$$

it follows that

$$\Gamma_k = \begin{pmatrix} u_k^* c_{k\uparrow} + v_k^* c^\dagger_{-k\downarrow} \\ +u^*_{-k} c_{k\downarrow} - v^*_{-k} c^\dagger_{-k\uparrow} \\ -v_k c_{k\uparrow} + u_k c^\dagger_{-k\downarrow} \\ -v_{-k} c_{k\downarrow} - u_{-k} c^\dagger_{-k\uparrow} \end{pmatrix} \tag{3.69}$$

The expression of $\mathcal{H}$ in terms of γ and $\gamma^\dagger$ is now

$$\mathcal{H} = \frac{1}{2}\sum_k \left(E^{(1)}_{k,+} \tilde{\gamma}^\dagger_{k\uparrow}\tilde{\gamma}_{k\uparrow} + E^{(2)}_{k,+}\tilde{\gamma}^\dagger_{k\downarrow}\tilde{\gamma}_{k\downarrow} - E^{(2)}_{-k,+}\tilde{\gamma}_{-k\downarrow}\tilde{\gamma}^\dagger_{-k\downarrow} - E^{(1)}_{-k,+}\tilde{\gamma}_{-k\uparrow}\tilde{\gamma}^\dagger_{-k\uparrow} \right) + C. \tag{3.70}$$

where the constant C is given in Eq.(3.7). Using Eq.(2.35) and relabeling the summation index $-k \rightarrow k$, the final form is

$$\begin{aligned} \mathcal{H} &= \frac{1}{2}\sum_k \left(2\,\xi^0_k - E^{(2)}_{k,+} - E^{(1)}_{k,+} \right) + \sum_k \left(E^{(1)}_{k,+}\tilde{\gamma}^\dagger_{k\uparrow}\tilde{\gamma}_{k\uparrow} + E^{(2)}_{k,+}\tilde{\gamma}^\dagger_{k\downarrow}\tilde{\gamma}_{k\downarrow} \right) = \\ &= \sum_k \xi^0_k + \sum_k \left\{ E^{(1)}_{k,+}\left(\tilde{\gamma}^\dagger_{k\uparrow}\tilde{\gamma}_{k\uparrow} - \frac{1}{2} \right) + E^{(2)}_{k,+}\left(\tilde{\gamma}^\dagger_{k\downarrow}\tilde{\gamma}_{k\downarrow} - \frac{1}{2} \right) \right\} \end{aligned} \tag{3.71}$$

Excitations
It is important to point out that, differently from the standard BCS case covered in chapter 2, here the energy $E^{(1)}_{k,+}$ and $E^{(2)}_{k,+}$, defined in Eqs.(3.54) and (3.60) respectively, may not be positive $\forall\, k$, due to the presence of the magnetic field b_z. Indeed, depending on the magnitude $|b_z|$ of the Zeeman field one can distinguish two cases:

1. **weak magnetic field** $\Delta_0 > |b_z|$
   In this case one has
   $$E^{(j)}_{k,+} > 0 \qquad \forall k$$
   and $E^{(j)}_{k,+}$ can be correctly interpreted as excitation energies. Indeed the ground state GS is obtained for
   $$\langle \tilde{\gamma}^\dagger_{k\sigma}\tilde{\gamma}_{k\sigma} \rangle = 0 \qquad \forall\, k, \sigma$$

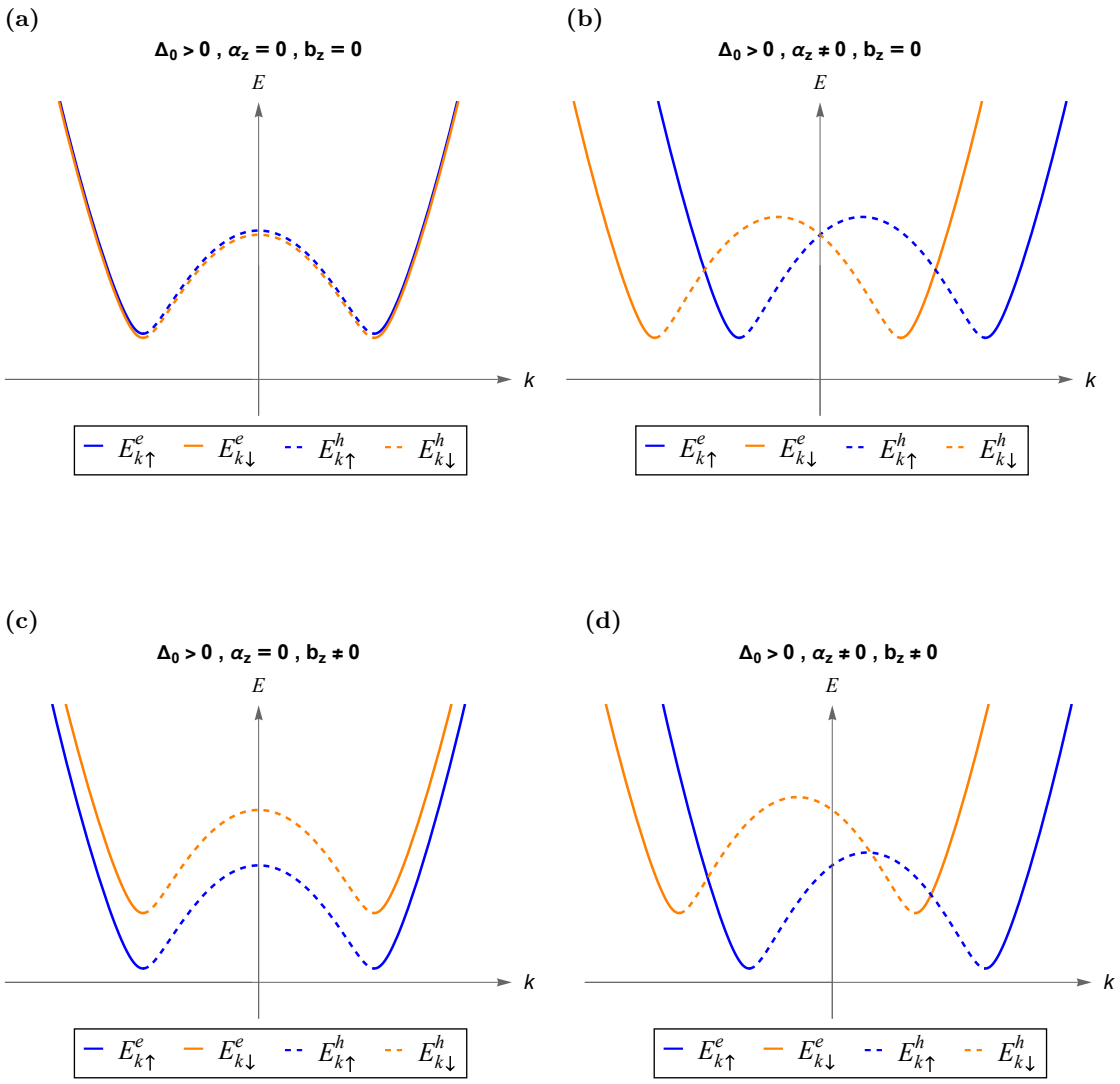

Figure 3.4: The spectrum of excitation energies $E_{k,\uparrow}$ and $E_{k\downarrow}$ of a proximized Nanowire [see Eqs.(3.72)] is plotted as a function of k, for various values of the parameters α and b_z, in the case $|b_z| < \Delta_0$. Solid and dashed lines refer to electron-like and hole-like branches of the excitations, where the quasi-particle operator $\gamma_{k\sigma}$ in Eq.(3.73) exhibits a predominant weight on the particle and in the hole sectors [see Eq.(3.57)]

Then, one can denote

$$\begin{aligned} E_{k\uparrow} &= E^{(1)}_{k,+} = -b_z + \sqrt{\left(\xi^0_k - \alpha_z k\right)^2 + \Delta_0^2} \\ E_{k\downarrow} &= E^{(2)}_{k,+} = +b_z + \sqrt{\left(\xi^0_k + \alpha_z k\right)^2 + \Delta_0^2} \end{aligned} \tag{3.72}$$

and the related excitations

$$\begin{aligned} \gamma_{k\uparrow} &= \tilde{\gamma}_{k,\uparrow} = u^*_k c_{k\uparrow} + v^*_k c^\dagger_{-k\downarrow} \\ \gamma_{k\downarrow} &= \tilde{\gamma}_{k,\downarrow} = u^*_{-k} c_{k\downarrow} - v^*_{-k} c^\dagger_{-k\uparrow} \end{aligned} \tag{3.73}$$

are superpositions of particle and hole states. At a given k, depending on the relative weights of u_k and v_k in Eqs.(3.57), the excitation is dubbed *electron-like* or *hole-like*. The Hamiltonian (3.71) is rewritten as

$$\mathcal{H} = \sum_k \left\{ E_{k,\uparrow} \left(\gamma^\dagger_{k\uparrow}\gamma_{k\uparrow} - \frac{1}{2} \right) + E_{k,\downarrow} \left(\gamma^\dagger_{k\downarrow}\gamma_{k\downarrow} - \frac{1}{2} \right) \right\} + \sum_k \xi^0_k \tag{3.74}$$

In Fig.3.4 the two bands are depicted as a function of k.

2. **strong magnetic field** $\Delta_0 < |b_z|$
In this case the energies $E^{(j)}_{k,+}$ may become negative for some k-values. When this occurs, the superconducting gap closes, and they cannot be interpreted as excitation energies. This means that, for those k-values, in the GS, the expectation value $\langle \tilde{\gamma}^\dagger_{k\uparrow}\tilde{\gamma}_{k\uparrow}\rangle$ is not equal to zero, and such operators do not describe excitations. Indeed, one may have two possible situations:

   (a) $E_{k,+} > 0 \quad \Rightarrow \quad$ GS is obtained for $\langle \tilde{\gamma}^\dagger_{k\sigma}\tilde{\gamma}_{k\sigma}\rangle = 0$, with energy contribution $-\frac{E_k}{2} = -\frac{|E_k|}{2}$

   (b) $E_{k,+} < 0 \quad \Rightarrow \quad$ GS is obtained for $\langle \tilde{\gamma}^\dagger_{k\sigma}\tilde{\gamma}_{k\sigma}\rangle = 1$, with energy contribution $+\frac{E_k}{2} = -\frac{|E_k|}{2}$

This implies that the $\tilde{\gamma}^\dagger_k$ operators appearing in the Hamiltonian (3.71) are related to the actual excitation operators γ_k's through the relation

$$\begin{aligned} E^{(1)}_{k,+} > 0 \;&\Rightarrow\; E^{(1)}_{k,+} = E_{k\uparrow} \;\rightarrow\; \tilde{\gamma}_{k,\uparrow} = \gamma_{k\uparrow} \\ E^{(1)}_{k,+} < 0 \;&\Rightarrow\; E^{(1)}_{k,+} = E_{-k\downarrow} \;\rightarrow\; \tilde{\gamma}_{k,\uparrow} = \gamma^\dagger_{-k\downarrow} \\ E^{(2)}_{k,+} > 0 \;&\Rightarrow\; E^{(2)}_{k,+} = E_{k\downarrow} \;\rightarrow\; \tilde{\gamma}_{k,\uparrow} = \gamma^\dagger_{-k\downarrow} \\ E^{(2)}_{k,+} < 0 \;&\Rightarrow\; E^{(2)}_{k,+} = E_{-k\uparrow} \;\rightarrow\; \tilde{\gamma}_{k,\downarrow} = \gamma^\dagger_{-k\uparrow} \end{aligned} \tag{3.75}$$

Thus, the GS energy is

$$E_0 = \sum_k \left(\xi^0_k - \frac{1}{2}|E^{(1)}_{k,+}| - \frac{1}{2}|E^{(2)}_{k,+}| \right) \tag{3.76}$$

3.3 The case of magnetic field perpendicular to the spin-orbit field: emergence of exotic superconducting pairing

In this section we want to show that, when the magnetic field and the spin-orbit field are orthogonal, a Nanowire proximized by an s-wave superconductor can also exhibit exotic p-wave superconducting pairings, controlled by the intensity of the spin-orbit coupling and the Zeeman field.

3.3.1 BdG Hamiltonian in the natural basis and effective pairings

Before implementing the hypothesis of orthogonality between the spin-orbit and the magnetic fields, let us start from the general expression (3.6) of the homogeneous NW proximized by the s-wave superconductor, and rewrite it in its 'natural basis', i.e. in the basis that diagonalizes the particle and hole sectors. To this purpose, we first rewrite Eq.(3.6) compactly as

$$H_{BdG}(k) = \begin{pmatrix} \xi_k^0\sigma_0 + \mathbf{m}(k)\cdot\boldsymbol{\sigma} & \Delta_0 e^{i\varphi}\sigma_0 \\ \Delta_0 e^{-i\varphi}\sigma_0 & -\xi_k^0\sigma_0 + \mathbf{m}(-k)\cdot\boldsymbol{\sigma} \end{pmatrix} \tag{3.77}$$

where

$$\mathbf{m}(k) = -(k\boldsymbol{\alpha} + \mathbf{b}) = (-\alpha_x k - b_x\,, -\alpha_y k - b_y,\ -\alpha_z k - b_z) \tag{3.78}$$

and the related unit vector

$$\hat{\mathbf{n}}(k) = \frac{\mathbf{m}(k)}{|\mathbf{m}(k)|} = (\sin\theta_k\cos\varphi_k, \sin\theta_k\sin\varphi_k, \cos\theta_k) \tag{3.79}$$

identifies the azimuthal and polar angles, $\varphi_k \in [0, 2\pi]$ and $\theta_k \in [0, \pi]$, respectively. Explicitly

$$\begin{cases} \cos\theta_k &= -\dfrac{\alpha_z k + b_z}{\sqrt{(\alpha_x k + b_x)^2 + (\alpha_y k + b_y)^2 + (\alpha_z k + b_z)^2}} \\ \sin\theta_k &= \sqrt{\dfrac{(\alpha_x k + b_x)^2 + (\alpha_y k + b_y)^2}{(\alpha_x k + b_x)^2 + (\alpha_y k + b_y)^2 + (\alpha_z k + b_z)^2}} \\ \varphi_k &= \arctan\left(\frac{\alpha_y k + b_y}{\alpha_x k + b_x}\right) + \pi\vartheta(\alpha_x k + b_x) \qquad \leftarrow \text{(here } \vartheta \text{ is the Heaviside function)} \end{cases} \tag{3.80}$$

where

$$\alpha = |\boldsymbol{\alpha}| \qquad\qquad b = |\mathbf{b}| \tag{3.81}$$

- **Diagonalization of the electron sector**
  To diagonalize the electron block of the BdG Hamiltonian (3.77), we exploit the general expression of the eigenvectors of $\mathbf{m}(k)\cdot\boldsymbol{\sigma}$, i.e.

$$\chi_k^{(+)} = \begin{pmatrix} \cos\frac{\theta_k}{2} \\ \\ e^{i\varphi_k}\sin\frac{\theta_k}{2} \end{pmatrix} \qquad\qquad \chi_k^{(-)} = \begin{pmatrix} -e^{-i\varphi_k}\sin\frac{\theta_k}{2} \\ \\ \cos\frac{\theta_k}{2} \end{pmatrix} \tag{3.82}$$

and introduce the unitary matrix U_k containing the vectors (3.82) as columns

$$U_k = \begin{pmatrix} \cos\frac{\theta_k}{2} & -e^{-i\varphi_k}\sin\frac{\theta_k}{2} \\ e^{i\varphi_k}\sin\frac{\theta_k}{2} & \cos\frac{\theta_k}{2} \end{pmatrix} \qquad U_k^\dagger = \begin{pmatrix} \cos\frac{\theta_k}{2} & e^{-i\varphi_k}\sin\frac{\theta_k}{2} \\ -e^{i\varphi_k}\sin\frac{\theta_k}{2} & \cos\frac{\theta_k}{2} \end{pmatrix} \tag{3.83}$$

Because U_k contains the eigenvectors of the electron block $h_e(k) = \xi_k^0 + \mathbf{m}(k)\cdot\boldsymbol{\sigma}$, a rotation by U_k diagonalizes the particle block $h_e(k) = U_k\tilde{h}_e(k)U_k^\dagger$, where $\tilde{h}_e(k) = \xi_k^0 + |\mathbf{m}(k)|\sigma_z$. In turn, this amounts to identify the new operators $\tilde{c}_{k\pm}$, in terms of which the electron Hamiltonian is diagonal

$$\begin{aligned} \mathcal{H}_e &= \frac{1}{2}\sum_k \left(c_{k\uparrow}^\dagger, c_{k\downarrow}^\dagger\right) h_e(k) \begin{pmatrix} c_{k\uparrow} \\ c_{k\downarrow} \end{pmatrix} = \\ &= \frac{1}{2}\sum_k \underbrace{\left(c_{k\uparrow}^\dagger, c_{k\downarrow}^\dagger\right) U_k}\, \tilde{h}_e(k)\, \underbrace{U_k^\dagger \begin{pmatrix} c_{k\uparrow} \\ c_{k\downarrow} \end{pmatrix}} \end{aligned} \tag{3.84}$$

whence

$$\begin{pmatrix} \tilde{c}_{k+} \\ \tilde{c}_{k-} \end{pmatrix} = U_k^\dagger \begin{pmatrix} c_{k\uparrow} \\ c_{k\downarrow} \end{pmatrix} \qquad \Leftrightarrow \qquad \begin{pmatrix} c_{k\uparrow} \\ c_{k\downarrow} \end{pmatrix} = U_k \begin{pmatrix} \tilde{c}_{k+} \\ \tilde{c}_{k-} \end{pmatrix} = \begin{pmatrix} \cos\frac{\theta_k}{2}\tilde{c}_{k+} - e^{-i\varphi_k}\sin\frac{\theta_k}{2}\,\tilde{c}_{k-} \\ e^{i\varphi_k}\sin\frac{\theta_k}{2}\tilde{c}_{k+} + \cos\frac{\theta_k}{2}\,\tilde{c}_{k-} \end{pmatrix} \tag{3.85}$$

Remark
We note that matrix U_k in Eq.(3.83) can be interpreted as a rotation by an angle θ_k around an axis $\hat{\mathbf{u}}(k)$ lying in the x-y plane and perpendicular to the projection of $\hat{\mathbf{n}}(k)$ in that plane. Indeed U_k can be compactly rewritten as

$$U_k = \cos\frac{\theta_k}{2}\,\mathbb{I} + i\sin\frac{\theta_k}{2}\left(\sin\varphi_k\cdot\sigma_x \;-\cos\varphi_k\cdot\sigma_y\right) = e^{i\frac{\theta_k}{2}\mathbf{u}_k\cdot\boldsymbol{\sigma}} \tag{3.86}$$

where $\mathbf{u}_k$ is

$$\mathbf{u}_k = (\sin\varphi_k, -\cos\varphi_k, 0) = \left(\cos\left(\varphi_k - \frac{\pi}{2}\right), \sin\left(\varphi_k - \frac{\pi}{2}\right), 0\right) \tag{3.87}$$

- **Diagonalization of the hole sector**
The above transformation (3.85) on the upper part of the Nambu spinor Ψ_k Eq.(3.5) directly determines, by consistency requirement, the transformation on the lower part of the Nambu spinor,

$$\begin{pmatrix} c_{-k\uparrow} \\ c_{-k\downarrow} \end{pmatrix} = U_{-k} \begin{pmatrix} \tilde{c}_{-k+} \\ \tilde{c}_{-k-} \end{pmatrix} = \begin{pmatrix} \cos\frac{\theta_{-k}}{2}\tilde{c}_{-k+} - e^{-i\varphi_{-k}}\sin\frac{\theta_{-k}}{2}\,\tilde{c}_{-k-} \\ e^{i\varphi_{-k}}\sin\frac{\theta_{-k}}{2}\tilde{c}_{-k+} + \cos\frac{\theta_{-k}}{2}\,\tilde{c}_{-k-} \end{pmatrix} \tag{3.88}$$

which in turn implies

$$\begin{aligned} \begin{pmatrix} c_{-k\downarrow}^\dagger \\ -c_{-k\uparrow}^\dagger \end{pmatrix} &= \begin{pmatrix} e^{-i\varphi_{-k}}\sin\frac{\theta_{-k}}{2}\tilde{c}_{-k+}^\dagger + \cos\frac{\theta_{-k}}{2}\,\tilde{c}_{-k-}^\dagger \\ -\cos\frac{\theta_{-k}}{2}\tilde{c}_{-k+}^\dagger + e^{i\varphi_{-k}}\sin\frac{\theta_{-k}}{2}\,\tilde{c}_{-k-}^\dagger \end{pmatrix} = \\ &= \underbrace{\begin{pmatrix} \cos\frac{\theta_{-k}}{2} & -e^{-i\varphi_{-k}}\sin\frac{\theta_{-k}}{2} \\ e^{i\varphi_{-k}}\sin\frac{\theta_{-k}}{2} & \cos\frac{\theta_{-k}}{2} \end{pmatrix}}_{=U_{-k}} \begin{pmatrix} \tilde{c}_{-k-}^\dagger \\ -\tilde{c}_{-k+}^\dagger \end{pmatrix} \end{aligned} \tag{3.89}$$

Combining Eqs.(3.85) and (3.89) we deduce that the Nambu spinor must rotate as

$$\begin{pmatrix} c_{k\uparrow} \\ c_{k\downarrow} \\ c^{\dagger}_{-k\downarrow} \\ -c^{\dagger}_{-k\uparrow} \end{pmatrix} = \begin{pmatrix} U_k & 0 \\ 0 & U_{-k} \end{pmatrix} \begin{pmatrix} \tilde{c}_{k+} \\ \tilde{c}_{k-} \\ \tilde{c}^{\dagger}_{-k-} \\ -\tilde{c}^{\dagger}_{-k+} \end{pmatrix} \tag{3.90}$$

We therefore apply the following rotation

$$\mathsf{U}_k = \begin{pmatrix} U_k & 0 \\ 0 & U_{-k} \end{pmatrix} \tag{3.91}$$

to $H_{BdG}(k)$

$$H_{BdG}(k) = \mathsf{U}_k \, \tilde{H}_{BdG}(k) \, \mathsf{U}_k^{\dagger} \qquad \Leftrightarrow \qquad \tilde{H}_{BdG}(k) = \mathsf{U}_k^{\dagger} \, H_{BdG}(k) \, \mathsf{U}_k \tag{3.92}$$

obtaining

$$\tilde{H}_{BdG}(k) = \begin{pmatrix} \xi^0_k \sigma_0 + |\mathbf{m}(k)|\sigma_z & \Delta_0 \, e^{i\varphi} U^{\dagger}_k \, U_{-k} \\ \Delta_0 \, e^{-i\varphi} U^{\dagger}_{-k} \, U_k & -\xi^0_k \sigma_0 + |\mathbf{m}(-k)|\sigma_z \end{pmatrix} \tag{3.93}$$

Note that $U^{\dagger}_{-k} U_k = (U^{\dagger}_k U_{-k})^{\dagger}$, as is expected from the Hermiticity of $\tilde{H}_{BdG}(k)$. Furthermore, recalling Eqs.(3.86)-(3.87) the products $U^{\dagger}_k U_{-k}$ and $U^{\dagger}_{-k} U_k$ can be compactly rewritten as

$$U^{\dagger}_k U_{-k} = e^{-i\frac{\theta_k}{2}\mathbf{u}_k \cdot \boldsymbol{\sigma}} \, e^{i\frac{\theta_{-k}}{2}\mathbf{u}_{-k} \cdot \boldsymbol{\sigma}} \tag{3.94}$$

$$U^{\dagger}_{-k} U_k = e^{-i\frac{\theta_{-k}}{2}\mathbf{u}_{-k} \cdot \boldsymbol{\sigma}} \, e^{i\frac{\theta_k}{2}\mathbf{u}_k \cdot \boldsymbol{\sigma}} \tag{3.95}$$

By construction, the rotated BdG Hamiltonian $\tilde{H}_{BdG}(k)$ in Eq.(3.93) exhibits particle and hole blocks that are diagonal. However, the off-diagonal blocks characterized by the superconducting pairing acquire a richer, k-dependent, texture. As we shall see, novel types of superconducting pairing arise, due to the products $U^{\dagger}_k U_{-k}$ and $U^{\dagger}_{-k} U_k$

$$U^{\dagger}_k U_{-k} = \begin{pmatrix} \cos\frac{\theta_k}{2}\cos\frac{\theta_{-k}}{2} + \sin\frac{\theta_k}{2}\sin\frac{\theta_{-k}}{2} e^{-i(\varphi_k - \varphi_{-k})} & \cos\frac{\theta_{-k}}{2}\sin\frac{\theta_k}{2} e^{-i\varphi_k} - \cos\frac{\theta_k}{2}\sin\frac{\theta_{-k}}{2} e^{-i\varphi_{-k}} \\ -\cos\frac{\theta_{-k}}{2}\sin\frac{\theta_k}{2} e^{i\varphi_k} + \cos\frac{\theta_k}{2}\sin\frac{\theta_{-k}}{2} e^{i\varphi_{-k}} & \cos\frac{\theta_k}{2}\cos\frac{\theta_{-k}}{2} + \sin\frac{\theta_k}{2}\sin\frac{\theta_{-k}}{2} e^{i(\varphi_k - \varphi_{-k})} \end{pmatrix} \tag{3.96}$$

$$U^{\dagger}_{-k} U_k = \begin{pmatrix} \cos\frac{\theta_k}{2}\cos\frac{\theta_{-k}}{2} + \sin\frac{\theta_k}{2}\sin\frac{\theta_{-k}}{2} e^{i(\varphi_k - \varphi_{-k})} & -\cos\frac{\theta_{-k}}{2}\sin\frac{\theta_k}{2} e^{-i\varphi_k} + \cos\frac{\theta_k}{2}\sin\frac{\theta_{-k}}{2} e^{-i\varphi_{-k}} \\ \cos\frac{\theta_{-k}}{2}\sin\frac{\theta_k}{2} e^{i\varphi_k} - \cos\frac{\theta_k}{2}\sin\frac{\theta_{-k}}{2} e^{i\varphi_{-k}} & \cos\frac{\theta_k}{2}\cos\frac{\theta_{-k}}{2} + \sin\frac{\theta_k}{2}\sin\frac{\theta_{-k}}{2} e^{-i(\varphi_k - \varphi_{-k})} \end{pmatrix} \tag{3.97}$$

In particular, in the next subsection, we shall explicitly show an example of how effective p-wave superconducting pairing can be generated from the interplay of superconductivity, spin-orbit coupling and magnetic field. Before doing that, let us briefly mention what happens in the case $\Delta_0 = 0$.

The case $\Delta_0 = 0$
When $\Delta_0 = 0$ the rotated BdG Hamiltonian (3.93) of the NW is completely diagonal

$$\tilde{H}_{BdG}(k) = \begin{pmatrix} \xi_k^0 \sigma_0 + |\mathbf{m}(k)|\sigma_z & 0 \\ 0 & -\xi_k^0 \sigma_0 + |\mathbf{m}(-k)|\sigma_z \end{pmatrix} \tag{3.98}$$

Its four eigenvalues are

$$\begin{cases} E^e_{k,\pm} &= \xi_k^0 \pm |\mathbf{m}(k)| \\ E^h_{k,\pm} &= -\xi_k^0 \mp |\mathbf{m}(-k)| \end{cases} \tag{3.99}$$

with corresponding eigenvectors

$$\tilde{\Phi}^e_{k,+} = \begin{pmatrix} 1 \\ 0 \\ 0 \\ 0 \end{pmatrix} \qquad \tilde{\Phi}^e_{k,-} = \begin{pmatrix} 0 \\ 1 \\ 0 \\ 0 \end{pmatrix} \qquad \tilde{\Phi}^h_{k,-} = \begin{pmatrix} 0 \\ 0 \\ 1 \\ 0 \end{pmatrix} \qquad \tilde{\Phi}^h_{k,+} = \begin{pmatrix} 0 \\ 0 \\ 0 \\ 1 \end{pmatrix} \tag{3.100}$$

Thus, the eigenstates $\Phi^{e/h}_{k,\pm}$ of $H_{BdG}(k)$ are straightforwardly obtained using Eq.(3.92)

$$H_{BdG}(k)\, \Phi^{e/h}_{k,\pm} = E^{e/h}_{k,\pm}\, \Phi^{e/h}_{k,\pm} \tag{3.101}$$

and read

$$\Phi^{e/h}_{k,\pm} = \mathsf{U}_k \tilde{\Phi}^{e/h}_{k,\pm} \tag{3.102}$$

In particular

$$\Phi^e_{k,+} = \begin{pmatrix} \cos\frac{\theta_k}{2} \\ \sin\frac{\theta_k}{2}\, e^{i\varphi_k} \\ 0 \\ 0 \end{pmatrix} \qquad \Phi^e_{k,-} = \begin{pmatrix} -\sin\frac{\theta_k}{2}\, e^{-i\varphi_k} \\ \cos\frac{\theta_k}{2} \\ 0 \\ 0 \end{pmatrix}$$

$$\Phi^h_{k,-} = \begin{pmatrix} 0 \\ 0 \\ \cos\frac{\theta_{-k}}{2} \\ \sin\frac{\theta_{-k}}{2}\, e^{i\varphi_{-k}} \end{pmatrix} \qquad \Phi^h_{k,+} = \begin{pmatrix} 0 \\ 0 \\ -\sin\frac{\theta_{-k}}{2}\, e^{-i\varphi_{-k}} \\ \cos\frac{\theta_{-k}}{2} \end{pmatrix} \tag{3.103}$$

3.3.2 The case of SO coupling along z and magnetic field along x-direction

In the previous Sec.3.3.1, we have kept the directions of $\boldsymbol{\alpha}$ and $\mathbf{b}$ completely arbitrary. As anticipated at the beginning of this section, we now want to focus on the case where the spin-orbit field and the magnetic field are mutually orthogonal. For definiteness, we shall choose

$$\boldsymbol{\alpha} = (0,0,\alpha_z) \tag{3.104}$$

$$\mathbf{b} = (b_x,0,0) \tag{3.105}$$

In this configuration, the general relations Eqs.(3.80) reduce to

$$\begin{cases} \cos\theta_k &= -\operatorname{sgn}(\alpha_z k)\sqrt{\frac{\alpha_z^2 k^2}{b_x^2+\alpha_z^2 k^2}} = -\operatorname{sgn}(\alpha_z k)\frac{|\alpha_z k|}{\sqrt{b_x^2+\alpha_z^2 k^2}} = -\frac{\alpha_z k}{\sqrt{b_x^2+\alpha_z^2 k^2}} \\ \sin\theta_k &= \sqrt{\frac{b_x^2}{b_x^2+\alpha_z^2 k^2}} = \frac{|b_x|}{\sqrt{b_x^2+\alpha_z^2 k^2}} = \frac{\operatorname{sgn}(b_x)\, b_x}{\sqrt{b_x^2+\alpha_z^2 k^2}} \\ \varphi_k &= \pi\vartheta(b_x) \quad \to e^{\pm i\varphi_k} = -\operatorname{sgn}(b_x) \end{cases} \tag{3.106}$$

Since $\frac{\theta_k}{2} \in [0,\frac{\pi}{2}]$, terms of type "$\cos\frac{\theta_k}{2}$, $\sin\frac{\theta_k}{2}$" shall be always positive, thus, in this interval, the following trigonometric relations are valid

$$\cos\frac{\theta_k}{2} = +\sqrt{\frac{1}{2}\left(1+\cos\theta_k\right)} \qquad\qquad \sin\frac{\theta_k}{2} = +\sqrt{\frac{1}{2}\left(1-\cos\theta_k\right)} \tag{3.107}$$

whence, given that in our particular case $\cos\theta_{-k} = -\cos\theta_k$, we have

$$\cos\frac{\theta_{-k}}{2} = \sin\frac{\theta_k}{2} \qquad \text{and} \qquad \sin\frac{\theta_{-k}}{2} = \cos\frac{\theta_k}{2} \tag{3.108}$$

Given that $\varphi_k = \varphi_{-k}$, the product $U_k^\dagger U_{-k}$ shall acquire the form

$$U_k^\dagger U_{-k} = \begin{pmatrix} 2\cos\frac{\theta_k}{2}\sin\frac{\theta_k}{2} & \left(\sin^2\frac{\theta_k}{2} - \cos^2\frac{\theta_k}{2}\right)e^{-i\varphi_k} \\ \left(\cos^2\frac{\theta_k}{2} - \sin^2\frac{\theta_k}{2}\right)e^{i\varphi_k} & 2\cos\frac{\theta_k}{2}\sin\frac{\theta_k}{2} \end{pmatrix} \tag{3.109}$$

Now, using the following trigonometric relations

$$2\cos\frac{\theta_k}{2}\sin\frac{\theta_k}{2} = \sin\theta_k \tag{3.110}$$

$$\cos^2\frac{\theta_k}{2} - \sin^2\frac{\theta_k}{2} = \cos\theta_k \tag{3.111}$$

then

$$U_k^\dagger U_{-k} = \begin{pmatrix} \sin\theta_k & -\cos\theta_k e^{-i\varphi_k} \\ \cos\theta_k e^{i\varphi_k} & \sin\theta_k \end{pmatrix} = \frac{\operatorname{sgn}(b_x)}{\sqrt{b_x^2+\alpha_z^2 k^2}}\begin{pmatrix} b_x & -\alpha_z k \\ \alpha_z k & b_x \end{pmatrix} \tag{3.112}$$

and $U_{-k}^{\dagger}U_k = \left(U_k^{\dagger}U_{-k}\right)^{\dagger}$.
Inserting this last result in Eq.(3.93), together with $|\mathbf{m}(k)| = \sqrt{b_x^2 + \alpha_z^2 k^2}$, we get

$$\tilde{H}_{BdG} = \begin{pmatrix} \xi_k^0 + \sqrt{b_x^2 + \alpha_z^2 k^2} & 0 & \Delta_s(k) & \Delta_p(k) \\ 0 & \xi_k^0 - \sqrt{b_x^2 + \alpha_z^2 k^2} & -\Delta_p(k) & \Delta_s(k) \\ \Delta_s^*(k) & -\Delta_p^*(k) & -\xi_k^0 + \sqrt{b_x^2 + \alpha_z^2 k^2} & 0 \\ \Delta_p^*(k) & \Delta_s^*(k) & 0 & -\xi_k^0 - \sqrt{b_x^2 + \alpha_z^2 k^2} \end{pmatrix} \tag{3.113}$$

where we have defined the k-dependent functions $\Delta_s(k)$ and $\Delta_p(k)$ as

$$\Delta_s(k) = \Delta_0 e^{i\varphi} \frac{\mathrm{sgn}(b_x) b_x}{\sqrt{b_x^2 + \alpha_z^2 k^2}} \tag{3.114}$$

$$\Delta_p(k) = -\Delta_0 e^{i\varphi} \frac{\mathrm{sgn}(b_x) \alpha_z k}{\sqrt{b_x^2 + \alpha_z^2 k^2}} \tag{3.115}$$

In particular, being the $\Delta_s(k)$ term even in k, it represents the conventional "s-wave" superconducting pairing, which couples electron from different band (interband coupling). In contrast, the $\Delta_p(k)$ term represents an effective superconducting pairing that is *odd* in k, defining it as "p-wave" pairing. It couples electron from the same band (intraband coupling) and results from the interplay between spin-orbit coupling and s-wave superconducting coupling.
It is this emergent pairing that is responsible for driving the system into the topological phase. Indeed when the Fermi level lies between the two bands, one can effectively describe the system in terms of a single band, i.e.the lower one. The electrons of this unique band can couple via the new effective p-wave term, obtaining an effective *spinless p-wave* superconducting system as proposed by Lutchyn and Oreg and discussed in Section 1.3.3.

Chapter 4

Hybrid junctions in proximized nanowires

In this chapter, we shall describe *hybrid junctions* involving nanowires, i.e setups where a portion of the nanowire is normal (N), while other portions exhibit superconducting (S) pairing induced through proximity effect by superconducting films deposited on the NW. These kinds of setups include the so called N-S junctions, or S-N-S junctions, also known as Josephson junctions, which are the backbone of various modern quantum devices. In these systems, inhomogeneities in the Rashba spin-orbit coupling are expected to arise and to affect the physical properties such as the differential conductance or the Josephson current. However, most theoretical studies on hybrid junctions with nanowires have neglected such inhomogeneities. In particular, a thorough analysis of how inhomogeneities of the spin-orbit coupling affect Andreev reflection is still lacking. Because such phenomenon underlies the physics of these quantum systems, our ultimate goal is to address this problem.

4.1 Model for an inhomogeneous proximized nanowire with spin-orbit coupling

Inhomogeneities in the Rashba spin-orbit coupling in systems with proximized nanowires emerge for various reasons. The first one is that Rashba spin-orbit coupling can be tuned locally. Indeed, since the SOC strength depends on the electric field characterizing the SIA, such field can be controlled by means of voltage applied to local metallic gates near the nanowire [35, 96, 97, 98, 99]. By designing suitable setup geometries involving various top-, side- or wrap-gates, one can realize inhomogeneous profiles $\boldsymbol{\alpha}(x)$ of the Rashba SOC, where both the magnitude $\alpha = |\boldsymbol{\alpha}|$ and the direction $\hat{\mathbf{n}}$ of the Rashba field depend on the longitudinal position. This sort of inhomogeneity occurs already without superconductivity, and is purposely generated with the aim of controlling the electron transmission through the nanowire, exploiting its spin texture.
The second source of inhomogeneities is usually unwanted. It arises from disorder effects, such as impurity doping, interface density fluctuations, or random variations in the nanowire shape, which may affect a geometry and structure dependent coupling such as

SOC [100, 101, 102, 103].

Finally, in the specific case of proximized nanowires, where a superconducting pairing is induced by proximity effect on the NW portions covered by superconducting metal films, the different SIA characterizing the covered and uncovered portions of the NW naturally gives rise to further inhomogeneities of the RSOC. These effects, combined with the inhomogeneity of the superconducting pairing, are expected to strongly affect the Andreev reflection process, the spectrum of bound states and the Josephson current.

While some works have analyzed the effects of RSOC inhomogeneities in normal NWs, showing that they can lead to control and significantly modulate the electron transmission through the NW [104, 105, 106, 107, 108] , when it comes to hybrid junctions involving NWs proximized by superconductors, most studies have either assumed a homogeneous SOC (see e.g. Refs.[85], [86] [109]) or have neglected the SOC in the proximized regions [110]. Only a few papers have investigated the effects of inhomogeneities of SOC in proximized NWs. However, the main focus of these studies was to distinguish topological Majorana bound states from trivial bound states originating from inhomogeneities [111, 112, 113]. So far, a detailed investigation of how Andreev reflection is affected by the RSOC inhomogeneities is still lacking.

Here below, we introduce a general model that enables us to account for spatial inhomogeneities both in the superconducting pairing and in the Rashba spin-orbit coupling. While in this chapter we shall highlight the symmetries of the model and illustrate how the Bogolubov de Gennes formalism can be exploited to attack these problems, in the next chapter we shall focus on the specific case of a N-S junction, and show that Andreev reflection can be strongly affected by inhomogeneities of the Rashba spin-orbit coupling.

Because hybrid systems are intrinsically spatially inhomogeneous, it is convenient to use a real-space description of the system. The Hamiltonian consists of five terms

$$\mathcal{H} = \mathcal{H}_{kin} + \mathcal{H}_{\mu} + \mathcal{H}_{SO} + \mathcal{H}_{Z} + \mathcal{H}_{SC} \tag{4.1}$$

where

$$\mathcal{H}_{kin} = \int dx \left(\Psi_{\uparrow}^{\dagger}(x), \Psi_{\downarrow}^{\dagger}(x)\right) \frac{\hat{P}^2}{2m^*}\sigma_0 \begin{pmatrix}\Psi_{\uparrow}(x)\\ \Psi_{\downarrow}(x)\end{pmatrix} \tag{4.2}$$

describes the kinetic term associated with the effective mass approximation,

$$\mathcal{H}_{\mu} = -\int dx \left(\Psi_{\uparrow}^{\dagger}(x), \Psi_{\downarrow}^{\dagger}(x)\right) \mu(x)\sigma_0 \begin{pmatrix}\Psi_{\uparrow}(x)\\ \Psi_{\downarrow}(x)\end{pmatrix} \tag{4.3}$$

is the term accounting for the chemical potential profile $\mu(x)$,

$$\mathcal{H}_{SO} = -\frac{1}{2\hbar}\int dx \left(\Psi_{\uparrow}^{\dagger}(x), \Psi_{\downarrow}^{\dagger}(x)\right) \left\{\boldsymbol{\alpha}(x), \hat{P}\right\} \cdot \boldsymbol{\sigma} \begin{pmatrix}\Psi_{\uparrow}(x)\\ \Psi_{\downarrow}(x)\end{pmatrix} \tag{4.4}$$

describes the inhomogeneous Rashba spin-orbit coupling. Here, the anticommutator $\{\cdot\,,\cdot\}$ in Eq.(4.4) term is necessary because the momentum $\hat{P} = -i\hbar\partial_x$ does not commute with a space-dependent vector field $\boldsymbol{\alpha}(x)$ characterizing the spin-orbit field. Moreover,

$$\mathcal{H}_Z = -\int dx \left(\Psi_\uparrow^\dagger(x), \Psi_\downarrow^\dagger(x)\right) \boldsymbol{b}(x)\cdot\boldsymbol{\sigma} \begin{pmatrix}\Psi_\uparrow(x)\\ \Psi_\downarrow(x)\end{pmatrix} \tag{4.5}$$

denotes the Zeeman coupling with a magnetic field $\boldsymbol{b}(x)$, whereas

$$\mathcal{H}_{SC} = \int dx \Big[\Delta(x)\Psi_\uparrow^\dagger(x)\Psi_\downarrow^\dagger(x) + \Delta^*(x)\Psi_\downarrow(x)\Psi_\uparrow(x)\Big] \tag{4.6}$$

is the inhomogeneous superconducting pairing potential, which vanishes in the N regions, while it is present in the proximized regions (S) of the NW. The combination (4.1) of the above five terms is compactly rewritten as

$$\begin{aligned}\mathcal{H} \;=\; & \int dx \left(\Psi_\uparrow^\dagger(x), \Psi_\downarrow^\dagger(x)\right) \left[\left(\frac{\hat{P}^2}{2m^*} - \mu(x)\right)\sigma_0 - \frac{1}{2\hbar}\Big\{\boldsymbol{\alpha}(x), \hat{P}\Big\}\cdot\boldsymbol{\sigma} - \mathbf{b}(x)\cdot\boldsymbol{\sigma}\right] \begin{pmatrix}\Psi_\uparrow(x)\\ \Psi_\downarrow(x)\end{pmatrix} \\ & + \int dx \left(\Delta(x)\Psi_\uparrow^\dagger(x)\Psi_\downarrow^\dagger(x) + \Delta^*(x)\Psi_\downarrow(x)\Psi_\uparrow(x)\right)\end{aligned} \tag{4.7}$$

Hamiltonian symmetries

- **Time-reversal transformation**
  The time-reversal (TR) transformation $\mathcal{T}$ is defined as a *anti-linear* transformation operating on the electron fields as follows

  $$\mathcal{T}\begin{pmatrix}\Psi_\uparrow\\ \Psi_\downarrow\end{pmatrix}\mathcal{T}^{-1} \doteq \begin{pmatrix}-\Psi_\downarrow\\ \Psi_\uparrow\end{pmatrix} \equiv -i\sigma_y \begin{pmatrix}\Psi_\uparrow\\ \Psi_\downarrow\end{pmatrix} \tag{4.8}$$

  and, correspondingly

  $$\mathcal{T}\left(\Psi_\uparrow^\dagger, \Psi_\downarrow^\dagger\right)\mathcal{T}^{-1} \doteq \left(-\Psi_\downarrow^\dagger, \Psi_\uparrow^\dagger\right) \equiv \left(\Psi_\uparrow^\dagger, \Psi_\downarrow^\dagger\right) i\sigma_y \tag{4.9}$$

  The Hamiltonian $\mathcal{H}$ is time-reversal invariant iff

  $$\mathcal{T}\mathcal{H}\mathcal{T}^{-1} = \mathcal{H} \tag{4.10}$$

- **Charge-conjugation transformation**
  The particle-hole or charge-conjugation transformation $\mathcal{C}$ is defined as the *linear* operation mapping each field onto its adjoint Pro

  $$\mathcal{C}\begin{pmatrix}\Psi_\uparrow\\ \Psi_\downarrow\end{pmatrix}\mathcal{C}^{-1} \doteq \begin{pmatrix}\Psi_\uparrow^\dagger\\ \Psi_\downarrow^\dagger\end{pmatrix} \tag{4.11}$$

  and, correspondingly

  $$\mathcal{C}\left(\Psi_\uparrow^\dagger, \Psi_\downarrow^\dagger\right)\mathcal{C}^{-1} \doteq \left(\Psi_\uparrow, \Psi_\downarrow\right) \tag{4.12}$$

The Hamiltonian $\mathcal{H}$ is particle-hole symmetric iff

$$\mathcal{C}\mathcal{H}\mathcal{C}^{-1} = \mathcal{H} \tag{4.13}$$

It is straightforward to verify that, differently from TR, C-symmetry typically does not hold for $\mathcal{H}$ given in Eq.(4.7), regardless of the parameter values. Indeed it is easy to realize that the kinetic term is not charge-conjugation symmetric.

4.2 Bogoliubov de Gennes form of the proximized nanowire Hamiltonian

It is possible to show that the proximized and inhomogenous NW Hamiltonian (4.7) can be rewritten in the Bogolubov de Gennes form [1, 90, 91], namely as

$$\mathcal{H} = \frac{1}{2}\int dx\, \Psi^\dagger(x)\, H_{BdG}(x)\Psi(x) \; + C \tag{4.14}$$

where

$$\Psi(x) = \begin{pmatrix} \Psi_\uparrow(x) \\ \Psi_\downarrow(x) \\ \Psi^\dagger_\downarrow(x) \\ -\Psi^\dagger_\uparrow(x) \end{pmatrix} \tag{4.15}$$

denotes the four components (real-space) Nambu spinor, and

$$H_{BdG}(x) = \begin{pmatrix} h_e(x) & \Delta(x)\sigma_0 \\ \Delta^*(x)\sigma_0 & h_h(x) \end{pmatrix} \tag{4.16}$$

is the Bogolubov de Gennes (BdG) Hamiltonian, i.e. the first-quantization matrix representation of the NW Hamiltonian operator $\mathcal{H}$. Finally, C is a constant.

In the BdG Hamiltonian $H_{BdG}(x)$ appearing in Eq.(4.16), the 2×2 electron-block $h_e(x)$ and the 2×2 hole-block $h_h(x)$ are mutually related through

$$\boxed{h_h(x) = -\sigma_y h_e^*(x)\sigma_y} \tag{4.17}$$

and are explicitly given by

$$h_e(x) = \hat{\xi}(x)\sigma_0 - \frac{1}{2\hbar}\Big\{\boldsymbol{\alpha}(x), \hat{P}\Big\}\cdot\boldsymbol{\sigma} - \mathbf{b}(x)\cdot\boldsymbol{\sigma} \tag{4.18}$$

$$h_h(x) = -\hat{\xi}(x)\sigma_0 + \frac{1}{2\hbar}\Big\{\boldsymbol{\alpha}(x), \hat{P}\Big\}\cdot\boldsymbol{\sigma} - \mathbf{b}(x)\cdot\boldsymbol{\sigma} \tag{4.19}$$

where

$$\hat{\xi}(x) = \frac{\hat{P}^2}{2m^*} - \mu(x) = -\frac{1}{2m^*}\frac{\partial^2}{\partial x^2} - \mu(x) \tag{4.20}$$

is the kinetic energy operator with respect to the chemical potential, and

$$\hat{\mathbf{b}}_{SO}(x) = \frac{1}{2\hbar}\Big\{\boldsymbol{\alpha}(x), \hat{P}\Big\} = -\frac{i}{2}\Big\{\boldsymbol{\alpha}(x), \frac{\partial}{\partial x}\Big\} = -i\left(\boldsymbol{\alpha}(x)\frac{\partial}{\partial x} + \frac{1}{2}(\partial_x \boldsymbol{\alpha}(x))\right) \tag{4.21}$$

describes the spin-orbit field operator. Note that, differently from the actual magnetic field $\mathbf{b}$, the spin-orbit $\hat{\mathbf{b}}_{SO}(x)$ is complex (in particular it is purely imaginary, i.e. $\hat{\mathbf{b}}^*_{SO}(x) = -\hat{\mathbf{b}}_{SO}(x)$).

Explicitly the BdG Hamiltonian $H_{BdG}(x)$ for the inhomogeneous proximized NW is written as

$$\boxed{H_{BdG}(x) = \begin{pmatrix} \hat{\xi}(x)\sigma_0 - \hat{\mathbf{b}}_{SO}(x)\cdot\boldsymbol{\sigma} - \mathbf{b}(x)\cdot\boldsymbol{\sigma} & \Delta(x)\sigma_0 \\ \Delta^*(x)\sigma_0 & -\hat{\xi}(x)\sigma_0 + \hat{\mathbf{b}}_{SO}(x)\cdot\boldsymbol{\sigma} - \mathbf{b}(x)\cdot\boldsymbol{\sigma} \end{pmatrix}} \tag{4.22}$$

or equivalently, in a compact form,

$$H_{BdG}(x) = \tau_z \otimes \Big(\hat{\xi}(x)\sigma_0 - \hat{\mathbf{b}}_{SO}(x)\cdot\boldsymbol{\sigma}\Big) - (\tau_0 \otimes (\mathbf{b}(x)\cdot\boldsymbol{\sigma})) + (\tau_+ \otimes \sigma_0)\,\Delta(x) + (\tau_- \otimes \sigma_0)\,\Delta^*(x) \tag{4.23}$$

where σ_j are Pauli matrices acting on spin space, while τ_i are Pauli matrices acting on Nambu space, and $\tau_\pm = (\tau_x \pm i\tau_y)/2$.
Moreover, the constant C in Eq.(4.14) is given by

$$C = \iint dx\, dx' \delta(x - x') \left(-\frac{\hbar^2}{2m^*}\frac{\partial^2}{\partial x^2} - \mu(x)\right) \delta(x - x') \tag{4.24}$$

The proof of Eq.(4.22) is given in Appendix A.

The spatially uniform case

In the case of a homogeneous system, where all parameters in the Hamiltonian (4.22) are spatially uniform

$$\begin{array}{rcl} \boldsymbol{\alpha}(x) & \equiv & \boldsymbol{\alpha} \\ \mathbf{b}(x) & \equiv & \mathbf{b} \\ \Delta(x) & \equiv & \Delta_0\, e^{i\varphi} \\ \mu(x) & \equiv & \mu \end{array} \tag{4.25}$$

it is worth rewriting the Hamiltonian (4.14) in k-space, by re-expressing the electron field operator $\Psi_\sigma(x)$ in its Fourier mode operators $c_{k\sigma}$

$$\Psi_\sigma(x) = \frac{1}{\sqrt{\Omega}}\sum_k e^{ikx} c_{k\sigma} \tag{4.26}$$

$$\Psi^\dagger_\sigma(x) = \frac{1}{\sqrt{\Omega}}\sum_k e^{-ikx} c^\dagger_{k\sigma} = \frac{1}{\sqrt{\Omega}}\sum_k e^{ikx} c^\dagger_{-k\sigma} \tag{4.27}$$

whence the Nambu spinor (4.15) can be expressed as

$$\Psi(x) = \begin{pmatrix} \Psi_\uparrow(x) \\ \Psi_\downarrow(x) \\ \Psi^\dagger_\downarrow(x) \\ -\Psi^\dagger_\uparrow(x) \end{pmatrix} = \frac{1}{\sqrt{\Omega}} \sum_k e^{ikx} \begin{pmatrix} c_{k\uparrow} \\ c_{k\downarrow} \\ c^\dagger_{-k\downarrow} \\ -c^\dagger_{-k\uparrow} \end{pmatrix} = \frac{1}{\sqrt{\Omega}} \sum_k e^{ikx} \Psi_k \tag{4.28}$$

where $\Omega \to \infty$ is the entire length of the system and, correspondingly

$$\Psi^\dagger(x) = \frac{1}{\sqrt{\Omega}} \sum_k e^{-ikx} \Psi^\dagger_k \tag{4.29}$$

Here,

$$\Psi_k = \begin{pmatrix} c_{k\uparrow} \\ c_{k\downarrow} \\ c^\dagger_{-k\downarrow} \\ -c^\dagger_{-k\uparrow} \end{pmatrix} \qquad \Psi^\dagger_k = \left(c^\dagger_{k\uparrow}, c^\dagger_{k\downarrow}, c_{-k\downarrow}, -c_{-k\uparrow} \right) \tag{4.30}$$

is the natural k-space version of the Nambu spinor [see Eq.(2.13)].
Inserting Eqs.(4.28)-(4.29) into Eq.(4.14), and taking into account Eq.(4.22), the Hamiltonian acquires a diagonal form in k-space

$$\mathcal{H} = \frac{1}{2} \sum_k \Psi^\dagger_k H_{BdG}(k) \Psi_k \ + C \tag{4.31}$$

where the k-space Bogolubov de Gennes Hamiltonian found for the homogeneous case [see Eq.(3.6)] is recovered

$$H_{BdG}(k) = \begin{pmatrix} \xi^0_k \sigma_0 - k\boldsymbol{\alpha}\cdot\boldsymbol{\sigma} - \mathbf{b}\cdot\boldsymbol{\sigma} & \Delta_0 e^{i\varphi}\sigma_0 \\ \Delta_0 e^{-i\varphi}\sigma_0 & -\xi^0_k \sigma_0 + k\boldsymbol{\alpha}\cdot\boldsymbol{\sigma} - \mathbf{b}\cdot\boldsymbol{\sigma} \end{pmatrix} \tag{4.32}$$

Proof of Eqs.(4.31-4.32)

Inserting Eqs.(4.28)-(4.29) into Eq.(4.14), one has

$$\begin{aligned} \mathcal{H} &= \frac{1}{2} \int dx\, \Psi^\dagger(x)\, H_{BdG}(x) \Psi(x) \ + C = \\ &= \frac{1}{2\Omega} \int dx \sum_k e^{-ikx} \Psi^\dagger_k H_{BdG}(x) \sum_{k_2} e^{ik_2 x} \Psi_{k_2} \ + C \\ &= \frac{1}{2\Omega} \int dx \sum_k \sum_{k_2} e^{-ikx} \Psi^\dagger_k H_{BdG}(x) e^{ik_2 x} \Psi_{k_2} \ + C \end{aligned} \tag{4.33}$$

Substituting $\hat{P} \to -i\hbar\frac{\partial}{\partial x}$ in Eq.(4.22), and considering that, in the homogeneous case, Eq.(4.25) holds, then $H_{BdG}(x)$ acquires the form

$$H_{BdG}(x) = \begin{pmatrix} -\left(\frac{\hbar^2\partial^2}{2m^*\partial x^2} + \mu\right)\sigma_0 + i\boldsymbol{\alpha}\cdot\boldsymbol{\sigma}\frac{\partial}{\partial x} - \mathbf{b}\cdot\boldsymbol{\sigma} & \Delta_0 e^{i\varphi}\sigma_0 \\ \Delta_0 e^{-i\varphi}\sigma_0 & \left(\frac{\hbar^2\partial^2}{2m^*\partial x^2} + \mu\right)\sigma_0 - i\boldsymbol{\alpha}\cdot\boldsymbol{\sigma}\frac{\partial}{\partial x} - \mathbf{b}\cdot\boldsymbol{\sigma} \end{pmatrix} \tag{4.34}$$

Applying now $H_{BdG}(x)$ to the exponential function e^{-ik_2x}, it follows that

$$H_{BdG}(x)e^{-ik_2x} = H_{BdG}(k_2)e^{-ik_2x} \tag{4.35}$$

where $H_{BdG}(k_2)$ is

$$H_{BdG}(k_2) = \begin{pmatrix} \left(\frac{\hbar^2 k_2^2}{2m^*} - \mu\right)\sigma_0 - k_2\,\boldsymbol{\alpha}\cdot\boldsymbol{\sigma} - \mathbf{b}\cdot\boldsymbol{\sigma} & \Delta_0 e^{i\varphi}\sigma_0 \\ \Delta_0 e^{-i\varphi}\sigma_0 & -\left(\frac{\hbar^2 k_2^2}{2m^*} - \mu\right)\sigma_0 + k_2\,\boldsymbol{\alpha}\cdot\boldsymbol{\sigma} - \mathbf{b}\cdot\boldsymbol{\sigma} \end{pmatrix} \tag{4.36}$$

i.e. Eq.(4.32). Finally, re-inserting $H_{BdG}(k_2)$ in $\mathcal{H}$, we get

$$\begin{aligned} \mathcal{H} &= \frac{1}{2\Omega}\int dx \sum_k \sum_{k_2} e^{-ikx}\Psi_k^\dagger H_{BdG}(k_2)e^{ik_2x}\Psi_{k_2} \quad + C = \\ &= \frac{1}{2}\sum_k \sum_{k_2} \Psi_k^\dagger H_{BdG}(k_2)\Psi_{k_2}\frac{1}{\Omega}\int dx e^{-i(k-k_2)x} \quad + C = \\ &= \frac{1}{2}\sum_k \sum_{k_2} \Psi_k^\dagger H_{BdG}(k_2)\Psi_{k_2}\delta_{k,k_2} \quad + C = \\ &= \frac{1}{2}\sum_k \Psi_k^\dagger H_{BdG}(k)\Psi_k \quad + C \end{aligned} \tag{4.37}$$

which proves Eq.(4.31).

4.3 Hamiltonian symmetries in the BdG formalism

- **Time-reversal in the BdG formalism**
  Since we are dealing with hybrid superconducting systems, it is worth rewriting the action of the TR transformation on the Nambu spinor (4.15), namely

$$\mathcal{T}\Psi\mathcal{T}^{-1} = \mathcal{T}\begin{pmatrix} \Psi_\uparrow \\ \Psi_\downarrow \\ \Psi_\downarrow^\dagger \\ -\Psi_\uparrow^\dagger \end{pmatrix}\mathcal{T}^{-1} \doteq \begin{pmatrix} -\Psi_\downarrow \\ \Psi_\uparrow \\ \Psi_\uparrow^\dagger \\ \Psi_\downarrow^\dagger \end{pmatrix} \equiv \begin{pmatrix} 0 & -1 & 0 & 0 \\ 1 & 0 & 0 & 0 \\ 0 & 0 & 0 & -1 \\ 0 & 0 & 1 & 0 \end{pmatrix}\begin{pmatrix} \Psi_\uparrow \\ \Psi_\downarrow \\ \Psi_\downarrow^\dagger \\ -\Psi_\uparrow^\dagger \end{pmatrix} = (\tau_0\otimes(-i\sigma_y))\Psi \tag{4.38}$$

  which implies that the TR transformation $\mathcal{T}$ on the Nambu spinor is implemented by the 4×4 matrix

$$\mathrm{T} = (\tau_0\otimes(-i\sigma_y))\,K \tag{4.39}$$

  where K is the complex conjugation characterizing any anti-linear transformation. Correspondingly

$$\mathcal{T}\Psi^\dagger\mathcal{T}^{-1} = \Psi^\dagger(\tau_0\otimes(i\sigma_y)) = \Psi^\dagger\,\mathrm{T}^\dagger \tag{4.40}$$

When applying the TR transformation on the Hamiltonian, one obtains

$$\begin{aligned}
\mathcal{T}\mathcal{H}\mathcal{T}^{-1} &= \mathcal{T}\left(\frac{1}{2}\int dx\,\Psi^\dagger(x)H_{BdG}(x)\Psi(x) \;+C\right)\mathcal{T}^{-1} = \\
&= \frac{1}{2}\int dx\,\mathcal{T}\Psi^\dagger(x)\mathcal{T}^{-1}\underbrace{\mathcal{T}H_{BdG}(x)\mathcal{T}^{-1}}_{=H^*_{BdG}(x)}\mathcal{T}\Psi(x)\mathcal{T}^{-1} \;+\underbrace{C^*}_{=C} = \\
&= \frac{1}{2}\int dx\,\Psi^\dagger(\tau_0\otimes(i\sigma_y))\,H^*_{BdG}(x)(\tau_0\otimes(-i\sigma_y)\Psi(x) \;+C = \\
&= \frac{1}{2}\int dx\,\Psi^\dagger(x)\,(\tau_0\otimes\sigma_y)\,H^*_{BdG}(x)\,(\tau_0\otimes\sigma_y)\Psi(x) \;+C = \\
&= \frac{1}{2}\int dx\,\Psi^\dagger(x)\;H'_{BdG}(x)\,\Psi(x) \;+C
\end{aligned}$$

where

$$H'_{BdG}(x) = (\tau_0\otimes\sigma_y)\,H^*_{BdG}(x)\,(\tau_0\otimes\sigma_y) \tag{4.41}$$

is the transformed BdG Hamiltonian.

From Eq.(4.41), TR symmetry is fulfilled by $\mathcal{H}$ if and only if the following constraint is fulfilled by the BdG Hamiltonian

$$\boxed{H_{BdG}(x) = (\tau_0\otimes\sigma_y)\,H^*_{BdG}(x)\,(\tau_0\otimes\sigma_y)} \tag{4.42}$$

Exploiting this condition, here we shall verify which of the five terms (Eqs.(4.2) to (4.6)) of Hamiltonian (4.7) fulfills TR symmetry.

– **Kinetic term (with respect the chemical potential)**
In this case we are dealing with the following term

$$H_{kin}(x) + H_\mu(x) = \hat{\xi}(x)(\tau_z\otimes\sigma_0) = \left(\frac{\hat{P}^2}{2m^*} - \mu(x)\right)(\tau_z\otimes\sigma_0) \tag{4.43}$$

from which, obviously, $\Big(H_{kin}(x)+H_\mu(x)\Big) = \Big(H_{kin}(x)+H_\mu(x)\Big)^*$.
Then, let us compute the quantity given in the rhs of condition (4.42)

$$\begin{aligned}
&(\tau_0\otimes\sigma_y)\Big(H_{kin}(x)+H_\mu(x)\Big)^*(\tau_0\otimes\sigma_y) = \\
&\qquad= \hat{\xi}(x)\underbrace{(\tau_0\otimes\sigma_y)(\tau_z\otimes\sigma_0)}_{=\tau_z\otimes\sigma_y}(\tau_0\otimes\sigma_y) = \\
&\qquad= \hat{\xi}(x)(\tau_z\otimes\sigma_y)(\tau_0\otimes\sigma_y) = \\
&\qquad= \hat{\xi}(x)(\tau_z\otimes\sigma_0)
\end{aligned} \tag{4.44}$$

Therefore the kinetic term (with respect the chemical potential) satisfies TR symmetry (and thus, both the kinetic and the chemical potential terms, individually, satisfy it).

– **Spin-orbit term**
The SO term has the form

$$H_{SO}(x) = -\tau_z \otimes \left(\hat{\mathbf{b}}_{SO}(x) \cdot \boldsymbol{\sigma}\right) \tag{4.45}$$

where $\hat{\mathbf{b}}_{SO}(x) = \frac{1}{2\hbar}\left\{\boldsymbol{\alpha}(x), \hat{P}\right\}$ and, consequently, $\hat{\mathbf{b}}^*_{SO}(x) = -\hat{\mathbf{b}}_{SO}(x)$. Thus

$$\begin{aligned} H^*_{SO}(x) &= -\tau_z \otimes \left(\hat{\mathbf{b}}_{SO}(x) \cdot \boldsymbol{\sigma}\right)^* = \\ &= \tau_z \otimes \left(\hat{\mathbf{b}}_{SO}(x) \cdot \boldsymbol{\sigma}^*\right) \end{aligned} \tag{4.46}$$

Then, given Eq.(4.42), we have to prove that

$$H_{SO}(x) = (\tau_0 \otimes \sigma_y)\, H^*_{SO}(x)\, (\tau_0 \otimes \sigma_y) \tag{4.47}$$

Considering that $\sigma_y\, \boldsymbol{\sigma}^*\, \sigma_y = -\boldsymbol{\sigma}$, it follows

$$\begin{aligned} &(\tau_0 \otimes \sigma_y) \left(\tau_z \otimes \sigma^*_{x,y,z}\right) (\tau_0 \otimes \sigma_y) = \\ &\quad = \begin{pmatrix} \sigma_y & 0 \\ 0 & \sigma_y \end{pmatrix} \begin{pmatrix} \sigma^*_{x,y,z} & 0 \\ 0 & -\sigma^*_{x,y,z} \end{pmatrix} \begin{pmatrix} \sigma_y & 0 \\ 0 & \sigma_y \end{pmatrix} = \\ &\quad = \begin{pmatrix} -\sigma_{x,y,z} & 0 \\ 0 & \sigma_{x,y,z} \end{pmatrix} = \\ &\quad = -\tau_z \otimes \sigma_{x,y,z} \end{aligned} \tag{4.48}$$

Hence

$$(\tau_0 \otimes \sigma_y) H^*_{SO}(x)\, (\tau_0 \otimes \sigma_y) = \tag{4.49}$$

$$= (\tau_0 \otimes \sigma_y) \left(\tau_z \otimes \left(\hat{\mathbf{b}}_{SO}(x) \cdot \boldsymbol{\sigma}^*\right)\right) (\tau_0 \otimes \sigma_y) = \tag{4.50}$$

$$= -\tau_z \otimes \left(\hat{\mathbf{b}}_{SO}(x) \cdot \boldsymbol{\sigma}\right) = \tag{4.51}$$

$$= H_{SO}(x) \tag{4.52}$$

In conclusion, we have proven that SO term fulfills TR symmetry.

– **Zeeman term**
The Zeeman term is

$$H_Z(x) = -\tau_0 \otimes (\mathbf{b}(x) \cdot \boldsymbol{\sigma}) \tag{4.53}$$

Therefore, using $\sigma_y\, \boldsymbol{\sigma}^*\, \sigma_y = -\boldsymbol{\sigma}$, we have

$$(\tau_0 \otimes \sigma_y) \left(\tau_0 \otimes \sigma^*_{x,y,z}\right) (\tau_0 \otimes \sigma_y) = -\tau_0 \otimes \sigma_{x,y,z} \tag{4.54}$$

whence

$$\begin{aligned}(\tau_0 \otimes \sigma_y) H_Z^*(x) (\tau_0 \otimes \sigma_y) = \\ = -(\tau_0 \otimes \sigma_y) \Big(\tau_0 \otimes (\mathbf{b}(x) \cdot \boldsymbol{\sigma}^*)\Big) (\tau_0 \otimes \sigma_y) = \\ = \tau_0 \otimes \Big(\mathbf{b}(x) \cdot \boldsymbol{\sigma}\Big) = \\ = -H_Z(x)\end{aligned} \tag{4.55}$$

We showed that, under TR transformation, the Zeeman term is mapped into its opposite and thus, it does not satisfy TR symmetry.

– **Superconducting term**
The superconducting pairing term has the form

$$H_{SC}(x) = (\tau_+ \otimes \sigma_0) \Delta(x) + (\tau_- \otimes \sigma_0) \Delta^*(x) = \begin{pmatrix} 0 & \Delta(x)\sigma_0 \\ \Delta^*(x)\sigma_0 & 0 \end{pmatrix} \tag{4.56}$$

Then, applying relation (4.42) one gets

$$\begin{aligned}(\tau_0 \otimes \sigma_y) H_{SC}^*(x) (\tau_0 \otimes \sigma_y) = \\ = \begin{pmatrix} \sigma_y & 0 \\ 0 & \sigma_y \end{pmatrix} \begin{pmatrix} 0 & \Delta^*(x)\sigma_0 \\ \Delta(x)\sigma_0 & 0 \end{pmatrix} \begin{pmatrix} \sigma_y & 0 \\ 0 & \sigma_y \end{pmatrix} = \\ = \begin{pmatrix} 0 & \Delta(x)^*\sigma_y \\ \Delta(x)\sigma_y & 0 \end{pmatrix} \begin{pmatrix} \sigma_y & 0 \\ 0 & \sigma_y \end{pmatrix} = \\ = \begin{pmatrix} 0 & \Delta(x)^*\sigma_0 \\ \Delta(x)\sigma_0 & 0 \end{pmatrix} = \\ = (\tau_+ \otimes \sigma_0) \Delta^*(x) + (\tau_- \otimes \sigma_0) \Delta(x)\end{aligned} \tag{4.57}$$

Hence, $H_{SC}(x) = (\tau_0 \otimes \sigma_y) H_{SC}^*(x) (\tau_0 \otimes \sigma_y)$ is valid, and therefore TR symmetry fulfilled, iff $\Delta(x) = \Delta^*(x)$, i.e. when $\Delta(x)$ represents a real quantity.

- **Particle-hole transformation**
It is worth noting that the action of the C-transformation onto the Nambu spinor (4.15)

$$\mathcal{C}\Psi\mathcal{C}^{-1} = \mathcal{C} \begin{pmatrix} \Psi_\uparrow \\ \Psi_\downarrow \\ \Psi_\downarrow^\dagger \\ -\Psi_\uparrow^\dagger \end{pmatrix} \mathcal{C}^{-1} \doteq \begin{pmatrix} \Psi_\uparrow^\dagger \\ \Psi_\downarrow^\dagger \\ \Psi_\downarrow \\ -\Psi_\uparrow \end{pmatrix} \equiv \begin{pmatrix} 0 & 0 & 0 & -1 \\ 0 & 0 & 1 & 0 \\ 0 & 1 & 0 & 0 \\ -1 & 0 & 0 & 0 \end{pmatrix} \begin{pmatrix} \Psi_\uparrow \\ \Psi_\downarrow \\ \Psi_\downarrow^\dagger \\ -\Psi_\uparrow^\dagger \end{pmatrix} = (\tau_y \otimes \sigma_y)\Psi \tag{4.58}$$

is implemented by the 4×4 matrix $\tau_y \otimes \sigma_y$. This is a consequence of the redundancy of the 4 components of the Nambu spinor, which contains *both* the fields and their adjoint.

4.4 Spin operator in BdG formalism

The *second-quantized* spin operator is defined as ($j = x, y, z$)

$$\begin{aligned}\hat{\mathcal{S}}^j(x) &= \left(\Psi^\dagger_\uparrow(x), \Psi^\dagger_\downarrow(x)\right) S^j \begin{pmatrix} \Psi_\uparrow(x) \\ \Psi_\downarrow(x) \end{pmatrix} = \\ &= \frac{\hbar}{2}\left(\Psi^\dagger_\uparrow(x), \Psi^\dagger_\downarrow(x)\right) \sigma^j \begin{pmatrix} \Psi_\uparrow(x) \\ \Psi_\downarrow(x) \end{pmatrix} = \\ &= \frac{\hbar}{2} \sum_{\sigma,\sigma'=\uparrow,\downarrow} \Psi^\dagger_\sigma(x) \left(\sigma^j\right)_{\sigma\sigma'} \Psi_{\sigma'}(x) \end{aligned} \tag{4.59}$$

where

$$S^j = \frac{\hbar}{2}\sigma^j \tag{4.60}$$

is the *first-quantized* spin operator. We shall now prove that the operator (4.59) can be rewritten in the BdG formalism as follows

$$\hat{\mathcal{S}}^j(x) = \frac{1}{2} \cdot \frac{\hbar}{2} \Psi^\dagger(x)(\tau_0 \otimes \sigma^j)\Psi(x) \tag{4.61}$$

where $\Psi(x)$ is the Nambu spinor (4.15). Thus, the *first-quantized* BdG spin-operator is

$$\boxed{S^j_{BdG} = \tfrac{\hbar}{2}(\tau_0 \otimes \sigma^j)} \tag{4.62}$$

Proof of Eqs.(4.61)-(4.62)
We rewrite Eq.(4.59) as

$$\hat{\mathcal{S}}^j(x) = \tag{4.63}$$

$$= \frac{\hbar}{2}\left\{ \frac{1}{2} \sum_{\sigma,\sigma'=\uparrow,\downarrow} \Psi^\dagger_\sigma(x) \left(\sigma^j\right)_{\sigma\sigma'} \Psi_{\sigma'}(x) + \frac{1}{2} \lim_{y\to x} \sum_{\sigma,\sigma'=\uparrow,\downarrow} \Psi^\dagger_\sigma(x) \left(\sigma^j\right)_{\sigma\sigma'} \Psi_{\sigma'}(y) \right\} =$$

$$= \frac{\hbar}{2}\left\{ \frac{1}{2} \sum_{\sigma,\sigma'=\uparrow,\downarrow} \Psi^\dagger_\sigma(x) \left(\sigma^j\right)_{\sigma\sigma'} \Psi_{\sigma'}(x) + \frac{1}{2} \lim_{y\to x} \sum_{\sigma,\sigma'=\uparrow,\downarrow} \left(\sigma^j\right)_{\sigma\sigma'} \left(\delta_{\sigma\sigma'}\delta(x-y) - \Psi_{\sigma'}(y)\Psi^\dagger_\sigma(x)\right) \right\} =$$

$$= \frac{\hbar}{4}\left\{ \sum_{\sigma,\sigma'=\uparrow,\downarrow} \Psi^\dagger_\sigma(x) \left(\sigma^j\right)_{\sigma\sigma'} \Psi_{\sigma'}(x) + \lim_{y\to x} \underbrace{\sum_{\sigma=\uparrow,\downarrow} \delta_{j,3}\,\sigma\delta(x-y)}_{=0} - \lim_{y\to x} \Psi_{\sigma'}(y) \left(\sigma^j\right)^*_{\sigma'\sigma} \Psi^\dagger_\sigma(x) \right\} =$$

$$= \frac{\hbar}{4}\left\{ \left(\Psi_\uparrow^\dagger(x), \Psi_\downarrow^\dagger(x)\right) \sigma^j \begin{pmatrix} \Psi_\uparrow(x) \\ \Psi_\downarrow(x) \end{pmatrix} - \left(\Psi_\uparrow(x), \Psi_\downarrow(x)\right) \left(\sigma^j\right)^* \begin{pmatrix} \Psi_\uparrow^\dagger(x) \\ \Psi_\downarrow^\dagger(x) \end{pmatrix} \right\} =$$

[insert identity $\sigma_0 = (-i\sigma_y)(i\sigma_y)$ on the left and on the right of $(\sigma^j)^*$]

$$= \frac{\hbar}{4}\left\{ \left(\Psi_\uparrow^\dagger(x), \Psi_\downarrow^\dagger(x)\right) \sigma^j \begin{pmatrix} \Psi_\uparrow(x) \\ \Psi_\downarrow(x) \end{pmatrix} - \left(\Psi_\uparrow(x), \Psi_\downarrow(x)\right) (-i\sigma_y) i\sigma_y \left(\sigma^j\right)^* (-i\sigma_y) i\sigma_y \begin{pmatrix} \Psi_\uparrow^\dagger(x) \\ \Psi_\downarrow^\dagger(x) \end{pmatrix} \right\} =$$

$$= \frac{\hbar}{4}\left\{ \left(\Psi_\uparrow^\dagger(x), \Psi_\downarrow^\dagger(x)\right) \sigma^j \begin{pmatrix} \Psi_\uparrow(x) \\ \Psi_\downarrow(x) \end{pmatrix} - \left(\Psi_\downarrow(x), -\Psi_\uparrow(x)\right) \sigma_y (\sigma^j)^* \sigma_y \begin{pmatrix} \Psi_\downarrow^\dagger(x) \\ -\Psi_\uparrow^\dagger(x) \end{pmatrix} \right\} =$$

$$= \frac{\hbar}{4}\left(\Psi_\uparrow^\dagger(x), \Psi_\downarrow^\dagger(x), \Psi_\downarrow(x), -\Psi_\uparrow(x)\right) \begin{pmatrix} \sigma^j & 0 \\ 0 & \underbrace{-\sigma_y \left(\sigma^j\right)^* \sigma_y}_{=-\sigma^j} \end{pmatrix} \begin{pmatrix} \Psi_\uparrow(x) \\ \Psi_\downarrow(x) \\ \Psi_\downarrow^\dagger(x) \\ -\Psi_\uparrow^\dagger(x) \end{pmatrix} =$$

$$= \frac{\hbar}{4}\left\{ \left(\Psi_\uparrow^\dagger(x), \Psi_\downarrow^\dagger(x), \Psi_\downarrow(x), -\Psi_\uparrow(x)\right) (\tau_0 \otimes \sigma^j) \begin{pmatrix} \Psi_\uparrow(x) \\ \Psi_\downarrow(x) \\ \Psi_\downarrow^\dagger(x) \\ -\Psi_\uparrow^\dagger(x) \end{pmatrix} \right\} \tag{4.64}$$

which is precisely Eq.(4.61) with Eq.(4.62).
End of Proof.

4.5 Bogolubov de Gennes formalism for a spatially inhomogeneous system

Whenever the second-quantized Hamiltonian $\mathcal{H}$ of a system can be written in the Bogolubov de Gennes form

$$\mathcal{H} = \frac{1}{2}\int dx\, \Psi^\dagger(x)\, H_{BdG}(x) \Psi(x) \; + C \tag{4.65}$$

where the Bogolubov de Gennes Hamiltonian exhibits the structure

$$H_{BdG}(x) = \begin{pmatrix} h_e(x) & \Delta(x)\sigma_0 \\ \Delta^*(x)\sigma_0 & -\sigma_y h_e^*(x) \sigma_y \end{pmatrix} \tag{4.66}$$

one can apply the Bogolubov de Gennes method for inhomogeneous system that we are going to describe here below.

4.6 Built-in symmetry of the BdG Hamiltonian

The very structure (4.66) of the BdG Hamiltonian shows that, by construction, H_{BdG} exhibits an intrinsic symmetry

$$C H_{BdG} C = -H_{BdG} \qquad \leftrightarrow \qquad \boxed{(\tau_y \otimes \sigma_y) H_{BdG}^* (\tau_y \otimes \sigma_y) = -H_{BdG}} \tag{4.67}$$

where

$$C = (\tau_y \otimes \sigma_y)K \tag{4.68}$$

is the *first-quantized* version of the particle-hole transformation $\mathcal{C}$ to the *second-quantized* operators of the Nambu spinor, and fulfills

$$C^{-1} = C \tag{4.69}$$

Note that particle-hole $\mathcal{C}$ is linear in *second-quantization*, while its first quantization action C in Eq.(4.68) is anti-linear, as it involves the complex conjugation K. Because it is the product of a unitary matrix $\tau_y \otimes \sigma_y$ and complex conjugation K, it is an anti-unitary operator, since the transformation C preserves the norm of any wavefunction Φ.
We emphasize that the relation (4.67) does *not* correspond to any physical symmetry of the second quantized Hamiltonian $\mathcal{H}$. Rather, it is a built-in symmetry characterizing the structure (4.66) of the first-quantized BdG Hamiltonian H_{BdG}. Because the BdG Hamiltonian results from re-writing the Hamiltonian $\mathcal{H}$ in the form (4.14) using the Nambu spinor, such built-in symmetry originates from the redundancy of Nambu degrees of freedom, which contains both the field operators and their adjoint.

4.7 Bogolubov quasi-particles

The built-in symmetry (4.67) implies that, for any given (4×1 spinor) eigenfunction

$$\Phi(x) = \begin{pmatrix} \begin{pmatrix} \mathbf{u}(x) \\ \mathbf{v}(x) \end{pmatrix} \end{pmatrix} = \begin{pmatrix} u_\uparrow(x) \\ u_\downarrow(x) \\ v_\downarrow(x) \\ v_\uparrow(x) \end{pmatrix} \tag{4.70}$$

of the BdG Hamiltonian with energy E,

$$H_{BdG}(x)\Phi(x) = E\Phi(x) \tag{4.71}$$

the wavefunction

$$\Phi'(x) = C\Phi(x) = (\tau_y \otimes \sigma_y)\Phi^*(x) = \begin{pmatrix} -i\sigma_y \mathbf{v}^*(x) \\ i\sigma_y \mathbf{u}^*(x) \end{pmatrix} = \begin{pmatrix} -v^*_\uparrow(x) \\ v^*_\downarrow(x) \\ u^*_\downarrow(x) \\ -u^*_\uparrow(x) \end{pmatrix} \tag{4.72}$$

is also an eigenfunction of the BdG Hamiltonian, with eigenvalue $-E$.
Indeed, taking the complex conjugate of Eq.(4.71)

$$\begin{gathered} H^*_{BdG}(x)\Phi^*(x) = E\Phi^*(x) \\ [\text{apply}(\tau_y \otimes \sigma_y)\text{to both sides}] \\ \Downarrow \\ \underbrace{(\tau_y \otimes \sigma_y)H^*_{BdG}(x)(\tau_y \otimes \sigma_y)}_{=-H_{BdG}(x) \text{ from Eq.(4.67)}} \underbrace{(\tau_y \otimes \sigma_y)\Phi^*(x)}_{=C\Phi(x)=\Phi'(x)} = E \underbrace{(\tau_y \otimes \sigma_y)\Phi^*(x)}_{=C\Phi(x)=\Phi'(x)} \\ \Downarrow \\ H_{BdG}(x)\Phi'(x) = -E\Phi'(x) \end{gathered} \tag{4.73}$$

As a consequence, the spectrum of the BdG equation is by construction symmetric around $E = 0$. Therefore, we can only look for solutions $\Phi_n^{(+)}$ with non-negative eigenvalues $E_n \geq 0$

$$H_{BdG}(x) \begin{pmatrix} \mathbf{u}_n(x) \\ \mathbf{v}_n(x) \end{pmatrix} = E_n \begin{pmatrix} \mathbf{u}_n(x) \\ \mathbf{v}_n(x) \end{pmatrix} \qquad E_n \geq 0 \tag{4.74}$$

Then, the entire set of eigenfunctions Φ_n can be split into two groups

$$\text{solutions with energy } E_n \geq 0 \qquad \Phi_n^{(+)}(x) = \begin{pmatrix} \mathbf{u}_n(x) \\ \mathbf{v}_n(x) \end{pmatrix} = \begin{pmatrix} u_{\uparrow,n}(x) \\ u_{\downarrow,n}(x) \\ v_{\downarrow,n}(x) \\ v_{\uparrow,n}(x) \end{pmatrix} \tag{4.75}$$

$$\text{solutions with energy } -E_n \leq 0 \qquad \Phi_n^{(-)}(x) = C \begin{pmatrix} \mathbf{u}_n(x) \\ \mathbf{v}_n(x) \end{pmatrix} = \begin{pmatrix} -v_{\uparrow,n}^*(x) \\ v_{\downarrow,n}^*(x) \\ u_{\downarrow,n}^*(x) \\ -u_{\uparrow,n}^*(x) \end{pmatrix} \tag{4.76}$$

that are mutually connected through charge-conjugation

$$\Phi_n^{(-)}(x) = C\Phi_n^{(+)}(x) \qquad \Phi_n^{(+)}(x) = C\Phi_n^{(-)}(x) \tag{4.77}$$

where C is given by Eq.(4.68) and the label n runs over a half of the eigenfunction quantum numbers, i.e. $E_n \geq 0$.

Zero energy solutions

In solving the BdG equations, there might be eigenfunctions at zero energy. Because the charge conjugation transformation (4.72) maps a zero energy eigenfunction into a zero energy eigenfunction, this means that, the zero-energy subspace of the Bogolubov de Gennes Equation can always be considered as spanned by a basis formed by eigenfunctions that are also eigenfunctions of the charge-conjugation operator

$$C\Phi_0(x) = \pm\Phi_0(x) \tag{4.78}$$

Recalling Eq.(4.68), this means that such wavefunction must fulfill

$$\begin{pmatrix} u_\uparrow(x) \\ u_\downarrow(x) \\ v_\downarrow(x) \\ v_\uparrow(x) \end{pmatrix} = \pm \begin{pmatrix} -v_\uparrow^*(x) \\ v_\downarrow^*(x) \\ u_\downarrow^*(x) \\ -u_\uparrow^*(x) \end{pmatrix} \tag{4.79}$$

In customary systems, when zero energy solutions exist, they always come in pairs. However, in topological systems, there might be under suitable conditions, only *one* single zero energy solution. In that case, it must be an eigenfunction of charge conjugation (4.78).

Direct relations

Because $H_{\rm BdG}$ is Hermitean, its entire set of eigenfunctions (with positive and negative energies) form an orthogonal complete set of the 4×1 wavefunction Hilbert space. Thus, we can expand the Nambu field operator in terms of the BdG eigenfunction Φ_n's multiplied by an operator each. In doing that, we separate the $\Phi_n^{(+)}(x)$ from the $\Phi_n^{(-)}(x)$

$$\Psi(x)=\sum_{E_n\geq 0}\left(\Phi_n^{(+)}(x)\gamma_n+\Phi_n^{(-)}(x)\gamma_n^\dagger\right)=\sum_{E_n\geq 0}\underbrace{\left(\begin{pmatrix}\\ \Phi_n^{(+)}(x)\\ \\ \end{pmatrix},\begin{pmatrix}\\ \Phi_n^{(-)}(x)\\ \\ \end{pmatrix}\right)}_{4\times 2}\underbrace{\begin{pmatrix}\gamma_n\\ \gamma_n^\dagger\end{pmatrix}}_{2\times 1} \tag{4.80}$$

which can be compactly rewritten as

$$\Psi(x)=\sum_{E_n\geq 0}\left(\Phi_n^{(+)}(x)\gamma_n+\Phi_n^{(-)}(x)\gamma_n^\dagger\right)=\sum_{E_n\geq 0}\mathsf{W}_n(x)\Gamma_n \tag{4.81}$$

by introducing the matrix-valued function

$$\mathsf{W}_n(x)\doteq\underbrace{\left(\begin{pmatrix}\\ \Phi_n^{(+)}(x)\\ \\ \end{pmatrix},\begin{pmatrix}\\ \Phi_n^{(-)}(x)\\ \\ \end{pmatrix}\right)}_{4\times 2}\qquad \mathsf{W}_n^\dagger(x)\doteq\underbrace{\begin{pmatrix}\left(\Phi_n^{(+)}(x)\right)^\dagger\\ \left(\Phi_n^{(-)}(x)\right)^\dagger\end{pmatrix}}_{2\times 4} \tag{4.82}$$

and the 2×1 operator spinor

$$\Gamma_n(x)\doteq\begin{pmatrix}\gamma_n\\ \gamma_n^\dagger\end{pmatrix} \tag{4.83}$$

The operators $\gamma_n,\gamma_n^\dagger$ are called Bogoliubov quasi-particle (second-quantized) operators.

Remark 1: Notice that in Eq.(4.80) the operator $\gamma_n^\dagger$ multiplying the negative energy solution $\Phi_n^{(-)}$ *must* be the Hermitean conjugate of the operator γ_n multiplying the positive energy solution $\Phi_n^{(+)}$ related through charge conjugation (4.77). This is a consistency condition arising from the intrinsic redundancy of the Nambu spinor

$$\mathcal{C}\Psi(x)\mathcal{C}^{-1} = C\Psi(x) \tag{4.84}$$

$$\Downarrow$$

$$\mathcal{C}\left(\sum_{E_n\geq 0}\left(\Phi_n^{(+)}(x)\gamma_n+\Phi_n^{(-)}(x)\gamma_n^\dagger\right)\right)\mathcal{C}^{-1} = C\sum_{E_n\geq 0}\left(\Phi_n^{(+)}(x)\gamma_n+\Phi_n^{(-)}(x)\gamma_n^\dagger\right) \tag{4.85}$$

$$\Downarrow$$

$$\sum_{E_n\geq 0}\left(\Phi_n^{(+)}(x)\gamma_n^\dagger+\Phi_n^{(-)}(x)\gamma_n\right) = \sum_{E_n\geq 0}\left(\Phi_n^{(-)}(x)\gamma_n+\Phi_n^{(+)}(x)\gamma_n^\dagger\right) \tag{4.86}$$

Remark 2: Notice that, in our notation, the quantum number n appearing in the operators $\gamma_n,\gamma_n^\dagger$ labels the *positive energy* solutions. Indeed in the Nambu spinor expansion Eq.(4.80), n denotes the quantum number of a solution $\Phi_n^{(+)}$, and the negative energy

solutions, labelled as $\Phi_n^{(-)}$, are the charge-conjugated of the positive energy ones [see Eq.(4.76)]. Of course, Eq.(4.80) could in principle be rewritten as

$$\Psi(x) = \sum_{E_n \geq 0} \left(\Phi_n^{(+)}(x)\gamma_n + \Phi_n^{(-)}(x)\gamma_{n_c} \right) \tag{4.87}$$

with n_c denoting the 'charge-conjugated' of n, i.e. the quantum number labelling the negative energy eigenfunctions obtained from charge-conjugation of the positive energy $\Phi_n^{(+)}$. However, the consistency imposed by the Nambu redundancy would impose the constraint

$$\gamma_n^\dagger(E) = \gamma_{n_c}(-E) \tag{4.88}$$

which elucidates that the γ-operators related to negative energies would not be independent of the one with positive energy.

In particular, notice that the operators related to zero energy solutions ($E = 0$) that are eigenstate of the charge conjugation transformation [see Eq.(4.78)] necessarily fulfill $n_c = n$ and

$$\gamma_0^\dagger = \gamma_0 \qquad \text{Majorana quasi-particle} \tag{4.89}$$

i.e. they are equal to their adjoint. These operators describe Majorana quasi-particles.

Remark 3: Taking into account the expression of $\Phi_n^{(-)}$ and $\Phi_n^{(+)}$ [see Eqs.(4.75)-(4.76)], the explicit expression of the electron field operators $\Psi_\uparrow$ and $\Psi_\downarrow$ in terms of the γ_n's can be gained from the upper two components in the expansion (4.80) of the Nambu electron field operator

$$\begin{cases} \Psi_\uparrow(x) &= \sum_n \left(u_{\uparrow,n}\gamma_n - v_{\uparrow,n}^*\gamma_n^\dagger \right) \\ \Psi_\downarrow(x) &= \sum_n \left(u_{\downarrow,n}\gamma_n + v_{\downarrow,n}^*\gamma_n^\dagger \right) \end{cases} \tag{4.90}$$

Inverse relations
The BdG eigenfunctions exhibit a mutual orthogonality

$$\int dx \, (\Phi_n^{(s)}(x))^\dagger \, (\Phi_m^{(s')}(x)) \, = \delta_{s,s'}\delta_{n,m} \qquad\qquad s, s' = \pm \tag{4.91}$$

which can be compactly rewritten using the matrix $\mathsf{W}_n(x)$ defined in Eq.(4.82)

$$\int dx \; \mathsf{W}_n^\dagger(x) \, \mathsf{W}_m(x) = \sigma_0 \, \delta_{n,m} \tag{4.92}$$

By multiplying Eq.(4.87) on the left by $\mathsf{W}_n^\dagger(x)$ and integrating over x, one can invert the transformation Eq.(4.80) or and express the Bogolubov quasi-particles in terms of the Nambu field operator

$$\Gamma_n = \int dx \, \mathsf{W}_n^\dagger(x) \, \Psi(x) \tag{4.93}$$

Recalling the definition (4.82) and (4.83), one obtains

$$\gamma_n = \int dx \, (\Phi_n^{(+)}(x))^\dagger \, \Psi(x) = \int dx \left(u^*_{\uparrow,n}, u^*_{\downarrow,n}, v^*_{\downarrow,n}, v^*_{\uparrow,n} \right)(x) \begin{pmatrix} \Psi_\uparrow \\ \Psi_\downarrow \\ \Psi^\dagger_\downarrow \\ -\Psi^\dagger_\uparrow \end{pmatrix}(x) \tag{4.94}$$

$$\gamma_n^\dagger = \int dx \, (\Phi_n^{(-)}(x))^\dagger \, \Psi(x) = \int dx \, (-v_{\uparrow,n}, v_{\downarrow,n}, u_{\downarrow,n}, -u_{\uparrow,n})(x) \begin{pmatrix} \Psi_\uparrow \\ \Psi_\downarrow \\ \Psi^\dagger_\downarrow \\ -\Psi^\dagger_\uparrow \end{pmatrix}(x) \tag{4.95}$$

Remark 1: By inspecting the scalar products in Eqs.(4.94)-(4.95), it is straightforward to realize that the above results can equivalently be expressed in two equivalent ways

$$\gamma_n = \int dx \, \Psi^\dagger(x) \, \Phi_n^{(-)}(x) \; = \int dx \left(\Psi^\dagger_\uparrow, \Psi^\dagger_\downarrow, \Psi_\downarrow, -\Psi_\uparrow \right)(x) \begin{pmatrix} -v^*_{\uparrow,n} \\ v^*_{\downarrow,n} \\ u^*_{\downarrow,n} \\ u^*_{\uparrow,n} \end{pmatrix}(x) \tag{4.96}$$

$$\gamma_n^\dagger = \int dx \, \Psi^\dagger(x) \, \Phi_n^{(+)}(x) \; = \int dx \left(\Psi^\dagger_\uparrow, \Psi^\dagger_\downarrow, \Psi_\downarrow, -\Psi_\uparrow \right)(x) \begin{pmatrix} u_{\uparrow,n} \\ u_{\downarrow,n} \\ v_{\downarrow,n} \\ v_{\uparrow,n} \end{pmatrix}(x) \tag{4.97}$$

Remark 2: It is possible to prove that the anti-commutation relations of the fermionic field operators $\{\Psi_\sigma(x), \Psi^\dagger_{\sigma'}(x')\} = \delta_{\sigma,\sigma'}\delta(x-x')$ imply that the Bogolubov operators are also fermionic

$$\{\gamma_n \, , \, \gamma_m^\dagger\} = \delta_{n,m} \tag{4.98}$$

4.8 Hamiltonian in the Bogolubov quasi-particle basis

One can now rewrite the Hamiltonian $\mathcal{H}$ in Eq.(4.14) in terms of the Bogolubov quasi-particle operators γ_n's. It is possible to show that

$$\boxed{\mathcal{H} = \sum_{n>0} E_n \left(\gamma_n^\dagger \gamma_n - \frac{1}{2} \right) + C} \tag{4.99}$$

which can be interpreted as a collection of two-level systems, labelled by n. Indeed, depending on whether the eigenvalue of number operator $\gamma_n^\dagger\gamma_n$ is 1 or 0, i.e. on whether the fermionic level is occupied or empty, the energy value is $\pm E_n/2$.

Proof of Eq.(4.99):
In order to prove that the Hamiltonian (4.14) can be rewritten as Eq.(4.99), we insert

the expression (4.80) of the Nambu field, and the related expression for its adjoint

$$\Psi(x) = \sum_{n>0} \underbrace{\left(\left(\Phi_n^{(+)}(x)\right), \left(\Phi_n^{(-)}(x)\right)\right)}_{=4\times 2} \underbrace{\begin{pmatrix}\gamma_n \\ \gamma_n^\dagger\end{pmatrix}}_{=2\times 1} \tag{4.100}$$

$$\Psi^\dagger(x) = \sum_{m>0} \underbrace{\left(\gamma_m^\dagger, \gamma_m\right)}_{=1\times 2} \underbrace{\begin{pmatrix}\left((\Phi_m^{(+)})^\dagger(x)\right) \\ \left((\Phi_m^{(-)})^\dagger(x)\right)\end{pmatrix}}_{2\times 4} \tag{4.101}$$

into the Hamiltonian (4.14), obtaining

$$\mathcal{H} = \frac{1}{2}\int dx \sum_{m,n>0} \left(\gamma_m^\dagger, \gamma_m\right) \begin{pmatrix}\left((\Phi_m^{(+)})^\dagger(x)\right) \\ \left((\Phi_m^{(-)})^\dagger(x)\right)\end{pmatrix} H_{BdG}(x) \left(\left(\Phi_n^{(+)}(x)\right), \left(\Phi_n^{(-)}(x)\right)\right) \begin{pmatrix}\gamma_n \\ \gamma_n^\dagger\end{pmatrix} + C \tag{4.102}$$

Recalling now that $\Phi_n^{(\pm)}(x)$ are the eigenfunctions of H_{BdG} with eigenvalues $\pm E_n$,

$$H_{BdG}(x)\Phi_n^{(\pm)}(x) = \pm E_n\, \Phi_n^{(\pm)}(x) \tag{4.103}$$

one has

$$\mathcal{H} = \frac{1}{2}\int dx \sum_{m,n>0} \left(\gamma_m^\dagger, \gamma_m\right) \begin{pmatrix}\left((\Phi_m^{(+)})^\dagger(x)\right) \\ \left((\Phi_m^{(-)})^\dagger(x)\right)\end{pmatrix} \begin{pmatrix}E_n & 0 \\ 0 & -E_n\end{pmatrix} \left(\left(\Phi_n^{(+)}(x)\right), \left(\Phi_n^{(-)}(x)\right)\right) \begin{pmatrix}\gamma_n \\ \gamma_n^\dagger\end{pmatrix} + C =$$
$$= \frac{1}{2}\sum_{m,n>0} \left\{E_n\gamma_m^\dagger\gamma_n \left(\int dx (\Phi_m^{(+)})^\dagger(x)\cdot\Phi_n^{(+)}(x)\right) - E_n\gamma_m\gamma_n^\dagger \left(\int dx (\Phi_n^{(-)})^\dagger(x)\cdot\Phi_m^{(-)}(x)\right)\right\} + C$$

exploiting the orthonormality conditions (4.91), one finds

$$\mathcal{H} = \frac{1}{2}\sum_{n>0} E_n \left(\gamma_n^\dagger\gamma_n - \gamma_n\gamma_n^\dagger\right) + C \tag{4.104}$$

Exploiting now the anti-commutation relations (4.98) of the Bogolubov quasi-particles, we finally obtain the claimed Eq.(4.99).

The ground state

Since by construction $E_n \geq 0$, for each of the two-level system appearing in Eq.(4.99) the ground state has an energy $-E_n/2$ (unoccupied level), while the excited state has an energy $+E_n/2$ (occupied level). This means that $E_n \geq 0$ represents the *excitation energy*, and that the ground state $|G\rangle$ of the inhomogeneous system is defined as

$$\gamma_n|G\rangle = 0 \qquad \forall n \tag{4.105}$$

The ground state energy $E_0 = \langle G|\mathcal{H}|G\rangle$ is obtained when all excited levels are left empty and is equal to

$$E_0 = C - \frac{1}{2}\sum_n E_n \tag{4.106}$$

Note that, although both $(1/2)\sum_n E_n$ and C are formally infinite constants, their difference E_0 is typically finite.

Chapter 5

The case of a single N/S interface in the nanowire

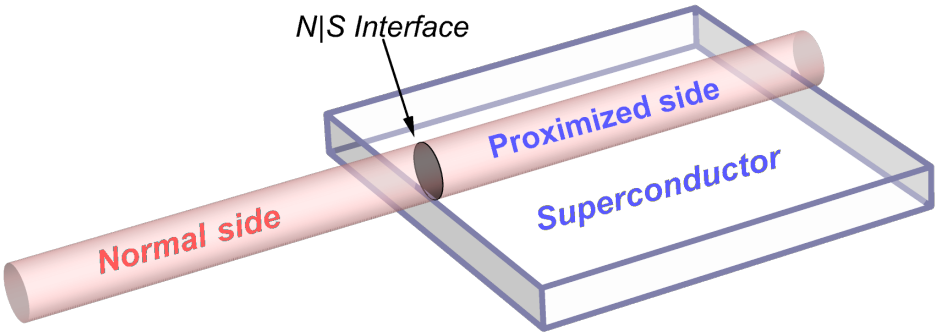

Figure 5.1: Schematic geometry of the Normal-Superconductor (N-S) junction. The system is modeled as a 1D nanowire. The Normal Region (N) and the Superconducting Region (S) are connected through a vertical planar interface, as illustrated in the figure.

Let us now consider the problem of an interface between a normal region N that is not proximized $\Delta_0 = 0$, and a nanowire region S proximized by a superconducting film, where the superconducting pairing $\Delta_0 > 0$ is present

$$\Delta(x) = \vartheta(x - x_0)\Delta_0 e^{i\varphi} \tag{5.1}$$

where x_0 is the location of the interface. Fig.5.1 shows a schematic representation of such a system.
Moreover, we shall assume that the hemical potential $\mu(x)$, the magnetic field $\mathbf{b}(x)$ and the spin-orbit coupling $\boldsymbol{\alpha}(x)$ can take different values on the two sides N and S of the

junction. For simplicity, we shall consider piecewise constant profiles, i.e.

$$\mu(x) = \vartheta(x_0 - x)\mu_N + \vartheta(x - x_0)\mu_S \tag{5.2}$$
$$\mathbf{b}(x) = \vartheta(x_0 - x)\mathbf{b}_N + \vartheta(x - x_0)\mathbf{b}_S \tag{5.3}$$
$$\boldsymbol{\alpha}(x) = \vartheta(x_0 - x)\boldsymbol{\alpha}_N + \vartheta(x - x_0)\boldsymbol{\alpha}_S \tag{5.4}$$

Equation (5.2) implies that the operator Eq.(4.20) is

$$\hat{\xi}(x) = -\frac{1}{2m^*}\frac{\partial^2}{\partial x^2} - \vartheta(x_0 - x)\mu_N - \vartheta(x - x_0)\mu_S \tag{5.5}$$

while Eq.(5.4) leads to the spin-orbit field operator Eq.(4.21)

$$\begin{aligned}\hat{\mathbf{b}}_{SO}(x) &= -i\left(\boldsymbol{\alpha}(x)\frac{\partial}{\partial x} + \frac{1}{2}(\partial_x\boldsymbol{\alpha}(x))\right) = \\ &= -i\left(\boldsymbol{\alpha}(x)\frac{\partial}{\partial x} + \frac{1}{2}(\boldsymbol{\alpha}_S - \boldsymbol{\alpha}_N)\,\delta(x - x_0)\right)\end{aligned} \tag{5.6}$$

The BdG Equations for the N-S junction are obtained from Eq.(4.22) and read

$$\begin{pmatrix}\hat{\xi}(x)\sigma_0 - \hat{\mathbf{b}}_{SO}(x)\cdot\boldsymbol{\sigma} - \mathbf{b}(x)\cdot\boldsymbol{\sigma} & \Delta(x)\sigma_0 \\ \Delta^*(x)\sigma_0 & -\hat{\xi}(x)\sigma_0 + \hat{\mathbf{b}}_{SO}(x)\cdot\boldsymbol{\sigma} - \mathbf{b}(x)\cdot\boldsymbol{\sigma}\end{pmatrix}\Phi(x) = E\,\Phi(x) \qquad E \geq 0 \tag{5.7}$$

where $\hat{\xi}(x)$ is given by Eq.(5.5), $\hat{\mathbf{b}}_{SO}(x)$ by Eq.(5.6) and $\Delta(x)$ by Eq.(5.1), and $\mathbf{b}(x)$ by Eq.(5.3), while the components read [see Eq.(4.70)]

$$\Phi(x) = \begin{pmatrix}\mathbf{u}(x)\\ \mathbf{v}(x)\end{pmatrix} = \begin{pmatrix}u_\uparrow(x)\\ u_\downarrow(x)\\ v_\downarrow(x)\\ v_\uparrow(x)\end{pmatrix} \quad . \tag{5.8}$$

5.1 Interface boundary conditions

At the interface x_0, the wavefunction $\Phi(x)$ must satisfy specific constraints at the interface. Here below we shall show that, the assumptions of piecewise constant profiles Eqs.(5.1),(5.2), (5.3) and (5.4) lead to the following boundary conditions at the N-S interface x_0

$$\boxed{\Phi(x_0^+) = \Phi(x_0^-) = \Phi(x_0)} \tag{5.9}$$

and

$$\boxed{\partial_x\Phi(x_0^+) - \partial_x\Phi(x_0^-) = i\frac{m^*}{\hbar^2}\left(\tau_0 \otimes \left((\boldsymbol{\alpha}_S - \boldsymbol{\alpha}_N)\cdot\boldsymbol{\sigma}\right)\right)\Phi(x_0)} \tag{5.10}$$

Notably, the wavefunction derivative exhibits a discontinuity at the interface location x_0, related to the abrupt jump of the spin-orbit coupling (5.4), whereas the discontinuities (5.2) and (5.3) in the chemical potential and magnetic field do not affect the boundary conditions. We now proceed by deriving these boundary conditions.

Rewriting the Bogoliubov equations (5.7) with the Hamiltonian Eq.(4.22) for the two 2×1 spinors $\mathbf{u}(x)$ and $\mathbf{v}(x)$ of the wavefunction (5.8), one obtains

$$\begin{cases} \Big(\hat{\xi}(x)\sigma_0 - \hat{\mathbf{b}}_{SO}(x)\cdot\boldsymbol{\sigma} - \mathbf{b}(x)\cdot\boldsymbol{\sigma}\Big)\mathbf{u}(x) + \Delta(x)\mathbf{v}(x) & = E\,\mathbf{u}(x) \\ \Delta^*(x)\mathbf{u}(x) - \Big(\hat{\xi}(x)\sigma_0 - \hat{\mathbf{b}}_{SO}(x)\cdot\boldsymbol{\sigma} + \mathbf{b}(x)\cdot\boldsymbol{\sigma}\Big)\mathbf{v}(x) & = E\,\mathbf{v}(x) \end{cases} \tag{5.11}$$

Substituting Eqs.(5.5) and (5.6), one obtains

$$-\frac{1}{2m^*}\,\partial_x^2\mathbf{u} - \mu(x)\mathbf{u}(x) + i\left(\boldsymbol{\alpha}(x)\cdot\boldsymbol{\sigma}\,\partial_x\mathbf{u}(x) + \frac{1}{2}(\boldsymbol{\alpha}_S - \boldsymbol{\alpha}_N)\cdot\boldsymbol{\sigma}\,\mathbf{u}(x)\,\delta(x-x_0)\right) + \\ -\mathbf{b}(x)\cdot\boldsymbol{\sigma}\,\mathbf{u}(x) + \Delta(x)\mathbf{v}(x) = E\mathbf{u}(x) \tag{5.12}$$

$$\frac{1}{2m^*}\,\partial_x^2\mathbf{v} + \mu(x)\mathbf{v}(x) - i\left(\boldsymbol{\alpha}(x)\cdot\boldsymbol{\sigma}\,\partial_x\mathbf{v}(x) + \frac{1}{2}(\boldsymbol{\alpha}_S - \boldsymbol{\alpha}_N)\cdot\boldsymbol{\sigma}\,\mathbf{v}(x)\,\delta(x-x_0)\right) + \\ -\mathbf{b}(x)\cdot\boldsymbol{\sigma}\,\mathbf{v}(x) + \Delta^*(x)\mathbf{u}(x) = E\mathbf{v}(x) \tag{5.13}$$

- **Continuity of the wavefunction**

  The first equation (5.12) implies that the function $\mathbf{u}(x)$ must be continuous at x_0. Indeed, if $\mathbf{u}(x)$ had a discontinuity at x_0, its first derivative would behave as $\partial_x\mathbf{u} \propto \delta(x-x_0)$, while its second derivative as $\partial_x^2\mathbf{u} \propto \partial_x\delta(x-x_0)$. However, the other equation terms do not exhibit a term $\partial_x\delta(x-x_0)$ and the equation could not be fulfilled. Similarly, the second equation (5.12) implies that the function $\mathbf{v}(x)$ must be continuous at x_0

  $$\begin{cases} \mathbf{u}(x_0^+) = \mathbf{u}(x_0^-) = \mathbf{u}(x_0) \\ \mathbf{v}(x_0^+) = \mathbf{v}(x_0^-) = \mathbf{v}(x_0) \end{cases} \qquad \Longrightarrow \qquad \Phi(x_0^+) = \Phi(x_0^-) = \Phi(x_0) \tag{5.14}$$

  which is the claimed Eq.(5.9).

- **Discontinuity of the first derivative of the wavefunction**

  To derive the boundary conditions for the first derivative, we integrate each of the two BdG equations over an infinitesimal interval $[x_0-\epsilon, x_0+\epsilon]$, taking the limit $\epsilon \to 0$,

  $$\lim_{\epsilon\to 0}\int_{x_0-\epsilon}^{x_0+\epsilon}\Big(H_{BdG}(x) - E\Big)\Phi(x)\;dx = 0 \qquad \Leftrightarrow \qquad \begin{cases} \lim\limits_{\epsilon\to 0}\int_{x_0-\epsilon}^{x_0+\epsilon} \text{Eq.(5.12)}\,dx \\ \lim\limits_{\epsilon\to 0}\int_{x_0-\epsilon}^{x_0+\epsilon} \text{Eq.(5.13)}\,dx \end{cases} \tag{5.15}$$

  When integrating, we observe that, because $\mathbf{u}$ and $\mathbf{v}$ are continuous, their derivatives $\partial_x\mathbf{u}$ and $\partial_x\mathbf{v}$ can at most exhibit a jump discontinuity (not a divergence), and are

bounded. Thus, their integral over the infinitesimally small domain $[x_0-\epsilon, x_0+\epsilon]$ vanishes. Integrating Eq.(5.12) one obtains

$$-\frac{\hbar^2}{2m^*}\Big(\partial_x \mathbf{u}(x_0^+) - \partial_x \mathbf{u}(x_0^-)\Big) - \underbrace{\int_{x_0-\epsilon}^{x_0+\epsilon} \mu(x)\mathbf{u}(x)\,dx}_{\to 0} + i\underbrace{\int_{x_0-\epsilon}^{x_0+\epsilon} \boldsymbol{\alpha}(x)\cdot\boldsymbol{\sigma}\,\partial_x \mathbf{u}(x)\,dx}_{\to 0} +$$
$$+\frac{i}{2}(\boldsymbol{\alpha}_S - \boldsymbol{\alpha}_N)\cdot\boldsymbol{\sigma}\underbrace{\int_{x_0-\epsilon}^{x_0+\epsilon} \mathbf{u}(x)\,\delta(x-x_0)\,dx}_{\mathbf{u}(x_0)} - \underbrace{\int_{x_0-\epsilon}^{x_0+\epsilon} \mathbf{b}(x)\cdot\boldsymbol{\sigma}\,\mathbf{u}(x)\,dx}_{\to 0} +$$
$$+\underbrace{\int_{x_0-\epsilon}^{x_0+\epsilon} \Delta(x)\mathbf{v}(x)\,dx}_{\to 0} = E\underbrace{\int_{x_0-\epsilon}^{x_0+\epsilon} \mathbf{u}(x)\,dx}_{\to 0} \tag{5.16}$$

which leads to

$$\partial_x \mathbf{u}(x_0^+) - \partial_x \mathbf{u}(x_0^-) = i\frac{m^*}{\hbar^2}\Big((\boldsymbol{\alpha}_S - \boldsymbol{\alpha}_N)\cdot\boldsymbol{\sigma}\Big)\,\mathbf{u}(x_0) \tag{5.17}$$

Similarly, integrating Eq.(5.13) one obtains

$$\frac{\hbar^2}{2m^*}\Big(\partial_x \mathbf{v}(x_0^+) - \partial_x \mathbf{v}(x_0^-)\Big) + \underbrace{\int_{x_0-\epsilon}^{x_0+\epsilon} \mu(x)\mathbf{v}(x)\,dx}_{\to 0} - i\underbrace{\int_{x_0-\epsilon}^{x_0+\epsilon} \boldsymbol{\alpha}(x)\cdot\boldsymbol{\sigma}\,\partial_x \mathbf{v}(x)\,dx}_{\to 0} +$$
$$-\frac{i}{2}(\boldsymbol{\alpha}_S - \boldsymbol{\alpha}_N)\cdot\boldsymbol{\sigma}\underbrace{\int_{x_0-\epsilon}^{x_0+\epsilon} \mathbf{v}(x)\,\delta(x-x_0)\,dx}_{\mathbf{v}(x_0)} - \underbrace{\int_{x_0-\epsilon}^{x_0+\epsilon} \mathbf{b}(x)\cdot\boldsymbol{\sigma}\,\mathbf{v}(x)\,dx}_{\to 0} +$$
$$+\underbrace{\int_{x_0-\epsilon}^{x_0+\epsilon} \Delta^*(x)\mathbf{u}(x)\,dx}_{\to 0} = E\underbrace{\int_{x_0-\epsilon}^{x_0+\epsilon} \mathbf{v}(x)\,dx}_{\to 0} \tag{5.18}$$

which leads to

$$\partial_x \mathbf{v}(x_0^+) - \partial_x \mathbf{v}(x_0^-) = i\frac{m^*}{\hbar^2}\Big((\boldsymbol{\alpha}_S - \boldsymbol{\alpha_N})\cdot\boldsymbol{\sigma}\Big)\,\mathbf{v}(x_0) \tag{5.19}$$

Finally, recalling Eq.(5.8), we can recast the two conditions Eqs.(5.16) and (5.18) into Eq.(5.10).

5.1.1 Scattering Matrix

In this section we shall illustrate how the boundary conditions defined in Eqs.(5.9)-(5.10) enable us to construct the Scattering Matrix, which enables us to extract all the relevant physical transport properties and, in particular, the Andreev reflection.

We start by observing that the wavefunction $\Phi(x)$ for the entire N-S system is expressed as the following piecewise function:

$$\Phi(x) = \begin{cases} \Phi_N(x) & \text{if} \quad x \le x_0 \\ \\ \Phi_S(x) & \text{if} \quad x > x_0 \end{cases} \tag{5.20}$$

where x_0 denotes the interface positions. Then, it is worth rewriting the boundary condition (5.10) describing the discontinuity of the first derivatives by separating the terms related to $\Phi_N(x)$ in N region from those of $\Phi_S(x)$ in S region. Then, the boundary conditions (5.9)-(5.10) for $\Phi(x)$ are rewritten as

$$\begin{cases} \Phi_N(x_0^-) = \Phi_S(x_0^+) \\ \partial_x \Phi_N(x_0^-) - i\dfrac{m^*}{\hbar^2}\Big(\tau_0 \otimes \big(\boldsymbol{\alpha}_N \cdot \boldsymbol{\sigma}\big)\Big)\,\Phi_N(x_0^-) = \partial_x \Phi_S(x_0^+) - i\dfrac{m^*}{\hbar^2}\Big(\tau_0 \otimes \big(\boldsymbol{\alpha}_S \cdot \boldsymbol{\sigma}\big)\Big)\,\Phi_S(x_0^+) \end{cases} \tag{5.21}$$

Since the wavefunctions are four-component spinors, Eq.(5.21) corresponds to a system of 8 linear equations. In order to proceed to the solution, we shall borrow some concepts from the Scattering formalism formulated by Landauer & Büttiker [114, 115].

At a given energy E, the wavefunctions $\Phi_N(x)$ and $\Phi_S(x)$ on each side of the junction, are superposition of planewaves eigenstates of the form $e^{ik_E x}$, each being multiplied by its complex amplitude. One can distinguish two types of waves.

- The wavefunctions characterized by a real wavevector k_E are called *propagating modes*. They might be particle or hole modes (in the N side) and particle-like or hole-like (in the S side). The sign of the group velocity $v = \hbar^{-1}\partial_k E_k$ determines the propagation direction of the mode (rightwards or leftwards). At each energy E, one always has an even number of propagating modes. Indeed for any propagating mode with a positive group velocity, there exists also another propagating mode with negative group velocity. Specifically, in the system considered here, for any mode with velocity $v_E > 0$, there exist a mode with the same energy E and opposite velocity $-v_E$ (although not necessarily with the opposite wavevector). Such a pair of counter-propagating modes form a *quantum propagating channel*. In each side of the interface, we shall label by a the amplitudes of propagating modes that are *incoming* towards the interface, and by b the amplitudes of the modes that are *outgoing* from the interface;
- At the energy E, one can also have wavefunctions characterized by a wavevector k with an imaginary part. Again, in each side of the interface, such modes come always in pairs with complex conjugate imaginary parts of the wavevectors. However, only the ones that do not diverge exponentially at $|x| \to \infty$ are physically acceptable and should be retained. These are dubbed *evanescent modes*.

The number of propagating and evanescent modes depend on the energy. For a given energy range, in each side $i = N, S$ of the interface, one has a number $N_{p,N}$ and $N_{p,S}$ of propagating channels, and each channel exhibits a mode incoming towards the interface (with an amplitude denoted by a) and a mode outgoing from the interface (with an amplitude denoted by b). Thus, in each side, one has $2N_{p,i}$ unknown amplitudes. Furthermore, each side can also exhibit a number $N_{e,N}$ (and $N_{e,S}$) of evanescent modes, whose amplitudes are denoted by c. We also note that, in the system considered here, at each given energy E, there are always 8 wavevectors in each side. Therefore, the following

relation holds

$$2(N_{p,i}+N_{e,i})=8 \quad \Leftrightarrow \quad N_{p,i}+N_{e,i}=4 \qquad\qquad i=N,S \tag{5.22}$$

In summary, one has

$$\begin{array}{rcl} N_N &=& 2N_{p,N}+N_{e,N} = \#\text{ of unknowns on the N side} \\ N_S &=& 2N_{p,S}+N_{e,S} = \#\text{ of unknowns on the S side} \end{array} \tag{5.23}$$

We now denote by

$$\begin{array}{rcl} \mathbf{v}_N &=& \left(\underbrace{a\ldots b\ldots}_{2N_{p;N}},\underbrace{c\ldots}_{N_{e;N}}\right)^T = \text{vector of the } N_N \text{ unknown amplitudes on the N side} \\ \mathbf{v}_S &=& \left(\underbrace{a\ldots b\ldots}_{2N_{p;S}},\underbrace{c\ldots}_{N_{e;S}}\right)^T = \text{vector of the } N_S \text{ unknown amplitudes on the S side} \end{array} \tag{5.24}$$

Then, Eq.(5.21) can be written as

$$\underbrace{\begin{pmatrix} \\ \mathsf{M}_N(x_0) \\ \\ \end{pmatrix}}_{8\times N_N} \underbrace{\begin{pmatrix}\mathbf{v}_N\end{pmatrix}}_{N_N\times 1} = \underbrace{\begin{pmatrix} \\ \mathsf{M}_S(x_0) \\ \\ \end{pmatrix}}_{8\times N_S} \underbrace{\begin{pmatrix}\mathbf{v}_S\end{pmatrix}}_{N_S\times 1} \tag{5.25}$$

where the matrices $\mathsf{M}_N(x_0)$ and $\mathsf{M}_S(x_0)$ contain the various waves (travelling or evanescent) on the N and S side, respectively, evaluated at x_0.
As a whole, this is a set of 8 linear equations for N_N+N_S unknowns. This implies that one will be able to fix only 8 unknowns in terms of the remaining N_N+N_S-8, which remain undetermined. Exploiting Eqs.(5.22) and (5.23) it is straightforward to see that total number of undetermined unknowns is

$$\begin{array}{rcl} N_p &\doteq& N_N+N_S-8 \text{ (total \# of undetermined unknowns)} = \\ &\equiv& N_{p,N}+N_{p,S} \text{ (total \# of propagating channels)} \end{array} \tag{5.26}$$

Notice also that

$$8 \;=\; \text{total \# of determined unknowns} = N_{p,N}+N_{p,S}+N_{e,N}+N_{e,S} \tag{5.27}$$

We shall choose the amplitudes a of the *incoming* propagating modes as the undetermined unknowns. Thus, the boundary conditions (5.25) will enables us to express all the b amplitudes of the *outgoing* propagating modes and all the c amplitudes of the evanescent modes in terms of the a amplitudes of the *incoming* propagating modes.

$$\underbrace{\left(\begin{array}{c} b \\ \vdots \\ \hline c \end{array}\right)}_{8\times 1} = \underbrace{\begin{pmatrix} \\ S \\ \\ \hline \end{pmatrix}}_{\Sigma\ (8\times N_p)} \underbrace{\begin{pmatrix} a \end{pmatrix}}_{N_p\times 1} \tag{5.28}$$

where the upper part of the Σ matrix, called the *Scattering matrix*, is a $N_p \times N_p$ matrix connecting the outgoing amplitudes to the incoming amplitudes. Then we have:

- **N region**

$$\text{Range 1} \quad \mathbf{v}_N = \left(a^e_{\nearrow,+}, a^e_{\swarrow,+}, a^h_{\nearrow,-}, a^h_{\swarrow,-}, b^e_{\nearrow,-}, b^e_{\swarrow,-}, b^h_{\nearrow,+}, b^h_{\swarrow,+}\right)^T \quad \begin{cases} N_{p,N} = 4 \\ N_{e,N} = 0 \end{cases}$$

$$\text{Range 2} \quad \mathbf{v}_N = \left(a^e_{\nearrow,+}, a^e_{\swarrow,+}, b^h_{\nearrow,-}, b^h_{\swarrow,-}, c^h_{\nearrow,-}, c^h_{\swarrow,-}\right)^T \quad \begin{cases} N_{p,N} = 2 \\ N_{e,N} = 2 \end{cases}$$

- **S region**

$$\text{Sub-Gap} \quad \mathbf{v}_S = \left(c^e_{\uparrow,+}, c^e_{\downarrow,+}, c^h_{\uparrow,+}, c^h_{\downarrow,+}\right)^T \quad \begin{cases} N_{p,S} = 0 \\ N_{e,S} = 4 \end{cases}$$

$$\begin{matrix}\text{Lower} \\ \text{Supra-gap}\end{matrix} \quad \mathbf{v}_S = \left(a^e_{\uparrow,-}, a^e_{\downarrow,-}, a^h_{\uparrow,+}, a^h_{\downarrow,+}, b^e_{\uparrow,+}, b^e_{\downarrow,+}, b^h_{\uparrow,-}, b^h_{\downarrow,-}\right)^T \quad \begin{cases} N_{p,S} = 4 \\ N_{e,S} = 0 \end{cases}$$

$$\begin{matrix}\text{Upper} \\ \text{Supra-gap}\end{matrix} \quad \mathbf{v}_S = \left(a^e_{\uparrow,-}, a^e_{\downarrow,-}, b^e_{\uparrow,+}, b^e_{\downarrow,+}, c^h_{\uparrow,+}, c^h_{\downarrow,+}\right)^T \quad \begin{cases} N_{p,S} = 2 \\ N_{e,S} = 2 \end{cases}$$

The explicit expression of the Matrix Σ in Eq.(5.28) can be obtained from solving the system (5.25) using Wolfram Mathematica.

Unitarity of the Scattering Matrix

The fundamental property of the scattering matrix S is its *unitarity*. This mathematical property encode a fundamental physical principle: the conservation of probability. We will now provide a qualitative explanation for this statement. For a bound quantum state, the normalization condition for a generic wavefunction $\Phi(x,t)$ reads

$$\int_{-\infty}^{+\infty} |\Phi(x,t)|^2 \, dx = 1. \tag{5.29}$$

In scattering problems, however, the wavefunctions are not square-integrable and are instead normalized with respect to their probability flux. The continuity equation still expresses the same principle — the local conservation of probability.
Defining the probability density $\rho(x,t)$ and the probability current $j(x,t)$ as

$$\rho(x,t) = \Phi^\dagger(x,t)\, \Phi(x,t) \tag{5.30}$$

$$j(x,t) = \Phi^\dagger(x,t)\, \hat{v}_x\, \Phi(x,t) \tag{5.31}$$

where $\hat{v}_x$ is the 4×4 velocity operator, then the conservation of probability implies that the temporal change of ρ in any volume V is balanced by the net flux through its boundaries:

$$\int_V \frac{\partial \rho}{\partial t}\, dx = -\int_V \frac{\partial j}{\partial x}\, dx. \tag{5.32}$$

Since this relation holds for any volume, one obtains the continuity equation in differential form:

$$\frac{\partial \rho}{\partial t} + \frac{\partial j}{\partial x} = 0. \tag{5.33}$$

In a scattering problem treated with stationary states, the density $\rho(x) = |\Phi(x)|^2$ is independent of time. Consequently, $\partial_t \rho = 0$, and the continuity equation reduces to the conservation of the current:

$$\frac{\partial j}{\partial x} = 0 \quad \Longrightarrow \quad j(x) = \text{constant}. \tag{5.34}$$

Considering now the scattering matrix S and denoting the vectors of incoming and outgoing components, respectively, as $\mathbf{b}$ and $\mathbf{a}$ one has

$$\mathbf{b} = S\mathbf{a} \tag{5.35}$$

Since each propagating mode in the wavefunctions Φ_N [see Eqs (5.67-5.76)] and Φ_S [see Eqs(5.120-5.105-5.109)] has been normalized with respect to its corresponding group velocity, the total probability flux for the incoming state is

$$\mathbf{P}_{in} = \mathbf{a}^\dagger \, \mathbf{a} \tag{5.36}$$

whereas, the total probability flux for the outgoing state is

$$\mathbf{P}_{out} = \mathbf{b}^\dagger \, \mathbf{b} = \mathbf{a}^\dagger \, S^\dagger \, S \, \mathbf{a} \tag{5.37}$$

Then the conservation of probability fluxes holds iff

$$\mathbf{P}_{in} = \mathbf{P}_{out} \qquad \Longleftrightarrow \qquad S^\dagger \, S = 1 \tag{5.38}$$

namely, iff S is unitary.

The conservation of flux implies that the current j_{inc} carried by the incoming modes, is exactly redistributed among all outgoing waves. Therefore, considering a single incoming modes (normalized to carry unit flux), we define the reflection and transmission probabilities as

$$R_m = \frac{|j_{R,m}|}{|j_{\text{inc}}|}, \qquad T_n = \frac{|j_{T,n}|}{|j_{\text{inc}}|}, \tag{5.39}$$

and the conservation of flux imposes

$$\sum_m R_m + \sum_n T_n = 1. \tag{5.40}$$

where $m/\, n$ span all possible reflected and transmitted modes, respectively.
Thus, the unitarity of S_E guarantees that the total probability for a particle to be either reflected or transmitted is exactly one.

5.2 The case without magnetic field

Let us start by analyzing the case where no magnetic field is applied to the system

$$\mathbf{b} \equiv 0 \tag{5.41}$$

We shall assume the spin-orbit field lies in the y-z spin plane. In fact, in a 1D nanowire where the confinement potential acts in the y-z plane, the electron motion is restricted to the x-axis, implying $k \equiv k_x$. Recalling that the Rashba SOC term is proportional to $(\mathbf{k} \times \boldsymbol{\sigma}) \cdot \hat{\mathbf{r}}$ [see Eq.(1.54)], where $\hat{\mathbf{r}}$ represents the direction of the applied electric field $\mathbf{E}(\mathbf{r})$, it follows that the spin-orbit vector $\boldsymbol{\alpha}$ lies entirely in the plane perpendicular to the electron propagation direction. Moreover, because we aim to take into account inhomogeneities of the spin-orbit field, we shall assume that

$$\boldsymbol{\alpha}_N = \alpha_N \left(0, \sin\Phi_{SO}, \cos\Phi_{SO}\right) \tag{5.42}$$

$$\boldsymbol{\alpha}_S = (0, 0, \alpha_S) \tag{5.43}$$

where α_S can take any sign and Φ_{SO} describes the mislignament angle of the spin-orbit field directions between the N and S regions. Here below, we shall compute the solutions in the N and S regions, and then apply the boundary conditions to match them properly and identifying the Andreev reflection and the transmission processes

5.2.1 Solution in the N region

In the N region, i.e. for $x < 0$, the BdG equations (5.7) reduce to

$$\begin{pmatrix} \left(-\frac{\partial_x^2}{2m^*} - \mu_N\right)\sigma_0 + i(\boldsymbol{\alpha}_N \cdot \boldsymbol{\sigma})\partial_x & 0 \\ 0 & \left(\frac{\partial_x^2}{2m^*} + \mu_N\right)\sigma_0 - i(\boldsymbol{\alpha}_N \cdot \boldsymbol{\sigma})\partial_x \end{pmatrix} \Phi(x) = E\Phi(x) \tag{5.44}$$

Introducing the matrix

$$\sigma_\Phi = \sigma_y \sin\Phi_{SO} + \sigma_z \cos\Phi_{SO} \tag{5.45}$$

one has

$$\boldsymbol{\alpha}_N \cdot \boldsymbol{\sigma} = \alpha_N \, \sigma_\Phi$$

Then, looking now for plane-wave solutions of Eq.(5.44)

$$\Phi_k(x) = \mathsf{w}_k \, e^{ikx} \tag{5.46}$$

with w_k denoting a 4×1 spinor, the Equation reduces to

$$H_{BdG,N}(k)\, \mathsf{w}_k = E\, \mathsf{w}_k \tag{5.47}$$

where the k-space Hamiltonian $H_{BdG,N}(k)$ in the N region is

$$H_{BdG,N}(k) = \begin{pmatrix} \xi_N^0(k)\sigma_0 - \alpha_N \, k\sigma_\Phi & 0 \\ 0 & -\xi_N^0(k)\sigma_0 + \alpha_N \, k\sigma_\Phi \end{pmatrix} \tag{5.48}$$

and

$$\xi_N^0(k) = \frac{\hbar^2 k^2}{2m^*} - \mu_N \tag{5.49}$$

The problem naturally decouples in two separate problems for the particle and the hole sectors. To find the eigenstates, we notice that the eigenvectors of σ_Φ are

$$w_{\nearrow} = \begin{pmatrix} \cos\frac{\Phi_{SO}}{2} \\ i\sin\frac{\Phi_{SO}}{2} \end{pmatrix} \qquad \sigma_\Phi w_{\nearrow} = +w_{\nearrow} \tag{5.50}$$

$$w_{\swarrow} = \begin{pmatrix} i\sin\frac{\Phi_{SO}}{2} \\ \cos\frac{\Phi_{SO}}{2} \end{pmatrix} \qquad \sigma_\Phi w_{\swarrow} = -w_{\swarrow} \tag{5.51}$$

Introducing the quantities

$$\xi_{\nearrow/\swarrow}(k) = \xi_k^0 \mp \alpha_N k \tag{5.52}$$

the positive spectrum of (5.48) is

$$\begin{cases} E^e_{\nearrow}(k) &= \theta(\xi_{\nearrow}(k))|\xi_{\nearrow}(k)| = \theta(\xi_N^0(k) - \alpha_N k)|\xi_N^0(k) - \alpha_N k| \\ E^h_{\nearrow}(k) &= \theta(-\xi_{\swarrow}(-k))| - \xi_{\swarrow}(-k)| = \theta(-\xi_N^0(k) + \alpha_N k)|\xi_N^0(k) - \alpha_N k| \\ E^e_{\swarrow}(k) &= \theta(\xi_{\swarrow}(k))|\xi_{\swarrow}(k)| = \theta(\xi_N^0(k) + \alpha_N k)|\xi_N^0(k) + \alpha_N k| \\ E^h_{\swarrow}(k) &= \theta(-\xi_{\nearrow}(-k))| - \xi_{\nearrow}(-k)| = \theta(-\xi_N^0(k) - \alpha_N k)|\xi_N^0(k) + \alpha_N k| \end{cases} \tag{5.53}$$

and is *independent* of the spin-orbit angle Φ_{SO}. The related eigenvectors read

$$\begin{aligned} \mathsf{w}^e_{N,\nearrow} &= \begin{pmatrix} \cos\frac{\Phi_{SO}}{2} \\ i\sin\frac{\Phi_{SO}}{2} \\ 0 \\ 0 \end{pmatrix} & \mathsf{w}^e_{N,\swarrow} &= \begin{pmatrix} i\sin\frac{\Phi_{SO}}{2} \\ \cos\frac{\Phi_{SO}}{2} \\ 0 \\ 0 \end{pmatrix} \\ \mathsf{w}^h_{N,\nearrow} &= \begin{pmatrix} 0 \\ 0 \\ \cos\frac{\Phi_{SO}}{2} \\ i\sin\frac{\Phi_{SO}}{2} \end{pmatrix} & \mathsf{w}^h_{N,\swarrow} &= \begin{pmatrix} 0 \\ 0 \\ i\sin\frac{\Phi_{SO}}{2} \\ \cos\frac{\Phi_{SO}}{2} \end{pmatrix} \end{aligned} \tag{5.54}$$

and are independent of k.

Eigenfunctions at fixed energy E

So far, we have found the eigenvalues and eigenvectors as a function of k. We now want to fix $E > 0$, and determine the wavevectors and the eigenfunctions. Inverting in favor of k the four equations (5.53), one realizes that there exist two energy regimes:

- **Range 1:** $\boxed{0 \leq E \leq E_{SO,N} + \mu_N}$

In this case each of the four eigenvalue branch leads to two wavevectors, and one obtains 8 wavevectors at a given energy E

$$E^e_{\nearrow} = \xi^0_N(k) - \alpha_N k > 0 \quad \rightarrow \quad \boxed{k^e_{\nearrow,\pm}(E) = k_{SO,N}\left(1 \pm \sqrt{1 + \frac{E+\mu_N}{E_{SO,N}}}\right)} \tag{5.55}$$

$$E^e_{\swarrow} = \xi^0_N(k) + \alpha_N k > 0 \quad \rightarrow \quad \boxed{k^e_{\swarrow,\pm}(E) = k_{SO,N}\left(-1 \pm \sqrt{1 + \frac{E+\mu_N}{E_{SO,N}}}\right)} \tag{5.56}$$

$$E^h_{\nearrow} = -(\xi^0_N(k) - \alpha_N k) > 0 \quad \rightarrow \quad \boxed{k^h_{\nearrow,\pm}(E) = k_{SO,N}\left(1 \pm \sqrt{1 - \frac{E-\mu_N}{E_{SO,N}}}\right)} \tag{5.57}$$

$$E^h_{\swarrow} = -(\xi^0_N(k) + \alpha_N k) > 0 \quad \rightarrow \quad \boxed{k^h_{\swarrow,\pm}(E) = k_{SO,N}\left(-1 \pm \sqrt{1 - \frac{E-\mu_N}{E_{SO,N}}}\right)} \tag{5.58}$$

where

$$k_{SO,N} = \frac{\alpha_N m^*}{\hbar^2} > 0 \qquad \text{(spin-orbit wavevector in N)} \tag{5.59}$$

$$E_{SO,N} = \frac{\alpha_N^2 m^*}{2\hbar^2} \equiv \frac{\hbar^2 k^2_{SO,N}}{2m^*} \qquad \text{(spin-orbit energy in N)} \tag{5.60}$$

At each of these wavevectors, the group velocity, defined as

$$v(E) = \frac{1}{\hbar}\frac{\partial E}{\partial k}\bigg|_{k=k(E)} \tag{5.61}$$

reads

$$v^e_{\nearrow,\pm}(E) = v^e_{\swarrow,\pm}(E) = \pm v^e_N(E) \tag{5.62}$$

$$v^h_{\nearrow,\pm}(E) = v^h_{\swarrow,\pm}(E) = \mp v^h_N(E) \tag{5.63}$$

where

$$\boxed{v^e_N(E) = \sqrt{\frac{2}{m^*}\left(E_{SO} + \mu_N + E\right)} \; = \; v_N\sqrt{1 + \frac{E}{E_{SO,N} + \mu_N}}} \tag{5.64}$$

$$\boxed{v^h_N(E) = \sqrt{\frac{2}{m^*}\left(E_{SO} + \mu_N - E\right)} \; = \; v_N\sqrt{1 - \frac{E}{E_{SO,N} + \mu_N}}} \tag{5.65}$$

and

$$\boxed{v_N \doteq \sqrt{\frac{2(E_{SO,N} + \mu_N)}{m^*}}} \tag{5.66}$$

is an energy-independent velocity.
The general expression of the wavefunction in the N side of the junction, in this energy

range, is

$$\begin{aligned}\Phi_N(x) = a^e_{\nearrow,+}\frac{e^{ik^e_{\nearrow,+}(E)\,x}}{\sqrt{2\pi\hbar v^e_N(E)}}\mathsf{w}^e_{N,\nearrow} \;+\; a^e_{\swarrow,+}\frac{e^{ik^e_{\swarrow,+}(E)\,x}}{\sqrt{2\pi\hbar v^e_N(E)}}\mathsf{w}^e_{N,\swarrow} \;+\\ + a^h_{\nearrow,-}\frac{e^{ik^h_{\nearrow,-}(E)\,x}}{\sqrt{2\pi\hbar v^h_N(E)}}\mathsf{w}^h_{N,\nearrow} \;+\; a^h_{\swarrow,-}\frac{e^{ik^h_{\swarrow,-}(E)\,x}}{\sqrt{2\pi\hbar v^h_N(E)}}\mathsf{w}^h_{N,\swarrow} \;+\\ + b^e_{\nearrow,-}\frac{e^{ik^e_{\nearrow,-}(E)\,x}}{\sqrt{2\pi\hbar v^e_N(E)}}\mathsf{w}^e_{N,\nearrow} \;+\; b^e_{\swarrow,-}\frac{e^{ik^e_{\swarrow,-}(E)\,x}}{\sqrt{2\pi\hbar v^e_N(E)}}\mathsf{w}^e_{N,\swarrow} \;+\\ + b^h_{\nearrow,+}\frac{e^{ik^h_{\nearrow,+}(E)\,x}}{\sqrt{2\pi\hbar v^h_N(E)}}\mathsf{w}^h_{N,\nearrow} \;+\; b^h_{\swarrow,+}\frac{e^{ik^h_{\swarrow,-}(E)\,x}}{\sqrt{2\pi\hbar v^h_N(E)}}\mathsf{w}^h_{N,\swarrow}\end{aligned} \tag{5.67}$$

where the $a^{e/h}$ are complex amplitudes denoting the states incoming from the N side towards the interface, i.e. right-moving, while the $b^{e/h}$ are complex amplitudes denoting the states outgoing from the interface to the N side, i.e. left-moving. The spinors $\mathsf{w}^{e/h}_{N,\nearrow\swarrow}$ are given in Eqs.(5.54).

- **Range 2:** $\boxed{E > E_{SO,N} + \mu_N}$

In this case, while the electron wavevectors are just the same as in the previous range, the wavevectors of the hole branches acquire an imaginary part

$$E^e_{\nearrow} = \xi^0_N(k) - \alpha_N k > 0 \quad \rightarrow \quad \boxed{k^e_{\nearrow,\pm}(E) = k_{SO,N}\left(1 \pm \sqrt{1 + \frac{E+\mu_N}{E_{SO,N}}}\right)} \tag{5.68}$$

$$E^e_{\swarrow} = \xi^0_N(k) + \alpha_N k > 0 \quad \rightarrow \quad \boxed{k^e_{\swarrow,\pm}(E) = k_{SO,N}\left(-1 \pm \sqrt{1 + \frac{E+\mu_N}{E_{SO,N}}}\right)} \tag{5.69}$$

$$E^h_{\nearrow} = -(\xi^0_N(k) - \alpha_N k) > 0 \quad \rightarrow \quad \boxed{k^h_{\nearrow,\pm}(E) = k_{SO,N}\left(1 \pm i\sqrt{-1 + \frac{E-\mu_N}{E_{SO,N}}}\right)} \tag{5.70}$$

$$E^h_{\swarrow} = -(\xi^0_N(k) + \alpha_N k) > 0 \quad \rightarrow \quad \boxed{k^h_{\swarrow,\pm}(E) = k_{SO,N}\left(-1 \pm i\sqrt{-1 + \frac{E-\mu_N}{E_{SO,N}}}\right)} \tag{5.71}$$

where $k_{SO,N}$ and $E_{SO,N}$ are defined in Eqs.(5.60)-(5.60).
Note that, in the case of a single N/S interface, only one of the two hole wavevectors $k^h_{\nearrow,\pm}$ can be retained. Specifically, since N is on the left-hand side of the interface, only $k^h_{\nearrow,-}$ can be retained since, when inserted in Eq.(5.46), it describes an evanescent wave decaying for $x \to -\infty$. In contrast, the solution related to $k^h_{\nearrow,+}$ grows exponentially

for $x \to -\infty$ and cannot be retained in the Hilbert space. The same occurs for the two hole wavevectors $k^h_{\swarrow,\pm}$.
The group velocity is well defined only for the propagating modes, i.e. the electron wavevectors,

$$v(E) = \frac{1}{\hbar}\frac{\partial E}{\partial k}\bigg|_{k=k(E)} \tag{5.72}$$

and reads again

$$v^e_{\nearrow,\pm}(E) = v^e_{\swarrow,\pm}(E) = \pm v^e_N(E) \tag{5.73}$$

with

$$\boxed{v^e_N(E) = \sqrt{\frac{2}{m^*}\left(E_{SO} + \mu_N + E\right)} = v_N\sqrt{1 + \frac{E}{E_{SO,N} + \mu_N}}} \tag{5.74}$$

where v_N is the energy-independent velocity defined in Eq.(5.66).
For the hole evanescent modes a velocity is meaningless. Nevertheless, in order for the amplitudes of the evanescent modes to be dimensionally consistent with the amplitudes of the propagating modes, one can formally attribute

$$\boxed{v^h_{\nearrow,-}(E) = v^h_{\swarrow,-}(E) = v_N} \qquad \text{(formal definition)} \tag{5.75}$$

where v_N is the energy-independent velocity (5.66).
The general expression of the wavefunction in the N side of the junction, in this energy range, is

$$\boxed{\begin{aligned}\Phi_N(x) \;=\;& a^e_{\nearrow,+}\frac{e^{ik^e_{\nearrow,+}(E)\,x}}{\sqrt{2\pi\hbar v^e_N(E)}}\,\mathsf{w}^e_{N,\nearrow} \;+\; a^e_{\swarrow,+}\frac{e^{ik^e_{\swarrow,+}(E)\,x}}{\sqrt{2\pi\hbar v^e_N(E)}}\,\mathsf{w}^e_{N,\swarrow} \;+\\ &+b^e_{\nearrow,-}\frac{e^{ik^e_{\nearrow,-}(E)\,x}}{\sqrt{2\pi\hbar v^e_N(E)}}\,\mathsf{w}^e_{N,\nearrow} \;+\; b^e_{\swarrow,-}\frac{e^{ik^e_{\swarrow,-}(E)\,x}}{\sqrt{2\pi\hbar v^e_N(E)}}\,\mathsf{w}^e_{N,\swarrow} \;+\\ &+c^h_{\nearrow,-}\frac{e^{ik^h_{\nearrow,-}(E)\,x}}{\sqrt{2\pi\hbar v_N}}\,\mathsf{w}^h_{N,\nearrow} \;+\; c^h_{\swarrow,-}\frac{e^{ik^h_{\swarrow,-}(E)\,x}}{\sqrt{2\pi\hbar v_N}}\,\mathsf{w}^h_{N,\swarrow}\end{aligned}} \tag{5.76}$$

where $c^h_{\nearrow/\swarrow,-}$ are amplitudes associated to the evanescent modes, while the spinors $\mathsf{w}^{e,h}_{N,\nearrow,\swarrow}$ are defined in Eqs.(5.54).

Fig.5.2 displays the energy spectrum in N region and highlights graphically the various energy ranges previously analyzed.

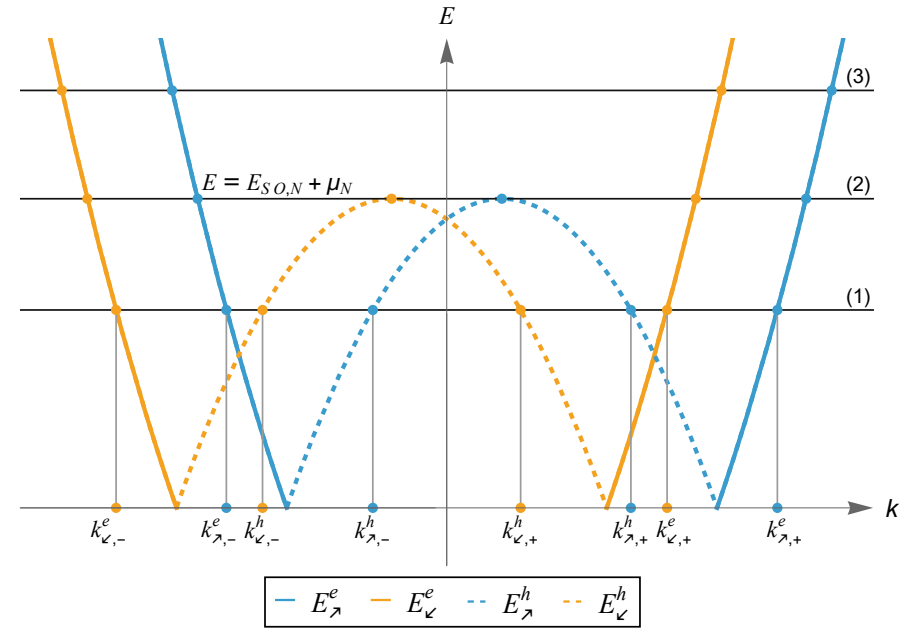

Figure 5.2: Graphic solution for the $k^{h,e}_{\nearrow,\swarrow}$ wavevectors in the N region. As already illustrated by solving analytically Eqs.(5.53) for a given $E > 0$, no real solutions in the hole sectors exist for $E > E_{SO} + \mu_N$ (line (3)), whereas for $E = E_{SO} + \mu_N$ (line (2)) the solutions $k^h_{\nearrow,\pm}$, as well as $k^h_{\swarrow,\pm}$, coincide. For energy values $E < E_{SO} + \mu_N$ the number of propagating modes are maximum as illustrated by highlighting the intersections with line 1.

5.2.2 Solution in the S region

In the region S, i.e. for $x > 0$, the spin-orbit field is supposed to point only along the z direction [see Eq.(5.43)] Then, the BdG equations (5.7) reduce to

$$\begin{pmatrix} \left(-\frac{\partial_x^2}{2m^*} - \mu_S\right)\sigma_0 + i\alpha_S\sigma_z\partial_x & \Delta_0 e^{i\varphi} \\ \Delta_0 e^{-i\varphi} & \left(\frac{\partial_x^2}{2m^*} + \mu_S\right)\sigma_0 - i\alpha_S\sigma_z\partial_x \end{pmatrix} \Phi(x) = E\Phi(x) \tag{5.77}$$

Looking for plane-wave solutions

$$\Phi_k(x) = \mathsf{w}_k\, e^{ikx} \tag{5.78}$$

with w_k denoting a 4×1 spinor, the Equation reduces to

$$H_{BdG,S}(k)\,\mathsf{w}_k = E\,\mathsf{w}_k \tag{5.79}$$

$$H_{BdG,S}(k) = \begin{pmatrix} \xi^0_S(k)\sigma_0 - \alpha_S\sigma_z k & \Delta_0 e^{i\varphi} \\ \Delta_0 e^{-i\varphi} & -\xi^0_S(k)\sigma_0 + \alpha_S\sigma_z k \end{pmatrix} \tag{5.80}$$

where

$$\xi^0_S(k) = \frac{\hbar^2 k^2}{2m^*} - \mu_S \tag{5.81}$$

A configuration of this type has already been discussed in Sec.(3.2), therefore, let us recall here the expressions of the excitation energies when $\mathbf{b} \equiv 0$ [see Hamiltonian (3.71)]

$$E_1(k) = \sqrt{\left(\xi_S^0(k) - \alpha_S k\right)^2 + \Delta_0^2} \tag{5.82}$$

$$E_2(k) = \sqrt{\left(\xi_S^0(k) + \alpha_S k\right)^2 + \Delta_0^2} \tag{5.83}$$

where $\xi_S^0(k)$ is given by Eq.(5.81) and we note that $E_2(k) = E_1(-k)$.
As shown in (3.62) the eigenvectors are

$$\mathsf{w}_{S,1}^e(k) = \begin{pmatrix} u_k \\ 0 \\ v_k \\ 0 \end{pmatrix} \quad \mathsf{w}_{S,2}^e(k) = \begin{pmatrix} 0 \\ u_{-k} \\ 0 \\ v_{-k} \end{pmatrix} \quad \mathsf{w}_{S,1}^h(k) = \begin{pmatrix} -v_k^* \\ 0 \\ u_k^* \\ 0 \end{pmatrix} \quad \mathsf{w}_{S,2}^h(k) = \begin{pmatrix} 0 \\ -v_{-k}^* \\ 0 \\ u_{-k}^* \end{pmatrix} \tag{5.84}$$

where

$$\begin{aligned} u_k &= \sqrt{\frac{1}{2}\left(1 + \frac{\xi_S^0(k) - \alpha_S k}{\sqrt{(\xi_S^0(k) - \alpha_S k)^2 + \Delta_0^2}}\right)} \\ v_k &= e^{-i\varphi}\sqrt{\frac{1}{2}\left(1 - \frac{\xi_S^0(k) - \alpha_S k}{\sqrt{(\xi_S^0(k) - \alpha_S k)^2 + \Delta_0^2}}\right)} \end{aligned} \tag{5.85}$$

We remind that, even when $\mathbf{b} \neq 0$, $u_k,\ v_k$ do not depend on the magnetic field.
Having revisited the solutions for the system in this region, it is important to clarify the notation used for the spin sectors. The choice of the indices 1,2 is a matter of convention adopted in Sec.3.2 to distinguish the superconducting case from the normal case [see Sec.3.2], for which the more explicit spin labels $\uparrow, \downarrow$ were used.However, it is crucial to remark that both sets of labels refer to the same physical reality, i.e. spin-up and spin-down excitations.
The eigenvectors presented in Eq.(5.84) are, in fact, eigenstates of the first quantized spin operator along the z-axis, which in the Nambu basis is written as $S_{BdG}^z = \frac{\hbar}{2}(\tau_0 \otimes \sigma^z)$[see Eq.(4.62)]. Indeed, it is easy to verify that :

- The eigenvectors $\mathsf{w}_{S,1}^{e,h}$ of sector 1 are eigenvectors of S_{BdG}^z with eigenvalue "+1";
- The eigenvectors $\mathsf{w}_{S,2}^{e,h}$ of sector 2 are eigenvectors of S_{BdG}^z with eigenvalue "−1";

This confirms that the Hamiltonian is block diagonal in the spin-basis and that, the energies $E_1(k),\ E_2(k)$ are the dispersion relation for the spin-up and spin-down quasiparticle excitations, respectively. Therefore, to maintain physical clarity, from this point on we shall adopt the more explicit spin labels $\uparrow, \downarrow$ in place of 1,2 to refer to the corresponding sector.

The very structure of the eigenvectors allows us to distinguish between "electron-like" and "hole-like" excitations. Indeed

$$\begin{cases} E^e_\uparrow(k) &= \theta\left(\xi^0_S(k)-\alpha_S k\right)|E_\uparrow(k)| = \theta\left(\xi^0_S(k)-\alpha_S k\right)\sqrt{\left(\xi^0_S(k)-\alpha_S k\right)^2+\Delta_0^2} \\ E^h_\uparrow(k) &= \theta\left(-\xi^0_S(k)+\alpha_S k\right)|E_\uparrow(k)| = \theta\left(-\xi^0_S(k)+\alpha_S k\right)\sqrt{\left(\xi^0_S(k)-\alpha_S k\right)^2+\Delta_0^2} \\ E^e_\downarrow(k) &= \theta\left(\xi^0_S(k)+\alpha_S k\right)|E_\downarrow(k)| = \theta\left(\xi^0_S(k)+\alpha_S k\right)\sqrt{\left(\xi^0_S(k)+\alpha_S k\right)^2+\Delta_0^2} \\ E^h_\downarrow(k) &= \theta\left(-\xi^0_S(k)-\alpha_S k\right)|E_\downarrow(k)| = \theta\left(-\xi^0_S(k)-\alpha_S k\right)\sqrt{\left(\xi^0_S(k)+\alpha_S k\right)^2+\Delta_0^2} \end{cases} \tag{5.86}$$

Eigenfunctions at fixed energy E

To determine the expressions for an "electron-like" and a "hole-like" eigenfunctions we have to compute the explicit expressions of the wavevectors. This can be achieved by solving the following equations for a given energy value $E \geq 0$,

$$E_\uparrow(k) = E \;\Rightarrow\; \sqrt{\left(\xi^0_S(k)-\alpha_S k\right)^2+\Delta_0^2} = E \;\Rightarrow\; \left(\xi^0_S(k)-\alpha_S k\right)^2 = E^2-\Delta_0^2 \tag{5.87}$$

$$E_\downarrow(k) = E \;\Rightarrow\; \sqrt{\left(\xi^0_S(k)+\alpha_S k\right)^2+\Delta_0^2} = E \;\Rightarrow\; \left(\xi^0_S(k)+\alpha_S k\right)^2 = E^2-\Delta_0^2 \tag{5.88}$$

Furthermore, let us define the SO wavevector and energy in the S region as

$$k_{SO,S} = \frac{\alpha_S\, m^*}{\hbar^2} \tag{5.89}$$

$$E_{SO,S} = \frac{\hbar^2 k^2_{SO,S}}{2m^*} = \frac{\alpha_S^2\, m^*}{2\hbar^2} \tag{5.90}$$

Now, we shall first analyze the solutions in the so called "Supra-gap regime"($E \geq \Delta_0$), and then in the so-called "Sub-gap regime"($E < \Delta_0$). Fig.5.3 illustrates graphically the possible en

- **Supra-gap regime** ($E > \Delta_0$)

  Similarly to the N region, in the Supra-gap regime we identify two different energy ranges:

  1. **Lower supra-gap regime:** $\boxed{\Delta_0 \leq E \leq \sqrt{\Delta_0^2+\left(E_{SO,S}+\mu_S\right)^2}}$

     In this energy range, each of the energy branch in Eq.(5.86) yields two wavevector

solutions for a fixed energy E:

$$\sqrt{(E^e_\uparrow)^2-\Delta_0^2} = +\left(\xi^0_S(k)-\alpha_S k\right) \quad \Rightarrow \quad \boxed{k^e_{\uparrow,\pm}(E) = k_{SO,S}\left(1\pm\sqrt{1+\frac{\mu_S+\sqrt{E^2-\Delta_0^2}}{E_{SO,S}}}\right)}$$

$$\sqrt{(E^e_\downarrow)^2-\Delta_0^2} = +\left(\xi^0_S(k)+\alpha_S k\right) \quad \Rightarrow \quad \boxed{k^e_{\downarrow,\pm}(E) = k_{SO,S}\left(-1\pm\sqrt{1+\frac{\mu_S+\sqrt{E^2-\Delta_0^2}}{E_{SO,S}}}\right)}$$

$$\sqrt{(E^h_\uparrow)^2-\Delta_0^2} = -\left(\xi^0_S(k)-\alpha_S k\right) \quad \Rightarrow \quad \boxed{k^h_{\uparrow,\pm}(E) = k_{SO,S}\left(1\pm\sqrt{1+\frac{\mu_S-\sqrt{E^2-\Delta_0^2}}{E_{SO,S}}}\right)}$$

$$\sqrt{(E^h_\downarrow)^2-\Delta_0^2} = -\left(\xi^0_S(k)+\alpha_S k\right) \quad \Rightarrow \quad \boxed{k^h_{\downarrow,\pm}(E) = k_{SO,S}\left(-1\pm\sqrt{1+\frac{\mu_S-\sqrt{E^2-\Delta_0^2}}{E_{SO,S}}}\right)} \tag{5.91}$$

Note that, as expected, $k^e_{\downarrow,\pm}(E) = -k^e_{\uparrow,\mp}(E)$ and $k^h_{\downarrow,\pm}(E) = -k^h_{\uparrow,\mp}(E)$.
Since in this energy range, we are describing propagating modes (only real solutions for the wavevectors exist), the group velocity is well defined and reads

$$v^e_{\sigma,\pm}(E) = \pm v^e_S(E) \qquad \sigma = \uparrow,\downarrow \tag{5.92}$$

$$v^h_{\sigma,\pm}(E) = \mp v^h_S(E) \tag{5.93}$$

where

$$\begin{aligned} v^e_S(E) &= \sqrt{\frac{2}{m^*}\left(1-\frac{\Delta_0^2}{E^2}\right)\left(E_{SO,S}+\mu_S+\sqrt{E^2-\Delta_0^2}\right)} \\ &= \boxed{v_S\sqrt{\left(1-\frac{\Delta_0^2}{E^2}\right)\left(1+\frac{\sqrt{E^2-\Delta_0^2}}{E_{SO,S}+\mu_S}\right)}} \end{aligned} \tag{5.94}$$

$$\begin{aligned} v^h_S(E) &= \sqrt{\frac{2}{m^*}\left(1-\frac{\Delta_0^2}{E^2}\right)\left(E_{SO,S}+\mu_S-\sqrt{E^2-\Delta_0^2}\right)} \\ &= \boxed{v_S\sqrt{\left(1-\frac{\Delta_0^2}{E^2}\right)\left(1-\frac{\sqrt{E^2-\Delta_0^2}}{E_{SO,S}+\mu_S}\right)}} \end{aligned} \tag{5.95}$$

and

$$\boxed{v_S \doteq \sqrt{\frac{2(E_{SO,S}+\mu_S)}{m^*}}} \tag{5.96}$$

is an energy independent velocity.

It is now possible to construct the general expression for the wavefunction in the S region, as a superposition of hole-like and electron-like waves, propagating towards(left-moving) and away(right-moving) from the interface, that is

$$\begin{aligned}\boxed{\Phi_S(x) = {} & a^e_{\uparrow,-}\frac{e^{ik^e_{\uparrow,-}(E)\,x}}{\sqrt{2\pi\hbar v^e_S(E)}}\mathsf{w}^e_{S,\uparrow}(k^e_{\uparrow,-}) \;+\; a^e_{\downarrow,-}\frac{e^{ik^e_{\downarrow,-}(E)\,x}}{\sqrt{2\pi\hbar v^e_S(E)}}\mathsf{w}^e_{S,\downarrow}(k^e_{\downarrow,-}) + \\ & + a^h_{\uparrow,+}\frac{e^{ik^h_{\uparrow,+}(E)\,x}}{\sqrt{2\pi\hbar v^h_S(E)}}\mathsf{w}^e_{S,\uparrow}(k^h_{\uparrow,+}) \;+\; a^h_{\downarrow,+}\frac{e^{ik^h_{\downarrow,+}(E)\,x}}{\sqrt{2\pi\hbar v^h_S(E)}}\mathsf{w}^e_{S,\downarrow}(k^h_{\downarrow,+}) + \\ & + b^e_{\uparrow,+}\frac{e^{ik^e_{\uparrow,+}(E)\,x}}{\sqrt{2\pi\hbar v^e_S(E)}}\mathsf{w}^e_{S,\uparrow}(k^e_{\uparrow,+}) \;+\; b^e_{\downarrow,+}\frac{e^{ik^e_{\downarrow,+}(E)\,x}}{\sqrt{2\pi\hbar v^e_S(E)}}\mathsf{w}^e_{S,\downarrow}(k^e_{\downarrow,+}) + \\ & + b^h_{\uparrow,-}\frac{e^{ik^h_{\uparrow,-}(E)\,x}}{\sqrt{2\pi\hbar v^h_S(E)}}\mathsf{w}^e_{S,\uparrow}(k^h_{\uparrow,-}) \;+\; b^h_{\downarrow,-}\frac{e^{ik^h_{\downarrow,-}(E)\,x}}{\sqrt{2\pi\hbar v^h_S(E)}}\mathsf{w}^e_{S,\downarrow}(k^h_{\downarrow,-})\end{aligned} \tag{5.97}$$

Each wave in the previous expression is weighted by a coefficient which represents the probability amplitude related to that specific modes. In particular, $a^{e/h}$ coefficients are associated to incoming (left-moving) particle with respect to the interface, while $b^{e/h}$ coefficients to outgoing (right-moving) ones.

Let us now make the following consideration: as alreay observed, for a fixed energy value E, the wavevectors exhibit the symmetry $k^{e/h}_{\downarrow,\pm}(E) = -k^{e/h}_{\uparrow,\mp}(E)$, due to the relation $E_\downarrow(k) = E_\uparrow(-k)$. This implies a corresponding symmetry in the coherence factors, that is

$$u_k\Big|_{k^{e/h}_{\uparrow,\pm}(E)} = u_{-k}\Big|_{k^{e/h}_{\downarrow,\pm}(E)} \qquad \text{and} \qquad v_k\Big|_{k^{e/h}_{\uparrow,\pm}(E)} = v_{-k}\Big|_{k^{e/h}_{\downarrow,\pm}(E)} \tag{5.98}$$

This symmetry allow us to define a new set of eigenvectors that depend only on the energy, rather than on the specific wavevector k. To this end, we introduce the energy dependent quantities $u_0(E),\ v_0(E)$ as

$$u_0(E) = \sqrt{\frac{1}{2}\left(1+\frac{\sqrt{E^2-\Delta_0^2}}{E}\right)} = \sqrt{\frac{\Delta_0}{2E}}e^{\frac{1}{2}\,\mathrm{arccosh}\,\frac{E}{\Delta_0}} \tag{5.99}$$

$$v_0(E) = \sqrt{\frac{1}{2}\left(1-\frac{\sqrt{E^2-\Delta_0^2}}{E}\right)} = \sqrt{\frac{\Delta_0}{2E}}e^{-\frac{1}{2}\,\mathrm{arccosh}\,\frac{E}{\Delta_0}} \tag{5.100}$$

We can thus define a simplified, energy-dependent, basis of eigenvectors $\bar{\mathsf{w}}^{e}_{\uparrow,\downarrow}(E)$ for an electron-like and hole-like states as

$$\bar{\mathsf{w}}^{e}_{S,\uparrow}(E) = \begin{pmatrix} u_0(E) \\ 0 \\ v_0(E)e^{-i\varphi} \\ 0 \end{pmatrix} \qquad \bar{\mathsf{w}}^{e}_{S,\downarrow}(E) = \begin{pmatrix} 0 \\ u_0(E) \\ 0 \\ v_0(E)e^{-i\varphi} \end{pmatrix} \tag{5.101}$$

$$\bar{\mathsf{w}}^{h}_{S,\uparrow}(E) = \begin{pmatrix} v_0(E) \\ 0 \\ u_0(E)e^{-i\varphi} \\ 0 \end{pmatrix} \qquad \bar{\mathsf{w}}^{h}_{S,\downarrow}(E) = \begin{pmatrix} 0 \\ v_0(E) \\ 0 \\ u_0(E)e^{-i\varphi} \end{pmatrix} \tag{5.102}$$

Note that, to ensure the normalization of the eigenvectors, the relation $|u_0(E)|^2 + |v_0(E)|^2 = 1$ must hold. Indeed, we have that

$$|u_0(E)|^2 + |v_0(E)|^2 = \frac{\Delta_0}{2E}\left(e^{\operatorname{arccosh}\frac{E}{\Delta_0}} + e^{-\operatorname{arccosh}\frac{E}{\Delta_0}}\right) \tag{5.103}$$

$$= \frac{\Delta_0}{E}\cosh\left(\operatorname{arccosh}\frac{E}{\Delta_0}\right) = 1 \tag{5.104}$$

Furthermore, being $u_0(E),\ v_0(E)$ real quantities, it is also true that $u_0^2 + v_0^2 = 1$. The general expression for the wavefunction in Eq.(5.97) can now be compactly rewritten as

$$\begin{aligned}\Phi_S(x) = {} & a^{e}_{\uparrow,-}\frac{e^{ik^{e}_{\uparrow,-}(E)\,x}}{\sqrt{2\pi\hbar v^{e}_S(E)}}\bar{\mathsf{w}}^{e}_{S,\uparrow}(E) \ + \ a^{e}_{\downarrow,-}\frac{e^{ik^{e}_{\downarrow,-}(E)\,x}}{\sqrt{2\pi\hbar v^{e}_S(E)}}\bar{\mathsf{w}}^{e}_{S,\downarrow}(E) \ + \\ & + a^{h}_{\uparrow,+}\frac{e^{ik^{h}_{\uparrow,+}(E)\,x}}{\sqrt{2\pi\hbar v^{h}_S(E)}}\bar{\mathsf{w}}^{h}_{S,\uparrow}(E) \ + \ a^{h}_{\downarrow,+}\frac{e^{ik^{h}_{\downarrow,+}(E)\,x}}{\sqrt{2\pi\hbar v^{h}_S(E)}}\bar{\mathsf{w}}^{h}_{S,\downarrow}(E) \ + \\ & + b^{e}_{\uparrow,+}\frac{e^{ik^{e}_{\uparrow,+}(E)\,x}}{\sqrt{2\pi\hbar v^{e}_S(E)}}\bar{\mathsf{w}}^{e}_{S,\uparrow}(E) \ + \ b^{e}_{\downarrow,+}\frac{e^{ik^{e}_{\downarrow,+}(E)\,x}}{\sqrt{2\pi\hbar v^{e}_S(E)}}\bar{\mathsf{w}}^{e}_{S,\downarrow}(E) \ + \\ & + b^{h}_{\uparrow,-}\frac{e^{ik^{h}_{\uparrow,-}(E)\,x}}{\sqrt{2\pi\hbar v^{h}_S(E)}}\bar{\mathsf{w}}^{h}_{S,\uparrow}(E) \ + \ b^{h}_{\downarrow,-}\frac{e^{ik^{h}_{\downarrow,-}(E)\,x}}{\sqrt{2\pi\hbar v^{h}_S(E)}}\bar{\mathsf{w}}^{h}_{S,\downarrow}(E)\end{aligned} \tag{5.105}$$

2. **Upper supra-gap regime:** $\boxed{E > \sqrt{\Delta_0^2 + (E_{SO,S} + \mu_S)^2}}$

From Eqs.(5.91) we note that, in this energy range, the hole solutions $k^{h}_{\uparrow,\pm},\ k^{h}_{\downarrow,\pm}$ acquire an imaginary part, indeed, as clear from Fig.(5.3) no intersections for the hole sectors exist. Thus, while the electron wavevectors remain unchanged, the hole

wavevectors acquire an imaginary part

$$\sqrt{(E^e_\uparrow)^2-\Delta_0^2} = +\left(\xi^0_S(k)-\alpha_S k\right) \quad \Rightarrow \quad \boxed{k^e_{\uparrow,\pm}(E) = k_{SO,S}\left(1\pm\sqrt{1+\frac{\mu_S+\sqrt{E^2-\Delta_0^2}}{E_{SO,S}}}\right)}$$

$$\sqrt{(E^e_\downarrow)^2-\Delta_0^2} = +\left(\xi^0_S(k)+\alpha_S k\right) \quad \Rightarrow \quad \boxed{k^e_{\downarrow,\pm}(E) = k_{SO,S}\left(-1\pm\sqrt{1+\frac{\mu_S+\sqrt{E^2-\Delta_0^2}}{E_{SO,S}}}\right)}$$

$$\sqrt{(E^h_\uparrow)^2-\Delta_0^2} = -\left(\xi^0_S(k)-\alpha_S k\right) \quad \Rightarrow \quad \boxed{k^h_{\uparrow,\pm}(E) = k_{SO,S}\left(1\pm i\sqrt{-1+\frac{\sqrt{E^2-\Delta_0^2}-\mu_S}{E_{SO,S}}}\right)}$$

$$\sqrt{(E^h_\downarrow)^2-\Delta_0^2} = -\left(\xi^0_S(k)+\alpha_S k\right) \quad \Rightarrow \quad \boxed{k^h_{\downarrow,\pm}(E) = k_{SO,S}\left(-1\pm i\sqrt{-1+\frac{\sqrt{E^2-\Delta_0^2}-\mu_S}{E_{SO,S}}}\right)} \tag{5.106}$$

$$k^h_{\uparrow,\pm}(E) = k_{SO,S}\left(1\pm i\sqrt{\left(-1+\frac{\sqrt{E^2-\Delta_0^2}-\mu_S}{E_{SO,S}}\right)}\right) \tag{5.107}$$

$$k^h_{\downarrow,\pm}(E) = k_{SO,S}\left(-1\pm i\sqrt{\left(-1+\frac{\sqrt{E^2-\Delta_0^2}-\mu_S}{E_{SO,S}}\right)}\right) \tag{5.108}$$

Differently from the expression of the wavefunction in the Lower Supra-Gap regime displayed in Eq.(5.105), in the upper supra gap regime the appearance of imaginary wavevectors implies that the hole solutions no longer represent propagating modes. Furthermore, given that the S region is on the right-hand side of the interface, the solutions related to wavevectors $k^h_{\uparrow,-}$, $k^h_{\downarrow,-}$ must be discard since they are diverging for $x\to+\infty$.
Thus, the wavefunction in this regime read

$$\begin{aligned}\boxed{\Phi_S(x) = {} & a^e_{\uparrow,-}\frac{e^{ik^e_{\uparrow,-}(E)\,x}}{\sqrt{2\pi\hbar v^e_S(E)}}\bar{\mathsf{w}}^e_{S,\uparrow}(E) \;+\; a^e_{\downarrow,-}\frac{e^{ik^e_{\downarrow,-}(E)\,x}}{\sqrt{2\pi\hbar v^e_S(E)}}\bar{\mathsf{w}}^e_{S,\downarrow}(E) + \\ & + b^e_{\uparrow,+}\frac{e^{ik^e_{\uparrow,+}(E)\,x}}{\sqrt{2\pi\hbar v^e_S(E)}}\bar{\mathsf{w}}^e_{S,\uparrow}(E) \;+\; b^e_{\downarrow,+}\frac{e^{ik^e_{\downarrow,+}(E)\,x}}{\sqrt{2\pi\hbar v^e_S(E)}}\bar{\mathsf{w}}^e_{S,\downarrow}(E) + \\ & + c^h_{\uparrow,+}\frac{e^{ik^h_{\uparrow,+}(E)\,x}}{\sqrt{2\pi\hbar v_S}}\bar{\mathsf{w}}^h_{S,\uparrow}(E) \;+\; c^h_{\downarrow,+}\frac{e^{ik^h_{\downarrow,+}(E)\,x}}{\sqrt{2\pi\hbar v_S}}\bar{\mathsf{w}}^h_{S,\downarrow}(E)\end{aligned} \tag{5.109}$$

where $v^e_S(E)$ represents the group velocity for the electron modes [see Eq.(5.94)] and it is well posed, whereas we adopt the energy independent velocity (5.96) to normalize the

coefficients of the evanescent modes, since for them the definition of group velocity become meaningless.

- **Sub-gap regime** $(0 < E < \Delta_0)$
  This energy regime is characterized by energies $E < \Delta_0$. Starting from the solutions computed in "Lower Upper-gap" regime and displayed in Eqs.(5.91), we observe that, in the current regime, the term $\sqrt{E^2 - \Delta_0^2}$ becomes purely immaginary, leading to complex wavevectors.
  Therefore, the latter now read

$$\boxed{\begin{aligned} k^e_{\uparrow,\pm}(E) &= k_{SO,S} \pm k^e_{CX} \\ k^h_{\uparrow,\pm}(E) &= k_{SO,S} \pm k^h_{CX} \\ k^e_{\downarrow,\pm}(E) &= -k_{SO,S} \pm k^e_{CX} \\ k^h_{\downarrow,\pm}(E) &= -k_{SO,S} \pm k^h_{CX} \end{aligned}} \tag{5.110}$$

  where k^e_{CX} and k^h_{CX} are complex quantity. We then define k^e_{CX} as the principal square root

$$k^e_{CX} = k_{SO,S}\sqrt{\left(1 + \frac{\mu_S + i\sqrt{\Delta_0^2 - E^2}}{E_{SO,S}}\right)} \tag{5.111}$$

  and k^h_{CX} being its complex conjugate, $k^h_{CX} = [k^e_{CX}]^*$.
  In polar coordinates they read

$$k^e_{CX} = |k_{CX}|e^{i\frac{\theta}{2}} = |k_{CX}|\Big(\cos\frac{\theta}{2} + i\sin\frac{\theta}{2}\Big) \tag{5.112}$$

$$k^h_{CX} = |k_{CX}|e^{-i\frac{\theta}{2}} = |k_{CX}|\Big(\cos\frac{\theta}{2} - i\sin\frac{\theta}{2}\Big) \tag{5.113}$$

  where the magnitude and angle are given by

$$|k_{CX}| = k_{SO,S}\left(\left(1 + \frac{\mu}{E_{SO,S}}\right)^2 + \frac{\Delta_0^2 - E^2}{E^2_{SO,S}}\right)^{\frac{1}{4}} \tag{5.114}$$

$$\theta = \arctan\left(\frac{\sqrt{\Delta_0^2 - E^2}}{E_{SO,S} + \mu}\right) + \pi\,\vartheta\left(-E_{SO,S} - \mu_S\right) \tag{5.115}$$

  As a consequence, in this regime, the wavefunction $\Phi_S(x)$ become a superposition of growing and decaying exponential solutions for $x \to +\infty$. Thus, for a physical acceptable wavefunction we must discard the diverging terms, which, in this case, are related to wavevectors $k^e_{\uparrow,-},\ k^e_{\downarrow,-},\ k^h_{\uparrow,+},\ k^h_{\downarrow,+}$.

Furthermore, for $E < \Delta_0$ we observe that the coherence factors $u_0(E),\ v_0(E)$ transform into

$$u_0(E) = \sqrt{\frac{\Delta_0}{2E}} e^{\frac{i}{2}\arccos\frac{E}{\Delta_0}} \qquad \text{and} \qquad v_0(E) = \sqrt{\frac{\Delta_0}{2E}} e^{-\frac{i}{2}\arccos\frac{E}{\Delta_0}} \tag{5.116}$$

i.e. the analityc continuation of Eq.(5.99).
The latter no longer satisfy the eigenvectors normalization condition

$$|u_0(E)|^2 + |v_0(E)|^2 = 1 \tag{5.117}$$

instead they are related by

$$u_0(E)^2 + v_0(E)^2 = \frac{\Delta_0}{2E}\left(e^{i\arccos\frac{E}{\Delta_0}} + e^{-i\arccos\frac{E}{\Delta_0}}\right) \tag{5.118}$$

$$= \frac{\Delta_0}{E}\cos\left(\arccos\frac{E}{\Delta_0}\right) = 1 \tag{5.119}$$

Finally, the wavefunction representing the superposition of evanescent modes reads

$$\begin{aligned}\Phi_S(x) = c^e_{\uparrow,+}\frac{e^{ik^e_{\uparrow,+}(E)\,x}}{\sqrt{2\pi\hbar v_S}}\,\bar{\mathsf{w}}^e_{S,\uparrow}(E) \;+\; c^e_{\downarrow,+}\frac{e^{ik^e_{\downarrow,+}(E)\,x}}{\sqrt{2\pi\hbar v_S}}\,\bar{\mathsf{w}}^e_{S,\downarrow}(E) \;+ \\ + c^h_{\uparrow,-}\frac{e^{ik^h_{\uparrow,-}(E)\,x}}{\sqrt{2\pi\hbar v_S}}\,\bar{\mathsf{w}}^h_{S,\uparrow}(E) \;+\; c^h_{\downarrow,-}\frac{e^{ik^h_{\downarrow,-}(E)\,x}}{\sqrt{2\pi\hbar v_S}}\,\bar{\mathsf{w}}^h_{S,\downarrow}(E)\end{aligned} \tag{5.120}$$

or, equivalently

$$\boxed{\begin{aligned}\Phi_S(x) \;=\; \frac{1}{\sqrt{2\pi\hbar v_S}}\Big\{c^e_{\uparrow,+}\,\bar{\mathsf{w}}^e_{S,\uparrow}(E)\,e^{ik^e_{\uparrow,+}(E)\,x} \;+\; c^e_{\downarrow,+}\,\bar{\mathsf{w}}^e_{S,\downarrow}(E)\,e^{ik^e_{\downarrow,+}(E)\,x} + \\ + \;c^h_{\uparrow,-}\bar{\mathsf{w}}^h_{S,\uparrow}(E)\,e^{ik^h_{\uparrow,-}(E)\,x} \;+\; c^h_{\downarrow,-}\,\bar{\mathsf{w}}^h_{S,\downarrow}(E)\,e^{ik^h_{\downarrow,-}(E)\,x}\Big\}\end{aligned}} \tag{5.121}$$

where v_S is given in Eq.(5.96) and the complex wavevectors are given in Eqs.(5.110).

Fig. 5.3 shows the graphic visualization of the obtained analytical derivation.

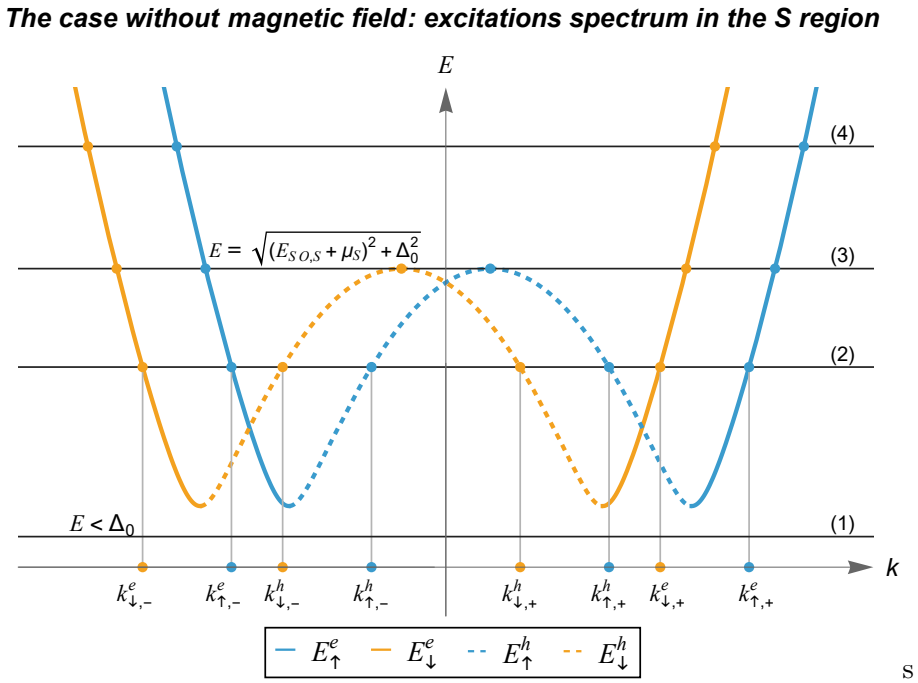

Figure 5.3: The excitations spectrum in the S region exhibits three different energy regimes, which have been discussed analytically: the "Sub-gap" regime, in which no intersection exists (line (1)), and the Supra-gap one, which consists of a Lower and an Upper part. Specifically, in the Lower regimes 8 different propagating solutions for the wavevectors are found, as clear from the intersections of line (2) with the spectrum in the figure; whereas, in Upper regimes only 4 (electron-like) propagating modes are allowed as shown from the intersection with line (4).

5.2.3 The regime of large spin-orbit energy ($E_{SO} > \Delta_0$)

We start by analyzing the regime of strong spin-orbit coupling, i.e. $E_{SO} \gg \Delta_0$. For definiteness, we shall adopt the following parameters

$$E_{SO,N} = E_{SO,S} = 10\Delta_0 \qquad \mu_N = \mu_S = 0 \tag{5.122}$$

The excitations spectra for both regions are illustrated in Fig. 5.4.

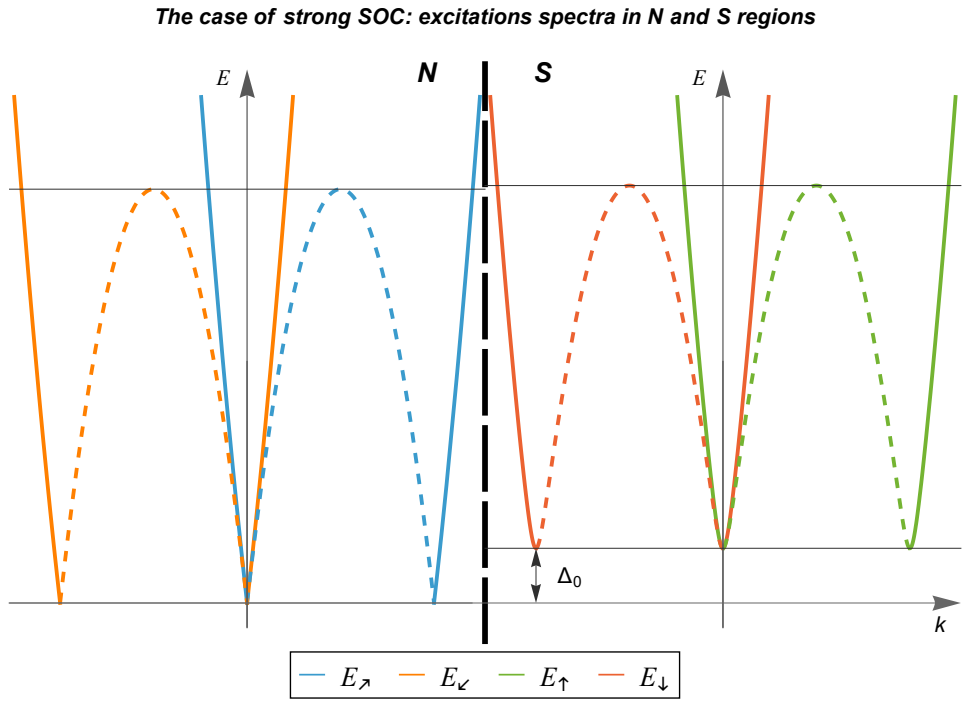

Figure 5.4: Plot of the excitations spectra of the two regions for the case of large spin-orbit energy $E_{SO} > \Delta_0$. This particular choice of parameters allows for four different energy ranges. The energy thresholds characterizing each range are marked by horizontal lines.

For this parameter set, there exist four energy ranges, which we shall analyze in details here below.

(I) $\boldsymbol{E < \Delta_0}$

This energy range corresponds to Range 1 in the N region and to the Sub-gap regime in the S region.
The Σ-matrix in Eq.(5.28) is an 8×4 matrix, and the upper 4×4 block is the Scattering matrix connecting the outgoing amplitude vector $\mathbf{b}$ to the incoming amplitude vector $\mathbf{a}$,

$$\begin{cases} \mathbf{a} &= \left(a^e_{\nearrow,+}, a^e_{\swarrow,+}, a^h_{\nearrow,-}, a^h_{\swarrow,-}\right)^T \\ \mathbf{b} &= \left(b^e_{\nearrow,-}, b^e_{\swarrow,-}, b^h_{\nearrow,+}, b^h_{\swarrow,+}\right)^T \end{cases} \tag{5.123}$$

thus, in this energy range we observe only the reflection phenomenon, since the outgoing coefficients are all related to the N-side.

The explicit expression of the scattering matrix S is

$$\begin{pmatrix} b^{e}_{\nearrow,-} \\ b^{e}_{\swarrow,-} \\ b^{h}_{\nearrow,+} \\ b^{h}_{\swarrow,+} \end{pmatrix} = \underbrace{\begin{pmatrix} r^{e,\nearrow}_{e,\nearrow} & r^{e,\nearrow}_{e,\swarrow} & r^{e,\nearrow}_{h,\nearrow} & r^{e,\nearrow}_{h,\swarrow} \\ r^{e,\swarrow}_{e,\nearrow} & r^{e,\swarrow}_{e,\swarrow} & r^{e,\swarrow}_{h,\nearrow} & r^{e,\swarrow}_{h,\swarrow} \\ r^{h,\nearrow}_{e,\nearrow} & r^{h,\nearrow}_{e,\swarrow} & r^{h,\nearrow}_{h,\nearrow} & r^{h,\nearrow}_{h,\swarrow} \\ r^{h,\swarrow}_{e,\nearrow} & r^{h,\swarrow}_{e,\swarrow} & r^{h,\swarrow}_{h,\nearrow} & r^{h,\swarrow}_{h,\swarrow} \end{pmatrix}}_{=S} \begin{pmatrix} a^{e}_{\nearrow,+} \\ a^{e}_{\swarrow,+} \\ a^{h}_{\nearrow,-} \\ a^{h}_{\swarrow,-} \end{pmatrix} \tag{5.124}$$

where the r^{β}_{α} denote the reflection amplitudes with the notation defined as follows:

- the superscript β (e.g.$e, \nearrow$) identifies the state of the outgoing (reflected) particle;
- the subscript α (e.g.$h, \swarrow$) identifies the state of the incoming (incident) particle;

For example, $r^{e,\nearrow}_{h,\swarrow}$ represents the reflection amplitude for an incoming hole in the $\swarrow$ state to be reflected as an electron in the $\nearrow$ state.

We define the reflection coefficient from α to β as

$$R^{\beta}_{\alpha} \;=\; |r^{\beta}_{\alpha}|^2 \qquad \forall\, \alpha,\ \beta \tag{5.125}$$

We have verified that

$$R^{e,\nearrow}_{\alpha} + R^{e,\swarrow}_{\alpha} + R^{h,\nearrow}_{\alpha} + R^{h,\swarrow}_{\alpha} = 1 \quad \forall\, \alpha \tag{5.126}$$

and that

$$R^{\beta}_{e,\nearrow} + R^{\beta}_{e,\swarrow} + R^{\beta}_{h,\nearrow} + R^{\beta}_{h,\swarrow} = 1 \quad \forall\, \beta \tag{5.127}$$

in agreement with the unitarity of the Scattering Matrix, stemming from the conservation of the probability flux. The numerical results for each single incoming mode are summarized in Table 5.1, from which we observe that the dominant process is the *Andreev Reflection* (AR).

Incident mode α	$\|r^{e,\nearrow}_{\alpha}\|^2$	$\|r^{e,\swarrow}_{\alpha}\|^2$	$\|r^{h,\nearrow}_{\alpha}\|^2$	$\|r^{h,\swarrow}_{\alpha}\|^2$	**Dominant process**
$(\nearrow,+)$	≈ 0	0	≈ 1	0	$e_{\nearrow,+} \to h_{\nearrow,+}$
$(\swarrow,+)$	0	≈ 0	0	≈ 1	$e_{\swarrow,+} \to h_{\swarrow,+}$
$(\nearrow,-)$	≈ 1	0	≈ 0	0	$h_{\nearrow,-} \to e_{\nearrow,-}$
$(\swarrow,-)$	0	≈ 1	0	≈ 0	$h_{\swarrow,-} \to e_{\swarrow,-}$

Table 5.1: Numerical reflection probabilities for the different incoming modes $\alpha = (\nearrow,\pm), (\swarrow,\pm)$. Each incoming particle is (almost) completely reflected into its corresponding Time-reversal partner.

As a result, defining the total Normal and Andreev Reflection for the electron and

hole modes as

$$R^N_{e\to e}(E) = \left(R^{e,\nearrow}_{e,\nearrow} + R^{e,\nearrow}_{e,\swarrow} + R^{e,\swarrow}_{e,\nearrow} + R^{e,\swarrow}_{e,\swarrow}\right) \quad \text{Electron Normal Reflection} \tag{5.128}$$

$$R^N_{h\to h}(E) = \left(R^{h,\nearrow}_{h,\nearrow} + R^{h,\nearrow}_{h,\swarrow} + R^{h,\swarrow}_{h,\nearrow} + R^{h,\swarrow}_{h,\swarrow}\right) \quad \text{Hole Normal Reflection} \tag{5.129}$$

$$R^N_{e\to h}(E) = \left(R^{h,\nearrow}_{e,\nearrow} + R^{h,\nearrow}_{e,\swarrow} + R^{h,\swarrow}_{e,\nearrow} + R^{h,\swarrow}_{e,\swarrow}\right) \quad \text{Electron Andreev Reflection} \tag{5.130}$$

$$R^N_{h\to e}(E) = \left(R^{e,\nearrow}_{h,\nearrow} + R^{e,\nearrow}_{h,\swarrow} + R^{e,\swarrow}_{h,\nearrow} + R^{e,\swarrow}_{h,\swarrow}\right) \quad \text{Hole Andreev Reflection} \tag{5.131}$$

we obtained that

$$R^N_{e\to e}(E) = R^N_{h\to h}(E) = 0 \tag{5.132}$$

$$R^N_{h\to e}(E) = R^N_{e\to h}(E) = 2 \tag{5.133}$$

as clear from Fig. 5.5.

We have observed up to this point that Normal Reflection is completely suppressed. This result can be perfectly understood by establishing an analogy between our spin-orbit model and the standard Blonder-Tinkham-Klapwijk (BTK) framework [12]. In this mapping, the spin-orbit energy E_{SO} assumes the physical role of the chemical potential μ of the standard BTK model.

The regime of large spin-orbit energy [see Eq.(5.122)] represents an ideal scenario defined by two conditions that suppress Normal Reflection .

First, the condition $E_{SO,N} = E_{SO,S} \gg \Delta_0$ places the system in the Andreev approximation limit. This is analogous to the $\mu \gg \Delta_0$ limit in the standard BTK model. This large energy scale ensures that the intrinsic momentum mismatch between the incident electron (k^e) and the reflected hole (k^h) is negligible, which removes the first potential source of normal reflection.

Second, the condition $E_{SO,N} = E_{SO,S}$ implies there is no "step" in the dominant energy scale at the interface. This is analogous to a perfectly transparent interface (zero barrier potential) in the BTK model, removing the second source of Normal Reflection. Indeed, even within our defined Andreev approximation ($E_{SO} \gg \Delta_0$), a non-negligible difference between the two energies ($E_{SO,N} \neq E_{SO,S}$) would act as an effective interface barrier, resulting in the appearance of Normal Reflection. Indeed, as derived in the boundary condition Eq.(5.10), any discontinuity in the spin-orbit vector at the interface ($\boldsymbol{\alpha}_N \neq \boldsymbol{\alpha}_S$) creates an additional, spin-dependent effective barrier. This term is mathematically analogous to the $V_0\delta(x)$ potential used in the BTK model to describe a non-ideal interface.

Furthermore, another key result is that, the Reflection coefficients are individually completely independent of the misalignment angle Φ_{SO}, representing the orientation of the SO vector in the $y-z$ plane for the N region. Indeed, in the absence of additional spin-anisotropic fields or perturbations, changing Φ_{SO} only amounts to a local choice of the reference frame in N and does not modify the reflection probabilities measured.

Specifically, in the N region, varying the angle Φ_{SO} is equivalent to a rigid rotation of

the local spin quantization axis around the x-axes. This rotation does not affect the spectrum or the group velocities of the incident modes; in practice, it is just a change of spin basis. Because the reflected basis in N is defined within the same region, it rotates in exactly the same way. As a result, a change in Φ_{SO} acts as a simultaneous rotation of the entire N-region, including the incident states, the reflected basis, and the N-component of the interface barrier. Since all components related to reflection phenomenon "rotate together", the Reflection probabilities remain unchanged.
Furthermore, in the S region, the superconducting pairing term is s-wave singlet and proportional to σ_0 in spin space, i.e. spin-isotropic. A global change of spin basis therefore does not alter the pairing term and cannot induce any residual sensitivity to the spin orientation chosen on the N side. Therefore, the case of strong spin-orbit coupling demonstrates the key feature of ideal Andreev scattering: the Normal Reflection is suppressed because the system is simultaneously in the Andreev approximation ($E_{SO,N}, E_{SO,S} \gg \Delta_0$) and possesses a transparent interface (guaranteed by $E_{SO,N} = E_{SO,S}$).

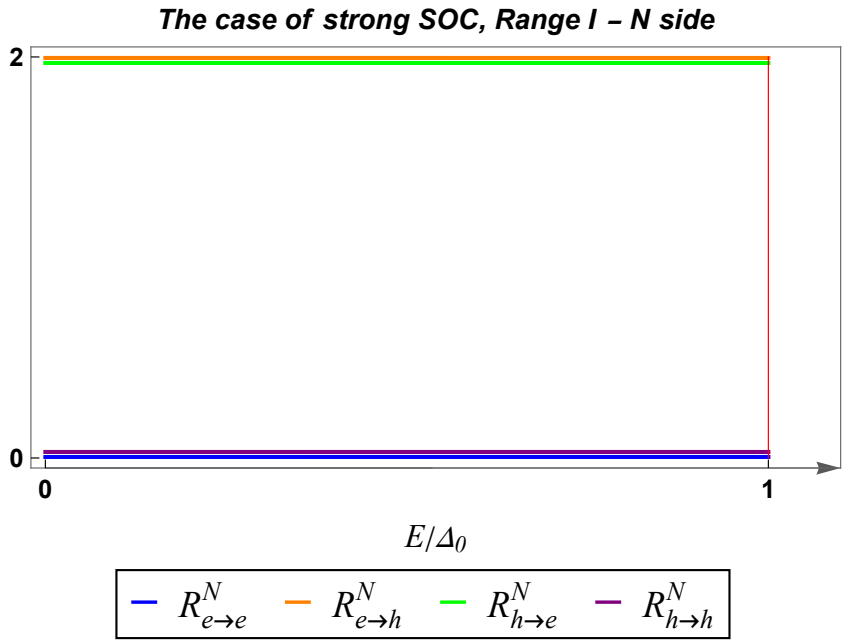

Figure 5.5: Plot of the total Normal and Andreev Reflection in the energy range I. The green and the purple curves are shown with a slight vertical offset to aid visualization, since the electron and hole ARs, as well as the electron and hole Normal Reflections, are perfectly coincident. The figure shows that the Normal Reflection is completely suppressed, while the AR is constant at its maximum probability value of 2 for both the electron and hole modes. There is no dependence on the SO misalignment angle Φ_{SO}.

(II) $\boldsymbol{\Delta_0 \leq E \leq E_{SO,N} + \mu_N \quad \leftrightarrow \quad \Delta_0 \leq E \leq 10\,\Delta_0}$

This energy range still corresponds to Range 1 in the Normal side while spans a large portion of the Lower Supra-gap regime in the Superconducting side . With respect

to the sub-gap regime, it includes both incoming and outgoing components in the S region. The vectors of propagating components read

$$\begin{cases} \mathbf{a} &= \left(a^{e}_{\nearrow,+}, a^{e}_{\swarrow,+}, a^{h}_{\nearrow,-}, a^{h}_{\swarrow,-}, a^{e}_{\uparrow,-}, a^{e}_{\downarrow,-}, a^{h}_{\uparrow,+}, a^{h}_{\downarrow,+}\right) \\ \mathbf{b} &= \left(b^{e}_{\nearrow,-}, b^{e}_{\swarrow,-}, b^{h}_{\nearrow,+}, b^{h}_{\swarrow,+}, b^{e}_{\uparrow,+}, b^{e}_{\downarrow,+}, b^{h}_{\uparrow,-}, b^{h}_{\downarrow,-}\right) \end{cases} \tag{5.134}$$

As a result, the Scattering matrix S is a 8×4 matrix and acquires the following form

$$\begin{pmatrix} b^{e}_{\nearrow,-} \\ b^{e}_{\swarrow,-} \\ b^{h}_{\nearrow,+} \\ b^{h}_{\swarrow,+} \\ b^{e}_{\uparrow,+} \\ b^{e}_{\downarrow,+} \\ b^{h}_{\uparrow,-} \\ b^{h}_{\downarrow,-} \end{pmatrix} = \underbrace{\begin{pmatrix} r^{e,\nearrow}_{e,\nearrow} & r^{e,\nearrow}_{e,\swarrow} & r^{e,\nearrow}_{h,\nearrow} & r^{e,\nearrow}_{h,\swarrow} & t^{e,\nearrow}_{e,\uparrow} & t^{e,\nearrow}_{e,\downarrow} & t^{e,\nearrow}_{h,\uparrow} & t^{e,\nearrow}_{h,\downarrow} \\ r^{e,\swarrow}_{e,\nearrow} & r^{e,\swarrow}_{e,\swarrow} & r^{e,\swarrow}_{h,\nearrow} & r^{e,\swarrow}_{h,\swarrow} & t^{e,\swarrow}_{e,\uparrow} & t^{e,\swarrow}_{e,\downarrow} & t^{e,\swarrow}_{h,\uparrow} & t^{e,\swarrow}_{h,\downarrow} \\ r^{h,\nearrow}_{e,\nearrow} & r^{h,\nearrow}_{e,\swarrow} & r^{h,\nearrow}_{h,\nearrow} & r^{h,\nearrow}_{h,\swarrow} & t^{h,\nearrow}_{e,\uparrow} & t^{h,\nearrow}_{e,\downarrow} & t^{h,\nearrow}_{h,\uparrow} & t^{h,\nearrow}_{h,\downarrow} \\ r^{h,\swarrow}_{e,\nearrow} & r^{h,\swarrow}_{e,\swarrow} & r^{h,\swarrow}_{h,\nearrow} & r^{h,\swarrow}_{h,\swarrow} & t^{h,\swarrow}_{e,\uparrow} & t^{h,\swarrow}_{e,\downarrow} & t^{h,\swarrow}_{h,\uparrow} & t^{h,\swarrow}_{h,\downarrow} \\ t^{e,\uparrow}_{e,\nearrow} & t^{e,\uparrow}_{e,\swarrow} & t^{e,\uparrow}_{h,\nearrow} & t^{e,\uparrow}_{h,\swarrow} & r^{e,\uparrow}_{e,\uparrow} & r^{e,\uparrow}_{e,\downarrow} & r^{e,\uparrow}_{h,\uparrow} & r^{e,\uparrow}_{h,\downarrow} \\ t^{e,\downarrow}_{e,\nearrow} & t^{e,\downarrow}_{e,\swarrow} & t^{e,\downarrow}_{h,\nearrow} & t^{e,\downarrow}_{h,\swarrow} & r^{e,\downarrow}_{e,\uparrow} & r^{e,\downarrow}_{e,\downarrow} & r^{e,\downarrow}_{h,\uparrow} & r^{e,\downarrow}_{h,\downarrow} \\ t^{h,\uparrow}_{e,\nearrow} & t^{h,\uparrow}_{e,\swarrow} & t^{h,\uparrow}_{h,\nearrow} & t^{h,\uparrow}_{h,\swarrow} & r^{h,\uparrow}_{e,\uparrow} & r^{h,\uparrow}_{e,\downarrow} & r^{h,\uparrow}_{h,\uparrow} & r^{h,\uparrow}_{h,\downarrow} \\ t^{h,\downarrow}_{e,\nearrow} & t^{h,\downarrow}_{e,\swarrow} & t^{h,\downarrow}_{h,\nearrow} & t^{h,\downarrow}_{h,\swarrow} & r^{h,\downarrow}_{e,\uparrow} & r^{h,\downarrow}_{e,\downarrow} & r^{h,\downarrow}_{h,\uparrow} & r^{h,\downarrow}_{h,\downarrow} \end{pmatrix}}_{=S} \begin{pmatrix} a^{e}_{\nearrow,+} \\ a^{e}_{\swarrow,+} \\ a^{h}_{\nearrow,-} \\ a^{h}_{\swarrow,-} \\ a^{e}_{\uparrow,-} \\ a^{e}_{\downarrow,-} \\ a^{h}_{\uparrow,+} \\ a^{h}_{\downarrow,+} \end{pmatrix} \tag{5.135}$$

The notation for the transmission amplitudes (t^{β}_{α}) follows the same structure as for the reflection ones. For example, $t^{e,\downarrow}_{e,\swarrow}$ represents the transmission amplitude for an incident $e,\swarrow$ electron to be transmitted as a $e,\downarrow$ quasi-electron.
The scattering matrix displayed in Eq.(5.135) is composed by four 4×4 sub-blocks. Specifically:

- the 4×4 upper-left block contains the reflection amplitudes (r^{β}_{α}) for the N-side modes;
- the 4×4 lower-left block contains the transmission amplitudes (t^{β}_{α}) for a particle incoming from the N region and transmitted in the S one;
- the 4×4 upper-right block contains the transmission amplitudes (t^{β}_{α}) for a particle incoming from the S region and transmitted in N one;
- the 4×4 lower-right block contains the reflection amplitudes (r^{β}_{α}) for the S-side modes;

Therefore, this energy interval supports all types of scattering processes.
The Transmission coefficient T^{β}_{α} from mode α to mode β is defined as

$$T^{\beta}_{\alpha} \;=\; |t^{\beta}_{\alpha}|^2 \qquad \forall\,\alpha,\;\beta \tag{5.136}$$

while the Reflection coefficient was already defined in Eq.(5.125).
The computation of each of the R^{β}_{α} and T^{β}_{α} coefficients $\forall\,\alpha,\,\beta$ via Wolfram Mathematica shows that, while the Reflection coefficients are independent of the Φ_{SO} angle also in this interval, the Transmission coefficients do depend on Φ_{SO} . To explain

this effect , let us consider, for example, the case of the $(e,\nearrow)$ incoming mode, which corresponds to analyzing the first column of the S-matrix in Eq.(5.135).
Let us recall here the expressions of the $(e,\nearrow)$ eigenvector in the N region and of the $(e,\uparrow),(e,\downarrow)$ eigenvectors in the S region for a fixed energy E. From Eq.(5.54-5.101) we have

$$\mathsf{w}^{e}_{N,\nearrow} = \begin{pmatrix} \cos\frac{\Phi_{SO}}{2} \\ i\sin\frac{\Phi_{SO}}{2} \\ 0 \\ 0 \end{pmatrix} \qquad \bar{\mathsf{w}}^{e}_{S,\uparrow}(E) = \begin{pmatrix} u_0(E) \\ 0 \\ v_0(E)e^{-i\varphi} \\ 0 \end{pmatrix} \qquad \bar{\mathsf{w}}^{e}_{S,\downarrow}(E) = \begin{pmatrix} 0 \\ u_0(E) \\ 0 \\ v_0(E)e^{-i\varphi} \end{pmatrix}$$

We observe that the first two components in $\mathsf{w}^{e}_{N,\nearrow}$ depend on the spin-orbit direction angle Φ_{SO} . In contrast the first two components of the eigenvectors on the S side, $\mathsf{w}^{e}_{S,\uparrow}(E)$ and $\mathsf{w}^{e}_{S,\downarrow}(E)$, cannot have such dependence.
Thus, the fractions of the incoming mode $(e,\nearrow)$, transmitted as electron-like $(e,\uparrow)$ and as electron-like $(e,\downarrow)$ shall depend on the value of the Φ_{SO}, causing such dependence in each of the Transmission coefficients $T^{e,\uparrow}_{e,\nearrow}$ and $T^{e,\downarrow}_{e,\nearrow}$. However, the total electron-electron transmission, i.e. the *sum* $T^{e,\uparrow}_{e,\nearrow} + T^{e,\downarrow}_{e,\nearrow}$ of the two Transmission coefficients, is *independent* of the Φ_{SO} angle. Similarly, a Φ_{SO} dependence is present also in $T^{h,\uparrow}_{e,\nearrow}$ and $T^{h,\downarrow}_{e,\nearrow}$, whereas the total electron-hole Transmission $T^{h,\uparrow}_{e,\nearrow} + T^{h,\downarrow}_{e,\nearrow}$ is *independent* of Φ_{SO}.
The same considerations hold when considering the Transmission coefficients regarding the other incoming modes, i.e. the other columns of the scattering matrix Eq.(5.135).
In addition, we verified that

$$\sum_{\beta}\left(R^{\beta}_{\alpha}+T^{\beta}_{\alpha}\right) = 1 \qquad \forall\ \alpha \tag{5.137}$$

$$\sum_{\alpha}\left(R^{\beta}_{\alpha}+T^{\beta}_{\alpha}\right) = 1 \qquad \forall\ \beta \tag{5.138}$$

in agreement with the conservation of the probability flux.
Finally, let us define the total Reflection and Transmission coefficients for each of the

possible scattering processes in the two side as

N side **S side**

$$\begin{cases} R^N_{e\to e}(E) = \left(R^{e,\nearrow}_{e,\nearrow} + R^{e,\swarrow}_{e,\swarrow} + R^{e,\swarrow}_{e,\nearrow} + R^{e,\swarrow}_{e,\swarrow}\right) \\ R^N_{h\to h}(E) = \left(R^{h,\nearrow}_{h,\nearrow} + R^{h,\nearrow}_{h,\swarrow} + R^{h,\swarrow}_{h,\nearrow} + R^{h,\swarrow}_{h,\swarrow}\right) \\ R^N_{h\to e}(E) = \left(R^{e,\nearrow}_{h,\nearrow} + R^{e,\nearrow}_{h,\swarrow} + R^{e,\swarrow}_{h,\nearrow} + R^{e,\swarrow}_{h,\swarrow}\right) \\ R^N_{e\to h}(E) = \left(R^{h,\nearrow}_{e,\nearrow} + R^{h,\nearrow}_{e,\swarrow} + R^{h,\swarrow}_{e,\nearrow} + R^{h,\swarrow}_{e,\swarrow}\right) \\ T^{N\to S}_{e\to e}(E) = \left(T^{e,\uparrow}_{e,\nearrow} + T^{e,\uparrow}_{e,\swarrow} + T^{e,\downarrow}_{e,\nearrow} + T^{e,\downarrow}_{e,\swarrow}\right) \\ T^{N\to S}_{h\to h}(E) = \left(T^{h,\uparrow}_{h,\nearrow} + R^{h,\uparrow}_{h,\swarrow} + T^{h,\downarrow}_{h,\nearrow} + T^{h,\downarrow}_{h,\swarrow}\right) \\ T^{N\to S}_{h\to e}(E) = \left(T^{e,\uparrow}_{h,\nearrow} + T^{e,\uparrow}_{h,\swarrow} + T^{e,\downarrow}_{h,\nearrow} + T^{e,\downarrow}_{h,\swarrow}\right) \\ T^{N\to S}_{e\to h}(E) = \left(T^{h,\uparrow}_{e,\nearrow} + T^{h,\uparrow}_{e,\swarrow} + T^{h,\downarrow}_{e,\nearrow} + T^{h,\downarrow}_{e,\swarrow}\right) \end{cases} \quad \begin{cases} R^S_{e\to e}(E) = \left(R^{e,\uparrow}_{e,\uparrow} + R^{e,\uparrow}_{e,\downarrow} + R^{e,\downarrow}_{e,\uparrow} + R^{e,\downarrow}_{e,\downarrow}\right) \\ R^S_{h\to h}(E) = \left(R^{h,\uparrow}_{h,\uparrow} + R^{h,\uparrow}_{h,\downarrow} + R^{h,\downarrow}_{h,\uparrow} + R^{h,\downarrow}_{h,\downarrow}\right) \\ R^S_{h\to e}(E) = \left(R^{e,\uparrow}_{h,\uparrow} + R^{e,\uparrow}_{h,\downarrow} + R^{e,\downarrow}_{h,\uparrow} + R^{e,\downarrow}_{h,\downarrow}\right) \\ R^S_{e\to h}(E) = \left(R^{h,\uparrow}_{e,\uparrow} + R^{h,\uparrow}_{e,\downarrow} + R^{h,\downarrow}_{e,\uparrow} + R^{h,\downarrow}_{e,\downarrow}\right) \\ T^{S\to N}_{e\to e}(E) = \left(T^{e,\uparrow}_{e,\uparrow} + T^{e,\uparrow}_{e,\downarrow} + T^{e,\downarrow}_{e,\uparrow} + T^{e,\downarrow}_{e,\downarrow}\right) \\ T^{S\to N}_{h\to h}(E) = \left(T^{h,\uparrow}_{h,\uparrow} + T^{h,\uparrow}_{h,\downarrow} + T^{h,\downarrow}_{h,\uparrow} + T^{h,\downarrow}_{h,\downarrow}\right) \\ T^{S\to N}_{h\to e}(E) = \left(T^{e,\uparrow}_{h,\uparrow} + T^{e,\uparrow}_{h,\downarrow} + T^{e,\downarrow}_{h,\uparrow} + T^{e,\downarrow}_{h,\downarrow}\right) \\ T^{S\to N}_{e\to h}(E) = \left(T^{h,\uparrow}_{e,\uparrow} + T^{h,\uparrow}_{e,\downarrow} + T^{h,\downarrow}_{e,\uparrow} + T^{h,\downarrow}_{e,\downarrow}\right) \end{cases} \tag{5.139}$$

Since there are two electron and two hole incident modes in each side of the junctions, then it holds that

$$\left(R^N_{e\to e} + R^N_{e\to h} + T^{N\to S}_{e\to e} + T^{N\to S}_{e\to h}\right)(E) \;=\; \left(R^N_{h\to e} + R^N_{h\to h} + T^{N\to S}_{h\to e} + T^{N\to S}_{h\to h}\right)(E) = 2 \tag{5.140}$$

$$\left(R^S_{e\to e} + R^S_{e\to h} + T^{S\to N}_{e\to e} + T^{S\to N}_{e\to h}\right)(E) \;=\; \left(R^S_{h\to e} + R^S_{h\to h} + T^{S\to N}_{h\to e} + T^{S\to N}_{h\to h}\right)(E) = 2 \tag{5.141}$$

The graphic representation of the total Reflection and Transmission coefficients for both sides is provided in Fig. 5.6.

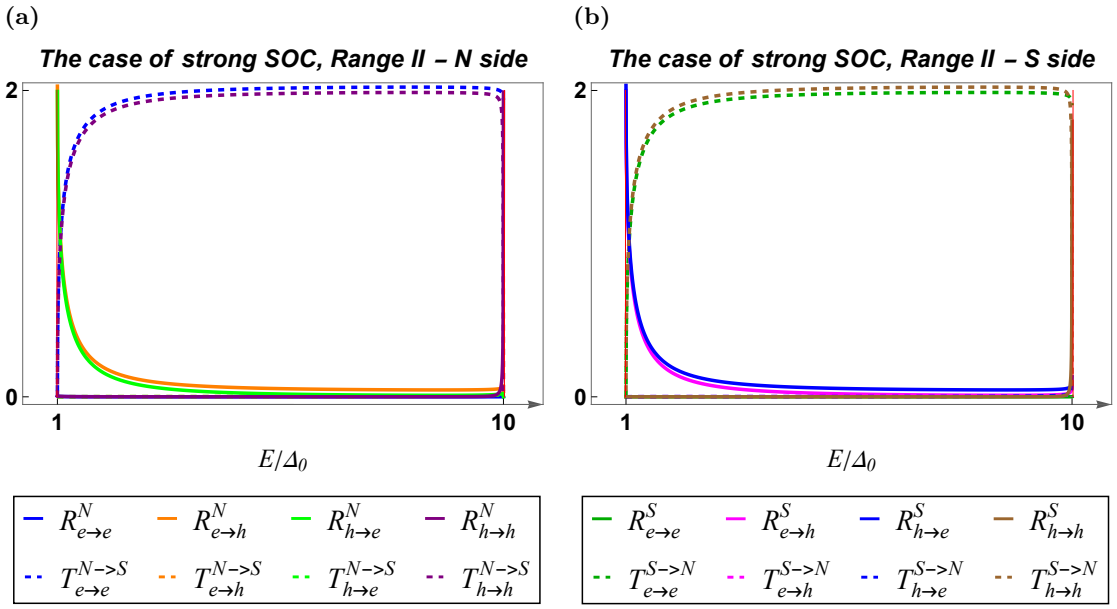

Figure 5.6: Graphic representation of the scattering process in the N side (left panel) and S side (right panel) in range II. To aid visualization a slight vertical offset has been added to the green and dashed blue curve in the left panel and to the blue and dashed brown curve in right panel. As clear from the figures, this energy range supports all the possible scattering process, since no evanescent modes are allowed. From the left panel we observe a pronounced decay of the Andreev Reflection which is almost completely suppressed for value of $4\Delta_0$. Furthermore we observe that the $h-h$ Transmission in both side of the junction abruptly drops to zero while the $h-h$ Reflection drastically increase around the energy value of $10\Delta_0$ as for energies greater than this value, the hole modes become evanescent in the N region.

(III) $\boldsymbol{E_{SO,N}+\mu_N \leq E \leq \sqrt{(E_{SO,S}+\mu_S)^2+\Delta_0^2} \quad \leftrightarrow \quad 10\,\Delta_0 \leq E \leq \sqrt{101}\,\Delta_0}$

This energy range corresponds to Range 2 in the N region, while also spanning a small and final portion of the Lower supra-gap regime. The vectors of propagating modes are

$$\begin{cases} \mathbf{a} &= \left(a^e_{\nearrow,+}, a^e_{\swarrow,+}, a^e_{\uparrow,-}, a^e_{\downarrow,-}, a^h_{\uparrow,+}, a^h_{\downarrow,+}\right) \\ \mathbf{b} &= \left(b^e_{\nearrow,-}, b^e_{\swarrow,-}, b^e_{\uparrow,+}, b^e_{\downarrow,+}, b^h_{\uparrow,-}, b^h_{\downarrow,-}\right) \end{cases} \tag{5.142}$$

The scattering matrix linearly connecting these two vectors reads

$$\begin{pmatrix} b^e_{\nearrow,-} \\ b^e_{\swarrow,-} \\ b^e_{\uparrow,+} \\ b^e_{\downarrow,+} \\ b^h_{\uparrow,-} \\ b^h_{\downarrow,-} \end{pmatrix} = \underbrace{\begin{pmatrix} r^{e,\nearrow}_{e,\nearrow} & r^{e,\nearrow}_{e,\swarrow} & t^{e,\nearrow}_{e,\uparrow} & t^{e,\nearrow}_{e,\downarrow} & t^{e,\nearrow}_{h,\uparrow} & t^{e,\nearrow}_{h,\downarrow} \\ r^{e,\swarrow}_{e,\nearrow} & r^{e,\swarrow}_{e,\swarrow} & t^{e,\swarrow}_{e,\uparrow} & t^{e,\swarrow}_{e,\downarrow} & t^{e,\swarrow}_{h,\uparrow} & t^{e,\swarrow}_{h,\downarrow} \\ t^{e,\uparrow}_{e,\nearrow} & t^{e,\uparrow}_{e,\swarrow} & r^{e,\uparrow}_{e,\uparrow} & r^{e,\uparrow}_{e,\downarrow} & r^{e,\uparrow}_{h,\uparrow} & r^{e,\uparrow}_{h,\downarrow} \\ t^{e,\downarrow}_{e,\nearrow} & t^{e,\downarrow}_{e,\swarrow} & r^{e,\downarrow}_{e,\uparrow} & r^{e,\downarrow}_{e,\downarrow} & r^{e,\downarrow}_{h,\uparrow} & r^{e,\downarrow}_{h,\downarrow} \\ t^{h,\uparrow}_{e,\nearrow} & t^{h,\uparrow}_{e,\swarrow} & r^{h,\uparrow}_{e,\uparrow} & r^{h,\uparrow}_{e,\downarrow} & r^{h,\uparrow}_{h,\uparrow} & r^{h,\uparrow}_{h,\downarrow} \\ t^{h,\downarrow}_{e,\nearrow} & t^{h,\downarrow}_{e,\swarrow} & r^{h,\downarrow}_{e,\uparrow} & r^{h,\downarrow}_{e,\downarrow} & r^{h,\downarrow}_{h,\uparrow} & r^{h,\downarrow}_{h,\downarrow} \end{pmatrix}}_{=S} \begin{pmatrix} a^e_{\nearrow,+} \\ a^e_{\swarrow,+} \\ a^e_{\uparrow,-} \\ a^e_{\downarrow,-} \\ a^h_{\uparrow,+} \\ a^h_{\downarrow,+} \end{pmatrix} \tag{5.143}$$

Thus, this energy range supports both the electron to electron and electron to hole transmissions, as well as the electron reflection in the N side. In contrast, Andreev Reflection is no longer allowed, since for this energy interval the hole modes in the N region become evanescent.
The dependence of the Transmission coefficients T_α^β on the spin-orbit angle Φ_{SO}, found in the previous energy regime, is also observed in this energy interval.
Here as well, we have verified that the conditions in Eq.(5.137), which ensure flux conservation, are satisfied.
Finally, given the definitions of the total Reflection and Transmission coefficients in Eq.(5.139), the following probability conservation relations must hold

$$\left(R^N_{e\to e} + T^{N\to S}_{e\to e} + T^{N\to S}_{e\to h}\right)(E) \;=\; 2 \tag{5.144}$$

$$\left(R^S_{e\to e} + R^S_{e\to h} + T^{S\to N}_{e\to e}\right)(E) \;=\; \left(R^S_{h\to e} + R^S_{h\to h} + T^{S\to N}_{h\to e}\right)(E) \;=\; 2 \tag{5.145}$$

Indeed, this energy interval supports two and four incoming modes in the N and S regions, respectively. As verification, we have plotted the total Reflection and Transmission coefficients For the N and S side in Fig.(5.6)

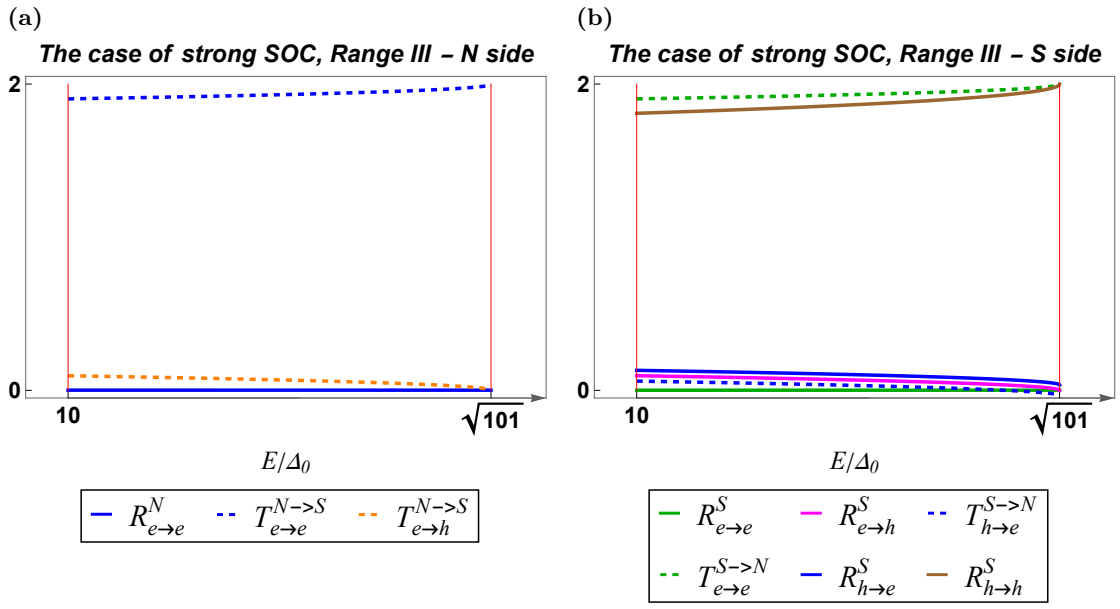

Figure 5.7: The energy range III does no support hole modes in the N side (left panel), thus the number of scattering process are limited in that region and the Andreev Reflection is no longer allowed. To aid visualization a slight vertical offset has been addedd to the blue and dashed blue curves, in continuity with the representation of the S side in range II.

(IV) $\boldsymbol{E > \sqrt{(E_{SO,S} + \mu_S)^2 + \Delta_0^2} \quad \leftrightarrow \quad E > \sqrt{101}\,\Delta_0}$

We now analyze the final range for the case of large SO energy. Here, the energy lies

within Range 2 in the N side and within the Upper supra-gap regime in the S side. The vectors of propagating components are

$$\begin{cases} \mathbf{a} &= \left(a^e_{\nearrow,+}, a^e_{\swarrow,+}, a^e_{\uparrow,-}, a^e_{\downarrow,-}\right) \\ \mathbf{b} &= \left(b^e_{\nearrow,-}, b^e_{\swarrow,-}, b^e_{\uparrow,+}, b^e_{\downarrow,+}\right) \end{cases} \tag{5.146}$$

The scattering matrix, which relates these two vectors, is

$$\begin{pmatrix} b^e_{\nearrow,-} \\ b^e_{\swarrow,-} \\ b^e_{\uparrow,+} \\ b^e_{\downarrow,+} \end{pmatrix} = \underbrace{\begin{pmatrix} r^{e,\nearrow}_{e,\nearrow} & r^{e,\nearrow}_{e,\swarrow} & t^{e,\nearrow}_{e,\uparrow} & t^{e,\nearrow}_{e,\downarrow} \\ r^{e,\swarrow}_{e,\nearrow} & r^{e,\swarrow}_{e,\swarrow} & t^{e,\swarrow}_{e,\uparrow} & t^{e,\swarrow}_{e,\downarrow} \\ t^{e,\uparrow}_{e,\nearrow} & t^{e,\uparrow}_{e,\swarrow} & r^{e,\uparrow}_{e,\uparrow} & r^{e,\uparrow}_{e,\downarrow} \\ t^{e,\downarrow}_{e,\nearrow} & t^{e,\downarrow}_{e,\swarrow} & r^{e,\downarrow}_{e,\uparrow} & r^{e,\downarrow}_{e,\downarrow} \end{pmatrix}}_{=S} \begin{pmatrix} a^e_{\nearrow,+} \\ a^e_{\swarrow,+} \\ a^e_{\uparrow,-}, \\ a^e_{\downarrow,-} \end{pmatrix} \tag{5.147}$$

This energy range no longer supports propagating hole modes, which, in fact, are evanescent in both sides of the junction. As a consequence, the only observable phenomena in the two regions are Normal electron Reflection and Transmission.
The spin-orbit angle Φ_{SO} dependence of the Transmission coefficients, observed in the previous two regimes, persists in this energy interval as well.
Furthermore, we have numerically verified that the conservation of the flux, expressed by the conditions in Eq.(5.137), is satisfied.
In the end, as clear from Fig. 5.8, it holds that

$$\left(R^N_{e\to e} + T^{N\to S}_{e\to e}\right)(E) \;=\; 2 \tag{5.148}$$

$$\left(R^S_{e\to e} + T^{S\to N}_{e\to e}\right)(E) \;=\; 2 \tag{5.149}$$

since this regime supports two electron incoming modes in both sides of the junction.

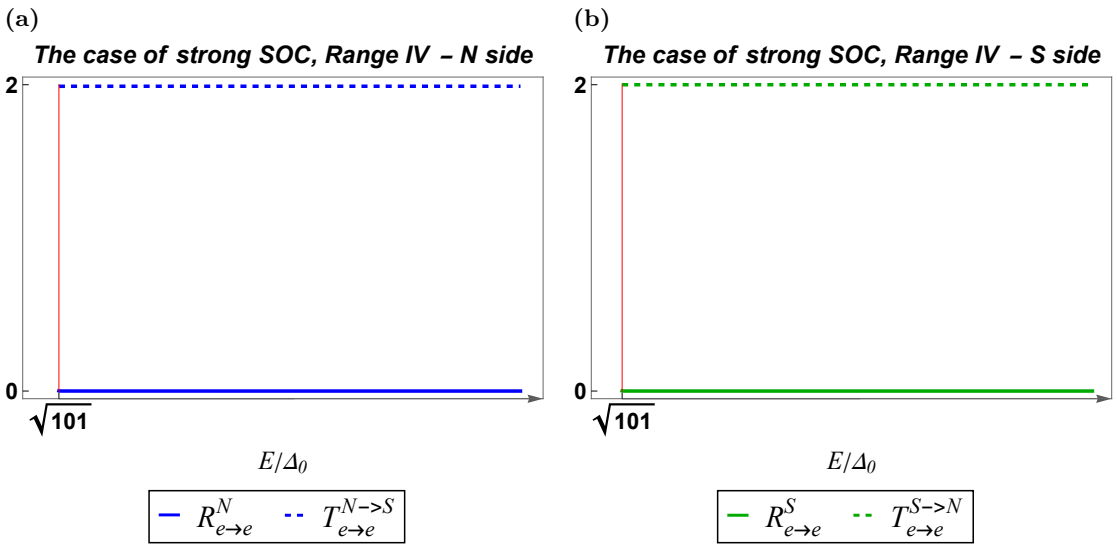

Figure 5.8: This energy range trivially supports only electron modes in both sides of the junction, therefore only Normal Reflection and electron-electron Transmission are allowed. As expected, for larger energy values, the Reflection probabilities are completely suppressed while the Transmission ones are maximized.

In conclusion, we have summarized the results obtained for the Normal and Andreev Reflection coefficients in Fig. 5.9 for energies up to $4\Delta_0$. This value marks the approximate threshold after which the Andreev Reflection is suppressed.
We remark here that the single Reflection coefficients R_α^β as well as the total Reflection ($\sum_\beta R_\alpha^\beta$) and Transmission coefficients ($\sum_\beta T_\alpha^\beta$) for each incoming mode α does not exhibit any dependence on the misalignment angle Φ_{SO}. In contrast, the individual Transmission coefficients (e.g. $T_{e,\nearrow}^{e,\uparrow}$) show a dependence on the Φ_{SO}, since the basis of N and S regions have a difference dependence on the SO angle.
Furthermore, in Fig.5.10 we have shown that it is possible to modulate the AR probabilities by varying the SO energy in the N region.

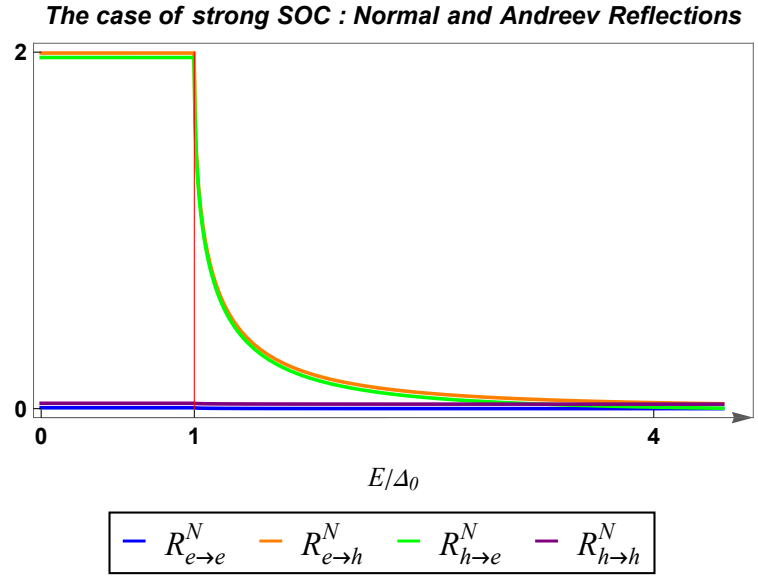

Figure 5.9: Plot of the total Normal and Andreev Reflections up to the energy value of $4\Delta_0$ for the electron and hole modes. Also here the green and the purple curves are shown with a slight vertical offset to aid visualization. The AR probability is maximum in the sub-gap regime, while strongly decades for energy values larger than Δ_0 and is completely suppressed for energy values around $4\Delta_0$. No dependence on the misalignment angle Φ_{SO} is observed.

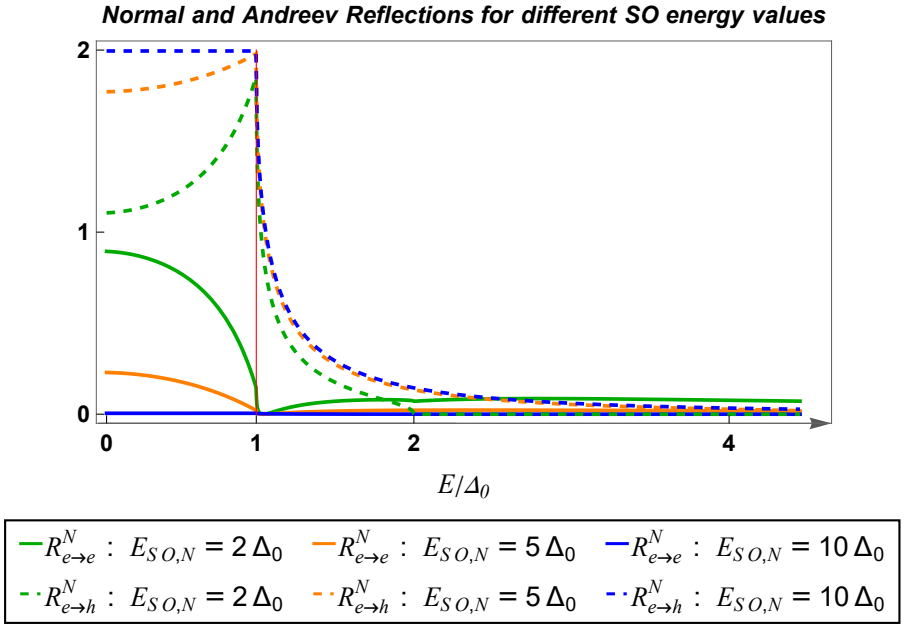

Figure 5.10: Normal and Andreev Reflections for a fixed SO energy in S region ($E_{SO,S} = 10\Delta_0$) and different values of $E_{SO,N}$ in N region. The value $E = 2\Delta_0$ marks the energy after which AR is no longer allowed for the $E_{SO.N} = 2\Delta_0$ case . Here we observe that changing the magnitude of the SO energy in N region causes the AR probabilities to vary.

5.2.4 The regime of weak spin-orbit energy ($E_{SO} < \Delta_0$)

Let us now turn to the case of weak spin-orbit energy $E_{SO} < \Delta_0$. Specifically, we shall adopt the following model parameters

$$E_{SO,N} = E_{SO,S} = \frac{\Delta_0}{3} \qquad \mu_N = \mu_S = 0 \tag{5.150}$$

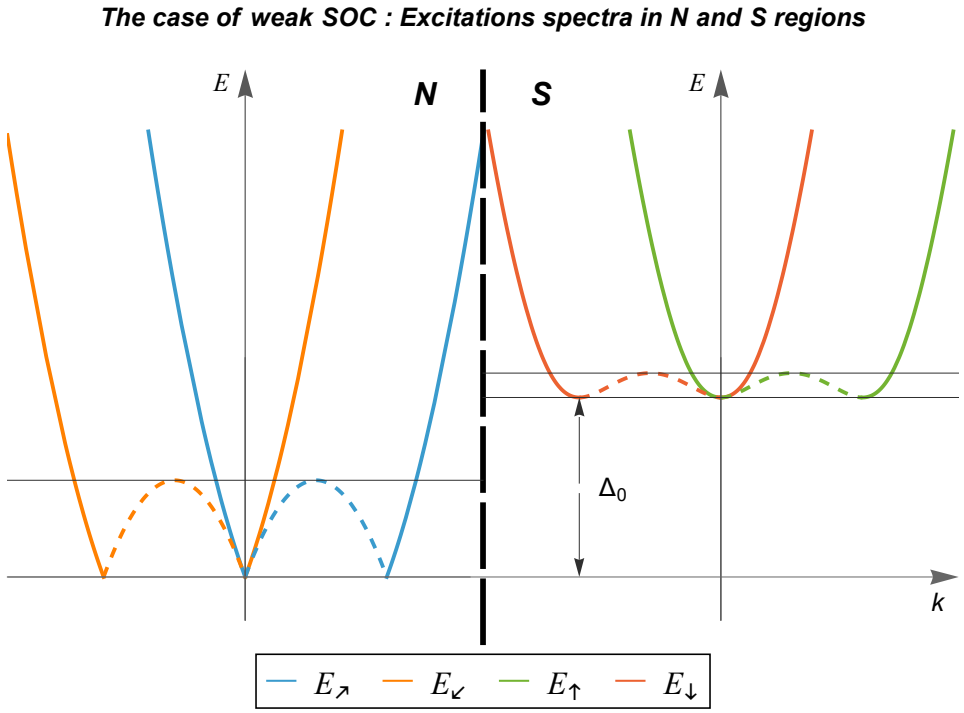

Figure 5.11: Plot of the excitations spectra in the two regions for the regime B of weak spin-orbit energy ($E_{SO} < \Delta_0$). This specific set of parameters leads to four different energy ranges, which are marked by horizontal lines.

The energy spectrum on the two sides of the junction is shown in Fig.5.11. As one can see, there are four different energy ranges, stemming from the combination of the energy ranges in the two sides of the junction. Let us now analyze each of these separately:

(I) $\boldsymbol{E \leq E_{SO,N} + \mu_N \quad \leftrightarrow \quad E \leq \frac{\Delta_0}{3}}$

This interval corresponds to Range 1 in the N side, and to the Sub-Gap regime in the S one. The vector of propagating components are

$$\begin{cases} \mathbf{a} &= \left(a^e_{\nearrow,+}, a^e_{\swarrow,+}, a^h_{\nearrow,-}, a^h_{\swarrow,-}\right)^T \\ \mathbf{b} &= \left(b^e_{\nearrow,-}, b^e_{\swarrow,-}, b^h_{\nearrow,+}, b^h_{\swarrow,+}\right)^T \end{cases} \tag{5.151}$$

The corresponding scattering matrix S for this pair of incoming vectors is presented in Eq.(5.124). Indeed, this energy interval is characterized by the same vectors **a** and

b as for the $E < \Delta_0$ regime of large spin-orbit energy [see Sec 5.2.3]. Consequently, the theoretical considerations regarding the structure of the S matrix and the allowed scattering process are identical.
We emphasize that, since the parameters under consideration in this configuration are different from those in large spin-orbit energy (5.122), the energy dependence of the individual Reflection coefficients R_α^β differs between the two cases.
In particular the most significant difference between the cases of large and weak spin-orbit energy -in the case of equal SO energy in the two regions ($E_{SO,N} = E_{SO,S}$)-, is the emergence of a finite Normal Reflection in the weak regime that was not observed in large regime.
The emergence of the Normal Reflection confirms that the current parameters place the system in a regime beyond the standard Andreev approximation. Indeed, as established in our analysis of the large spin-orbit regime, this setup is analogous to the BTK framework, but with the spin-orbit energy E_{SO} playing the role of the chemical potential μ. In contrast, here the spin-orbit energy is smaller than the superconducting gap $E_{SO,N} = E_{SO,N} < \Delta_0$, and the Andreev approximation ($E_{SO} \gg \Delta_0$) no longer holds. Consequently, an intrinsic momentum mismatch $k^e \neq k^h$ arises between the incident electron (hole) and the reflected hole (electron) in the Andreev Reflection process. This mismatch acts as an effective barrier, generating the appearance of a Normal Reflection.
Finally, we remark that even in this regime, the individual Reflection coefficients (R_α^β) are still independent of the angle Φ_{SO}. Indeed, a change in Φ_{SO} acts as a rotation of the entire N-region. Since all parts related to the reflection phenomenon rotate together, the reflection probabilities are left invariant.

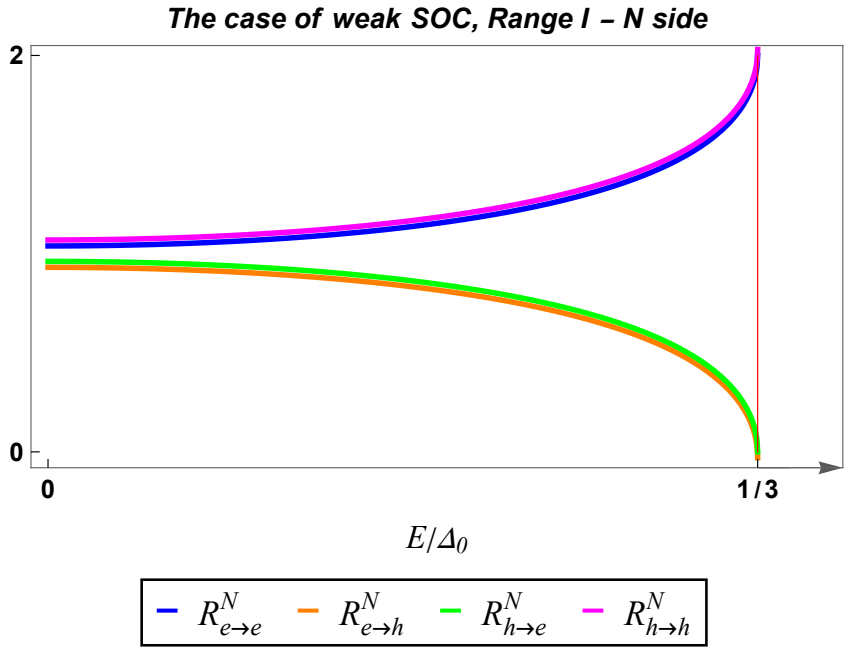

Figure 5.12: Plot of the Andreev and Normal Reflection for Range I in the case of weak SOC. The green and purple curves are shown with a slight vertical offset to aid visualization, since the electron and hole AR curves, as well as the electron and hole Normal Reflection ones, are perfectly coincident. Differently from the case of strong SO energy, here the Normal Reflection is not suppressed, conversely it approaches its maximum probability value as the energy tends to $\frac{\Delta_0}{3}$. No dependence on the SO misalignment angle is observed also for this choice of the parameters.

(II) $\boldsymbol{E_{SO.N} + \mu_N \;<\; E \;< \Delta_0 \quad \leftrightarrow \quad \frac{\Delta_0}{3} \;< E \;< \Delta_0}$

This energy range spans a second and final portion of the Sub-Gap regime, while it refers to Range 2 regime for the Normal region. Notably, for all higher energy intervals, the N region remains in Range 2, and consequently, hole modes in this side are no longer allowed. The vector of propagating components are

$$\begin{cases} \mathbf{a} &= \left(a^e_{\nearrow,+}, a^e_{\swarrow,+}\right)^T \\ \mathbf{b} &= \left(b^e_{\nearrow,-}, b^e_{\swarrow,-}\right)^T \end{cases} \tag{5.152}$$

and the corresponding scattering matrix is

$$\begin{pmatrix} b^e_{\nearrow,-} \\ b^e_{\swarrow,-} \end{pmatrix} = \underbrace{\begin{pmatrix} r^{e,\nearrow}_{e,\nearrow} & r^{e,\nearrow}_{e,\swarrow} \\ r^{e,\swarrow}_{e,\nearrow} & r^{e,\swarrow}_{e,\swarrow} \end{pmatrix}}_{=S} \begin{pmatrix} a^e_{\nearrow,+} \\ a^e_{\swarrow,+} \end{pmatrix} \tag{5.153}$$

The S-matrix reveals that the system is trivial in this energy interval. Indeed, the only permitted process is Normal Reflection. We have specifically verified that $R^{e,\nearrow}_{e,\nearrow}$ and $R^{e,\swarrow}_{e,\swarrow}$ are equal to 1.

(III) $\boldsymbol{\Delta_0} \leq \boldsymbol{E} \leq \sqrt{\boldsymbol{\Delta_0^2} + (\boldsymbol{E_{SO,N}} + \boldsymbol{\mu_S})^2} \quad \leftrightarrow \quad \boldsymbol{\Delta_0} \leq \boldsymbol{E} \leq \sqrt{\frac{10}{9}}\boldsymbol{\Delta_0}$

This energy interval spans all the Lower Supra-Gap regime, while, as already discussed, it corresponds to Range 2 for the Normal region. The vectors **a** and **b** of propagating components are

$$\begin{cases} \mathbf{a} &= \left(a^e_{\nearrow,+}, a^e_{\swarrow,+}, a^e_{\uparrow,-}, a^e_{\downarrow,-}, a^h_{\uparrow,+}, a^h_{\downarrow,+}\right)^T \\ \mathbf{b} &= \left(b^e_{\nearrow,-}, b^e_{\swarrow,-}, b^e_{\uparrow,+}, b^e_{\downarrow,+}, b^h_{\uparrow,-}, b^h_{\downarrow,-}\right)^T \end{cases} \tag{5.154}$$

and the Scattering matrix reads

$$\begin{pmatrix} b^e_{\nearrow,-} \\ b^e_{\swarrow,-} \\ b^e_{\uparrow,+} \\ b^e_{\downarrow,+} \\ b^h_{\uparrow,-} \\ b^h_{\downarrow,-} \end{pmatrix} = \underbrace{\begin{pmatrix} r^{e,\nearrow}_{e,\nearrow} & r^{e,\nearrow}_{e,\swarrow} & t^{e,\nearrow}_{e,\uparrow} & t^{e,\nearrow}_{e,\downarrow} & t^{e,\nearrow}_{h,\uparrow} & t^{e,\nearrow}_{h,\downarrow} \\ r^{e,\swarrow}_{e,\nearrow} & r^{e,\swarrow}_{e,\swarrow} & t^{e,\swarrow}_{e,\uparrow} & t^{e,\swarrow}_{e,\downarrow} & t^{e,\swarrow}_{h,\uparrow} & t^{e,\swarrow}_{h,\downarrow} \\ t^{e,\uparrow}_{e,\nearrow} & t^{e,\uparrow}_{e,\swarrow} & r^{e,\uparrow}_{e,\uparrow} & r^{e,\uparrow}_{e,\downarrow} & r^{e,\uparrow}_{h,\uparrow} & r^{e,\uparrow}_{h,\downarrow} \\ t^{e,\downarrow}_{e,\nearrow} & t^{e,\downarrow}_{e,\swarrow} & r^{e,\downarrow}_{e,\uparrow} & r^{e,\downarrow}_{e,\downarrow} & r^{e,\downarrow}_{h,\uparrow} & r^{e,\downarrow}_{h,\downarrow} \\ t^{h,\uparrow}_{e,\nearrow} & t^{h,\uparrow}_{e,\swarrow} & r^{h,\uparrow}_{e,\uparrow} & r^{h,\uparrow}_{e,\downarrow} & r^{h,\uparrow}_{h,\uparrow} & r^{h,\uparrow}_{h,\downarrow} \\ t^{h,\downarrow}_{e,\nearrow} & t^{h,\downarrow}_{e,\swarrow} & r^{h,\downarrow}_{e,\uparrow} & r^{h,\downarrow}_{e,\downarrow} & r^{h,\downarrow}_{h,\uparrow} & r^{h,\downarrow}_{h,\downarrow} \end{pmatrix}}_{=S} \begin{pmatrix} a^e_{\nearrow,+} \\ a^e_{\swarrow,+} \\ a^e_{\uparrow,-} \\ a^e_{\downarrow,-} \\ a^h_{\uparrow,+} \\ a^h_{\downarrow,+} \end{pmatrix} \tag{5.155}$$

This energy range has already been encountered in the analyses of the case of strong SO energy. Therefore, we refer the reader to that specific section for the details of the allowed scattering processes.
We remark here that the Andreev Reflection phenomenon is no longer allowed since hole modes in N side are evanescent in this energy range.
Fig.(5.13) displays the total Reflection and Transmission probabilities, and clearly demonstrates the unitarity of the Scattering matrix.

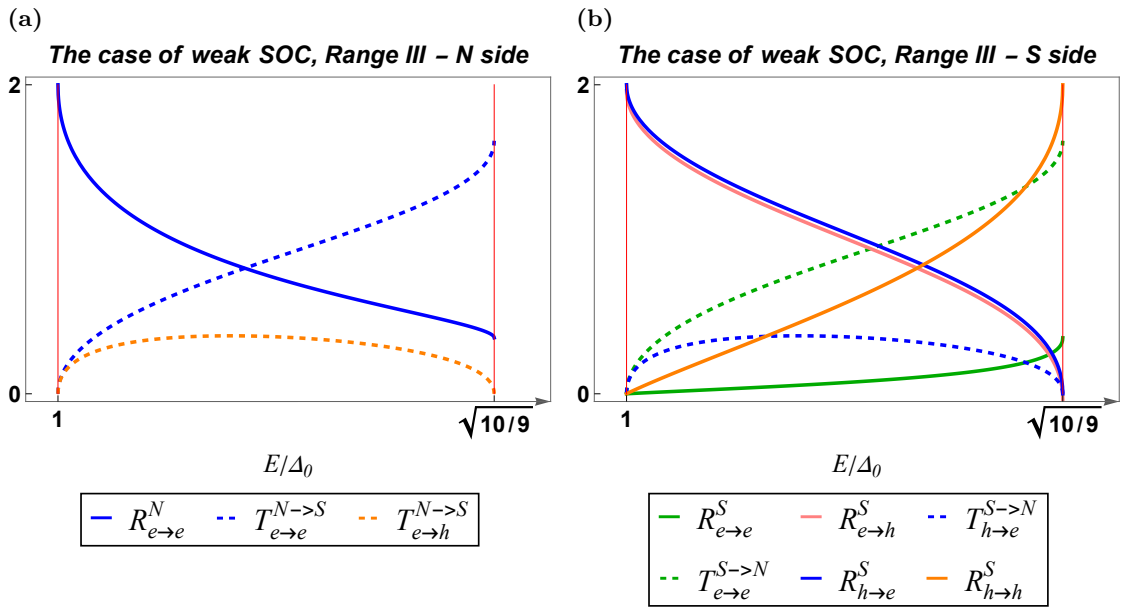

Figure 5.13: Graphic representation of the total Reflection and Transmission probabilities for the N (left panel) and S regions (right panel) in Range III. A slight vertical offset has been added to the pink curve to aid visualization.

(IV) $\boldsymbol{E \geq \sqrt{\Delta_0^2 + (E_{SO,N} + \mu_S)^2}} \quad \leftrightarrow \quad \boldsymbol{E \geq \sqrt{\frac{10}{9}}\Delta_0}$

The vectors of propagating components are

$$\begin{cases} \mathbf{a} &= \left(a^e_{\nearrow,+}, a^e_{\swarrow,+}, a^e_{\uparrow,-}, a^e_{\downarrow,-}\right) \\ \mathbf{b} &= \left(b^e_{\nearrow,-}, b^e_{\swarrow,-}, b^e_{\uparrow,+}, b^e_{\downarrow,+}\right) \end{cases} \tag{5.156}$$

The Scattering matrix, which relates these two vectors, is

$$\begin{pmatrix} b^e_{\nearrow,-} \\ b^e_{\swarrow,-} \\ b^e_{\uparrow,+} \\ b^e_{\downarrow,+} \end{pmatrix} = \underbrace{\begin{pmatrix} r^{e,\nearrow}_{e,\nearrow} & r^{e,\nearrow}_{e,\swarrow} & t^{e,\nearrow}_{e,\uparrow} & t^{e,\nearrow}_{e,\downarrow} \\ r^{e,\swarrow}_{e,\nearrow} & r^{e,\swarrow}_{e,\swarrow} & t^{e,\swarrow}_{e,\uparrow} & t^{e,\swarrow}_{e,\downarrow} \\ t^{e,\uparrow}_{e,\nearrow} & t^{e,\uparrow}_{e,\swarrow} & r^{e,\uparrow}_{e,\uparrow} & r^{e,\uparrow}_{e,\downarrow} \\ t^{e,\downarrow}_{e,\nearrow} & t^{e,\downarrow}_{e,\swarrow} & r^{e,\downarrow}_{e,\uparrow} & r^{e,\downarrow}_{e,\downarrow} \end{pmatrix}}_{=S} \begin{pmatrix} a^e_{\nearrow,+} \\ a^e_{\swarrow,+} \\ a^e_{\uparrow,-}, \\ a^e_{\downarrow,-} \end{pmatrix} \tag{5.157}$$

This last energy range trivially admits only electron modes in both sides of the junction. The total Transmission and Reflection probabilities are presented in Fig.5.14, which clearly demonstrate the unitary of the Scattering matrix.
As expected, the electron reflection are completely suppressed for larger energy values and the Transmission coefficient reaches its maximum value.

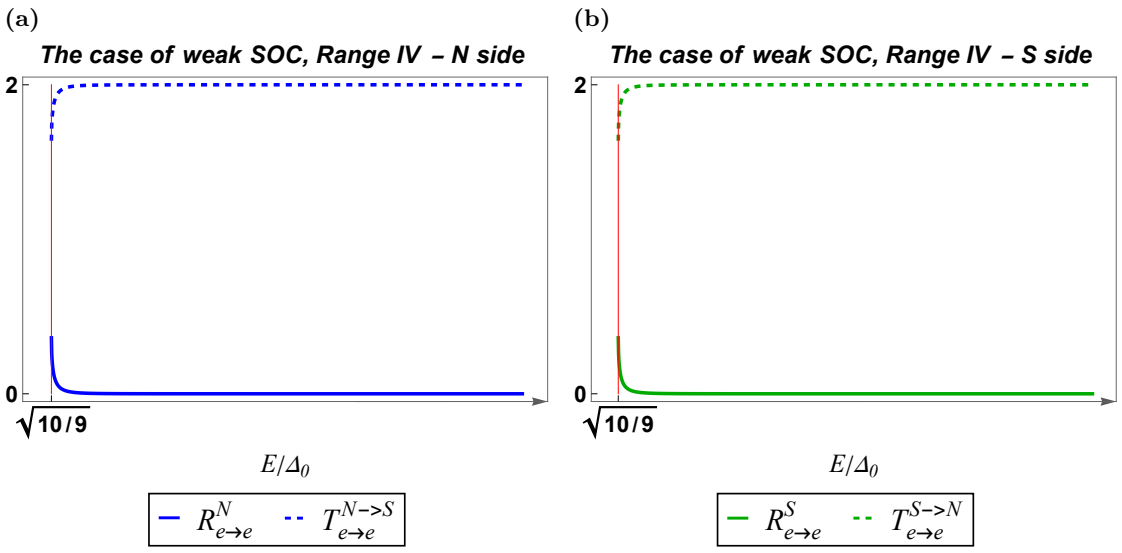

Figure 5.14: This energy range trivially supports only electron modes in both side of the junction, therefore only Normal Reflection and electron-electron Transmission are allowed. As expected, for large energy values, the Normal Reflection is completely suppressed and the Transmission probabilities are maximized.

In conclusion, we summarize here the main result obtained for the current choice of parameters. No dependence on the *misalignment* angle Φ_{SO} is observed for the total Reflection and Transmission coefficients. In Fig.5.15 we have plotted the Normal and Andreev Reflection up to an energy of $1.5\Delta_0$. We remark that AR is allowed up to an energy value of $\frac{\Delta_0}{3}$, since hole modes turn evanescent at higher energies; Normal Reflection remains allowed however is completely suppressed for energy values around $1.5\Delta_0$.
In contrast, a dependence on the *magnitude* of the SO vector is always observed, as showed in Fig.5.16.
Specifically, we have represented the Normal and Andreev Reflection probabilities up to the energy value of Δ_0 for a fixed SO energy in S region of $E_{SO,S} = \frac{\Delta_0}{3}$, while varying the magnitude of the SO vector in the N side. This amounts to change the value of the SO energy E_{SO} in the N region, thus Fig.5.16 demonstrates the possibility to tune the AR probabilities by modulating the value of the SO energy $E_{SO,N}$. Tuning the Rashba SOC can be experimentally realized by implementing electrostatic gates (wrap/side/back) in the N side of the junction, through which it is possible to control the applied electrical field $\mathbf{E}(\mathbf{r})$ and thus the Rashba interaction term [35].

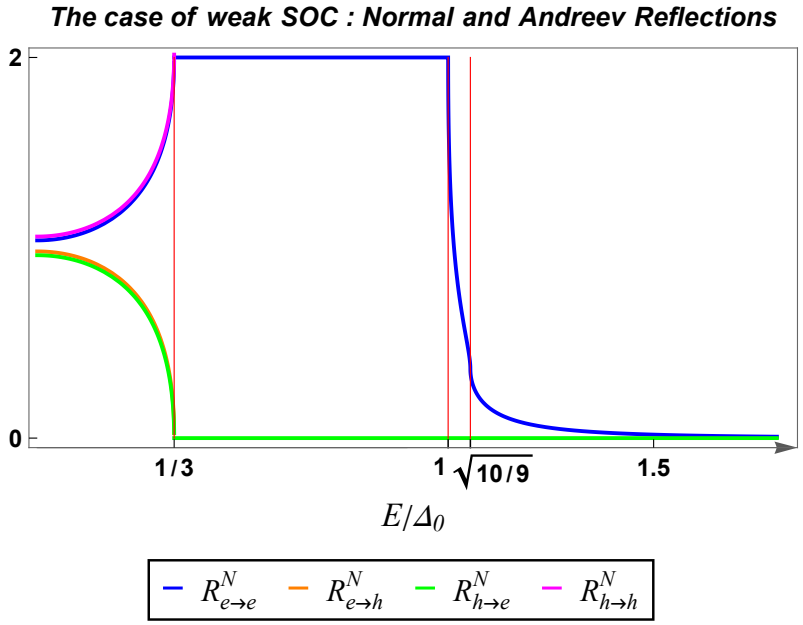

Figure 5.15: Plot of the total Normal and Andreev Reflection up to the energy value of $1.5\Delta_0$. Also here a slight vertical offset has been added to aid visualization, as the electron and hole ARs, as well as the electron and hole Normal Reflections, are perfectly coincident. There is no dependence on the spin-orbit misalignment angle Φ_{SO}.

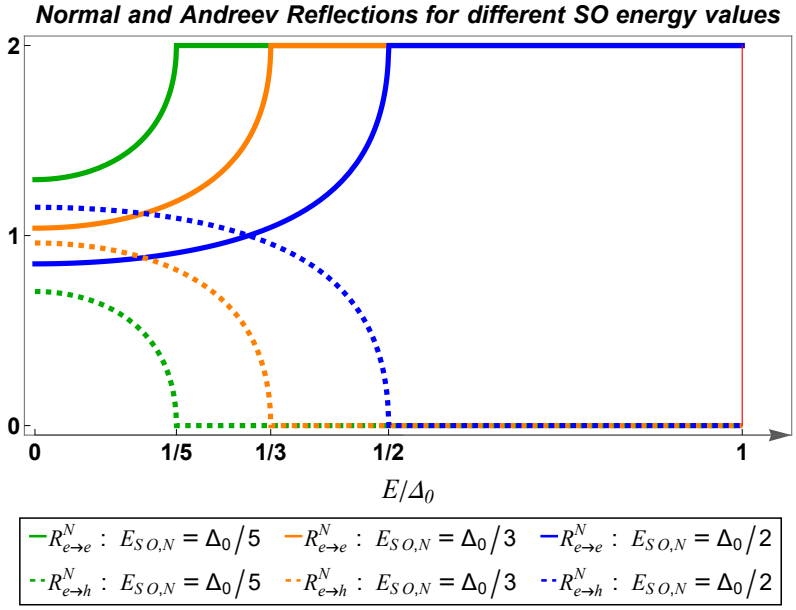

Figure 5.16: Plot of the total Normal and Andreev Reflection up to the energy value of Δ_0, for a fixed value of $E_{SO,S} = 0.5\Delta_0$ in the S region and for different values of $E_{SO,N}$ in the N region. The inhomogeneities in the magnitude α_N of the SOC, which enters the spin-orbit energy on each side of the interface, affect the AR process.

5.3 Effects of a perpendicular magnetic field

Building upon the system structure delineated at the beginning of Section 5, we now extend our analysis of the N-S interface to include a uniform magnetic field that is orthogonal to the spin-orbit field. Specifically, since the spin-orbit field lies in $y-z$ plane

$$\boldsymbol{\alpha}_N = \alpha_N \left(0, \sin\Phi_{SO}, \cos\Phi_{SO}\right) \tag{5.158}$$

$$\boldsymbol{\alpha}_S = (0,0,\alpha_S) \tag{5.159}$$

with Φ_{SO} denoting the mislignament angle between the N and S regions, we shall assume that the magnetic field $\mathbf{b}$ is applied along the NW axis x, i.e.

$$\mathbf{b} = (b_x,0,0) \tag{5.160}$$

Similarly to what we did in the previous section for the case without magnetic field, we shall compute the solutions in the N and S regions, and then impose the boundary conditions to determine the reflection and transmission properties.

5.3.1 Solution in the N region

We start by the Bogoliubov-de Gennes Hamiltonian (3.6) derived in Section 3.1. By specifying it to the N region, where the superconducting pairing vanishes ($\Delta_0 = 0$), we obtain the block-diagonal Hamiltonian

$$H_{BdG}(k) = \begin{pmatrix} \xi_k^0\sigma_0 - k\,\boldsymbol{\alpha_N}\cdot\boldsymbol{\sigma} - \mathbf{b}\cdot\boldsymbol{\sigma} & 0 \\ 0 & -\xi_k^0\sigma_0 + k\,\boldsymbol{\alpha_N}\cdot\boldsymbol{\sigma} - \mathbf{b}\cdot\boldsymbol{\sigma} \end{pmatrix} \tag{5.161}$$

The diagonalization of such matrix was already performed in Section 3.3.1, by rotating the basis and moving to the natural basis [see Eq.(3.98)]

$$\tilde{H}_{BdG}(k) = \begin{pmatrix} \xi_k^0\sigma_0 + |\mathbf{m}(k)|\sigma_z & 0 \\ 0 & -\xi_k^0\sigma_0 + |\mathbf{m}(-k)|\sigma_z \end{pmatrix} \tag{5.162}$$

In particular, in the present case (5.158)-(5.160) the effective field vector $\mathbf{m}(k)$, which includes both the SO and Zeeman terms, is

$$|\mathbf{m}(k)| = \sqrt{(\alpha_N k)^2 + b_x^2} \tag{5.163}$$

and, the eigenvalues (3.99) read

$$\begin{cases} \xi^e_{\Uparrow/\Downarrow}(k) = \xi^0_N(k) \pm \sqrt{(\alpha_N k)^2 + b_x^2} \\ \xi^h_{\Uparrow/\Downarrow}(k) = -\xi^0_N(k) \mp \sqrt{(\alpha_N k)^2 + b_x^2} \end{cases} \tag{5.164}$$

The eigenvectors (3.103) acquire the form

$$\Phi^e_{k,\Uparrow}=\begin{pmatrix}\cos\frac{\theta_k}{2}\\ \sin\frac{\theta_k}{2}\,e^{i\varphi_k}\\ 0\\ 0\end{pmatrix}\qquad\qquad \Phi^e_{k,\Downarrow}=\begin{pmatrix}-\sin\frac{\theta_k}{2}\,e^{-i\varphi_k}\\ \cos\frac{\theta_k}{2}\\ 0\\ 0\end{pmatrix}$$

$$\Phi^h_{k,\Downarrow}=\begin{pmatrix}0\\ 0\\ \cos\frac{\theta_{-k}}{2}\\ \sin\frac{\theta_{-k}}{2}\,e^{i\varphi_{-k}}\end{pmatrix}\qquad\qquad \Phi^h_{k,\Uparrow}=\begin{pmatrix}0\\ 0\\ -\sin\frac{\theta_{-k}}{2}\,e^{-i\varphi_{-k}}\\ \cos\frac{\theta_{-k}}{2}\end{pmatrix} \tag{5.165}$$

where

$$\begin{cases}\cos\theta_k &=& -\dfrac{\alpha_z k}{\sqrt{b_x^2+(\alpha_N k)^2}}\\[2ex] \sin\theta_k &=& \sqrt{\dfrac{b_x^2+(\alpha_N\,k\sin\Phi_{SO})^2}{b_x^2+(\alpha_N k)^2}}\\[2ex] \varphi_k &=& \arctan\left(\frac{\alpha_N\,k\sin\Phi_{SO}}{b_x}\right)+\pi\vartheta(b_x)\end{cases} \tag{5.166}$$

and $\varphi_k\in[0,2\pi]$, $\theta_k\in[0,\pi]$, with ϑ denoting the Heaviside function.
We observe that, since $\frac{\theta_k}{2}\in[0,\frac{\pi}{2}]$, terms of type "$\cos\frac{\theta_k}{2},\ \sin\frac{\theta_k}{2}$" shall be always positive, thus, in this interval, the following trigonometric relations are valid

$$\cos\frac{\theta_k}{2}=+\sqrt{\frac{1}{2}\,(1+\cos\theta_k)}\qquad\qquad \sin\frac{\theta_k}{2}=+\sqrt{\frac{1}{2}\,(1-\cos\theta_k)} \tag{5.167}$$

whence, given that in our particular case $\cos\theta_{-k}=-\cos\theta_k$, we get

$$\cos\frac{\theta_{-k}}{2}=\sin\frac{\theta_k}{2}\qquad\text{and}\qquad\sin\frac{\theta_{-k}}{2}=\cos\frac{\theta_k}{2} \tag{5.168}$$

Finally the positive spectrum of (5.162) read

$$\begin{cases}E^e_{\Uparrow}(k) &=& \vartheta(\xi^e_{\Uparrow}(k))|\xi^e_{\Uparrow}(k)|=\vartheta\Big(\xi^0_N(k)+\sqrt{(\alpha_N k)^2+b_x^2}\Big)\Big|\xi^0_N(k)+\sqrt{(\alpha_N k)^2+b_x^2}\Big|\\[2ex] E^h_{\Uparrow}(k) &=& \vartheta(\xi^h_{\Uparrow}(k))|\xi^h_{\Uparrow}(k)|=\vartheta\Big(-\xi^0_N(k)-\sqrt{(\alpha_N k)^2+b_x^2}\Big)\Big|\xi^0_N(k)+\sqrt{(\alpha_N k)^2+b_x^2}\Big|\\[2ex] E^e_{\Downarrow}(k) &=& \vartheta(\xi^e_{\Downarrow}(k))|\xi^e_{\Downarrow}(k)|=\vartheta\Big(\xi^0_N(k)-\sqrt{(\alpha_N k)^2+b_x^2}\Big)\Big|\xi^0_N(k)-\sqrt{(\alpha_N k)^2+b_x^2}\Big|\\[2ex] E^h_{\Downarrow}(k) &=& \vartheta(\xi^h_{\Downarrow}(k))|\xi^h_{\Downarrow}(k)|=\vartheta\Big(-\xi^0_N(k)+\sqrt{(\alpha_N k)^2+b_x^2}\Big)\Big|\xi^0_N(k)-\sqrt{(\alpha_N k)^2+b_x^2}\Big|\end{cases} \tag{5.169}$$

From the expression of $E^h_{\Uparrow}(k)$ in Eq.(5.169), we observe that this branch only exists in the positive spectrum if the argument of the Heaviside ϑ-function is positive. Let us analyze

this condition, which is

$$\vartheta(\xi^h_{\Uparrow}(k)) = \vartheta\left(-\frac{\hbar^2k^2}{2m^*} + \mu_N - \sqrt{(\alpha_N k)^2 + b_x^2}\right) \tag{5.170}$$

The terms $-\frac{\hbar^2k^2}{2m^*}$ and $-\sqrt{(\alpha_N k)^2 + b_x^2}$ both provide a negative contribution that increases in magnitude with k. Therefore, the maximum of$E^h_+(k)$ occurs at $k = 0$, and it is $\mu_N - |b_x|$. If this maximum value is negative (i.e., if $|b_x| > \mu_N$), then $E^h_+(k)$ will be negative for all k. Consequently, the ϑ-function will be zero for all k, and the Hole-$\Uparrow$ branch of the spectrum vanishes from the positive energy range, thus losing its capacity to support propagating modes. Despite that, in such a situation, this branch still contributes to the total solution through evanescent modes.
We now have all the necessary ingredients to compute the wavefunction $\Phi_N(x)$ in the N region.

Remark
A crucial difference from the case with vanishing magnetic field is that here the eigenvectors are now necessarily k-dependent. The electron bands acquire a k-dependent spin texture. This is a fundamental consequence of the competition between the two spin-aligning fields in the system: the constant Zeeman field $\mathbf{b}$ and the momentum-dependent spin-orbit (SO) field, $k\boldsymbol{\alpha}$.
The total effective field, $\mathbf{m}(k) = -(k\boldsymbol{\alpha} + \mathbf{b})$, defines the spin quantization axis for the system, given by $\hat{\mathbf{n}}(k) = \mathbf{m}(k)/|\mathbf{m}(k)|$. Due to the competition between its two constituent terms, this axis rotates as a function of momentum k. Specifically, the spin axis precesses from being aligned with the Zeeman field at $k = 0$ (where $\mathbf{m}(0) = -\mathbf{b}$) to being asymptotically aligned with the SO-field at large k (where $\mathbf{m}(k) \approx -k\boldsymbol{\alpha}$. Since the eigenvectors of the Hamiltonian are, by definition, the spin states that align with this k-dependent axis, they must inherit this strong k-dependence to form the correct basis.

Eigenfunctions at fixed energy E

To determine the eigenfunctions for our system at a fixed energy $E > 0$, we must first find the corresponding wavevectors. These are obtained by inverting the four equations

of the positive spectrum given in Eq.(5.169) in favour of k, namely

$$\begin{aligned}
E^e_{\Uparrow}(k) = E \quad &\Rightarrow \quad \xi^0_N(k) + \sqrt{(\alpha_N k)^2 + b_x^2} = E \quad \Rightarrow \quad (\alpha_N k)^2 + b_x^2 = \Big(E - \xi^0_N(k)\Big)^2 \\
E^h_{\Uparrow}(k) = E \quad &\Rightarrow \quad \xi^0_N(k) + \sqrt{(\alpha_N k)^2 + b_x^2} = -E \quad \Rightarrow \quad (\alpha_N k)^2 + b_x^2 = \Big(E + \xi^0_N(k)\Big)^2 \\
E^e_{\Downarrow}(k) = E \quad &\Rightarrow \quad \xi^0_N(k) - \sqrt{(\alpha_N k)^2 + b_x^2} = E \quad \Rightarrow \quad (\alpha_N k)^2 + b_x^2 = \Big(E - \xi^0_N(k)\Big)^2 \\
E^h_{\Downarrow}(k) = E \quad &\Rightarrow \quad \xi^0_N(k) - \sqrt{(\alpha_N k)^2 + b_x^2} = -E \quad \Rightarrow \quad (\alpha_N k)^2 + b_x^2 = \Big(E + \xi^0_N(k)\Big)^2
\end{aligned} \tag{5.171}$$

As is evident from the equations above, the two electron equations once squared, collapse into a single algebraic equation. The same holds true for the two hole sectors ($E^h_{\Uparrow}$ and $E^h_{\Downarrow}$).
Since $\xi^0_N(k)$ is a quadratic function of k (i.e., $\xi^0_N(k) = \frac{\hbar^2 k^2}{2m^*} - \mu_N$), both of these resulting equations are biquadratic in k (i.e., of the form $Ak^4 + Bk^2 + C = 0$).
Solving each of these two biquadratic equations yields four distinct roots for k.
The correct correspondence between these solutions and the four original dispersion branches is recovered by considering the sign constraints in the unsquared equations. For example, the roots belonging to $E^e_{\Uparrow}$ must satisfy the constraint $E - \xi^0_N(k) \geq 0$, while those belonging to $E^e_{\Downarrow}$ must satisfy $E - \xi^0_N(k) \leq 0$. An analogous sorting applies to the two hole branches.
As a result the number of solutions for each branch strictly depends on the competition between the energy parameters $\mu_N\,, E_{SO,N}$, E_Z, where the definition of $E_{SO,N}$ is given in Eq.(5.60) and the Zeeman Energy E_Z is defined as

$$E_Z = |b_x| \tag{5.172}$$

Specifically, we start our analysis by considering the case $E_Z > \mu_N$. We have already noted that, in this situation, the Hole-$\Uparrow$ branch in Eq.(5.169) is shifted entirely below the Fermi level ($E = 0$) and thus it is unable to carry propagating modes, but only evanescent ones.
Furthermore, we will structure our analysis based on a critical condition that dictates the Hole-$\Downarrow$ sector band structure. Indeed, we observe that the competition between the Zeeman energy (E_Z) and the spin-orbit energy ($E_{SO,N}$) fundamentally alters the shape of the $E^h_{\Downarrow}(k)$ branch, thereby changing the number of available propagating channels.
In particular, it is possible to distinguish between two regimes, namely the Rashba-dominated regime, defined by the condition $E_Z < 2E_{SO,N}$ and the Zeeman dominated-regime $E_Z > 2E_{SO,N}$.
When the spin-orbit interaction is dominant($E_Z < 2E_{SO,S}$), the $E^h_{\Downarrow}(k)$ band exhibits a "double-well" (or inverted Mexican hat) structure and it is characterized by a local minimum at $k = 0$ and two global maxima at $k = \pm k_{max}$. The crucial consequence is the emergence of a finite energy window between the local minimum $E^h_{\Downarrow}(0)$ and the global

maxima $E^h_{\Downarrow}(\pm k_{max})$ where a line of constant energy E intersects the band four times. Therefore, in this specific energy interval, the hole-$\Downarrow$ sector can support four propagating solutions (i.e., four real k-vectors).
Conversely, when the Zeeman field is strong enough to overcome the spin-orbit splitting ($E_Z > 2E_{SO,S}$), the double-well structure collapses. The band's shape is now featuring by only a single global maximum at $k = 0$. In this regime, any line of constant energy E can intersect the band Hole-$\Downarrow$ at most twice.
Consequently, the hole sector can only support a maximum of two propagating solutions. This distinction is extremely important, as the number of "open" propagating channels (four vs two) at given energy depends on it.
Finally, in what follows we will analyze only the case of the Rashba-dominated regime, as the main focus of this thesis lies in the study of how SOC changes the scattering process in an N/S junction.

Rashba-dominated regime $E_Z < 2E_{SO,N}$

Let us start by solving the equations (5.171) for a fixed energy E to identify the various energy regimes governing the scattering process.
In doing so, we first identify two critical energy thresholds derived from the band extrema: $I_1 = E_Z - \mu_N$ and $I_2 = \mu_N + \frac{E_Z^2}{4E_{SO,N}}$. We observe that the relative order of these two thresholds depends on the specific system parameters. In particular, if $\mu_N > \frac{1}{2}\left(E_Z - \frac{E_Z^2}{4E_{SO,N}}\right)$, then I_1 marks the lower energy threshold, whereas if this condition is not met, I_2 becomes the lower threshold. As will be clear, the primary consequence of this ordering relates to the nature and presence of evanescent modes within the different energy intervals defined by I_1 and I_2.
Regardless, for the remainder of this derivation, we shall focus on the specific situation where $\mu_N < \frac{1}{2}\left(E_Z - \frac{E_Z^2}{4E_{SO,N}}\right)$.
In particular we identify five possible regimes:

- **Range 1** : $\boxed{E < \mu_N + \dfrac{E_Z^2}{4E_{SO,N}}}$

  The solution of the Eqs defined in (5.171) are

  $$(\alpha_N k)^2 + b_x^2 = \left(E^e_{\Uparrow} - \xi^0_N(k)\right)^2$$

  $$\boxed{k^e_{\Uparrow,\pm} = \pm i\sqrt{\frac{2m^*}{\hbar^2}\left(\sqrt{4E_{SO,N}\left(\mu_N + E + E_{SO,N}\right) + E_Z^2} - \left(\mu_N + E + 2E_{SO,N}\right)\right)}} \tag{5.173}$$

  $$(\alpha_N k)^2 + b_x^2 = \left(E^h_{\Uparrow} + \xi^0_N(k)\right)^2$$

  $$\boxed{k^h_{\Uparrow,\pm} = \pm i\sqrt{\frac{2m^*}{\hbar^2}\left(\sqrt{4E_{SO,N}\left(\mu_N - E + E_{SO,N}\right) + E_Z^2} - \left(\mu_N - E + 2E_{SO,N}\right)\right)}} \tag{5.174}$$

$$(\alpha_N k)^2 + b_x^2 = \left(E_{\Downarrow}^e - \xi_N^0(k)\right)^2$$

$$\boxed{k_{\Downarrow,\pm}^e = \pm\sqrt{\frac{2m^*}{\hbar^2}\Big((\mu_N + E + 2E_{SO,N}) + \sqrt{4E_{SO,N}\left(\mu_N + E + E_{SO,N}\right) + E_Z^2}\Big)}} \tag{5.175}$$

$$(\alpha_N k)^2 + b_x^2 = \left(E_{\Downarrow}^h + \xi_N^0(k)\right)^2$$

$$\boxed{k_{\Downarrow,\pm}^{h,1} = \pm\sqrt{\frac{2m^*}{\hbar^2}\Big((\mu_N - E + 2E_{SO,N}) + \sqrt{4E_{SO,N}\left(\mu_N - E + E_{SO,N}\right) + E_Z^2}\Big)}} \tag{5.176}$$

and we assign the index "1" to the $k_{\Downarrow,\pm}^{h,1}$ wavevectors, since in the following ranges the $E_{\Downarrow}^h$ branch will admit more than two solutions. Therefore, we obtain 4 real solutions, describing propagating modes, and 4 complex ones describing evanescent ones. Indeed the electron $k_{\Uparrow,\pm}$ solutions possess an imaginary part for the energy constraint $E < E_Z - \mu_N$ that, by hypothesis, Range 1 always satisfies. Similarly, the hole $E_{\Uparrow}^h$ branch admits two evanescent solutions for $E < E_Z + \mu_N$, which is also true for all energies within Range 1.
In fact, as previously discussed, this last branch only admits complex solutions for $E > 0$, since it lies entirely below the Fermi level. In particular, as will become evident in the following ranges, this Hole branch will cease to contribute any solutions, including evanescent ones.
However, since N is on the left-hand side of the interface, only solutions with a negative imaginary part can be retained, since describing evanescent waves decaying for $x \to -\infty$. As a result $k_{\Uparrow,-}^e, k_{\Uparrow,-}^h$ modes represents the only permitted solutions here, whereas $k_{\Uparrow,+}^e, k_{\Uparrow,+}^e$ modes bring to a divergent contribution and must be discarded.
For the propagating modes the group velocity is defined as

$$v_g(E) = \frac{1}{\hbar}\frac{\partial E}{\partial k}\bigg|_{k=k(E)} \tag{5.177}$$

and reads

$$v_{\Downarrow,\pm}^e(E) = \frac{\hbar}{m^*}\, k_{\Downarrow,\pm}^e(E)\, \frac{D_e}{2E_{SO,N} + D_e} \quad \text{and} \quad D_e = \sqrt{4E_{SO,N}\left(\mu_N + E + E_{SO,N}\right) + E_Z^2} \tag{5.178}$$

$$v_{\Downarrow,\pm}^{h,1}(E) = -\frac{\hbar}{m^*}\, k_{\Downarrow,\pm}^{h,1}(E)\, \frac{D_h}{2E_{SO,N} + D_h} \quad \text{and} \quad D_h = \sqrt{4E_{SO,N}\left(\mu_N - E + E_{SO,N}\right) + E_Z^2} \tag{5.179}$$

The general expression of the wavefunction in the N side of the junction for this energy

range is

$$\begin{aligned}\Phi_N(x) = a^e_{\Downarrow,+}\frac{e^{ik^e_{\Downarrow,+}(E)\,x}}{\sqrt{2\pi\hbar v^e_{\Downarrow,+}(E)}}\Phi^e_{\Downarrow}(k^e_{\Downarrow,+}) \;+\; a^{h,1}_{\Downarrow,-}\frac{e^{ik^{h,1}_{\Downarrow,-}(E)\,x}}{\sqrt{2\pi\hbar v^{h,1}_{\Downarrow,-}(E)}}\Phi^h_{\Downarrow}(k^{h,1}_{\Downarrow,-}) + \\ + b^e_{\Downarrow,-}\frac{e^{ik^e_{\Downarrow,-}(E)\,x}}{\sqrt{2\pi\hbar v^e_{\Downarrow,-}(E)}}\Phi^e_{\Downarrow}(k^e_{\Downarrow,-}) \;+\; b^{h,1}_{\Downarrow,+}\frac{e^{ik^{h,1}_{\Downarrow,+}(E)\,x}}{\sqrt{2\pi\hbar v^{h,1}_{\Downarrow,+}(E)}}\Phi^h_{\Downarrow}(k^{h,1}_{\Downarrow,+}) + \\ + c^e_{\Uparrow,-}\frac{e^{ik^e_{\Uparrow,-}(E)\,x}}{\sqrt{2\pi\hbar v_N}}\Phi^e_{\Uparrow}(k^e_{\Uparrow,-}) \;+\; c^h_{\Uparrow,-}\frac{e^{ik^h_{\Uparrow,-}(E)\,x}}{\sqrt{2\pi\hbar v_N}}\Phi^h_{\Uparrow}(k^h_{\Uparrow,-})\end{aligned} \tag{5.180}$$

where v_N is defined as

$$v_N \doteq \sqrt{\frac{2(E_{SO,N}+\mu_N)}{m^*}} \tag{5.181}$$

and represent a formal definition of velocity, introduced to correctly normalize the evanescent mode in Φ_N, similarly to the propaganting ones.

- **Range 2** : $\mu_N + \dfrac{E_Z^2}{4E_{SO,N}} \leq E < E_Z - \mu_N$

  We observe that for energies $E \geq \mu_N + \frac{E_Z^2}{4E_{SO,N}}$ hole-$\Uparrow$ branch stops contributing solutions altogether, not even evanescent ones, whereas the solution of Eqs (5.171) for the hole-$\Downarrow$ branch always yields four solutions.
  In particular, the real ones solutions for the $\Downarrow$-Hole branch were already computed for the Range 1 energy interval, whereas the remaining two solutions represent always complex quantity for energy E such that $E_Z > |\mu_N - E|$, which for our choice of the

parameters traduces to $E < \mu_N + E_Z$. Therefore, we have

$$(\alpha_N k)^2 + b_x^2 = \Big(E^e_{\Uparrow} - \xi^0_N(k)\Big)^2$$

$$\boxed{k^e_{\Uparrow,\pm} = \pm i\sqrt{\frac{2m^*}{\hbar^2}\Big(\sqrt{4E_{SO,N}\left(\mu_N + E + E_{SO,N}\right) + E_Z^2} - \left(\mu_N + E + 2E_{SO,N}\right)\Big)}} \tag{5.182}$$

$$(\alpha_N k)^2 + b_x^2 = \Big(E^e_{\Downarrow} - \xi^0_N(k)\Big)^2$$

$$\boxed{k^e_{\Downarrow,\pm} = \pm\sqrt{\frac{2m^*}{\hbar^2}\Big(\left(\mu_N + E + 2E_{SO,N}\right) + \sqrt{4E_{SO,N}\left(\mu_N + E + E_{SO,N}\right) + E_Z^2}\Big)}} \tag{5.183}$$

$$(\alpha_N k)^2 + b_x^2 = \Big(E^h_{\Downarrow} + \xi^0_N(k)\Big)^2$$

$$\begin{cases} \boxed{k^{h,1}_{\Downarrow,\pm} = \pm\sqrt{\frac{2m^*}{\hbar^2}\Big(\left(\mu_N - E + 2E_{SO,N}\right) + \sqrt{4E_{SO,N}\left(\mu_N - E + E_{SO,N}\right) + E_Z^2}\Big)}} \\ \boxed{k^{h,2}_{\Downarrow,\pm} = \pm i\sqrt{\frac{2m^*}{\hbar^2}\Big(\sqrt{4E_{SO,N}\left(\mu_N - E + E_{SO,N}\right) + E_Z^2} - \left(\mu_N - E + 2E_{SO,N}\right)\Big)}} \end{cases} \tag{5.184}$$

Note that the $k^{h,2}_{\Downarrow,\pm}$ solutions are equal to $k^h_{\Uparrow,\pm}$ ones, since the two equations for the Hole branch in (5.171), once squared, represents the same unique equation. The difference between the two ranges clearly lies in the specific energy regimes of validity for the 4 solutions.
From the four evanescent solutions, we must discard the ones indentified by $k^{h,2}_{\Downarrow,+}$, $k^e_{\Uparrow,+}$, since characterized by a positive imaginary part and thus diverging for $x \to -\infty$. Given the definition of velocity group in Eq.(5.178) for the propagating $\Downarrow$-modes, the wavefunction $\Phi_N(x)$ in this regime reads

$$\begin{aligned} \boxed{\Phi_N(x) = a^e_{\Downarrow,+}\frac{e^{ik^e_{\Downarrow,+}(E)\,x}}{\sqrt{2\pi\hbar v^e_{\Downarrow,+}(E)}}\Phi^e_{\Downarrow}(k^e_{\Downarrow,+}) \;+\; a^{h,1}_{\Downarrow,-}\frac{e^{ik^{h,1}_{\Downarrow,-}(E)\,x}}{\sqrt{2\pi\hbar v^{h,1}_{\Downarrow,-}(E)}}\Phi^h_{\Downarrow}(k^{h,1}_{\Downarrow,-}) +} \\ + b^e_{\Downarrow,-}\frac{e^{ik^e_{\Downarrow,-}(E)\,x}}{\sqrt{2\pi\hbar v^e_{\Downarrow,-}(E)}}\Phi^e_{\Downarrow}(k^e_{\Downarrow,-}) \;+\; b^{h,1}_{\Downarrow,+}\frac{e^{ik^{h,1}_{\Downarrow,+}(E)\,x}}{\sqrt{2\pi\hbar v^{h,1}_{\Downarrow,+}(E)}}\Phi^h_{\Downarrow}(k^{h,1}_{\Downarrow,+}) + \\ c^e_{\Uparrow,-}\frac{e^{ik^e_{\Uparrow,-}(E)\,x}}{\sqrt{2\pi\hbar v_N}}\Phi^e_{\Uparrow}(k^e_{\Uparrow,-}) \;+\; c^{h,2}_{\Downarrow,-}\frac{e^{ik^{h,2}_{\Downarrow,-}(E)\,x}}{\sqrt{2\pi\hbar v_N}}\Phi^h_{\Downarrow}(k^{h,2}_{\Downarrow,-}) \end{aligned} \tag{5.185}$$

where v_N is defined in (5.181).

- **Range 3** : $\boxed{E_Z - \mu_N \leq E < E_Z + \mu_N}$

  The value $E_Z - \mu_N$ represents the onset energy for propagating modes within the $E^e_{\Uparrow}$ branch, as determined by Eqs.(5.171). This marks the energy threshold above which

the solutions for the $E^e_{\Uparrow}$ branch transition from evanescent to permanently propagating. It follows that

$$(\alpha_N k)^2 + b_x^2 = \Big(E^e_{\Uparrow} - \xi^0_N(k)\Big)^2$$

$$\boxed{k^e_{\Uparrow,\pm} = \pm\sqrt{\frac{2m*}{\hbar^2}\Big(\,(\mu_N + E + 2E_{SO,N}) - \sqrt{4E_{SO,N}\,(\mu + E + E_{SO,N}) + b_x^2}\Big)}} \tag{5.186}$$

$$(\alpha_N k)^2 + b_x^2 = \Big(E^e_{\Downarrow} - \xi^0_N(k)\Big)^2$$

$$\boxed{k^e_{\Downarrow,\pm} = \pm\sqrt{\frac{2m*}{\hbar^2}\Big(\,(\mu_N + E + 2E_{SO,N}) + \sqrt{4E_{SO,N}\,(\mu + E + E_{SO,N}) + E_Z^2}\Big)}} \tag{5.187}$$

$$(\alpha_N k)^2 + b_x^2 = \Big(E^h_{\Downarrow} + \xi^0_N(k)\Big)^2$$

$$\begin{cases} \boxed{k^{h,1}_{\Downarrow,\pm} = \pm\sqrt{\frac{2m^*}{\hbar^2}\Big(\,(\mu_N - E + 2E_{SO,N}) + \sqrt{4E_{SO,N}\,(\mu - E + E_{SO,N}) + E_Z^2}\Big)}} \\ \boxed{k^{h,2}_{\Downarrow,\pm} = \pm i\sqrt{\frac{2m^*}{\hbar^2}\Big(\sqrt{4E_{SO,N}\,(\mu - E + E_{SO,N}) + E_Z^2} - (\mu_N - E + 2E_{SO,N})\Big)}} \end{cases} \tag{5.188}$$

The computation of velocity group $v_g(E) = \frac{1}{\hbar}\frac{\partial E}{\partial k}$ for the two Electron-$\Uparrow$ modes brings to

$$v^e_{\Uparrow,\pm}(E) = \frac{\hbar}{m^*}\,k^e_{\Uparrow,\pm}(E)\,\frac{D_e}{D_e - 2E_{SO,N}} \quad \text{and} \quad D_e = \sqrt{4E_{SO,N}\,(\mu + E + E_{SO,N}) + E_Z^2} \tag{5.189}$$

We observe that the quantity $D_e - 2E_{SO,N}$ is always positive, therefore assigning the right sign to the velocities of the two electron modes. The wavefunctions in the N side reads

$$\begin{boxed}
\begin{aligned}
\Phi_N(x) = {} & a^e_{\Downarrow,+}\frac{e^{ik^e_{\Downarrow,+}(E)\,x}}{\sqrt{2\pi\hbar v^e_{\Downarrow,+}(E)}}\Phi^e_{\Downarrow}(k^e_{\Downarrow,+}) \;+\; a^{h,1}_{\Downarrow,-}\frac{e^{ik^{h,1}_{\Downarrow,-}(E)\,x}}{\sqrt{2\pi\hbar v^h_{\Downarrow,-}(E)}}\Phi^h_{\Downarrow}(k^{h,1}_{\Downarrow,-}) + \\
& + a^e_{\Uparrow,+}\frac{e^{ik^e_{\Uparrow,+}(E)\,x}}{\sqrt{2\pi\hbar v^e_{\Uparrow,+}(E)}}\Phi^e_{\Uparrow}(k^e_{\Uparrow,+}) \;+\; b^e_{\Downarrow,-}\frac{e^{ik^e_{\Downarrow,-}(E)\,x}}{\sqrt{2\pi\hbar v^e_{\Downarrow,-}(E)}}\Phi^e_{\Downarrow}(k^e_{\Downarrow,-}) \\
& + b^{h,1}_{\Downarrow,+}\frac{e^{ik^{h,1}_{\Downarrow,+}(E)\,x}}{\sqrt{2\pi\hbar v^{h,1}_{\Downarrow,+}(E)}}\Phi^h_{\Downarrow}(k^h_{\Downarrow,+}) \;+\; b^e_{\Uparrow,-}\frac{e^{ik^e_{\Uparrow,-}(E)\,x}}{\sqrt{2\pi\hbar v^e_{\Uparrow,-}(E)}}\Phi^e_{\Uparrow}(k^e_{\Uparrow,-}) \\
& + c^{h,2}_{\Downarrow,-}\frac{e^{ik^{h,2}_{\Downarrow,-}(E)\,x}}{\sqrt{2\pi\hbar v_N}}\Phi^h_{\Downarrow}(k^{h,2}_{\Downarrow,-})
\end{aligned}
\end{boxed} \tag{5.190}$$

- **Range 4** : $\boxed{E_Z + \mu_N \leq E \leq E_{SO,N} + \dfrac{E_Z^2}{4E_{SO,N}} + \mu_N}$

This particular energy range is unique within the SO-dominated regime ($E_Z < 2E_{SO,N}$). Within this window, the hole-$\Downarrow$ sector supports four propagating modes. Indeed, all four real roots generated by the corresponding biquadratic equation in (5.171) satisfy the constraint for the $E^h_{\Downarrow}$ branch. Furthermore, the electrons sector remain unchanged compared to adjacent energy regimes and the corresponding biquadratic equations for each of the two electron sectors continue to yield two real (propagating) solutions. Thus, the wavevectors solutions read

$$(\alpha_N k)^2 + b_x^2 = \Big(E^e_{\Uparrow} - \xi^0_N(k)\Big)^2$$

$$\boxed{k^e_{\Uparrow,\pm} = \pm\sqrt{\frac{2m*}{\hbar^2}\Big((\mu_N + E + 2E_{SO,N}) - \sqrt{4E_{SO,N}\,(\mu + E + E_{SO,N}) + b_x^2}\Big)}} \tag{5.191}$$

$$(\alpha_N k)^2 + b_x^2 = \Big(E^e_{\Downarrow} - \xi^0_N(k)\Big)^2$$

$$\boxed{k^e_{\Downarrow,\pm} = \pm\sqrt{\frac{2m*}{\hbar^2}\Big((\mu_N + E + 2E_{SO,N}) + \sqrt{4E_{SO,N}\,(\mu + E + E_{SO,N}) + E_Z^2}\Big)}} \tag{5.192}$$

$$(\alpha_N k)^2 + b_x^2 = \Big(E^h_{\Downarrow} + \xi^0_N(k)\Big)^2$$

$$\begin{cases} \boxed{k^{h,1}_{\Downarrow,\pm} = \pm\sqrt{\dfrac{2m^*}{\hbar^2}\Big((\mu_N - E + 2E_{SO,N}) + \sqrt{4E_{SO,N}\,(\mu - E + E_{SO,N}) + E_Z^2}\Big)}} \\ \boxed{k^{h,2}_{\Downarrow,\pm} = \pm\sqrt{\dfrac{2m^*}{\hbar^2}\Big((\mu_N - E + 2E_{SO,N}) - \sqrt{4E_{SO,N}\,(\mu - E + E_{SO,N}) + E_Z^2}\Big)}} \end{cases} \tag{5.193}$$

The group velocity for the propagating $k^{h,2}_{\Downarrow,\pm}$ modes is

$$v^{h,2}_{\Downarrow,\pm}(E) = \frac{\hbar}{m^*}\, k^{h,2}_{\Downarrow,\pm}(E)\, \frac{D_h}{2E_{SO,N} - D_h} \quad \text{and} \quad D_h = \sqrt{4E_{SO,N}\,(\mu - E + E_{SO,N}) + E_Z^2} \tag{5.194}$$

From Eq.(5.194) we note that the quantity $2E_{SO,N} - D_h$ is always positive in the present regime. Consequently, unlike "traditional holes", for which the wavevector (k) and the velocity group (v_g) have opposite sign, the two $k^{h,2}_{\Downarrow,\pm}(E)$ solutions yield to waves which propagates to the right for $k = k^{h,2}_{\Downarrow,+}(E) > 0$ and to the left for $k = k^{h,2}_{\Downarrow,-}(E) < 0$. The emergence of this unconventional behaviour is observed only in the SO-dominated regime ($E_Z < 2E_{SO,N}$. Indeed as already discussed previosly, the $E^h_{\Downarrow}(k)$ band exhibits a "double-well" (or inverted Mexican hat) structure and it is characterized by a local minimum at $k = 0$ and two global maxima at $k = \pm k_{max}$. Then, the wavefunction

$\Phi_N(x)$ in this regime reads

$$\boxed{\begin{aligned}\Phi_N(x) = a^e_{\Downarrow,+}\frac{e^{ik^e_{\Downarrow,+}(E)\,x}}{\sqrt{2\pi\hbar v^e_{\Downarrow,+}(E)}}\Phi^e_{\Downarrow}(k^e_{\Downarrow,+}) \;+\; a^e_{\Uparrow,+}\frac{e^{ik^e_{\Uparrow,+}(E)\,x}}{\sqrt{2\pi\hbar v^e_{\Uparrow,+}(E)}}\Phi^e_{\Uparrow}(k^e_{\Uparrow,+}) \;+\\ + a^{h,1}_{\Downarrow,-}\frac{e^{ik^{h,1}_{\Downarrow,-}(E)\,x}}{\sqrt{2\pi\hbar v^{h,1}_{\Downarrow,-}(E)}}\Phi^h_{\Downarrow}(k^{h,1}_{\Downarrow,-}) \;+\; a^{h,2}_{\Downarrow,+}\frac{e^{ik^{h,2}_{\Downarrow,+}(E)\,x}}{\sqrt{2\pi\hbar v^{h,2}_{\Downarrow,+}(E)}}\Phi^h_{\Downarrow}(k^{h,2}_{\Downarrow,+}) \;+\\ + b^e_{\Downarrow,-}\frac{e^{ik^e_{\Downarrow,-}(E)\,x}}{\sqrt{2\pi\hbar v^e_{\Downarrow,-}(E)}}\Phi^e_{\Downarrow}(k^e_{\Downarrow,-}) \;+\; b^e_{\Uparrow,-}\frac{e^{ik^e_{\Uparrow,-}(E)\,x}}{\sqrt{2\pi\hbar v^e_{\Uparrow,-}(E)}}\Phi^e_{\Uparrow}(k^e_{\Uparrow,-}) \;+\\ + b^{h,1}_{\Downarrow,+}\frac{e^{ik^{h,1}_{\Downarrow,+}(E)\,x}}{\sqrt{2\pi\hbar v^{h,1}_{\Downarrow,+}(E)}}\Phi^h_{\Downarrow}(k^{h,1}_{\Downarrow,+}) \;+\; b^{h,2}_{\Downarrow,-}\frac{e^{ik^{h,2}_{\Downarrow,-}(E)\,x}}{\sqrt{2\pi\hbar v^{h,2}_{\Downarrow,-}(E)}}\Phi^h_{\Downarrow}(k^{h,2}_{\Downarrow,-})\end{aligned}}$$

- **Range 5** : $\boxed{E > E_{SO,N} + \dfrac{E_Z^2}{4E_{SO,N}} + \mu_N}$

Finally, in this last energy range the entire set of hole solutions exhibits an imaginary part, thereby leading to possible evanescent modes.
Furthermore, the situation for electron sector remains unchanged compared to adjacent energy regimes. Each of the two electron branches ($E^e_{\Uparrow}$ and $E^e_{\Downarrow}$) is associated with two real solutions originating from the electron biquadratic equation in Eq.(5.171), supporting, therefore, propagating modes The solution of Eq.(5.171) for the three branches yields the following wavevectors

$$(\alpha_N k)^2 + b_x^2 = \Big(E^e_{\Uparrow} - \xi^0_N(k)\Big)^2$$

$$\boxed{k^e_{\Uparrow,\pm} = \pm\sqrt{\frac{2m*}{\hbar^2}\Big(\,(\mu_N + E + 2E_{SO,N}) - \sqrt{4E_{SO,N}\,(\mu + E + E_{SO,N}) + b_x^2}\Big)}} \tag{5.195}$$

$$(\alpha_N k)^2 + b_x^2 = \Big(E^e_{\Downarrow} - \xi^0_N(k)\Big)^2$$

$$\boxed{k^e_{\Downarrow,\pm} = \pm\sqrt{\frac{2m*}{\hbar^2}\Big(\,(\mu_N + E + 2E_{SO,N}) + \sqrt{4E_{SO,N}\,(\mu + E + E_{SO,N}) + E_Z^2}\Big)}} \tag{5.196}$$

$$(\alpha_N k)^2 + b_x^2 = \Big(E^h_{\Downarrow} + \xi^0_N(k)\Big)^2$$

$$\begin{cases} \boxed{k^{h,1}_{\Downarrow,\pm} = \pm\sqrt{\dfrac{2m^*}{\hbar^2}\Big(\,(\mu_N - E + 2E_{SO,N}) + i\sqrt{4E_{SO,N}\,(E - \mu_N - E_{SO,N}) - E_Z^2}\Big)}} \\ \boxed{k^{h,2}_{\Downarrow,\pm} = \pm\sqrt{\dfrac{2m^*}{\hbar^2}\Big(\,(\mu_N - E + 2E_{SO,N}) - i\sqrt{4E_{SO,N}\,(E - \mu_N - E_{SO,N}) - E_Z^2}\Big)}} \end{cases} \tag{5.197}$$

To determine which solutions causes diverging modes for $x \to -\infty$, we rewrite the Hole wavevectors as

$$k^{h,1}_{\Downarrow,\pm} = \pm\sqrt{Z} \tag{5.198}$$

$$k^{h,2}_{\Downarrow,\pm} = \pm\sqrt{Z^*} \tag{5.199}$$

where

$$\sqrt{Z} = \sqrt{\frac{|Z|+A}{2}} + i\sqrt{\frac{|Z|-A}{2}} \tag{5.200}$$

$$\text{where} \quad |Z| = \sqrt{A^2+B^2}$$

$$\sqrt{Z^*} = \sqrt{\frac{|Z|+A}{2}} - i\sqrt{\frac{|Z|-A}{2}} \tag{5.201}$$

and we have defined A and B as

$$A = \frac{2m^*}{\hbar^2}\left(\mu_N - E + 2E_{SO,N}\right) \tag{5.202}$$

$$B = \frac{2m^*}{\hbar^2}\sqrt{4E_{SO,N}\left(E-\mu-E_{SO,N}\right) - E_Z^2}\Big) \tag{5.203}$$

Consequently, we conclude that the solutions $k^{h,1}_{\Downarrow,+}, k^{h,2}_{\Downarrow,-}$ must be discarded, since diverging for $x \to -\infty$, whereas the solutions $k^{h,1}_{\Downarrow,-}, k^{h,2}_{\Downarrow,+}$ must be retained since represent exponentially decaying evanescent modes. Therefore, the wavefunction $\Phi_N(x)$ for this final regime read

$$\begin{aligned}\Phi_N(x) = {} & a^e_{\Downarrow,+}\frac{e^{ik^e_{\Downarrow,+}(E)\,x}}{\sqrt{2\pi\hbar v^e_{\Downarrow,+}(E)}}\Phi^e_{\Downarrow}(k^e_{\Downarrow,+}) \;+\; a^e_{\Uparrow,+}\frac{e^{ik^e_{\Uparrow,+}(E)\,x}}{\sqrt{2\pi\hbar v^e_{\Uparrow,+}(E)}}\Phi^e_{\Uparrow}(k^e_{\Uparrow,+}) \;+ \\ & + b^e_{\Downarrow,-}\frac{e^{ik^e_{\Downarrow,-}(E)\,x}}{\sqrt{2\pi\hbar v^e_{\Downarrow,-}(E)}}\Phi^e_{\Downarrow}(k^e_{\Downarrow,-}) \;+\; b^e_{\Uparrow,-}\frac{e^{ik^e_{\Uparrow,-}(E)\,x}}{\sqrt{2\pi\hbar v^e_{\Uparrow,-}(E)}}\Phi^e_{\Uparrow}(k^e_{\Uparrow,-}) \;+ \\ & + c^{h,1}_{\Downarrow,-}\frac{e^{ik^{h,1}_{\Downarrow,-}(E)\,x}}{\sqrt{2\pi\hbar v_N}}\Phi^h_{\Downarrow}(k^{h,1}_{\Downarrow,-}) \;+\; c^{h,2}_{\Downarrow,+}\frac{e^{ik^{h,2}_{\Downarrow,+}(E)\,x}}{\sqrt{2\pi\hbar v_N}}\Phi^h_{\Downarrow}(k^{h,2}_{\Downarrow,+})\end{aligned} \tag{5.204}$$

Fig.5.17 shows the excitations spectrum in N region and highlights the various energy ranges which have been previously discussed.

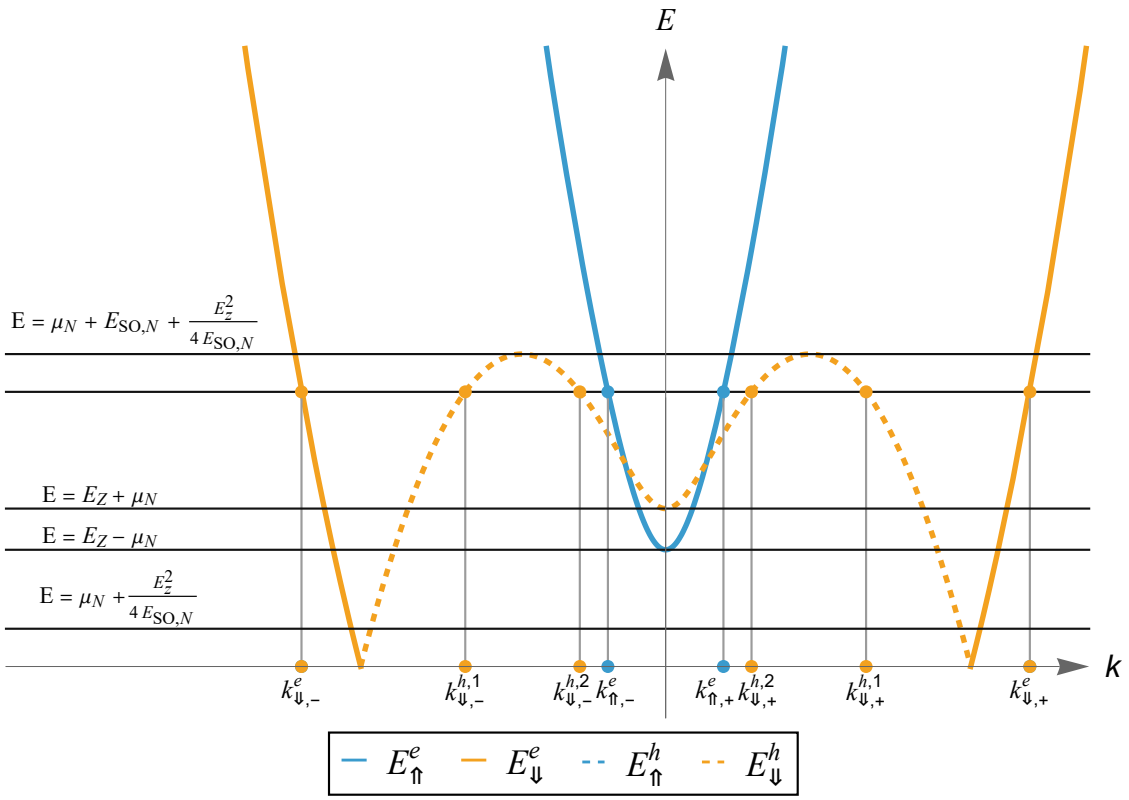

Figure 5.17: Excitations spectrum in the N region for the Rashba-dominated regime. The horizontal lines mark the various energy regimes which have been discussed analitically. Specifically, in the energy interval $E_Z + \mu_N < E < E_{SO,N} + \frac{E_Z^2}{4E_{SO,N}} + \mu_N$ the eight allowed propagating solutions are highlighted and associated with their corresponding wavevectors.

5.3.2 Solution in the S region

We discuss here the solutions in the S region in the presence of a magnetic field lying along the x-axis [see Eq.(5.160)] and of a SOC pointing along the z-direction [see Eq.(5.158)]. Let us start by writing here the BdG Hamiltonian (3.6) in k-space for such a choice of the SOC and magnetic field, namely

$$H_{BdG}(k) = \begin{pmatrix} \xi_k^0\sigma_0 - k\,\alpha_S\sigma_z - b_x\sigma_x & \Delta_0 e^{i\varphi}\sigma_0 \\ \Delta_0 e^{-i\varphi}\sigma_0 & -\xi_k^0\sigma_0 + k\,\alpha_S\sigma_z - b_x\sigma_x \end{pmatrix} \tag{5.205}$$

Although the direct diagonalization of this matrix is not algebraically trivial, its eigenvalues can be derived by squaring the Hamiltonian H_{BdG}. This approach exploits the intrinsic particle-hole symmetry satisfied by H_{BdG}, which arises from the redundancy of the Nambu spinor in the BdG formalism. Specifically, if $\Phi(k)$ is an eigenvector of H_{BdG} with eigenvalue $+E$, then its particle-hole partner $\Phi'(k) = C\Phi(k)$ (where C is the charge-conjugation operator defined in Eq.(4.68)) will be an eigenvector with eigenvalue

$-E$ [see Sec. (4.67)]. Applying the operator H_{BdG} twice to these eigenvectors, we find

$$H_{BdG}(k)\Big[H_{BdG}(k)\Phi(k)\Big] = H_{BdG}(k)\Big(+E\,\Phi(k)\Big) = E^2\Phi(k) \tag{5.206}$$

$$H_{BdG}(k)\Big[H_{BdG}(k)\Phi'(k)\Big] = H_{BdG}(k)\Big(-E\,\Phi'(k)\Big) = (-E)\Big(-E\,\Phi'(k)\Big) = E^2\Phi'(k)$$

This implies that the electron-hole pair is characterized by the same squared eigenvalue. Consequently, the squared matrix H^2_{BdG} becomes block-diagonal and exhibits two pairs of degenerate eigenvalues. Denoting these squared eigenvalues as $(\xi^2)_\pm(k)$, we have:

$$(\xi^2)_\pm(k) = \xi_k^2 + \alpha_S^2 k^2 + b_x^2 + \Delta_0^2 \pm 2\sqrt{\xi_k^2(\alpha_S^2 k^2 + b_x^2) + b_x^2\Delta_0^2} \tag{5.207}$$

Thus, the four eigenvalues of the original Hamiltonian H_{BdG} reads

$$\xi^e_\pm(k) = \sqrt{\xi_k^2 + \alpha_S^2 k^2 + b_x^2 + \Delta_0^2 \pm 2\sqrt{\xi_k^2(\alpha_S^2 k^2 + b_x^2) + b_x^2\Delta_0^2)}} \tag{5.208}$$

$$\xi^h_\pm(k) = -\sqrt{\xi_k^2 + \alpha_S^2 k^2 + b_x^2 - \Delta_0^2 \pm 2\sqrt{\xi_k^2(\alpha_S^2 k^2 + b_x^2) + b_x^2\Delta_0^2)}}$$

It is worth noting that, while the eigenvalues admit a compact analytical form, the analytical derivation of the eigenvectors is algebraically cumbersome. Nevertheless, it can be achieved by writing a code in Wolfram Mathematica.
Exploiting the general structure of the eigenfunctions in real space defined in Eq.(5.8), a generic eigenvector of H_{BdG} can be decomposed as

$$\Phi(k) = \begin{pmatrix} \mathbf{u}(k) \\ \mathbf{v}(k) \end{pmatrix} = \begin{pmatrix} u_\uparrow(k) \\ u_\downarrow(k) \\ v_\downarrow(k) \\ v_\uparrow(k) \end{pmatrix} \tag{5.209}$$

Therefore, the generic eigenvectors for H_{BdG} Hamiltonian read

$$\Phi^e_1(k) = \begin{pmatrix} u_{1,\uparrow}(k) \\ u_{1,\downarrow}(k) \\ v_{1,\uparrow}(k) \\ v_{1,\downarrow}(k) \end{pmatrix} \qquad \Phi^h_1(k) = C\,\Phi^e_1(k) = \begin{pmatrix} -v^*_{1,\uparrow(k)} \\ v^*_{1,\downarrow(k)} \\ u^*_{1,\downarrow(k)} \\ -u^*_{1,\uparrow(k)} \end{pmatrix}$$

$$\Phi^e_2(k) = \begin{pmatrix} u_{2,\uparrow}(k) \\ u_{2,\downarrow}(k) \\ v_{2,\uparrow}(k) \\ v_{2,\downarrow}(k) \end{pmatrix} \qquad \Phi^h_2(k) = C\,\Phi^e_2(k) = \begin{pmatrix} -v^*_{2,\uparrow(k)} \\ v^*_{2,\downarrow(k)} \\ u^*_{2,\downarrow(k)} \\ -u^*_{2\uparrow(k)} \end{pmatrix} \tag{5.210}$$

where the u-components and the v-component characterize, respectively, the electron part and the hole part of the eigenvector.
The physical interpretation of the spinor components is given by their squared moduli,

representing the probability weight of the quasiparticle. To characterize whether an excitation is electron-like or hole-like, we define the charge character $\mathcal{Q}(k)$ as

$$\mathcal{Q}(k) = \Big(|u_\uparrow(k)|^2 + |u_\downarrow(k)|^2\Big) - \Big(|v_\uparrow(k)|^2 + |v_\downarrow(k)|^2\Big) \tag{5.211}$$

Using this quantity, we can classify the nature of the states

$$\begin{aligned} \mathcal{Q}(k) > 0 \quad &\Longrightarrow \quad \text{Electron-like state} \\ \mathcal{Q}(k) < 0 \quad &\Longrightarrow \quad \text{Hole-like state} \end{aligned} \tag{5.212}$$

Thus, the excitation spectrum can be labelled according to the dominant character of the bands

$$\begin{cases} E_1^e(k) &= \vartheta\big(\mathcal{Q}_1(k)\big)\xi_+^e(k) \\ E_1^h(k) &= \vartheta\big(-\mathcal{Q}_1(k)\big)\xi_+^e(k) \\ E_2^e(k) &= \vartheta\big(\mathcal{Q}_2(k)\big)\xi_-^e(k) \\ E_2^h(k) &= \vartheta\big(-\mathcal{Q}_2(k)\big)\xi_-^e(k) \end{cases} \tag{5.213}$$

where ϑ denotes the Heaviside function.

Eigenfunctions at fixed energy E

To construct the spatial wavefunction at a fixed energy E, it is necessary to determine the expression of wavevectors characterizing the different modes. This requires inverting the dispersion relations derived above, which amounts to solving the following equations for k

$$E_1(k) = E \quad \Rightarrow \quad \sqrt{\xi_k^2 + \alpha_S^2 k^2 + b_x^2 + \Delta_0^2 + 2\sqrt{\xi_k^2(\alpha_S^2 k^2 + b_x^2) + b_x^2\Delta_0^2)}} = E \tag{5.214}$$

$$E_2(k) = E \quad \Rightarrow \quad \sqrt{\xi_k^2 + \alpha_S^2 k^2 + b_x^2 + \Delta_0^2 - 2\sqrt{\xi_k^2(\alpha_S^2 k^2 + b_x^2) + b_x^2\Delta_0^2)}} = E \tag{5.215}$$

Once the solutions are found, the electron-like or hole-like nature of the wavevectors must be assigned according to the sign of the charge character $\mathcal{Q}(k)$.
Unfortunately, the algebraic inversion of these relations is non-trivial, as it corresponds to finding the roots of an eighth-degree polynomial in k (or, equivalently, a quartic equation in k^2). The algebraic complexity of the spectrum in this region prevents us from pursuing the fully analytical approach employed in Sections 5.2 and 5.3. Consequently, we must proceed by using a numerical approach implemented via Wolfram Mathematica.
Despite the lack of closed-form analytical solutions for the wavevectors, a graphical analysis of the dispersion relation allows us to extract crucial information regarding the allowed propagating and evanescent modes.
Specifically, we will assume $\mu_S = 0$, and, consistently with our analysis of the Normal region, we restrict our study to the Rashba-dominated regime, i.e. $E_Z < 2E_{SO,S}$

($E_Z = |b_x|$), within the trivial superconducting phase. Accordingly, the constraints imposed on the parameters are

$$\mu_S = 0 \ , \qquad E_Z < 2E_{SO,S} \ , \qquad E_Z < \Delta_0 \tag{5.216}$$

Based on a graphical analysis, this parameter configuration reveals the following extrema for the E_2 band:

(i) A global minimum at $k = 0$ with energy $E_2(0) = E_Z - \Delta_0$. This minimum corresponds to the excitation gap in the presence of a magnetic field, i.e., the lowest possible energy for an excitation.

(ii) Two local minima located at $k = \pm k_{Min}$ and energy E_{Min}. Unfortunately, an exact analytical expression for these points cannot be derived, as it would require solving a higher-order polynomial equation in k. These points are highlighted in Fig.5.18. It is important to emphasize that these minima do not coincide with the "transition point" between electron-like and hole-like states within band 2. Indeed, the mathematical conditions defining the band minimum ($dE_2/dk = 0$) and the charge character transition [Eq.(5.211)] are analytically distinct. However, these two points are typically numerically proximal, rendering them virtually indistinguishable in a standard graphical representation.

(iii) Two local maxima located at $\pm k_{Max}$ and energy E_{Max} (see Fig.5.18), for which no closed-form expression exists. For a fixed Zeeman energy E_Z the value of this maximum strongly depends on the SO energy $E_{SO,N}$.

The E_1 band is characterized by a global minimum at $k = 0$ with energy $E_1(0) = E_Z + \Delta_0$. The condition $Q_1(k) < 0$, which identifies the hole-like states for the E_1 band, is generally satisfied only within an extremely narrow range around the minimum, consequently, this feature is not visually resolvable in the given plot representation.
As a result the four quantities $E_1(0), E_{Min}, E_{Max}, E_2(0)$ represent the energy extrema characterizing the number of propagating modes of the scattering process in the superconducting region.

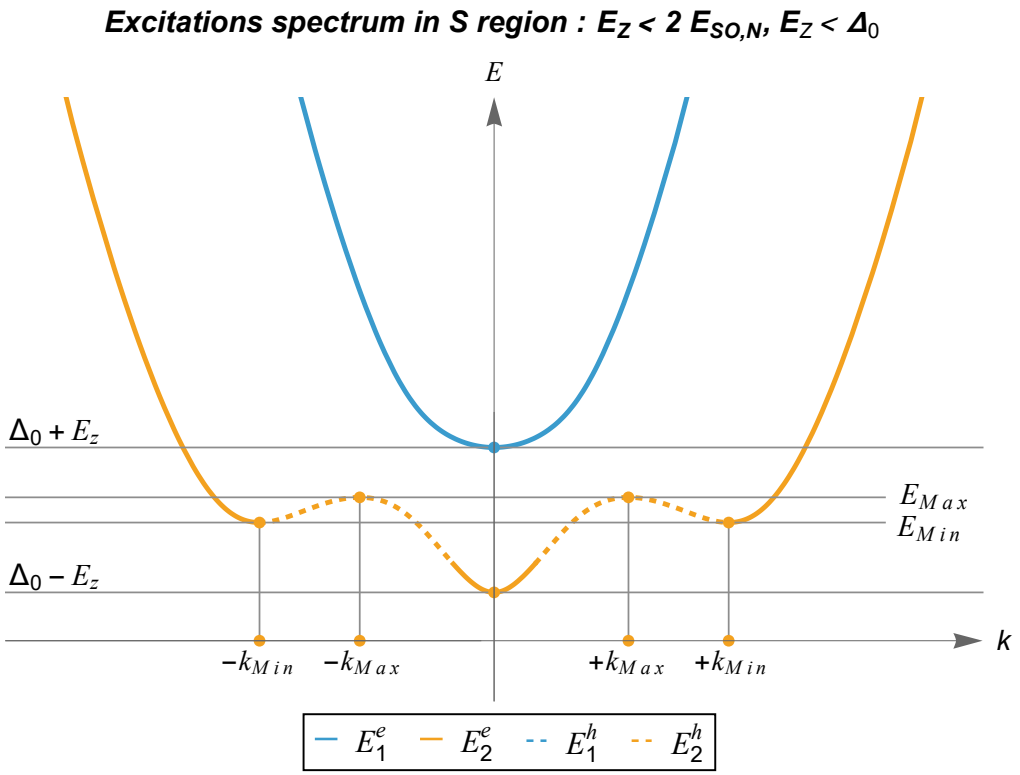

Figure 5.18: The excitations spectrum in S region exhibits two *well* separated energy band E_1, E_2. In particular E_2 represents the lower bands and is characterized by a global minimum at $k = 0$ and energy $E_2(0) = E_Z - \Delta_0$, which represents the bulk gap of the spectrum. Furthermore, this energy band shows two local minima at $\pm k_{Min}$ and energy E_{Min} and two local maxima at $\pm k_{Max}$ and energy E_{Max}. In contrast, the upper band E_1 exhibits a global minimum at $k = 0$ and energy $E_1(0) = E_Z + \Delta_0$. Each gray line is associated to one of the extrema of the spectrum. We remark that, depending on the specific parameters of the system, the local maxima of the E_2 band may be larger than the minimum of the E_1 band.

Although it is not possible to gain an analytical derivation of the eigenfunctions, as for the N region, we remark that the general expressions of the wavevefunctions $\Phi(x)$ represents a superposition of propagating and evanescent modes, namely

$$\Phi_S(x) = \frac{1}{\sqrt{2\pi\hbar}} \left(\sum_{a_i} \frac{a_i}{\sqrt{v_{a_i}}} \Phi(k_{a_i}) e^{-ik_{a_i}x} + \sum_{b_j} \frac{b_j}{\sqrt{v_{b_j}}} \Phi(k_{b_j}) e^{-ik_{b_j}} + \sum_{c_l} \frac{c_l}{\sqrt{v_{c_l}}} \Phi(k_{c_l}) e^{-ik_{c_l}x} \right) \tag{5.217}$$

where the label "a_i" denotes incident propagating modes (left-moving), the label "b_j" denotes outgoing propagating modes (right-moving) and the label "c_l" denotes evanescent modes. In particular, the wavevectors associated to the latter modes shall be characterized by a positive imaginary part, in order to avoid divergence for $x \to +\infty$. Furthermore, we have introduced a formal definition of velocity v_c related to the evanescent modes to

correctly normalize them , whereas the velocity group for the propagating modes is

$$v_g(E) = \frac{1}{\hbar}\frac{\partial E}{\partial k}\bigg|_{k=k(E)} \tag{5.218}$$

5.3.3 Andreev Reflection in the case of a magnetic field perpendicular to the SO vector

In this section we shall investigate the Andreev Reflection phenomenon for two specific sets of parameters in the Rashba-dominated regime ($E_Z < 2E_{SO} < \Delta_0$). Specifically, we shall analyze the cases of moderate ($E_Z = E_{SO}$) and strong ($E_Z > E_{SO}$) Zeeman field, adopting the two following sets of parameters:

moderate Zeeman field :
$$E_Z = 0.4\Delta_0\,, \quad E_{SO,N} = E_{SO,S} = 0.4\Delta_0\,, \quad \mu_S = \mu_N = 0 \tag{5.219}$$

(5.220)

strong Zeeman field :
$$E_Z = 0.8\Delta_0\,, \quad E_{SO,N} = E_{SO,S} = 0.5\Delta_0\,, \quad \mu_S = \mu_N = 0 \tag{5.221}$$

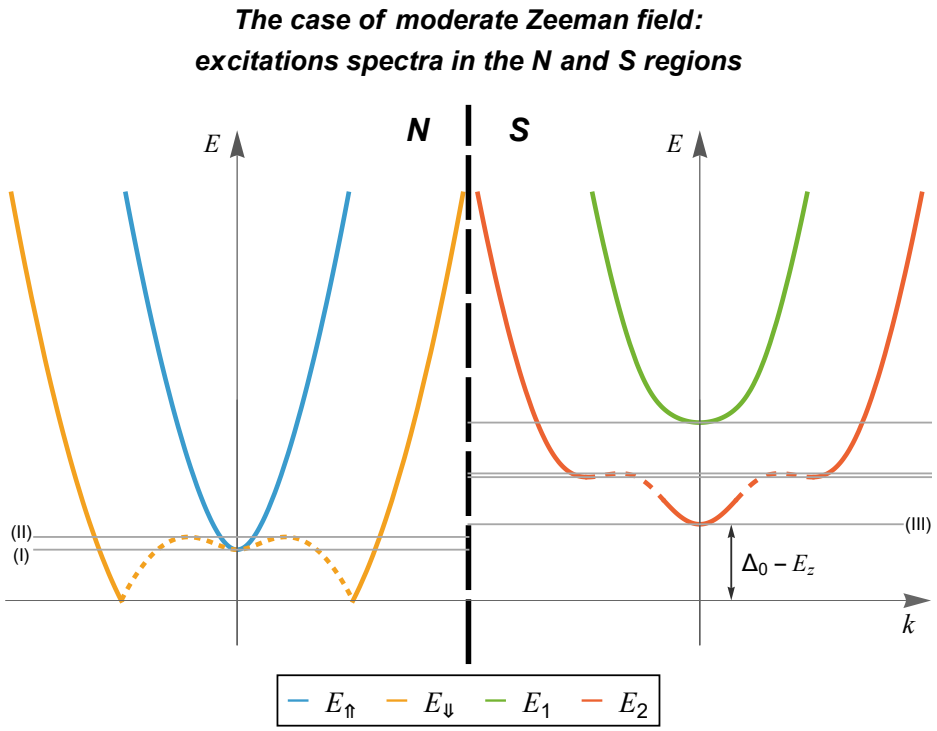

Figure 5.19: Comparison of the excitations spectra of the N and S regions in the case of moderate Zeeman field. Line (I) and marks, the energy values $E_I = 0.4\Delta_0$ while line (II) marks the energy value $E_{II} = 0.5\Delta_0$, above which the AR phenomenon is no longer allowed. Line (III) marks the energy value of the bulk gap $E_{III} = E_2(0) = 0.6\Delta_0$. For this specific choice of the parameters AR occurs entirely in bulk sub-gap regime.

The case of moderate Zeeman field

The excitations spectra in the N and S regions for this set of parameters are shown in Fig.5.19. As illustrated in the analytical derivation of the solutions in the region N, the threshold energy value after which the hole modes turn evanescent, and thus Andreev Reflection no longer occurs, is

$$E_{II} = E_{SO,N} + \mu_N + \frac{E_Z^2}{4E_{SO,N}} \tag{5.222}$$

which for this choice of the parameters yields $E_{II} = 0.5\Delta_0$. This energy value is highlighted in Fig.5.19 by "line (II)", while "line (I)" marks the energy values $E_I = 0.4\Delta_0$ at which further propagating modes are available for transport. In Fig.5.20, we present the electron and hole AR probabilities for three different values of the misalignment angle, namely $\Phi_{SO} = \{0, \frac{\pi}{2}, \pi\}$.
Although the AR probabilities undergo only some slight modifications when the Φ_{SO} varies, this dependence can be fully appreciated graphically . Furthermore, from 5.20 we observe that, at fixed Φ_{SO}, the electron ($R^N_{e\to h}$) and the hole ($R^N_{h\to e}$) AR probabilities coincide exactly. In fact, although the application of a magnetic field breaks Time Reversal symmetry, for this specific choice of the parameters AR occurs completely at lower energy with respect to the bulk sub-gap ($E_{II} < E_{III}$ in Fig.5.19). Consequently, since there are no propagating modes in the S region, AR represents a purely internal process of the N region and the $e \to h$ process is perfectly symmetrical with respect to the $h \to e$ one.

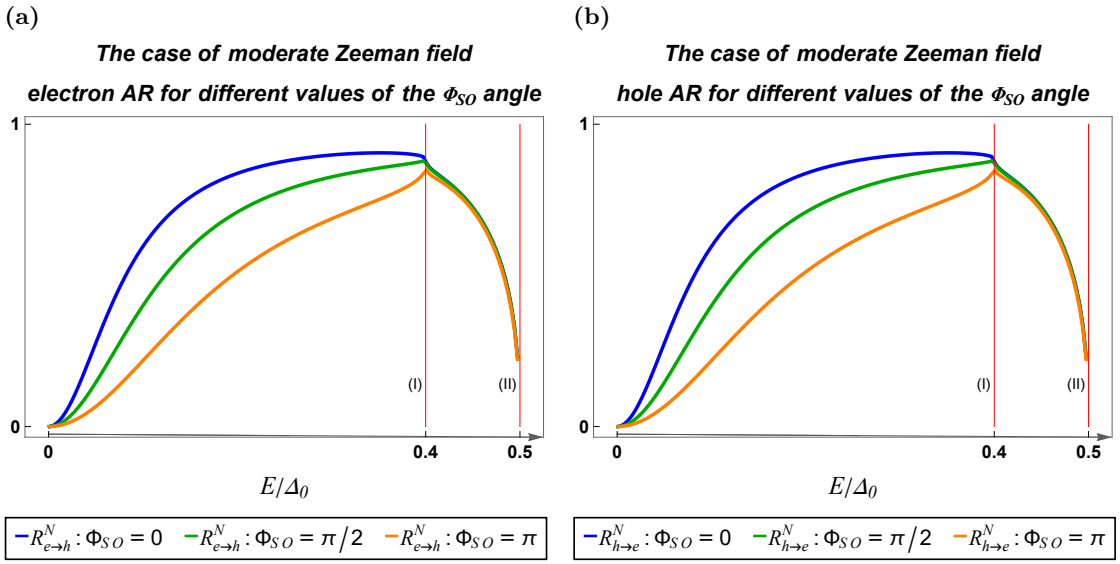

Figure 5.20: Electron (left panel) and hole (right panel) Andreev Reflection probabilities for three different SO angle values, namely $\Phi_{SO} = \{0, \frac{\pi}{2}, \pi\}$. Line (I) and (II) marks the energies $E_I = 0.4\Delta_0$ and $E_{II} = 0.5\Delta_0$. The AR phenomenon is limited to energy value below E_{II}, since at higher energies hole modes become evanescent. In the energy interval $0.4\Delta_0 < E < 0.5\Delta_0$ the three curves collapse into a single one. We observe that the $e \to h$ and $h \to e$ processes are perfectly coincident.

The case of strong Zeeman field ($E_{SO} < E_Z < 2E_{SO}$)

We have plotted the excitations spectra in the N and S region for this set of parameters in Fig.5.21. The three energy values of interest for the Andreev Reflection are

$$E_I = 0.2\Delta_0 \qquad E_{II} = 0.8\Delta_0 \qquad E_{III} = 0.82\Delta_0 \tag{5.223}$$

and are marked by lines (I),(II),(III) in Fig.5.21 and Fig.5.22. In particular, $E_I = E_1(0)$ here represents the bulk gap energy in the S side of the junction, while E_{III} represents the energy threshold above which hole modes become evanescent in the N region and AR no longer occurs. We observe in Fig.5.22 that both electron and hole ARs show a strong dependence on the misalignment Φ_{SO} angle. In particular, for $\Phi_{SO} = \pi$, AR is almost completely suppressed, while for $\Phi_{SO} = 0$, reaches almost the maximum value of 1, near E_I. Furthermore, for energy values higher than E_I (i.e. beyond the bulk sub-gap energy), we observe that the hole and electron AR differ for the angle $\Phi_{SO} = \frac{\pi}{2}$.

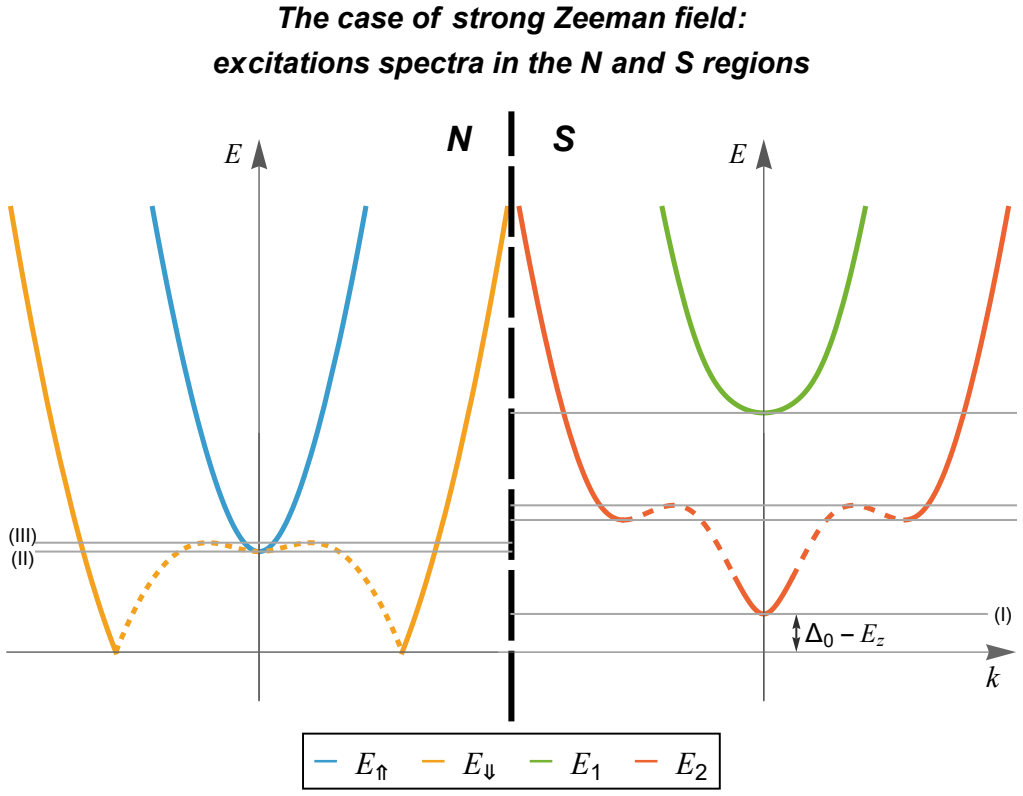

Figure 5.21: Excitations spectra of the N and S regions in the case of a strong Zeeman field. Line (I) marks the energy of the bulk gap in the S region ($E_I = 0.2\Delta_0$), while line (III) marks the threshold energy for the Andreev Reflection phenomenon ($E_{III} = 0.82\Delta_0$). For this choice of the parameters AR also occurs for energy values beyond the bulk gap.

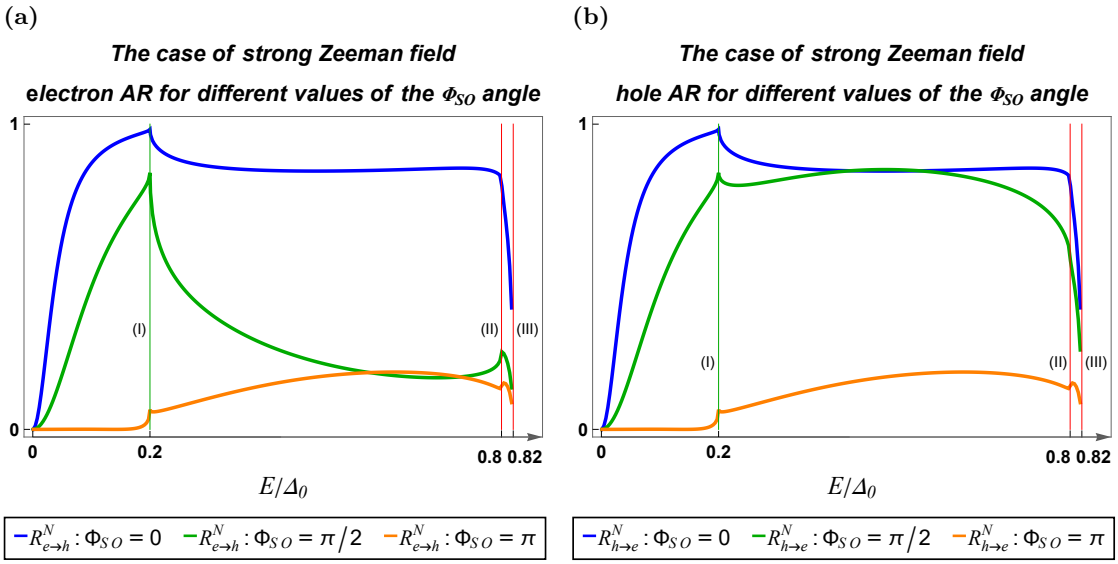

Figure 5.22: Electron (left panel) and hole (right panel) Andreev Reflection probabilities for three different SO angle values, namely $\Phi_{SO} = \{0, \frac{\pi}{2}, \pi\}$. Line (I),(II) and (III) mark, respectively the energies $E_I = 0.2\Delta_0$, $E_{II} = 0.8\Delta_0$, and $E_{III} = 0.82\Delta_0$. We observe in this case a strong dependence on the Φ_{SO} angle. Furthermore, while in the bulk sub-gap the electron and hole AR are coincident, for energy beyond E_I, we observe a difference between them Φ_{SO}.

In conclusion we demonstrated that applying a perpendicular magnetic field gives rise to a dependence of the Andreev Reflection process on the spin orbit misalignment angle Φ_{SO}. This result can be understood by considering that the field and the SOC fix two different axes in spin space, and their competition results in a non-trivial spin-texture along the wire.
Indeed, differently from the case without magnetic field, here rotating the SOC vector (i.e. changing Φ_{SO}) cannot be reabsorbed by a simple basis transformation and the matching conditions at the interface become genuinely angle-dependent. This explains why, in the presence of a perpendicular magnetic field, the Andreev Reflection phenomenon develops a clear dependence on Φ_{SO}.

Chapter 6

Conclusions

In this MS Thesis I have investigated the Andreev Reflection process in nanowires characterized by strong spin-orbit coupling and proximized by a superconductor. Andreev Reflection represents the fundamental effect characterizing all quantum devices based on nanowires and superconductors, which are currently on the spotlight of scientific research in condensed matter, in view of their promising applications as Andreev spin qubits and in the study of topological superconductivity and Majorana quasi-particles.

Specifically, I have investigated how the inhomogeneities of the Rashba spin-orbit coupling emerging across the interface between a Normal (N) and a Superconducting (S) nanowire portion affect the Andreev reflection. While most theoretical models have overlooked these effects, such inhomogeneities are actually present in any typical setup, due to the change in structural inversion asymmetry across the interface and to the presence of gate voltages applied to the nanowire. The research work of this MS Thesis bridges this gap of knowledge, providing a thorough analysis of the Andreev Reflection process in the presence of inhomogeneities in both the direction and the magnitude of the spin-orbit coupling, and taking also into account the presence of an applied magnetic field.

The first part of the Thesis includes some introductory material, where -to the benefit of the reader- I have reviewed some fundamental concepts regarding superconductivity, the Andreev Reflection phenomenon, and I have summarized the most relevant applications of nanowires with spin-orbit. Then, after providing a brief primer on the standard Bardeen-Cooper-Schrieffer (BCS) model describing bulk low-temperature superconductors, I have generalized the BCS model to include the effects of the spin-orbit coupling and the presence of a magnetic field. This enables one to describe a homogeneous single channel semiconductor NW proximized by a superconducting pairing.

The second part of the Thesis is concerned with genuine research work. Specifically, in Chapter 4, by adopting the Bogoliubov-de Gennes method, I have further extended the model to include inhomogeneities in both the superconducting pairing and in the spin-orbit coupling. Then, in Chapter 5 I have applied such model to the specific case of a Normal-Superconducting (N/S) nanowire junction in order to investigate how spin-orbit

inhomogeneities affect the phenomenon of Andreev Reflection. This chapter contains most of the novel and original results of the MS Thesis, which were obtained by combining analytical calculations and numerical analysis carried out by writing a Wolfram Mathematica code. Specifically, I have considered two types of inhomogeneities. The first one is an inhomogeneity in the direction of the spin-orbit coupling field, i.e. where a misalignment angle Φ_{SO} exists between the N side and the S side of the junction. The second type of inhomogeneity is in the magnitude of the Rashba spin-orbit coupling characterizing the N and the S side of the junction.
I started by analyzing their effects in the absence of an external magnetic field, considering two different regimes, where the spin-orbit energy is much larger or smaller than the superconducting gap. In both cases I found that, while the misalignment angle Φ_{SO} has no effect on the Andreev Reflection phenomenon, the difference in the spin-orbit magnitude can significantly affect it.
Then, I turned to discuss how these effects are modified by the presence of a magnetic field. In particular, I focused on the most interesting case where the magnetic field is perpendicular to the spin orbit vector, where an actual spin texture in the electronic states emerges, and unconventional superconducting pairing is generated by its interplay with superconductivity. Interestingly, in this case Andreev reflection exhibits a dependence on the spin-orbit misalignment angle Φ_{SO}. Specifically, the investigation of two different sets of system parameters reveals that such dependence can be more or less pronounced depending on the relative ratio between spin-orbit energy and Zeeman energy. By electrically tuning the direction of the spin-orbit coupling, one can either enhance or strongly suppress the Andreev reflection phenomenon, which is the building block of any hybrid quantum system involving NWs and superconductors.

In conclusion, this MS Thesis work provides a general theoretical framework to model quantum transport in hybrid systems involving spin-orbit NWs and superconductors. The results obtained for the case of a N/S junction demonstrate the feasibility of modulating the phenomenon of Andreev Reflection by tuning either the magnitude or the direction of the spin-orbit coupling, in the presence of a suitably applied magnetic field. The work also provides interesting perspectives for future research. In particular, the established framework and the obtained results are quite promising to address the case of a S-N-S junctions, in view of potential applications for Andreev spin qubits and topological superconductors.

Appendix A

Details about the BdG Hamiltonian of the inhomogeneous nanowire

In this Appendix we provide the proof that Eq.(4.7) can be written in the BdG form (4.14), with the Bogolubov de Gennes Hamiltonian given by Eq.(4.22). We start by rewriting each of the five terms of the Hamiltonian Eq.(4.7), namely Eqs.(4.2) to (4.6), in another equivalent form. To this purpose, we shall make use of the following anticommutation relations of the electron field operators

$$\Big\{\Psi_\sigma(x),\Psi^\dagger_{\sigma'}(x')\Big\}=\Psi_\sigma(x)\Psi^\dagger_{\sigma'}(x')+\Psi^\dagger_{\sigma'}(x')\Psi_\sigma(x)=\delta(x-x')\delta_{\sigma\sigma'} \tag{A.1}$$

$$\frac{\partial}{\partial x}\Big\{\Psi_\sigma(x),\Psi^\dagger_{\sigma'}(x')\Big\}=\frac{\partial\Psi_\sigma(x)}{\partial x}\Psi^\dagger_{\sigma'}(x')+\Psi^\dagger_{\sigma'}(x')\frac{\partial\Psi_\sigma(x)}{\partial x}=\frac{\partial}{\partial x}\delta(x-x')\delta_{\sigma\sigma'} \tag{A.2}$$

$$\frac{\partial^2}{\partial x^2}\Big\{\Psi_\sigma(x),\Psi^\dagger_{\sigma'}(x')\Big\}=\frac{\partial^2\Psi_\sigma(x)}{\partial x^2}\Psi^\dagger_{\sigma'}(x')+\Psi^\dagger_{\sigma'}(x')\frac{\partial^2\Psi_\sigma(x)}{\partial x^2}=\frac{\partial^2}{\partial x^2}\delta(x-x')\delta_{\sigma\sigma'} \tag{A.3}$$

$$\Big\{\Psi^\dagger_\sigma(x),\Psi^\dagger_{\sigma'}(x')\Big\}=\Psi^\dagger_\sigma(x)\Psi^\dagger_{\sigma'}(x')+\Psi^\dagger_{\sigma'}(x')\Psi^\dagger_\sigma(x)=0 \tag{A.4}$$

$$\int dx f(x)g(x)=\int dx f(x)\int dx' g(x')\delta(x-x') \tag{A.5}$$

where $\sigma,\sigma'=\uparrow\downarrow$.

Let us then rewrite each of the five terms in Eq.(4.7) one by one.

Kinetic term

Let us start by the kinetic term (4.2)

$$\begin{aligned}
\mathcal{H}_{kin} &= \int dx \left(\Psi_\uparrow^\dagger(x), \Psi_\downarrow^\dagger(x)\right) \frac{\hat{P}^2}{2m^*}\sigma_0 \begin{pmatrix}\Psi_\uparrow(x)\\ \Psi_\downarrow(x)\end{pmatrix} = \\
&= \sum_{\sigma=\uparrow,\downarrow} \int dx\, \Psi_\sigma^\dagger(x) \frac{\hat{P}^2}{2m^*} \Psi_\sigma(x) = \\
&\quad \text{[substitute } \hat{P} \to -i\hbar\tfrac{\partial}{\partial x} \text{ and use Eq.(A.5)]} \\
&= -\frac{\hbar^2}{2m^*} \sum_{\sigma=\uparrow,\downarrow} \iint dx\, dx'\, \Psi_\sigma^\dagger(x') \frac{\partial^2 \Psi_\sigma(x)}{\partial x^2}\, \delta(x-x') = \\
&\quad \text{[we now use Eq.(A.3)]} \\
&= -\frac{\hbar^2}{2m^*} \sum_{\sigma=\uparrow,\downarrow} \iint dx\, dx' \left[\frac{\partial^2}{\partial x^2}\delta(x-x') - \frac{\partial^2 \Psi_\sigma(x)}{\partial x^2}\Psi_\sigma^\dagger(x')\right] \delta(x-x') = \\
&= \sum_{\sigma=\uparrow,\downarrow} \left(C_p + \frac{\hbar^2}{2m^*} \iint dx\, dx' \frac{\partial^2 \Psi_\sigma}{\partial x^2} \Psi_\sigma^\dagger(x')\, \delta(x-x') \right)
\end{aligned} \tag{A.6}$$

where we have introduced the constant

$$C_p = -\frac{\hbar^2}{2m^*} \iint dx\, dx' \delta(x-x') \frac{\partial^2}{\partial x^2} \delta(x-x') \tag{A.7}$$

The second term in Eq.(A.6) can be rewritten by repeatedly integrating by parts

$$\begin{aligned}
&\frac{\hbar^2}{2m^*} \iint dx\, dx' \frac{\partial^2 \Psi_\sigma}{\partial x^2} \Psi_\sigma^\dagger(x')\, \delta(x-x') = \\
&= \frac{\hbar^2}{2m^*} \int dx \frac{\partial^2 \Psi_\sigma}{\partial x^2} \Psi_\sigma^\dagger(x) = \\
&= \underbrace{\frac{\hbar^2}{2m^*} \frac{\partial \Psi_\sigma(x)}{\partial x} \Psi_\sigma^\dagger(x)\Big|_{-\infty}^{+\infty}}_{=0} - \frac{\hbar^2}{2m^*} \int dx \frac{\partial \Psi_\sigma(x)}{\partial x} \frac{\partial \Psi_\sigma^\dagger(x)}{\partial x} = \\
&= \underbrace{-\frac{\hbar^2}{2m^*} \Psi_\sigma(x) \frac{\partial \Psi_\sigma^\dagger(x)}{\partial x}\Big|_{-\infty}^{+\infty}}_{=0} + \frac{\hbar^2}{2m^*} \int dx\, \Psi_\sigma(x) \frac{\partial^2 \Psi_\sigma^\dagger(x)}{\partial x^2} = \\
&= -\frac{\hbar^2}{2m^*} \int dx\, \Psi_\sigma(x) \frac{\hat{P}^2}{2m^*} \Psi_\sigma^\dagger(x)
\end{aligned} \tag{A.8}$$

where we exploited the fact that the field (and its derivative) vanishes at large distance, $\Psi_\sigma(x \to \pm\infty) = 0$.

The kinetic term in Eq.(A.6) acquires the form

$$\begin{aligned}\mathcal{H}_{kin} &= 2C_p - \sum_{\sigma=\uparrow,\downarrow}\int dx\,\Psi_\sigma(x)\frac{\hat{P}^2}{2m^*}\Psi^\dagger_\sigma(x) = \\ &= 2C_p - \int dx\left(\Psi_\uparrow(x),\Psi_\downarrow(x)\right)\frac{\hat{P}^2}{2m^*}\sigma_0\begin{pmatrix}\Psi^\dagger_\uparrow(x)\\ \Psi^\dagger_\downarrow(x)\end{pmatrix} = \\ &\text{[now write } \sigma_0 = (-i\sigma_y)(i\sigma_y)\text{]} \\ &= 2C_p - \int dx\left(\Psi_\uparrow(x),\Psi_\downarrow(x)\right)\frac{\hat{P}^2}{2m^*}(-i\sigma_y)(i\sigma_y)\begin{pmatrix}\Psi^\dagger_\uparrow(x)\\ \Psi^\dagger_\downarrow(x)\end{pmatrix} = \\ &= 2C_p - \int dx\left(\Psi_\downarrow(x),-\Psi_\uparrow(x)\right)\frac{\hat{P}^2}{2m^*}\sigma_0\begin{pmatrix}\Psi^\dagger_\downarrow(x)\\ -\Psi^\dagger_\uparrow(x)\end{pmatrix} \qquad \text{(A.9)}\end{aligned}$$

In conclusion, we have rewritten the kinetic term in Eq.(4.2) as

$$\mathcal{H}_{kin} = 2C_p - \int dx\left(\Psi_\downarrow(x),-\Psi_\uparrow(x)\right)\frac{\hat{P}^2}{2m^*}\sigma_0\begin{pmatrix}\Psi^\dagger_\downarrow(x)\\ -\Psi^\dagger_\uparrow(x)\end{pmatrix} \qquad \text{(A.10)}$$

Chemical potential term

$$\begin{aligned}\mathcal{H}_\mu &= -\int dx\left(\Psi^\dagger_\uparrow(x),\Psi^\dagger_\downarrow(x)\right)\mu(x)\sigma_0\begin{pmatrix}\Psi_\uparrow(x)\\ \Psi_\downarrow(x)\end{pmatrix} = \\ &= -\sum_{\sigma=\uparrow,\downarrow}\int dx\,\Psi^\dagger_\sigma(x)\,\mu(x)\,\Psi_\sigma(x) = \\ &= -\sum_{\sigma=\uparrow,\downarrow}\iint dx\,dx'\Psi^\dagger_\sigma(x')\,\mu(x)\,\Psi_\sigma(x)\,\delta(x-x') = \\ &\text{using Eq.(A.1), we have} \\ &= -\sum_{\sigma=\uparrow,\downarrow}\iint dx\,dx'\,\mu(x)\,\delta(x-x')\,\delta(x-x') + \sum_{\sigma=\uparrow,\downarrow}\iint dx\,dx'\Psi_\sigma(x)\,\mu(x)\,\Psi^\dagger_\sigma(x')\,\delta(x-x') = \\ &= -\sum_{\sigma=\uparrow,\downarrow}\iint dx\,dx'\,\mu(x)\,\delta(x-x')\,\delta(x-x') \;+\; \sum_{\sigma=\uparrow,\downarrow}\iint dx\,\Psi_\sigma(x)\,\mu(x)\,\Psi^\dagger_\sigma(x) \qquad \text{(A.11)}\end{aligned}$$

By defining

$$C_\mu = \iint dx\,dx'\,\mu(x)\,\delta(x-x')\,\delta(x-x') \qquad \text{(A.12)}$$

the chemical potential term acquires the form

$$\mathcal{H}_\mu = -2C_\mu + \sum_{\sigma=\uparrow,\downarrow} \int dx\, \Psi_\sigma(x)\, \mu(x)\, \Psi^\dagger_\sigma(x) \; =$$

$$= -2C_\mu + \int dx \left(\Psi_\uparrow(x), \Psi_\downarrow(x)\right) \mu(x)\sigma_0 \begin{pmatrix} \Psi^\dagger_\uparrow(x) \\ \Psi^\dagger_\downarrow(x) \end{pmatrix} =$$

$$[\text{now write } \sigma_0 = (-i\sigma_y)(i\sigma_y)]$$

$$= -2C_\mu + \int dx \mu(x) \left(\Psi_\uparrow(x), \Psi_\downarrow(x)\right) (-i\sigma_y)(i\sigma_y) \begin{pmatrix} \Psi^\dagger_\uparrow(x) \\ \Psi^\dagger_\downarrow(x) \end{pmatrix} =$$

$$= -2C_\mu + \int dx \mu(x) \left(\Psi_\downarrow(x), -\Psi_\uparrow(x)\right) \sigma_0 \begin{pmatrix} \Psi^\dagger_\downarrow(x) \\ -\Psi^\dagger_\uparrow(x) \end{pmatrix} \tag{A.13}$$

In conclusion, we have rewritten the chemical potential term (4.3) in the form

$$\mathcal{H}_\mu = -2C_\mu + \int dx \mu(x) \left(\Psi_\downarrow(x), -\Psi_\uparrow(x)\right) \sigma_0 \begin{pmatrix} \Psi^\dagger_\downarrow(x) \\ -\Psi^\dagger_\uparrow(x) \end{pmatrix} \tag{A.14}$$

Spin-orbit term

Let us now consider the spin-orbit term (4.4), which consists of three component terms

$$\mathcal{H}_{SO} = -\frac{1}{2\hbar} \int dx \left(\Psi^\dagger_\uparrow(x), \Psi^\dagger_\downarrow(x)\right) \left\{\boldsymbol{\alpha}(x), \hat{P}\right\} \cdot \boldsymbol{\sigma} \begin{pmatrix} \Psi_\uparrow(x) \\ \Psi_\downarrow(x) \end{pmatrix} =$$

$$= \sum_{m=x,y,z} \mathcal{H}_{SO,m} \tag{A.15}$$

where

$$\mathcal{H}_{SO,m} = -\sum_{\sigma,\sigma'=\uparrow,\downarrow} \frac{1}{2\hbar} \int dx\, \Psi^\dagger_\sigma(x) \left\{\alpha_m(x), \hat{P}\right\} (\sigma_m)_{\sigma\sigma'}\, \Psi_{\sigma'}(x) \tag{A.16}$$

and $\hat{P} \to -i\hbar\frac{\partial}{\partial x}$ in Eq.(4.4).
Since such term consists of three components, we analyze separately the cases of the α_z component and the cases of the $\alpha_{x,y}$ components.

- **the z-component**
  For the z-component, one has

$$(\sigma_z)_{\sigma\sigma'} = \sigma\, \delta_{\sigma\sigma'} \tag{A.17}$$

and

$$\begin{aligned}\mathcal{H}_{SO,z} &= -\sum_{\sigma=\uparrow,\downarrow}\frac{\sigma}{2\hbar}\int dx\Psi^\dagger_\sigma(x)\left\{\alpha_z(x),\hat{P}\right\}\Psi_\sigma(x) = \\ &= \sum_{\sigma=\uparrow,\downarrow}\frac{i\sigma}{2}\int dx\ \Psi^\dagger_\sigma(x)\left\{\alpha_z(x),\partial_x\right\}\Psi_\sigma(x) = \\ &= \sum_{\sigma=\uparrow,\downarrow}\frac{i\sigma}{2}\int dx\,\Psi^\dagger_\sigma(x)\left[\alpha_z(x)\frac{\partial\Psi_\sigma(x)}{\partial x}+\frac{\partial}{\partial x}\Big(\alpha_z(x)\Psi_\sigma(x)\Big)\right] = \\ &= \sum_{\sigma=\uparrow,\downarrow}\frac{i\sigma}{2}\int dx\left[2\alpha_z(x)\Psi^\dagger_\sigma(x)\frac{\partial\Psi_\sigma(x)}{\partial x}+\Psi^\dagger_\sigma(x)\frac{\partial\,\alpha_z(x)}{\partial x}\Psi_\sigma(x)\right] = \\ &= \sum_{\sigma=\uparrow,\downarrow} i\sigma\int dx\left[\alpha_z(x)\Psi^\dagger_\sigma(x)\frac{\partial\Psi_\sigma(x)}{\partial x}+\frac{1}{2}\Psi^\dagger_\sigma(x)\frac{\partial\,\alpha_z(x)}{\partial x}\Psi_\sigma(x)\right] \end{aligned} \tag{A.18}$$

By applying Eq.(A.5) one can rewrite

$$\begin{aligned}&\mathcal{H}_{SO,z} = \\ &= \sum_{\sigma=\uparrow,\downarrow} i\sigma\iint dx\,dx'\left[\alpha_z(x)\Psi^\dagger_\sigma(x')\frac{\partial\Psi_\sigma(x)}{\partial x}+\frac{1}{2}\Psi^\dagger_\sigma(x')\frac{\partial\,\alpha_z(x)}{\partial x}\Psi_\sigma(x)\right]\delta(x-x')\end{aligned} \tag{A.19}$$

Let us focus on each term individually.

1. The first term of (A.19) can be rewritten applying the relation (A.2)

$$\begin{aligned}&+i\sigma\iint dx\,dx'\,\alpha_z(x)\Psi^\dagger_\sigma(x')\frac{\partial\Psi_\sigma(x)}{\partial x}\delta(x-x') = \\ &= \ +i\sigma\iint dx\,dx'\,\alpha_z(x)\Big[\partial_x\delta(x-x')-\frac{\partial\Psi_\sigma(x)}{\partial x}\Psi^\dagger_\sigma(x')\Big]\delta(x-x') = \\ &= \ \sigma C^{(1)}_\alpha - i\sigma\iint dx\,dx'\,\alpha_z(x)\frac{\partial\Psi_\sigma(x)}{\partial x}\Psi^\dagger_\sigma(x')\delta(x-x') = \\ &= \ \sigma C^{(1)}_\alpha - i\sigma\int dx\,\alpha_z(x)\frac{\partial\Psi_\sigma(x)}{\partial x}\Psi^\dagger_\sigma(x)\end{aligned} \tag{A.20}$$

where we have introduced the σ-independent constant

$$C^{(1)}_\alpha = i\iint dx\,dx'\,\alpha_z(x)\delta(x-x')\partial_x\delta(x-x') \tag{A.21}$$

Now, integrating by part the last integral in Eq.(A.20) it follows that

$$\begin{aligned}&-i\sigma\int dx\,\alpha_z(x)\frac{\partial\Psi_\sigma(x)}{\partial x}\Psi^\dagger_\sigma(x) = \\ &= \ \underbrace{-i\sigma\,\alpha_z(x)\Psi_\sigma(x)\Psi^\dagger_\sigma(x)\Big|^{+\infty}_{-\infty}}_{=0}+i\sigma\int dx\,\Psi_\sigma(x)\frac{\partial\left(\alpha_z(x)\Psi^\dagger_\sigma(x)\right)}{\partial x} = \\ &= \ +i\sigma\int dx\,\frac{\partial\alpha_z(x)}{\partial x}\Psi_\sigma(x)\Psi^\dagger_\sigma(x)+i\sigma\int dx\,\alpha_z(x)\Psi_\sigma(x)\frac{\partial\Psi^\dagger_\sigma(x)}{\partial x}\end{aligned} \tag{A.22}$$

and the first term of Eq.(A.19) acquires the form

$$i\sigma \iint dx\,dx'\,\alpha_z(x)\Psi^\dagger_\sigma(x')\frac{\partial\Psi_\sigma(x)}{\partial x}\delta(x-x') = \tag{A.23}$$
$$= \sigma C^{(1)}_\alpha + i\sigma\int dx\,\frac{\partial\alpha_z(x)}{\partial x}\Psi_\sigma(x)\Psi^\dagger_\sigma(x) + i\sigma\int dx\,\alpha_z(x)\Psi_\sigma(x)\frac{\partial\Psi^\dagger_\sigma(x)}{\partial x}$$

2. Regarding the second term of Eq.(A.19), it can be rewritten as

$$\frac{i\sigma}{2}\iint dx\,dx'\,\Psi^\dagger_\sigma(x')\frac{\partial\,\alpha_z(x)}{\partial x}\Psi_\sigma(x)\delta(x-x') =$$
$$= \frac{i\sigma}{2}\iint dx\,dx'\,\frac{\partial\,\alpha_z(x)}{\partial x}\delta(x-x')\,\delta(x-x') +$$
$$- \frac{i\sigma}{2}\iint dx\,dx'\,\Psi_\sigma(x)\frac{\partial\,\alpha_z(x)}{\partial x}\Psi^\dagger_\sigma(x')\delta(x-x') =$$
$$= \sigma C^{(2)}_\alpha - \frac{i\sigma}{2}\int dx\,\Psi_\sigma(x)\frac{\partial\,\alpha_z(x)}{\partial x}\Psi^\dagger_\sigma(x) \tag{A.24}$$

where we have introduced the σ-independent constant

$$C^{(2)}_\alpha = \frac{i}{2}\iint dx\,dx'\,\frac{\partial\,\alpha_z(x)}{\partial x}\delta(x-x')\,\delta(x-x') \tag{A.25}$$

Inserting Eqs.(A.23) and (A.24) into Eq.(A.19), the z-component of the spin-orbit term can be rewritten as

$$\mathcal{H}_{SO,z} = \sum_{\sigma=\uparrow,\downarrow}\Bigg[\sigma C^{(1)}_\alpha + i\sigma\int dx\,\frac{\partial\alpha_z(x)}{\partial x}\Psi_\sigma(x)\Psi^\dagger_\sigma(x) + i\sigma\int dx\,\alpha_z(x)\Psi_\sigma(x)\frac{\partial\Psi^\dagger_\sigma(x)}{\partial x} +$$
$$+\sigma C^{(2)}_\alpha - \frac{i\sigma}{2}\int dx\,\Psi_\sigma(x)\frac{\partial\,\alpha_z(x)}{\partial x}\Psi^\dagger_\sigma(x)\Bigg] =$$
$$= (C^{(1)}_\alpha + C^{(2)}_\alpha)\underbrace{\sum_{\sigma=\uparrow,\downarrow}\sigma}_{=0} +$$
$$+ \sum_{\sigma=\uparrow,\downarrow}\left[i\sigma\int dx\,\alpha_z(x)\Psi_\sigma(x)\frac{\partial\Psi^\dagger_\sigma(x)}{\partial x} + \frac{i\sigma}{2}\int dx\,\Psi_\sigma(x)\frac{\partial\,\alpha_z(x)}{\partial x}\Psi^\dagger_\sigma(x)\right] \tag{A.26}$$

The contribution of the constant term vanishes. In pass, we note that the sum of the two constants (A.21) and (A.25) would return

$$C_\alpha \doteq C^{(1)}_\alpha + C^{(2)}_\alpha = i\iint dx\,dx'\,\delta(x-x')\,\{\alpha_z(x),\partial_x\}\,\delta(x-x') \tag{A.27}$$

Moreover, by comparing the last two terms of Eq.(A.26) with Eq.(A.18), one finally obtains that the z-component of the spin-orbit term can be rewritten as

$$\mathcal{H}_{SO,z} = -\sum_{\sigma=\uparrow,\downarrow}\frac{\sigma}{2\hbar}\int dx\Psi^\dagger_\sigma(x)\left\{\alpha_z(x),\hat{P}\right\}\Psi_\sigma(x) =$$
$$= -\sum_{\sigma=\uparrow,\downarrow}\frac{\sigma}{2\hbar}\int dx\Psi_\sigma(x)\left\{\alpha_z(x),\hat{P}\right\}\Psi^\dagger_\sigma(x) \tag{A.28}$$

- **the x, y-components**
  Let us recall here Eq.(A.16),

$$\mathcal{H}_{SO,(x,y)} = -\sum_{\sigma,\sigma'=\uparrow,\downarrow} \frac{1}{2\hbar} \int dx\, \Psi^\dagger_\sigma(x) \Big\{ \alpha_{x,y}(x), \hat{P} \Big\} \, (\sigma_{x,y})_{\sigma\sigma'} \, \Psi_{\sigma'}(x) \tag{A.29}$$

  where

$$(\sigma_x)_{\sigma,\sigma'} = 1 - \delta_{\sigma,\sigma'} \tag{A.30}$$

$$(\sigma_y)_{\sigma,\sigma'} = i\,\sigma\,(\delta_{\sigma,\sigma'} - 1) \tag{A.31}$$

  Substituting $\hat{P} \to -i\hbar\frac{\partial}{\partial x}$, it follows that

$$\begin{aligned}
\mathcal{H}_{SO,(x,y)} &= -\sum_{\sigma,\sigma'=\uparrow,\downarrow} \frac{1}{2\hbar} \int dx\, \Psi^\dagger_\sigma(x) \Big\{ \alpha_{x,y}(x), \hat{P} \Big\} \, (\sigma_{x,y})_{\sigma\sigma'} \, \Psi_{\sigma'}(x) = \\
&= \frac{i}{2} \sum_{\sigma,\sigma'=\uparrow,\downarrow} \int dx\, \Psi^\dagger_\sigma(x) \Big\{ \alpha_{x,y}(x), \frac{\partial}{\partial x} \Big\} \, (\sigma_{x,y})_{\sigma\sigma'} \, \Psi_{\sigma'}(x) = \\
&= \frac{i}{2} \sum_{\sigma,\sigma'=\uparrow,\downarrow} \int dx\, \Psi^\dagger_\sigma(x) \left[\alpha_{x,y}(x) \frac{\partial \Psi_{\sigma'}(x)}{\partial x} + \frac{\partial}{\partial x} \Big(\alpha_{x,y}(x) \Psi_{\sigma'}(x) \Big) \right] (\sigma_{x,y})_{\sigma\sigma'} = \\
&= \frac{i}{2} \sum_{\sigma,\sigma'=\uparrow,\downarrow} \int dx \left[2\alpha_{x,y}(x) \Psi^\dagger_\sigma(x) \frac{\partial \Psi_{\sigma'}(x)}{\partial x} + \Psi^\dagger_\sigma(x) \frac{\partial\, \alpha_{x,y}(x)}{\partial x} \Psi_{\sigma'}(x) \right] (\sigma_{x,y})_{\sigma\sigma'} = \\
&= i \sum_{\sigma,\sigma'=\uparrow,\downarrow} \int dx \left[\alpha_{x,y}(x) \Psi^\dagger_\sigma(x) \frac{\partial \Psi_{\sigma'}(x)}{\partial x} + \frac{1}{2} \Psi^\dagger_\sigma(x) \frac{\partial\, \alpha_{x,y}(x)}{\partial x} \Psi_{\sigma'}(x) \right] (\sigma_{x,y})_{\sigma\sigma'}
\end{aligned} \tag{A.32}$$

  Exploiting now that the non-zero $\sigma_{x,y}$-elements are off diagonal ones (see Eqs.(A.30) and (A.31), by applying relations (A.1) and (A.2), one obtain

$$\mathcal{H}_{SO,(x,y)} = -i \sum_{\sigma,\sigma'=\uparrow,\downarrow} \int dx \left[\alpha_{x,y}(x) \frac{\partial \Psi_{\sigma'}(x)}{\partial x} \Psi^\dagger_\sigma(x) + \frac{1}{2} \Psi_{\sigma'}(x) \frac{\partial\, \alpha_{x,y}(x)}{\partial x} \Psi^\dagger_\sigma(x) \right] (\sigma_{x,y})_{\sigma\sigma'} \tag{A.33}$$

  Intergrating by part the first integral of the last equation, it can be rewritten as

$$\begin{aligned}
&-i \int dx\, \alpha_{x,y}(x) \frac{\partial \Psi_{\sigma'}(x)}{\partial x} \Psi^\dagger_\sigma(x) = \\
&= \underbrace{-i\, \alpha_{x,y}(x) \Psi_{\sigma'}(x) \Psi^\dagger_\sigma(x) \Big|_{-\infty}^{+\infty}}_{=0} + i \int dx\, \Psi_{\sigma'}(x) \frac{\partial \left(\alpha_{x,y}(x) \Psi^\dagger_\sigma(x) \right)}{\partial x} = \\
&= +i \int dx\, \frac{\partial \alpha_{x,y}(x)}{\partial x} \Psi_{\sigma'}(x) \Psi^\dagger_\sigma(x) + i \int dx\, \alpha_{x,y}(x) \Psi_{\sigma'}(x) \frac{\partial \Psi^\dagger_\sigma(x)}{\partial x}
\end{aligned} \tag{A.34}$$

and inserting this last result in (A.33), it follows that

$$\begin{aligned}
\mathcal{H}_{SO,(x,y)} &= -i \sum_{\sigma,\sigma'=\uparrow,\downarrow} \int dx \left[\alpha_{x,y}(x)\frac{\partial \Psi_{\sigma'}(x)}{\partial x}\Psi^{\dagger}_{\sigma}(x) + \frac{1}{2}\Psi_{\sigma'}(x)\frac{\partial\, \alpha_{x,y}(x)}{\partial x}\Psi^{\dagger}_{\sigma}(x)\right](\sigma_{x,y})_{\sigma\sigma'} = \\
&= +i \sum_{\sigma,\sigma'=\uparrow,\downarrow} \int dx \left[\, \alpha_{x,y}(x)\Psi_{\sigma'}(x)\frac{\partial \Psi^{\dagger}_{\sigma}(x)}{\partial x} + \Psi_{\sigma'}(x)\frac{\partial \alpha_{x,y}(x)}{\partial x}\Psi^{\dagger}_{\sigma}(x) + \right. \\
&\quad \left. - \frac{1}{2}\Psi_{\sigma'}(x)\frac{\partial \alpha_{x,y}(x)}{\partial x}\Psi^{\dagger}_{\sigma}(x)\right](\sigma_{x,y})_{\sigma\sigma'} = \qquad \text{(A.35)} \\
&= +i \sum_{\sigma,\sigma'=\uparrow,\downarrow} \int dx \left[\, \alpha_{x,y}(x)\Psi_{\sigma'}(x)\frac{\partial \Psi^{\dagger}_{\sigma}(x)}{\partial x} + \frac{1}{2}\Psi_{\sigma'}(x)\frac{\partial \alpha_{x,y}(x)}{\partial x}\Psi^{\dagger}_{\sigma}(x)\right](\sigma_{x,y})_{\sigma\sigma'}
\end{aligned}$$

Finally, by comparing Eq.(A.35) with Eq.(A.32) we can state that

$$\begin{aligned}
\mathcal{H}_{SO,(x,y)} &= -\sum_{\sigma,\sigma'=\uparrow,\downarrow} \frac{1}{2\hbar}\int dx\, \Psi^{\dagger}_{\sigma}(x)\left\{\alpha_{x,y}(x), \hat{P}\right\}(\sigma_{x,y})_{\sigma\sigma'}\,\Psi_{\sigma'}(x) = \\
&= +i \sum_{\sigma,\sigma'=\uparrow,\downarrow} \int dx \left[\alpha_{x,y}(x)\Psi^{\dagger}_{\sigma}(x)\frac{\partial \Psi_{\sigma'}(x)}{\partial x} + \frac{1}{2}\Psi^{\dagger}_{\sigma}(x)\frac{\partial\, \alpha_{x,y}(x)}{\partial x}\Psi_{\sigma'}(x)\right](\sigma_{x,y})_{\sigma\sigma'} = \\
&= +i \sum_{\sigma,\sigma'=\uparrow,\downarrow} \int dx \left[\, \alpha_{x,y}(x)\Psi_{\sigma'}(x)\frac{\partial \Psi^{\dagger}_{\sigma}(x)}{\partial x} + \frac{1}{2}\Psi_{\sigma'}(x)\frac{\partial \alpha_{x,y}(x)}{\partial x}\Psi^{\dagger}_{\sigma}(x)\right](\sigma_{x,y})_{\sigma\sigma'} = \\
&= -\sum_{\sigma,\sigma'=\uparrow,\downarrow} \frac{1}{2\hbar}\int dx\, \Psi_{\sigma'}(x)\left\{\alpha_{x,y}(x), \hat{P}\right\}(\sigma_{x,y})^{*}_{\sigma'\sigma}\,\Psi^{\dagger}_{\sigma}(x) \qquad \text{(A.36)}
\end{aligned}$$

where we used the following property

$$(\sigma_{x,y})_{\sigma\sigma'} = (\sigma_{x,y})^{*}_{\sigma'\sigma} \qquad \text{(A.37)}$$

In conclusion, recollecting the three components, the spin-orbit term gets rewritten as

$$\begin{aligned}
\mathcal{H}_{SO} &= -\frac{1}{2\hbar}\sum_{m=x,y,z}\sum_{\sigma,\sigma'=\uparrow,\downarrow}\int dx\,\Psi_\sigma(x)\Big\{\alpha_m(x),\hat{P}\Big\}\,(\sigma_m)^*_{\sigma\sigma'}\,\Psi^\dagger_{\sigma'}(x) = \\
&= -\frac{1}{2\hbar}\sum_{m=x,y,z}\int dx\,\Big(\Psi_\uparrow(x),\Psi_\downarrow(x)\Big)\Big\{\alpha_m(x),\hat{P}\Big\}\sigma^*_m\begin{pmatrix}\Psi^\dagger_\uparrow(x)\\ \Psi^\dagger_\downarrow(x)\end{pmatrix} = \\
&\quad \text{[now insert two identities } \sigma_0 \text{ on the left and on the right of } \sigma^*_m\text{]} \\
&= -\frac{1}{2\hbar}\sum_{m=x,y,z}\int dx\,\Big(\Psi_\uparrow(x),\Psi_\downarrow(x)\Big)\Big\{\alpha_m(x),\hat{P}\Big\}(-i\sigma_y)(i\sigma_y)\sigma^*_m(-i\sigma_y)(i\sigma_y)\begin{pmatrix}\Psi^\dagger_\uparrow(x)\\ \Psi^\dagger_\downarrow(x)\end{pmatrix} = \\
&= -\frac{1}{2\hbar}\sum_{m=x,y,z}\int dx\,\Big(\Psi_\uparrow(x),\Psi_\downarrow(x)\Big)(-i\sigma_y)\Big\{\alpha_m(x),\hat{P}\Big\}(i\sigma_y)\sigma^*_m(-i\sigma_y)(i\sigma_y)\begin{pmatrix}\Psi^\dagger_\uparrow(x)\\ \Psi^\dagger_\downarrow(x)\end{pmatrix} = \\
&= -\frac{1}{2\hbar}\sum_{m=x,y,z}\int dx\,\Big(\Psi_\downarrow(x),-\Psi_\uparrow(x)\Big)\Big\{\alpha_m(x),\hat{P}\Big\}\underbrace{\sigma_y\sigma^*_m\sigma_y}_{=-\sigma_m}\begin{pmatrix}\Psi^\dagger_\downarrow(x)\\ -\Psi^\dagger_\uparrow(x)\end{pmatrix} = \\
&= +\frac{1}{2\hbar}\sum_{m=x,y,z}\int dx\,\Big(\Psi_\downarrow(x),-\Psi_\uparrow(x)\Big)\Big\{\alpha_m(x),\hat{P}\Big\}\sigma_m\begin{pmatrix}\Psi^\dagger_\downarrow(x)\\ -\Psi^\dagger_\uparrow(x)\end{pmatrix} \qquad \text{(A.38)}
\end{aligned}$$

and again

$$\mathcal{H}_{SO} = +\frac{1}{2\hbar}\int dx\,\Big(\Psi_\downarrow(x),-\Psi_\uparrow(x)\Big)\Big\{\boldsymbol{\alpha}(x),\hat{P}\Big\}\cdot\boldsymbol{\sigma}\begin{pmatrix}\Psi^\dagger_\downarrow(x)\\ -\Psi^\dagger_\uparrow(x)\end{pmatrix} \qquad \text{(A.39)}$$

Zeeman term

The Zeeman term (4.5) consists of three components

$$\mathcal{H}_Z = -\sum_{m=x,y,z}\sum_{\sigma,\sigma'=\uparrow,\downarrow}\int dx\,\Psi^\dagger_\sigma(x)b_m(x)\,(\sigma_m)_{\sigma\sigma'}\,\Psi_{\sigma'}(x) \qquad \text{(A.40)}$$

Let us separately analyze the z-component and the x,y-components.

- **the z-component**
  Inserting definition (A.17) and then applying relation (A.5) to the z-component of Eq.(A.40), we have that

$$\begin{aligned}
\mathcal{H}_{Z,z} &= -\sum_{\sigma,\sigma'=\uparrow,\downarrow}\int dx\,\Psi^\dagger_\sigma(x)b_z(x)\,(\sigma_z)_{\sigma\sigma'}\,\Psi_{\sigma'}(x) = \\
&= -\sum_{\sigma,\sigma'=\uparrow,\downarrow}\int dx\,\Psi^\dagger_\sigma(x)b_z(x)\,\sigma\delta_{\sigma\sigma'}\Psi_{\sigma'}(x) = \\
&= -\sum_{\sigma,\sigma'=\uparrow,\downarrow}\iint dx\,dx'\,\Psi^\dagger_\sigma(x)b_z(x)\,\sigma\delta_{\sigma\sigma'}\Psi_{\sigma'}(x)\delta(x-x') = \\
&= -\sum_{\sigma=\uparrow,\downarrow}\sigma\iint dx\,dx'\,\Psi^\dagger_\sigma(x')b_z(x)\,\Psi_\sigma(x)\delta(x-x') \qquad \text{(A.41)}
\end{aligned}$$

Using relation (A.1), Eq.(A.41) gets rewritten as

$$\begin{aligned}\mathcal{H}_{Z,z} = &- \underbrace{\sum_{\sigma=\uparrow,\downarrow} \sigma}_{=0} \iint dx\, dx'\, b_z(x)\delta^2(x-x') + \\ &+ \sum_{\sigma=\uparrow,\downarrow} \sigma \iint dx\, dx'\, \Psi_\sigma(x) b_z(x)\, \Psi^\dagger_\sigma(x')\delta(x-x') = \\ &= \sum_{\sigma=\uparrow,\downarrow} \sigma \iint dx\, dx'\, \Psi_\sigma(x) b_z(x)\, \Psi^\dagger_\sigma(x')\delta(x-x') = \\ &= \sum_{\sigma=\uparrow,\downarrow} \sigma \int dx\, \Psi_\sigma(x) b_z(x)\, \Psi^\dagger_\sigma(x) \end{aligned} \tag{A.42}$$

and thus

$$\mathcal{H}_{Z,z} = + \sum_{\sigma,\sigma'=\uparrow,\downarrow} \int dx\, \Psi_\sigma(x) b_z(x)\, (\sigma_z)_{\sigma\sigma'}\, \Psi^\dagger_{\sigma'}(x)$$

- **the x, y-components**
  Let us start from Eq(A.40) for the x, y-components, i.e.

$$\mathcal{H}_{Z,(x,y)} = - \int dx\, \Psi^\dagger_\sigma(x) b_{x,y}(x)\, (\sigma_{x,y})_{\sigma\sigma'}\, \Psi_{\sigma'}(x) \tag{A.43}$$

  As for the SO x, y-terms, the non-zero $\sigma_{x,y}$-elements are off diagonal ones, thus we may directly apply relation (A.1), obtaning

$$\mathcal{H}_{Z,(x,y)} = + \sum_{\sigma,\sigma'=\uparrow,\downarrow} \int dx\, \Psi_{\sigma'}(x) b_{x,y}(x)\, (\sigma_{x,y})^*_{\sigma'\sigma}\, \Psi^\dagger_\sigma(x) \tag{A.44}$$

  where again we use $(\sigma_{x,y})_{\sigma\sigma'} = (\sigma_{x,y})^*_{\sigma'\sigma}$.

Recollecting now the three components of the Zeeman term, it follows that

$$\begin{aligned}
\mathcal{H}_Z &= + \sum_{m=x,y,z} \sum_{\sigma,\sigma'=\uparrow,\downarrow} \int dx\, \Psi_\sigma(x) b_m(x)\ (\sigma_m)^*_{\sigma\sigma'}\, \Psi^\dagger_{\sigma'}(x) = \\
&= + \sum_{m=x,y,z} \int dx\, (\Psi_\uparrow(x), \Psi_\downarrow(x)) b_m(x)\, \sigma^*_m \begin{pmatrix} \Psi^\dagger_\uparrow(x) \\ \Psi^\dagger_\downarrow(x) \end{pmatrix} = \\
&\quad \text{[now insert two identities } \sigma_0 \text{ on the left and on the right of } \sigma^*_m\text{]} \\
&= + \sum_{m=x,y,z} \int dx\, (\Psi_\uparrow(x), \Psi_\downarrow(x)) b_m(x)\, (-i\sigma_y)(i\sigma_y)\sigma^*_m(-i\sigma_y)(i\sigma_y) \begin{pmatrix} \Psi^\dagger_\uparrow(x) \\ \Psi^\dagger_\downarrow(x) \end{pmatrix} = \\
&= + \sum_{m=x,y,z} \int dx\, (\Psi_\uparrow(x), \Psi_\downarrow(x))(-i\sigma_y) b_m(x)\, (i\sigma_y)\sigma^*_m(-i\sigma_y)(i\sigma_y) \begin{pmatrix} \Psi^\dagger_\uparrow(x) \\ \Psi^\dagger_\downarrow(x) \end{pmatrix} = \\
&= + \sum_{m=x,y,z} \int dx\, (\Psi_\downarrow(x), -\Psi_\uparrow(x)) b_m(x)\, (i\sigma_y)\sigma^*_m(-i\sigma_y) \begin{pmatrix} \Psi^\dagger_\downarrow(x) \\ -\Psi^\dagger_\uparrow(x) \end{pmatrix} = \\
&= - \sum_{m=x,y,z} \int dx\, (\Psi_\downarrow(x), -\Psi_\uparrow(x)) b_m(x)\, \sigma_m \begin{pmatrix} \Psi^\dagger_\downarrow(x) \\ -\Psi^\dagger_\uparrow(x) \end{pmatrix}
\end{aligned}$$

In conclusion, the Zeeman term can be rewritten as

$$\mathcal{H}_Z = - \int dx\, (\Psi_\downarrow(x), -\Psi_\uparrow(x))\, \boldsymbol{b}(x) \cdot \boldsymbol{\sigma} \begin{pmatrix} \Psi^\dagger_\downarrow(x) \\ -\Psi^\dagger_\uparrow(x) \end{pmatrix} \tag{A.45}$$

Superconducting term

The superconducing term (4.6) can be rewritten as

$$\begin{aligned}
\mathcal{H}_{SC} &= \int dx \Big[\Delta(x) \Psi^\dagger_\uparrow(x) \Psi^\dagger_\downarrow(x) + \Delta^*(x) \Psi_\downarrow(x) \Psi_\uparrow(x) \Big] = \\
&= - \int dx \Big[\Delta(x) \Psi^\dagger_\downarrow(x) \Psi^\dagger_\uparrow(x) + \Delta^*(x) \Psi_\uparrow(x) \Psi_\downarrow(x) \Big]
\end{aligned} \tag{A.46}$$

Thus, Eqs.(A.10), (A.14), (A.39), (A.45) and (A.46) are equivalent expressions for the five terms (4.2), (4.3), (4.4), (4.5) and (4.6), respectively, i.e.

$$\mathcal{H}_{kin} = 2C_p - \int dx \left(\Psi_\downarrow(x), -\Psi_\uparrow(x) \right) \frac{\hat{P}^2}{2m^*} \sigma_0 \begin{pmatrix} \Psi^\dagger_\downarrow(x) \\ -\Psi^\dagger_\uparrow(x) \end{pmatrix} \tag{A.47}$$

$$\mathcal{H}_\mu = -2C_\mu + \int dx \mu(x) \left(\Psi_\downarrow(x), -\Psi_\uparrow(x) \right) \sigma_0 \begin{pmatrix} \Psi^\dagger_\downarrow(x) \\ -\Psi^\dagger_\uparrow(x) \end{pmatrix} \tag{A.48}$$

$$\mathcal{H}_{SO} = + \frac{1}{2\hbar} \int dx \left(\Psi_\downarrow(x), -\Psi_\uparrow(x) \right) \left\{ \boldsymbol{\alpha}(x), \hat{P} \right\} \cdot \boldsymbol{\sigma} \begin{pmatrix} \Psi^\dagger_\downarrow(x) \\ -\Psi^\dagger_\uparrow(x) \end{pmatrix} \tag{A.49}$$

$$\mathcal{H}_Z = - \int dx\, (\Psi_\downarrow(x), -\Psi_\uparrow(x))\, \boldsymbol{b}(x) \cdot \boldsymbol{\sigma} \begin{pmatrix} \Psi^\dagger_\downarrow(x) \\ -\Psi^\dagger_\uparrow(x) \end{pmatrix} \tag{A.50}$$

$$\mathcal{H}_{SC} = - \int dx \Big[\Delta(x) \Psi^\dagger_\downarrow(x) \Psi^\dagger_\uparrow(x) + \Delta^*(x) \Psi_\uparrow(x) \Psi_\downarrow(x) \Big] \tag{A.51}$$

We can therefore rewrite the full Hamitonian as

$$\mathcal{H} = \frac{1}{2}\left(\mathcal{H} + \mathcal{H}\right) \tag{A.52}$$

Now, for the first $\mathcal{H}$ appearing on the right hand side of Eq.(A.52) we adopt the sum of the expressions (4.2), (4.3), (4.4), (4.5) and (4.6), whereas for the second $\mathcal{H}$ we exploit the sum of the 5 equivalent expressions (A.47), (A.48), (A.49), (A.50) and (A.51). By exploiting the definition (4.15) of the Nambu spinor, Eq.(A.52) acquires the form (4.14) where $H_{BdG}(x)$ is given by Eq.(4.22).

End of proof

List of Figures

Bibliography

[1] John B. Ketterson and Shengnian N. Song. *Superconductivity*. Cambridge: Cambridge University Press, 1999. ISBN: 978-1-139-17109-0. DOI: 10.1017/CBO9781139171090.

[2] Michael Tinkham. *Introduction to superconductivity*. 2. ed. International series in pure and applied physics. New York: McGraw-Hill, 1996. ISBN: 978-0-07-064878-4.

[3] Emanuel Maxwell. ≪Isotope Effect in the Superconductivity of Mercury≫. In: *Physical Review* 78.4 (May 1950), pp. 477–477. ISSN: 0031-899X. DOI: 10.1103/PhysRev.78.477.

[4] W. Meissner and R. Ochsenfeld. ≪Ein neuer Effekt bei Eintritt der Supraleitfähigkeit≫. In: *Naturwissenschaften* 21.44 (Nov. 1933), pp. 787–788. ISSN: 1432-1904. DOI: 10.1007/BF01504252.

[5] J. G. Bednorz and K. A. Müller. ≪Possible highTc superconductivity in the Ba-La-Cu-O system≫. In: *Zeitschrift für Physik B Condensed Matter* 64.2 (June 1986), pp. 189–193. ISSN: 1431-584X. DOI: 10.1007/BF01303701.

[6] J. Bardeen, L. N. Cooper, and J. R. Schrieffer. ≪Theory of Superconductivity≫. In: *Physical Review* 108.5 (Dec. 1957), pp. 1175–1204. ISSN: 0031-899X. DOI: 10.1103/PhysRev.108.1175.

[7] Gerald D. Mahan. *Many particle physics*. 3rd ed. Physics of solids and liquids. New York: Kluwer academic/Plenum pub, 2000. ISBN: 978-0-306-46338-9.

[8] Neil W. Ashcroft and N. David Mermin. *Solid state physics*. Australia Brazil Canada Mexico Singapore United Kingdom United States Boston, MA: Cengage, 2023. ISBN: 978-81-315-0052-1.

[9] H. Fröhlich. ≪Theory of the Superconducting State. I. The Ground State at the Absolute Zero of Temperature≫. In: *Physical Review* 79.5 (Sept. 1950), pp. 845–856. ISSN: 0031-899X. DOI: 10.1103/PhysRev.79.845.

[10] Leon N. Cooper. ≪Bound Electron Pairs in a Degenerate Fermi Gas≫. In: *Physical Review* 104.4 (Nov. 1956), pp. 1189–1190. ISSN: 0031-899X. DOI: 10.1103/PhysRev.104.1189.

[11] A F Andreev. ≪Thermal conductivity of the intermediate state of superconductors≫. In: *Zh. Eksperim. i Teor. Fiz.* Vol: 46 (May 1964). Place: Country unknown/Code not available.

[12] G. E. Blonder, M. Tinkham, and T. M. Klapwijk. «Transition from metallic to tunneling regimes in superconducting microconstrictions: Excess current, charge imbalance, and supercurrent conversion». In: *Physical Review B* 25.7 (Apr. 1982), pp. 4515–4532. ISSN: 0163-1829. DOI: 10.1103/PhysRevB.25.4515.

[13] B.D. Josephson. «Possible new effects in superconductive tunnelling». In: *Physics Letters* 1.7 (July 1962), pp. 251–253. ISSN: 00319163. DOI: 10.1016/0031-9163(62)91369-0.

[14] B. D. Josephson. «The discovery of tunnelling supercurrents». In: *Reviews of Modern Physics* 46.2 (Apr. 1974), pp. 251–254. ISSN: 0034-6861. DOI: 10.1103/RevModPhys.46.251.

[15] R. Holm and W. Meissner. «Einige Kontaktwiderstandsmessungen bei tiefen Temperaturen». In: *Zeitschrift für Physik* 86.11 (Nov. 1933), pp. 787–791. ISSN: 0044-3328. DOI: 10.1007/BF01337880.

[16] Leslie L. Foldy and Siegfried A. Wouthuysen. «On the Dirac Theory of Spin 1/2 Particles and Its Non-Relativistic Limit». In: *Physical Review* 78.1 (Apr. 1950), pp. 29–36. ISSN: 0031-899X. DOI: 10.1103/PhysRev.78.29.

[17] Franz Schwabl. *Advanced Quantum Mechanics*. Trans. by R. Hilton and Angela Lahee. 4. 4th ed. 2008. Berlin, Heidelberg: Springer Berlin Heidelberg, 2008. ISBN: 978-3-540-85061-8. DOI: 10.1007/978-3-540-85062-5.

[18] David J. Griffiths and Darrell F. Schroeter. *Introduction to Quantum Mechanics*. 3rd ed. Cambridge University Press, Aug. 2018. ISBN: 978-1-316-99543-3. DOI: 10.1017/9781316995433.

[19] Franco Ciccacci. *Fondamenti di fisica atomica e quantistica*. 3. ed. OCLC: 1310141196. Napoli: EdiSES Università, 2019. ISBN: 978-88-3319-067-9.

[20] Roland Winkler. *Spin-orbit coupling effects in two-dimensional electron and hole systems*. Springer tracts in modern physics v. 191. Berlin ; New York: Springer, 2003. ISBN: 978-3-540-01187-3.

[21] Yu A Bychkov and E I Rashba. «Oscillatory effects and the magnetic susceptibility of carriers in inversion layers». In: *Journal of Physics C: Solid State Physics* 17.33 (Nov. 1984), pp. 6039–6045. ISSN: 0022-3719. DOI: 10.1088/0022-3719/17/33/015.

[22] A. Manchon et al. «New perspectives for Rashba spin-orbit coupling». In: *Nature Materials* 14.9 (Sept. 2015), pp. 871–882. ISSN: 1476-1122, 1476-4660. DOI: 10.1038/nmat4360.

[23] G. Dresselhaus. «Spin-Orbit Coupling Effects in Zinc Blende Structures». In: *Physical Review* 100.2 (Oct. 1955), pp. 580–586. ISSN: 0031-899X. DOI: 10.1103/PhysRev.100.580.

[24] A. Bringer, S. Heedt, and Th. Schäpers. «Dresselhaus spin-orbit coupling in [111]-oriented semiconductor nanowires». In: *Physical Review B* 99.8 (Feb. 2019), p. 085437. ISSN: 2469-9950, 2469-9969. DOI: 10.1103/PhysRevB.99.085437.

[25] Dario Bercioux and Procolo Lucignano. «Quantum transport in Rashba spin–orbit materials: a review». In: *Reports on Progress in Physics* 78.10 (Oct. 2015), p. 106001. ISSN: 0034-4885, 1361-6633. DOI: 10.1088/0034-4885/78/10/106001.

[26] Hannah J Joyce et al. «Electronic properties of GaAs, InAs and InP nanowires studied by terahertz spectroscopy». In: *Nanotechnology* 24.21 (May 2013), p. 214006. ISSN: 0957-4484, 1361-6528. DOI: 10.1088/0957-4484/24/21/214006.

[27] B. J. Van Wees et al. «Quantized conductance of point contacts in a two-dimensional electron gas». In: *Physical Review Letters* 60.9 (Feb. 1988), pp. 848–850. ISSN: 0031-9007. DOI: 10.1103/PhysRevLett.60.848.

[28] Supriyo Datta. *Electronic transport in mesoscopic systems*. Cambridge studies in semiconductor physics and microelectronic engineering 3. Cambridge: Cambridge University Press, 1995. ISBN: 978-0-511-80577-6. DOI: 10.1017/CBO9780511805776.

[29] C.W.J. Beenakker and H. van Houten. «Quantum transport in semiconductor nanostructures». In: *Semiconductor heterostructures and nanostructures*. Ed. by Henry Ehrenreich and David Turnbull. Vol. 44. Solid state physics. ISSN: 0081-1947. Academic Press, 1991, pp. 1–228. DOI: https://doi.org/10.1016/S0081-1947(08)60091-0.

[30] Stephan Furthmeier et al. «Enhanced spin–orbit coupling in core/shell nanowires». In: *Nature Communications* 7.1 (Aug. 2016), p. 12413. ISSN: 2041-1723. DOI: 10.1038/ncomms12413.

[31] Paweł Wójcik, Andrea Bertoni, and Guido Goldoni. «Tuning Rashba spin-orbit coupling in homogeneous semiconductor nanowires». In: *Physical Review B* 97.16 (Apr. 2018), p. 165401. ISSN: 2469-9950, 2469-9969. DOI: 10.1103/PhysRevB.97.165401.

[32] Yong-Joo Doh et al. «Tunable Supercurrent Through Semiconductor Nanowires». In: *Science* 309.5732 (July 2005), pp. 272–275. ISSN: 0036-8075, 1095-9203. DOI: 10.1126/science.1113523.

[33] Yi Cui et al. «Nanowire Nanosensors for Highly Sensitive and Selective Detection of Biological and Chemical Species». In: *Science* 293.5533 (Aug. 2001), pp. 1289–1292. ISSN: 0036-8075, 1095-9203. DOI: 10.1126/science.1062711.

[34] J. H. Davies. *The physics of low-dimensional semiconductors: an introduction*. Cambridge, U.K. ; New York, NY, USA: Cambridge University Press, 1998. ISBN: 978-0-521-48148-9.

[35] Zoltán Scherübl et al. «Electrical tuning of Rashba spin-orbit interaction in multi-gated InAs nanowires». In: *Physical Review B* 94.3 (July 2016), p. 035444. ISSN: 2469-9950, 2469-9969. DOI: 10.1103/PhysRevB.94.035444.

[36] Jouri D. S. Bommer et al. «Spin-Orbit Protection of Induced Superconductivity in Majorana Nanowires». In: *Physical Review Letters* 122.18 (May 2019), p. 187702. ISSN: 0031-9007, 1079-7114. DOI: 10.1103/PhysRevLett.122.187702.

[37] Paweł Wójcik, Andrea Bertoni, and Guido Goldoni. «Anisotropy of the spin-orbit coupling driven by a magnetic field in InAs nanowires». In: *Physical Review B* 103.8 (Feb. 2021), p. 085434. ISSN: 2469-9950, 2469-9969. DOI: 10.1103/PhysRevB.103.085434.

[38] Igor Žutić, Jaroslav Fabian, and S. Das Sarma. «Spintronics: Fundamentals and applications». In: *Reviews of Modern Physics* 76.2 (Apr. 2004), pp. 323–410. ISSN: 0034-6861, 1539-0756. DOI: 10.1103/RevModPhys.76.323.

[39] S. A. Wolf et al. «Spintronics: A Spin-Based Electronics Vision for the Future». In: *Science* 294.5546 (Nov. 2001), pp. 1488–1495. ISSN: 0036-8075, 1095-9203. DOI: 10.1126/science.1065389.

[40] Supriyo Datta and Biswajit Das. «Electronic analog of the electro-optic modulator». In: *Applied Physics Letters* 56.7 (Feb. 1990), pp. 665–667. ISSN: 0003-6951, 1077-3118. DOI: 10.1063/1.102730.

[41] C. Padurariu and Yu. V. Nazarov. «Theoretical proposal for superconducting spin qubits». In: *Physical Review B* 81.14 (Apr. 2010), p. 144519. ISSN: 1098-0121, 1550-235X. DOI: 10.1103/PhysRevB.81.144519.

[42] Nikolai M. Chtchelkatchev and Yu. V. Nazarov. «Andreev Quantum Dots for Spin Manipulation». In: *Physical Review Letters* 90.22 (June 2003), p. 226806. ISSN: 0031-9007, 1079-7114. DOI: 10.1103/PhysRevLett.90.226806.

[43] Sunghun Park and A. Levy Yeyati. «Andreev spin qubits in multichannel Rashba nanowires». In: *Physical Review B* 96.12 (Sept. 2017), p. 125416. ISSN: 2469-9950, 2469-9969. DOI: 10.1103/PhysRevB.96.125416.

[44] L. Tosi et al. «Spin-Orbit Splitting of Andreev States Revealed by Microwave Spectroscopy». In: *Physical Review X* 9.1 (Jan. 2019), p. 011010. ISSN: 2160-3308. DOI: 10.1103/PhysRevX.9.011010.

[45] M. Hays et al. «Coherent manipulation of an Andreev spin qubit». In: *Science* 373.6553 (July 2021), pp. 430–433. ISSN: 0036-8075, 1095-9203. DOI: 10.1126/science.abf0345.

[46] Arno Bargerbos et al. «Singlet-Doublet Transitions of a Quantum Dot Josephson Junction Detected in a Transmon Circuit». In: *PRX Quantum* 3.3 (July 2022), p. 030311. ISSN: 2691-3399. DOI: 10.1103/PRXQuantum.3.030311.

[47] Marta Pita-Vidal et al. «Direct manipulation of a superconducting spin qubit strongly coupled to a transmon qubit». In: *Nature Physics* 19.8 (Aug. 2023), pp. 1110–1115. ISSN: 1745-2473, 1745-2481. DOI: 10.1038/s41567-023-02071-x.

[48] David Van Driel et al. «Spin-filtered measurements of Andreev bound states in semiconductor-superconductor nanowire devices». In: *Nature Communications* 14.1 (Oct. 2023), p. 6880. ISSN: 2041-1723. DOI: 10.1038/s41467-023-42026-7.

[49] Masatoshi Sato and Yoichi Ando. «Topological superconductors: a review». In: *Reports on Progress in Physics* 80.7 (July 2017), p. 076501. ISSN: 0034-4885, 1361-6633. DOI: 10.1088/1361-6633/aa6ac7.

[50] Alexander Altland and Martin R. Zirnbauer. ≪Nonstandard symmetry classes in mesoscopic normal-superconducting hybrid structures≫. In: *Physical Review B* 55.2 (Jan. 1997), pp. 1142–1161. ISSN: 0163-1829, 1095-3795. DOI: 10.1103/PhysRevB.55.1142.

[51] Andreas P. Schnyder et al. ≪Classification of topological insulators and superconductors in three spatial dimensions≫. In: *Physical Review B* 78.19 (Nov. 2008), p. 195125. ISSN: 1098-0121, 1550-235X. DOI: 10.1103/PhysRevB.78.195125.

[52] Alexei Kitaev. ≪Periodic table for topological insulators and superconductors≫. In: *AIP Conference Proceedings* 1134.1 (May 2009), pp. 22–30. ISSN: 0094-243X. DOI: 10.1063/1.3149495.

[53] Yukio Tanaka, Masatoshi Sato, and Naoto Nagaosa. ≪Symmetry and Topology in Superconductors –Odd-Frequency Pairing and Edge States–≫. In: *Journal of the Physical Society of Japan* 81.1 (Jan. 2012), p. 011013. ISSN: 0031-9015, 1347-4073. DOI: 10.1143/JPSJ.81.011013.

[54] Jeffrey C. Y. Teo and C. L. Kane. ≪Topological defects and gapless modes in insulators and superconductors≫. In: *Physical Review B* 82.11 (Sept. 2010), p. 115120. ISSN: 1098-0121, 1550-235X. DOI: 10.1103/PhysRevB.82.115120.

[55] Jeffrey C. Y. Teo and Taylor L. Hughes. ≪Existence of Majorana-Fermion Bound States on Disclinations and the Classification of Topological Crystalline Superconductors in Two Dimensions≫. In: *Physical Review Letters* 111.4 (July 2013), p. 047006. ISSN: 0031-9007, 1079-7114. DOI: 10.1103/PhysRevLett.111.047006.

[56] Wladimir A. Benalcazar, Jeffrey C. Y. Teo, and Taylor L. Hughes. ≪Classification of two-dimensional topological crystalline superconductors and Majorana bound states at disclinations≫. In: *Physical Review B* 89.22 (June 2014), p. 224503. ISSN: 1098-0121, 1550-235X. DOI: 10.1103/PhysRevB.89.224503.

[57] Ken Shiozaki and Masatoshi Sato. ≪Topology of crystalline insulators and superconductors≫. In: *Physical Review B* 90.16 (Oct. 2014), p. 165114. ISSN: 1098-0121, 1550-235X. DOI: 10.1103/PhysRevB.90.165114.

[58] Ettore Majorana. ≪Teoria simmetrica dell'elettrone e del positrone≫. In: *Il Nuovo Cimento* 14.4 (Apr. 1937), pp. 171–184. ISSN: 0029-6341, 1827-6121. DOI: 10.1007/BF02961314.

[59] Frank Wilczek. ≪Majorana returns≫. In: *Nature Physics* 5.9 (Sept. 2009), pp. 614–618. ISSN: 1745-2473, 1745-2481. DOI: 10.1038/nphys1380.

[60] Jason Alicea. ≪New directions in the pursuit of Majorana fermions in solid state systems≫. In: *Reports on Progress in Physics* 75.7 (July 2012), p. 076501. ISSN: 0034-4885, 1361-6633. DOI: 10.1088/0034-4885/75/7/076501.

[61] Pasquale Marra. ≪Majorana nanowires for topological quantum computation≫. In: *Journal of Applied Physics* 132.23 (Dec. 2022), p. 231101. ISSN: 0021-8979, 1089-7550. DOI: 10.1063/5.0102999.

[62] Shinsei Ryu and Yasuhiro Hatsugai. ≪Topological Origin of Zero-Energy Edge States in Particle-Hole Symmetric Systems≫. In: *Physical Review Letters* 89.7 (July 2002), p. 077002. ISSN: 0031-9007, 1079-7114. DOI: 10.1103/PhysRevLett.89.077002.

[63] Masatoshi Sato and Satoshi Fujimoto. ≪Majorana Fermions and Topology in Superconductors≫. In: *Journal of the Physical Society of Japan* 85.7 (July 2016), p. 072001. ISSN: 0031-9015, 1347-4073. DOI: 10.7566/JPSJ.85.072001.

[64] David J. Clarke, Jay D. Sau, and Sumanta Tewari. ≪Majorana fermion exchange in quasi-one-dimensional networks≫. In: *Physical Review B* 84.3 (July 2011), p. 035120. ISSN: 1098-0121, 1550-235X. DOI: 10.1103/PhysRevB.84.035120.

[65] D. A. Ivanov. ≪Non-Abelian Statistics of Half-Quantum Vortices in p -Wave Superconductors≫. In: *Physical Review Letters* 86.2 (Jan. 2001), pp. 268–271. ISSN: 0031-9007, 1079-7114. DOI: 10.1103/PhysRevLett.86.268.

[66] Bertrand I. Halperin et al. ≪Adiabatic manipulations of Majorana fermions in a three-dimensional network of quantum wires≫. In: *Physical Review B* 85.14 (Apr. 2012), p. 144501. ISSN: 1098-0121, 1550-235X. DOI: 10.1103/PhysRevB.85.144501.

[67] Jason Alicea et al. ≪Non-Abelian statistics and topological quantum information processing in 1D wire networks≫. In: *Nature Physics* 7.5 (May 2011), pp. 412–417. ISSN: 1745-2473, 1745-2481. DOI: 10.1038/nphys1915.

[68] Ady Stern, Felix Von Oppen, and Eros Mariani. ≪Geometric phases and quantum entanglement as building blocks for non-Abelian quasiparticle statistics≫. In: *Physical Review B* 70.20 (Nov. 2004), p. 205338. ISSN: 1098-0121, 1550-235X. DOI: 10.1103/PhysRevB.70.205338.

[69] Ady Stern. ≪Non-Abelian states of matter≫. In: *Nature* 464.7286 (Mar. 2010), pp. 187–193. ISSN: 0028-0836, 1476-4687. DOI: 10.1038/nature08915.

[70] Karsten Flensberg. ≪Non-Abelian Operations on Majorana Fermions via Single-Charge Control≫. In: *Physical Review Letters* 106.9 (Mar. 2011), p. 090503. ISSN: 0031-9007, 1079-7114. DOI: 10.1103/PhysRevLett.106.090503.

[71] A.Yu. Kitaev. ≪Fault-tolerant quantum computation by anyons≫. In: *Annals of Physics* 303.1 (Jan. 2003), pp. 2–30. ISSN: 00034916. DOI: 10.1016/S0003-4916(02)00018-0.

[72] Chetan Nayak et al. ≪Non-Abelian anyons and topological quantum computation≫. In: *Reviews of Modern Physics* 80.3 (Sept. 2008), pp. 1083–1159. ISSN: 0034-6861, 1539-0756. DOI: 10.1103/RevModPhys.80.1083.

[73] Tudor D. Stanescu. *Introduction to topological quantum matter & quantum computation*. Boca Raton, FL: CRC Press, Taylor & Francis Group, 2017. ISBN: 978-1-4822-4593-6.

[74] Sankar Das Sarma, Michael Freedman, and Chetan Nayak. ≪Majorana zero modes and topological quantum computation≫. In: *npj Quantum Information* 1.1 (Oct. 2015), p. 15001. ISSN: 2056-6387. DOI: 10.1038/npjqi.2015.1.

[75] Jay D. Sau, Sumanta Tewari, and S. Das Sarma. ≪Universal quantum computation in a semiconductor quantum wire network≫. In: *Physical Review A* 82.5 (Nov. 2010), p. 052322. ISSN: 1050-2947, 1094-1622. DOI: 10.1103/PhysRevA.82.052322.

[76] Liang Jiang, Charles L. Kane, and John Preskill. ≪Interface between Topological and Superconducting Qubits≫. In: *Physical Review Letters* 106.13 (Mar. 2011), p. 130504. ISSN: 0031-9007, 1079-7114. DOI: 10.1103/PhysRevLett.106.130504.

[77] Parsa Bonderson and Roman M. Lutchyn. ≪Topological Quantum Buses: Coherent Quantum Information Transfer between Topological and Conventional Qubits≫. In: *Physical Review Letters* 106.13 (Mar. 2011), p. 130505. ISSN: 0031-9007, 1079-7114. DOI: 10.1103/PhysRevLett.106.130505.

[78] N. Read and Dmitry Green. ≪Paired states of fermions in two dimensions with breaking of parity and time-reversal symmetries and the fractional quantum Hall effect≫. In: *Physical Review B* 61.15 (Apr. 2000), pp. 10267–10297. ISSN: 0163-1829, 1095-3795. DOI: 10.1103/PhysRevB.61.10267.

[79] A Yu Kitaev. ≪Unpaired Majorana fermions in quantum wires≫. In: *Physics-Uspekhi* 44.10S (Oct. 2001), pp. 131–136. ISSN: 1468-4780. DOI: 10.1070/1063-7869/44/10S/S29.

[80] Masatoshi Sato. ≪Topological properties of spin-triplet superconductors and Fermi surface topology in the normal state≫. In: *Physical Review B* 79.21 (June 2009), p. 214526. ISSN: 1098-0121, 1550-235X. DOI: 10.1103/PhysRevB.79.214526.

[81] Masatoshi Sato. ≪Topological odd-parity superconductors≫. In: *Physical Review B* 81.22 (June 2010), p. 220504. ISSN: 1098-0121, 1550-235X. DOI: 10.1103/PhysRevB.81.220504.

[82] S. Raghu, A. Kapitulnik, and S. A. Kivelson. ≪Hidden Quasi-One-Dimensional Superconductivity in Sr 2 RuO 4≫. In: *Physical Review Letters* 105.13 (Sept. 2010), p. 136401. ISSN: 0031-9007, 1079-7114. DOI: 10.1103/PhysRevLett.105.136401.

[83] Zhiyuan Zhang et al. *Evidence of P-wave Pairing in K$_2$Cr$_3$As$_3$ Superconductors from Phase-sensitive Measurement*. arXiv:2408.07342 [cond-mat]. Feb. 2025. DOI: 10.48550/arXiv.2408.07342.

[84] Catherine Kallin. ≪Chiral p-wave order in Sr_2 RuO_4≫. In: *Reports on Progress in Physics* 75.4 (Apr. 2012), p. 042501. ISSN: 0034-4885, 1361-6633. DOI: 10.1088/0034-4885/75/4/042501.

[85] Roman M. Lutchyn, Jay D. Sau, and S. Das Sarma. ≪Majorana Fermions and a Topological Phase Transition in Semiconductor-Superconductor Heterostructures≫. In: *Physical Review Letters* 105.7 (Aug. 2010), p. 077001. ISSN: 0031-9007, 1079-7114. DOI: 10.1103/PhysRevLett.105.077001.

[86] Yuval Oreg, Gil Refael, and Felix Von Oppen. ≪Helical Liquids and Majorana Bound States in Quantum Wires≫. In: *Physical Review Letters* 105.17 (Oct. 2010), p. 177002. ISSN: 0031-9007, 1079-7114. DOI: 10.1103/PhysRevLett.105.177002.

[87] Hans Meissner. ≪Superconductivity of Contacts with Interposed Barriers≫. In: *Physical Review* 117.3 (Feb. 1960), pp. 672–680. ISSN: 0031-899X. DOI: 10.1103/PhysRev.117.672.

[88] Tudor D. Stanescu and S. Das Sarma. ≪Superconducting proximity effect in semiconductor nanowires≫. In: *Physical Review B* 87.18 (May 2013), p. 180504. ISSN: 1098-0121, 1550-235X. DOI: 10.1103/PhysRevB.87.180504.

[89] T D Stanescu and S Tewari. ≪Majorana fermions in semiconductor nanowires: fundamentals, modeling, and experiment≫. In: *Journal of Physics: Condensed Matter* 25.23 (June 2013), p. 233201. ISSN: 0953-8984, 1361-648X. DOI: 10.1088/0953-8984/25/23/233201.

[90] N. N. Bogoljubov. ≪On a new method in the theory of superconductivity≫. In: *Il Nuovo Cimento* 7.6 (Mar. 1958), pp. 794–805. ISSN: 0029-6341, 1827-6121. DOI: 10.1007/BF02745585.

[91] Pierre-Gilles de Gennes. *Superconductivity of metals and alloys*. Trans. by Philip A. Pincus. Advanced book classics. Boca Raton: CRC Press, Taylor & Francis Group, 2018. ISBN: 978-0-7382-0101-6. DOI: 10.1201/9780429497032.

[92] Manfred Sigrist and Kazuo Ueda. ≪Phenomenological theory of unconventional superconductivity≫. In: *Reviews of Modern Physics* 63.2 (Apr. 1991), pp. 239–311. ISSN: 0034-6861, 1539-0756. DOI: 10.1103/RevModPhys.63.239.

[93] E. F. Talantsev et al. ≪p-wave superconductivity in iron-based superconductors≫. In: *Scientific Reports* 9.1 (Oct. 2019), p. 14245. ISSN: 2045-2322. DOI: 10.1038/s41598-019-50687-y.

[94] C. C. Tsuei and J. R. Kirtley. ≪Pairing symmetry in cuprate superconductors≫. In: *Reviews of Modern Physics* 72.4 (Oct. 2000), pp. 969–1016. ISSN: 0034-6861, 1539-0756. DOI: 10.1103/RevModPhys.72.969.

[95] B. Keimer et al. ≪From quantum matter to high-temperature superconductivity in copper oxides≫. In: *Nature* 518.7538 (Feb. 2015), pp. 179–186. ISSN: 0028-0836, 1476-4687. DOI: 10.1038/nature14165.

[96] Yaroslav Tserkovnyak et al. ≪Boundary spin Hall effect in a two-dimensional semiconductor system with Rashba spin-orbit coupling≫. In: *Physical Review B* 76.8 (Aug. 2007), p. 085319. ISSN: 1098-0121, 1550-235X. DOI: 10.1103/PhysRevB.76.085319.

[97] Mariana Malard et al. ≪Modulated Rashba interaction in a quantum wire: Spin and charge dynamics≫. In: *Physical Review B* 84.7 (Aug. 2011), p. 075466. ISSN: 1098-0121, 1550-235X. DOI: 10.1103/PhysRevB.84.075466.

[98] Almas F. Sadreev and E. Ya. Sherman. ≪Effect of gate-driven spin resonance on the conductance through a one-dimensional quantum wire≫. In: *Physical Review B* 88.11 (Sept. 2013), p. 115302. ISSN: 1098-0121, 1550-235X. DOI: 10.1103/PhysRevB.88.115302.

[99] K. Takase et al. «Highly gate-tuneable Rashba spin-orbit interaction in a gate-all-around InAs nanowire metal-oxide-semiconductor field-effect transistor». In: *Scientific Reports* 7.1 (Apr. 2017), p. 930. ISSN: 2045-2322. DOI: 10.1038/s41598-017-01080-0.

[100] E. Ya. Sherman. «Random spin–orbit coupling and spin relaxation in symmetric quantum wells». In: *Applied Physics Letters* 82.2 (Jan. 2003), pp. 209–211. ISSN: 0003-6951, 1077-3118. DOI: 10.1063/1.1533839.

[101] M. M. Glazov and E. Ya. Sherman. «Theory of Spin Noise in Nanowires». In: *Physical Review Letters* 107.15 (Oct. 2011), p. 156602. ISSN: 0031-9007, 1079-7114. DOI: 10.1103/PhysRevLett.107.156602.

[102] S. Kudła et al. «Charge and spin conductivity of a two-dimensional electron gas with a random Rashba interaction». In: *Physical Review B* 97.24 (June 2018), p. 245307. ISSN: 2469-9950, 2469-9969. DOI: 10.1103/PhysRevB.97.245307.

[103] Jan Raphael Bindel et al. «Probing variations of the Rashba spin–orbit coupling at the nanometre scale». In: *Nature Physics* 12.10 (Oct. 2016), pp. 920–925. ISSN: 1745-2473, 1745-2481. DOI: 10.1038/nphys3774.

[104] David Sánchez and Llorenç Serra. «Fano-Rashba effect in a quantum wire». In: *Physical Review B* 74.15 (Oct. 2006), p. 153313. ISSN: 1098-0121, 1550-235X. DOI: 10.1103/PhysRevB.74.153313.

[105] David Sánchez, Llorenç Serra, and Mahn-Soo Choi. «Strongly modulated transmission of a spin-split quantum wire with local Rashba interaction». In: *Physical Review B* 77.3 (Jan. 2008), p. 035315. ISSN: 1098-0121, 1550-235X. DOI: 10.1103/PhysRevB.77.035315.

[106] Fabrizio Dolcini and Fausto Rossi. «Magnetic field effects on a nanowire with inhomogeneous Rashba spin-orbit coupling: Spin properties at equilibrium». In: *Physical Review B* 98.4 (July 2018), p. 045436. ISSN: 2469-9950, 2469-9969. DOI: 10.1103/PhysRevB.98.045436.

[107] Leonid Gogin, Fausto Rossi, and Fabrizio Dolcini. «Electron transport in quantum channels with spin–orbit interaction: effects of the sign of the Rashba coupling and applications to nanowires». In: *New Journal of Physics* 24.9 (Sept. 2022), p. 093025. ISSN: 1367-2630. DOI: 10.1088/1367-2630/ac8f66.

[108] Leonid Gogin et al. «The Dirac paradox in 1 + 1 dimensions and its realization with spin–orbit coupled nanowires». In: *New Journal of Physics* 24.5 (May 2022), p. 053045. ISSN: 1367-2630. DOI: 10.1088/1367-2630/ac6cfe.

[109] Jorge Cayao et al. «SNS junctions in nanowires with spin-orbit coupling: Role of confinement and helicity on the subgap spectrum». In: *Physical Review B* 91.2 (Jan. 2015), p. 024514. ISSN: 1098-0121, 1550-235X. DOI: 10.1103/PhysRevB.91.024514.

[110] G Campagnano et al. «Spin–orbit coupling and anomalous Josephson effect in nanowires». In: *Journal of Physics: Condensed Matter* 27.20 (May 2015), p. 205301. ISSN: 0953-8984, 1361-648X. DOI: 10.1088/0953-8984/27/20/205301.

[111] Christopher Reeg et al. ≪Zero-energy Andreev bound states from quantum dots in proximitized Rashba nanowires≫. In: *Physical Review B* 98.24 (Dec. 2018), p. 245407. ISSN: 2469-9950, 2469-9969. DOI: 10.1103/PhysRevB.98.245407.

[112] Jelena Klinovaja and Daniel Loss. ≪Fermionic and Majorana bound states in hybrid nanowires with non-uniform spin-orbit interaction≫. In: *The European Physical Journal B* 88.3 (Mar. 2015), p. 62. ISSN: 1434-6028, 1434-6036. DOI: 10.1140/epjb/e2015-50882-2.

[113] Lorenzo Rossi, Fabrizio Dolcini, and Fausto Rossi. ≪Majorana-like localized spin density without bound states in topologically trivial spin-orbit coupled nanowires≫. In: *Physical Review B* 101.19 (May 2020), p. 195421. ISSN: 2469-9950, 2469-9969. DOI: 10.1103/PhysRevB.101.195421.

[114] R. Landauer. ≪Spatial Variation of Currents and Fields Due to Localized Scatterers in Metallic Conduction≫. In: *IBM Journal of Research and Development* 1.3 (July 1957), pp. 223–231. ISSN: 0018-8646, 0018-8646. DOI: 10.1147/rd.13.0223.

[115] M. Büttiker. ≪Absence of backscattering in the quantum Hall effect in multiprobe conductors≫. In: *Physical Review B* 38.14 (Nov. 1988), pp. 9375–9389. ISSN: 0163-1829. DOI: 10.1103/PhysRevB.38.9375.